This electronic thesis or dissertation has been downloaded from the King's Research Portal at https://kclpure.kcl.ac.uk/portal/



Muscle precursor dynamics during growth and repair

Roy, Shukolpa Dutta

Awarding institution:
King's College London

The copyright of this thesis rests with the author and no quotation from it or information derived from it may be published without proper acknowledgement.

END USER LICENCE AGREEMENT



Unless another licence is stated on the immediately following page this work is licensed

under a Creative Commons Attribution-NonCommercial-NoDerivatives 4.0 International

licence. https://creativecommons.org/licenses/by-nc-nd/4.0/

You are free to copy, distribute and transmit the work

Under the following conditions:

- Attribution: You must attribute the work in the manner specified by the author (but not in any way that suggests that they endorse you or your use of the work).
- Non Commercial: You may not use this work for commercial purposes.
- No Derivative Works - You may not alter, transform, or build upon this work.

Any of these conditions can be waived if you receive permission from the author. Your fair dealings and other rights are in no way affected by the above.

Take down policy

If you believe that this document breaches copyright please contact librarypure@kcl.ac.uk providing details, and we will remove access to the work immediately and investigate your claim.

Download date: 08. Oct. 2023

Muscle precursor dynamics during growth and repair

Thesis submitted to the University of London in partial fulfillment of the requirements for the degree of Doctor of Philosophy

By
Shukolpa Dutta Roy

Randall Division of Cell & Molecular Biophysics
King's College London
New Hunts House
Guys Campus
London SE1 1UL

July 2013

Abstract

To date, knowledge of stem cell behavior during growth and muscle regeneration is limited by an inability to follow the repair process over time *in vivo*. Zebrafish larvae are amenable to *in vivo* imaging and possess muscle precursor cells (putative muscle stem cells). However, it has not been demonstrated whether the precursor cells marked by Pax7-expression are involved in post-hatched larval muscle growth and repair as in amniotes. With this aim in mind, the dynamics of $Pax7^{+}$ precursors was quantitated. $Myogenin^{+}$ precursor cells were also quantified as a marker of differentiation and along with $Pax7^{+}$ precursors were found to peak preceding myotomal recovery in $myod^{fh261}$ and wild type wounded fish, providing strong evidence for a role of $Pax7^{+}$ and $Myogenin^{+}$ muscle precursors in zebrafish growth and repair. Moreover, the spatiotemporal dynamics of precursors showed distinct proliferation, differentiation and migration behavior based on location in the somite. Roles of the niche at each somitic location are proposed based on the differences observed during growth and repair in the larval zebrafish.

Abbreviations

BrdU	Bromodeoxyuridine
BHLH	Basic Helix Loop Helix
cb	central body
de	dorsal edge
dpf	days post fertilization
dpw	days post wounding
EdU	5-ethynyl-2´-deoxyuridine
EER	Ectopic embryonic red
GFP	Green Fluorescent Protein
Hh	Hedgehog
Hm	horizontal myoseptum
Hpf	hours post fertilization
Hpw	hours post wounding
Hpi	hours post injury
LSM	laser scanning microscope
MAPK	Mitogen activated protein kinase
MRF	Myogenic regulatory factor
Myf5	Myogenic factor
Myod	Myogenic determination factor
n/nc	notochord
nt	neural tube
Pax	Paired box gene
PBS	Phosphate buffered saline
PBSTx	Phosphate buffered saline with Triton-X
PBST	Phosphate buffered saline with Tween-20
Penstrep	Penicillin Streptomycin antibiotic
PFA	Paraformaldehyde
PTU	Phenylthiourea
Shh	Sonic hedgehog
Tg	Transgenic
Vb	Vertical border

Table of Contents

Abstract **3**

Abbreviations **4**

Table of Contents **5**

List of Figures **9**

List of Tables **12**

Chapter 1: General introduction **13**

1.1 Skeletal muscle 13

1.2 Evidence for the role of satellite cells in muscle growth and repair 14

1.3 Molecular markers of satellite cells 16

1.4 Satellite cell activation 17

1.5 Factors involved in satellite cell activation 17

1.6 Satellite cell self-renewal and the role of Notch signaling 21

1.7 Potential therapeutic role of satellite cells 22

1.8 Amniote satellite cells arise in the dermomyotome 24

1.9 Evidence of a dermomyotome in *Xenopus* and *Danio rerio* (Zebrafish) 26

1.10 Role of Pax3 and Pax7 in early myogenesis and adult satellite cells of amniotes 28

1.11 Progenitors with myogenic potential are located in the zebrafish dermomyotome 30

1.12 Role of MRFs Myf5 and MyoD in skeletal muscle growth and repair in amniotes 32

1.13 Role of Pax 3/7 and MRFs in skeletal muscle growth and regeneration in zebrafish 33

1.14 Role of Myogenin in myoblast fusion and differentiation in amniotes and zebrafish 35

1.15 Thesis proposal 35

Chapter 2: Materials and Methods **38**

2.1 Fish maintenance 38

2.1.1 Identification of adult myod^{fh261} carriers 39

2.1.2 Identification of myod^{fh261} mutant larvae 41

2.2 Zebrafish embryo manipulations 42

2.2.1 PTU treatment 42

2.2.2 Wounding 42

2.2.3 Live imaging of embryos/larvae 43

2.2.4 Embryo fixation 44

2.2.5 Wholemount embryo and larval immunohistochemistry 44

2.2.6 BrdU treatment and detection in 4 dpf wholemount zebrafish 45
2.2.7 EdU treatment and detection in wholemount zebrafish 46
2.3 Wound area calculations 46
2.4 Counting of nuclei labeled with EdU/Pax7/Myogenin antibodies 47
2.5 Statistics 47
Chapter 3: Characterization of muscle progenitor cells during growth 48
3.1 Summary 48
3.2 Introduction 50
3.3 Results 53
3.3.1 $Pax7^+$ cells are clustered at the borders and located close to muscle fibres in the central body of zebrafish somites 53
3.3.2 The number of $Pax7^+$ cells increases in somites between day 3 and 6 of development 54
3.3.3 $Pax7^+$ cells increase in the deeper myotome during muscle growth 62
3.3.4 The fraction of $Pax7^+$ cells in S-phase varies with the somitic location 66
3.3.5 Spatio-temporal distribution of putative myogenic precursors expressing differentiation marker Myogenin 71
3.3.6 Spatio-temporal dynamics of putative myogenic precursors is altered in *myod*^{fh261} mutants 78
3.4 Discussion 88
3.4.1 Origin of $Pax7^+$ muscle progenitors in zebrafish muscle 88
3.4.2 The stem cell niche 88
3.4.3 Number of somitic $Pax7^+$ cells in zebrafish larvae and larvae 89
3.4.4 A model of myotomal myogenesis 91
3.4.5 Regional variation in the proliferation behaviour of muscle precursors in growing zebrafish 94
3.4.6 Myogenin expression in Myod mutants 95
3.5 Conclusion 96
Chapter 4: Characterization of muscle regeneration in zebrafish 97
4.1 Summary 97
4.2 Introduction 98
4.3 Results 101
4.3.1 Muscle wounds repair within 7 days post injury 101

4.3.2 Slow and fast muscle fibres regenerate at a similar rate 105
4.3.3 Structural proteins are lost and recover during muscle regeneration asynchronously 110
4.3.4 Nuclear recovery in wounded somites occurs by 2 days post wound 116
4.3.5 Rapid response of immune cells post muscle injury 124
4.3.6 Pax7:gfp^{+} cells contribute to muscle regeneration 128
4.3.7 The number of Pax7^{+} cells and Myogenin^{+} cells in wounded somites increases during muscle regeneration 143
4.3.8 The fraction of Pax7^{+} cells in the S-phase increases at the borders and central body during muscle regeneration 153
4.4 Discussion 170
4.4.1 Rapid but error prone repair 171
4.4.2 Proliferation and differentiation dynamics of muscle precursor cells during muscle repair and the role of Pax7^{+} cells at the various locations 172
4.4.3 Immune cell dynamics in muscle wounds 175
4.4.4 Wound size vs. rate of repair 176
4.4.5 Slow and fast muscle repair 176
4.4.6 Slow muscle fibres in fast muscle region 177
4.4.7 Model of myogenic cell dynamics 178
4.6 Conclusion 180
Chapter 5: General discussion 181
5.1 Dermomyotomal Pax7^{+} cells are precursors of muscle growth and repair in larval zebrafish 182
5.2 Variation in Myogenin expressing myogenic cells as a marker of muscle growth 184
5.3 Regional heterogeneity in muscle precursor dynamics 185
5.3.1 Central body 185
5.3.2 Vertical Borders 186
5.3.3 Dorsal edge 187
5.3.4 Horizontal myoseptum 188
5.3.5 Deciphering signaling pathways 190
5.4 Evidence of homeostatic control of myogenic precursors and future perspectives 196
5.5 Clinical relevance of the zebrafish model 198
5.6 Conclusion 199

Acknowledgements **201**
Bibliography **202**

List of Figures

Fig. 1.1 Schematic of a sarcomere 13

Fig. 1.2 Skeletal muscle and its mode of hyperplastic growth 14

Fig. 1.3 Myogenesis in zebrafish embryos 32

Fig. 2.1 Results of genotyping PCR 40

Fig. 2.2 Chromatograms from genotyping sequencing 41

Fig. 2.3 Identifying live and fixed myod^{fh261} mutant larvae 41

Fig. 3.1 Pax7^{+} cells are located at the borders and central body of somites 53

Fig. 3.2 Identification of Pax7^{+} cells at the borders 57

Fig. 3.3 Variation in the number of Pax7^{+} cells in individual larvae 58

Fig. 3.4 Pax7^{+} cells increase in epaxial somites at specific locations 59

Fig. 3.5 Pax7:gfp^{+} cells co-localize with Pax7 antibody stained nuclei 61

Fig. 3.6 Quantification of Pax7:gfp^{+} cells versus Pax7 antibody stained nuclei 62

Fig. 3.7 Pax7:gfp^{+} cells increase in the deep central body 64

Fig. 3.8 Pax7^{+} cells increase in deep myotome 65

Fig. 3.9 Somitic Pax7^{+} cells are proliferative 69

Fig. 3.10 The fraction of Pax7^{+} cells in S-phase varies based on somitic location 70

Fig. 3.11 Pax7:gfp^{+} cells differentiate into muscle fibres 74

Fig. 3.12 Myogenin^{+} cells are located at the dorsal edge and central body 75

Fig. 3.13 Differentiating Pax7^{+} cells increase significantly in the central body between 3 and 6 dpf 77

Fig. 3.14 Myotome growth recovers in 5 dpf *myod*^{fh261} mutants 81

Fig. 3.15 Pax7^{+} cells revert to normal levels by 5 dpf in *myod*^{fh261} mutants 82

Fig. 3.16 Pax7^{+}Myogenin^{+} cells revert to normal levels by 5 dpf in *myod*^{fh261} mutants 84

Fig. 3.17 Myogenin^{+} cells revert to normal levels by 5 dpf in *myod*^{fh261} mutants 85

Fig. 3.18 The number of myonuclei in *myod*^{fh261} mutants increases by 1.5 fold between 3 and 5 dpf 87

Fig. 3.19 Staining regimens tested for DP312 antibody staining 91

Fig. 3.20 Model of muscle growth and movement of Pax7^{+} precursor in 3-6 dpf zebrafish larvae 93

Fig. 4.1: Reduction of non-birefringent area in muscle wounds 101
Fig. 4.2 Average wound area reduction with time 102
Fig. 4.3 Confocal imaging of wound repair in live embryos 103
Fig. 4.4 Rate of wound resolution is independent of projected wound area 104
Fig. 4.5 Slow and fast muscle in zebrafish larvae muscle wounds repair at a similar rate 107
Fig. 4.6 Slow fibres are detected in the fast muscle layer in wounded muscle 109
Fig. 4.7 Loss and recovery of myosin heavy chain positive muscle fibres in wounded epaxial somites 112
Fig. 4.8 Loss of ß-catenin and striated actin positive muscle fibres in wounded muscle at 4 hpw 113
Fig. 4.9 Brightly stained ß-catenin material in wounds coincide with a concentration of nuclei but not striated actin 114
Fig. 4.10 Wound site is filled with striated material at 2 dpw 115
Fig. 4.11 Changes in the distribution of myosin and nuclei in wounded sections at 1 dpw 119
Fig. 4.12 Changes in the distribution of nuclei in wounded sections at 2 dpw 121
Fig. 4.13 Quantification of myonuclei in wounds at 1 and 2 dpw 123
Fig. 4.14: Dynamics of macrophages in zebrafish muscle wounds 126
Fig. 4.15 Quantification of macrophage dynamics in muscle wounds 127
Fig. 4.16 Neutrophils are more numerous in muscle wounds compared to macrophages 128
Fig. 4.17 Pax7:gfp^{+} cells contribute to muscle regeneration 131
Fig. 4.18 Pax7:gfp^{+} cells communicate with each other 133
Fig. 4.19 GFP perdurance of Pax7:gfp^{+} cells coincides with large caliber myosin positive fibres 134
Fig. 4.20 Pax7:gfp^{+} cells enter the wounds primarily from vertical borders and dorsal edge 136
Fig. 4.21 Entry route of Pax7:gfp^{+} cells in wounds 138
Fig. 4.22 Pax7:gfp^{+} cells loss and recovery at the horizontal myoseptum 140
Fig. 4.23 Pax7:gfp^{+} cells adjacent to wounds are mitotic 142

Fig. 4.24 $Pax7^+$ and $Myogenin^+$ cells are decimated in wounds at 4 hpw 147
Fig. 4.25 Numerous $Pax7^+$ and $Myogenin^+$ cells are present in wounds at 1 dpw 148
Fig. 4.26 $Pax7^+$ and $Myogenin^+$ cells appear more numerous in wounds compared to adjacent unwounded at 3 dpw 150
Fig. 4.27 $Pax7^+$ cells increase spatiotemporally in wounded muscle 152
Fig. 4.28 $Pax7^+EdU^+$ nuclei in wounded and unwounded epaxial somites at 5 hpw 158
Fig. 4.29 Numerous $Pax7^+EdU^+$ nuclei appear in wounds by 1 dpw 160
Fig. 4.30 $Pax7^+EdU^+$ nuclei in the central body of wounds compared to adjacent unwounded at 2 dpw 162
Fig. 4.31 At 5 hpw $Pax7^+$ cells in S-phase are located at the vertical borders of both wounded and adjacent unwounded somites 164
Fig. 4.32 At 1 dpw $Pax7^+$ cells in S-phase are located at the vertical borders and in the wounded central body 166
Fig. 4.33 At 2 dpw $Pax7^+$ cells in S-phase are primarily located in the wounded central body 168

List of Tables

Table 2.1 Transgenic/mutant zebrafish lines used 38

Table 2.2 List of objectives utilized 44

Table 2.3. Primary antibodies 45

Chapter 1: General introduction

1.1 Skeletal muscle

Skeletal muscle is a type of striated muscle that is attached to the bone via tendons and is involved in voluntary movement as well as maintaining posture. Skeletal muscle is made up of muscle cells or muscle fibres which in turn contain the functional units of muscle known as sarcomeres. The striated appearance of striated muscle arises from the ordered array of sarcomeres. A sarcomere (Fig. 1.1) is bordered by Z-discs and contains thin actin and thick myosin filaments (Gregorio et al., 1999; Squire, 1997). The region on either side of Z-discs is occupied by thin filaments and not thick filaments, and this region is called the I-band. The A-band encompasses the region spanned by thick filaments. Within the A-band lies the H-zone which is occupied by thick filaments alone but not thin filaments. The thick filaments are connected to titin extending from the Z-line to the M-band which lies within the H-zone. Thin filaments are coiled with nebulin filaments and also connected to titin and anchored in the Z-disc via non-contractile protein structures such as alpha-actinin in the Z-line. Muscle contraction is generated by the sliding action of thin filaments past the thick filaments leading to shortening of the sarcomere.

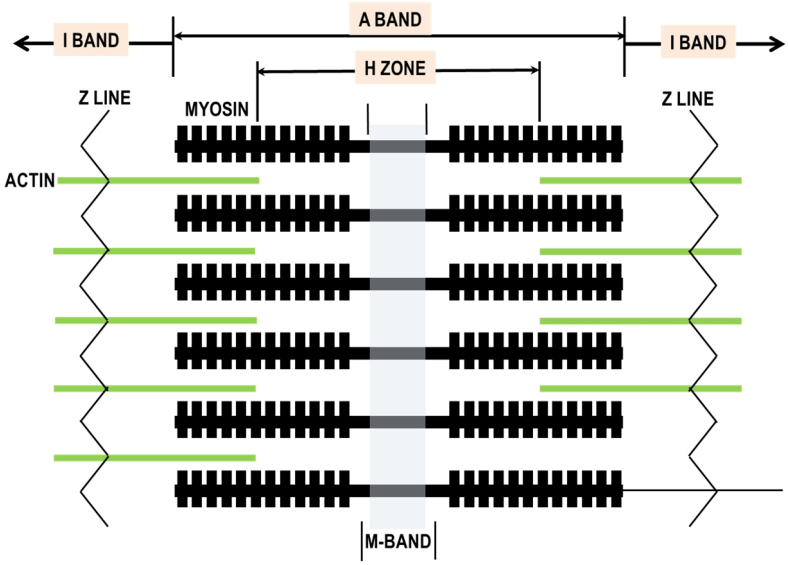


Fig. 1.1 Schematic of a sarcomere

A single unit of muscle consisting of thick myosin (black) and thin actin (green) filaments and bordered by Z discs to form the Z line. Myosin filaments are anchored within the M band whereas actin filaments are anchored in Z-discs. Also depicted with arrows are regions encompassed by A band, I band, M band and H zone. Adapted from Squire et al., 1997.

Skeletal muscle in adults is maintained and grows by the addition of satellite cells. Satellite cells give rise to precursors (upon activation if they are quiescent as in adults) that fuse to each other to give rise to new fibres or aid in fibre growth by fusing with existing fibres (Fig. 1.2).

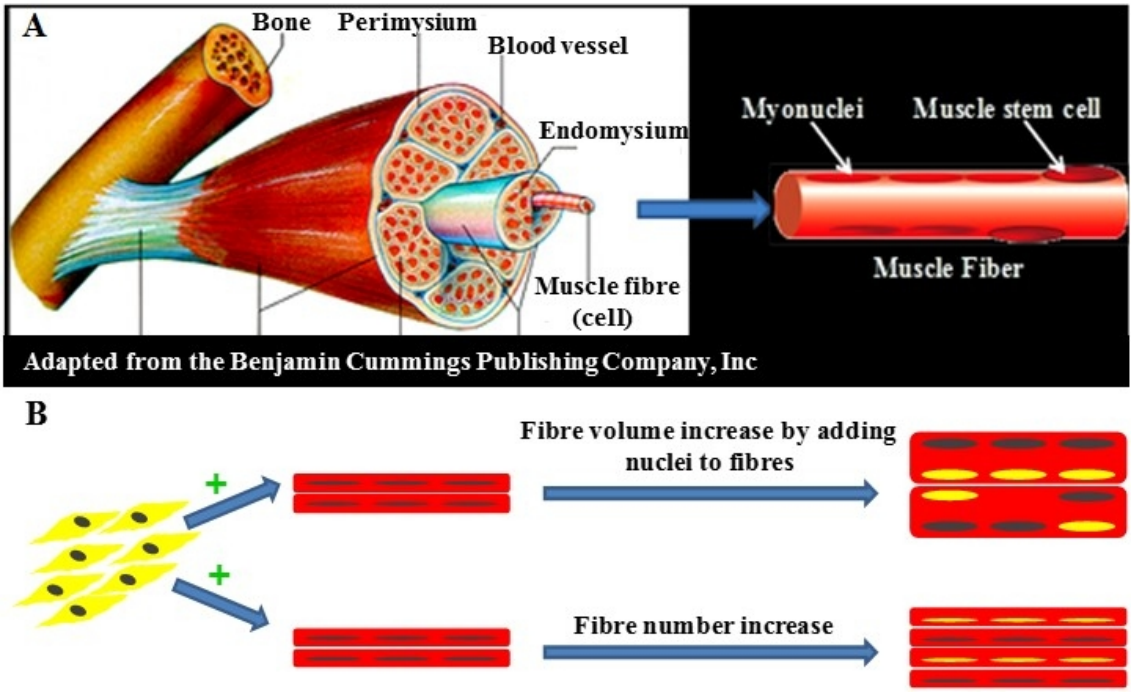


Fig. 1.2 Skeletal muscle and its mode of hyperplastic growth
A: Muscle is attached to the bone via tendon**.** Blue arrow points to a muscle fibre with its myonuclei and the muscle stem cell adjacent but separated from the plasmalemma of the muscle fibre. **B:** Skeletal muscle progenitors fuse with existing fibres to increase fibre volume or fuse with each other to give rise to new fibres.

1.2 Evidence for the role of satellite cells in muscle growth and repair

Satellite cells are a group of adult muscle stem cells that are capable of giving rise by proliferation to myogenic cells which further differentiate to produce muscle tissue. Additionally satellite cells have the ability to not be lost by differentiation but maintain themselves via self-renewal. Both of the above attributes satisfy the classic criteria for stem cells. Moreover, satellite cells have also been shown to be multipotent and thereby satisfy another criteria classically attributed to stem cells (Wada et al., 2002). As described later in Section 1.8, satellite cells originate from $Pax3^+$ and $Pax7^+$ cells in the embryonic dermomyotome. In intact adult skeletal muscle, satellite cells reside between the basal lamina and plasmalemma of mature muscle fibres separated from their

surroundings by their own plasma membrane (Mauro, 1961). Satellite cells have reduced cytoplasm and highly condensed nuclear material reflective of their quiescent state. Approximately 28% of muscle nuclei in 7 day old mice belong to satellite cells. However, in 30 day mice, about 5% of nuclei are those of satellite cells (Schultz, 1974). This reduction in the number of nuclei is likely a reflection of satellite cells fusing to each other or existing fibres resulting in postnatal muscle growth. The role of satellite cells in muscle growth was demonstrated in vivo by the work of Moss and Leblond (Moss and Leblond, 1971) in growing rats. They showed that satellite cell division correlated with an increase in the number of labeled nuclei within myofibres in growing animals, suggesting that dividing satellite cells produce muscle precursors which lead to muscle growth by fusing with each other or to existing fibres. Moreover, immediately following a tritiated thymidine pulse, only satellite cells were labeled whereas after a longer interval between pulse and assay, both satellite cells and nuclei within fibres were labeled, demonstrating that satellite cells contribute nuclei for muscle growth. Similarly, when muscle tissue labeled with tritiated thymidine where the only labeled cells were satellite cells was transplanted in non-tritiated littermates, regenerating myotube nuclei were labeled, demonstrating that satellite cells contribute nuclei during muscle regeneration. Satellite cells in the adult tissue are generally quiescent (Schultz et al., 1978), and are activated to proliferate rapidly to provide myogenic cells following injury to muscle fibres which could occur from weight bearing exercise, denervation, trauma, injury or disease (Bischoff and Heintz, 1994; Darr and Schultz, 1987; Snow, 1977; Snow, 1983). Repair to muscle fibres was shown to occur in vitro by the fusion of the satellite cell progeny to damaged fibres, thereby repairing them, or to each other to form new fibres (Bintliff and Walker, 1960; Capers, 1960; Cooper and Konigsberg, 1961; Grounds et al., 1980; Grounds and McGeachie, 1987; Konigsberg et al., 1960; Lipton and Schultz, 1979; Mintz and Baker, 1967; Partridge et al., 1978; Snow, 1978; Watt et al., 1982). Tritiated thymidine labeling in vivo studies suggested that myoblasts involved in muscle repair in vivo largely arise from satellite cells (Reznik, 1969; Snow, 1977; Snow, 1978) and fibre regeneration from transplantation of intact myofibres containing satellite cells into irradiated mice provided in vivo evidence of satellite cell-aided muscle repair (Collins et al., 2005).

1.3 Molecular markers of satellite cells

Electron microscopy was the key method used to identify satellite cells by their location under the basal lamina (Mauro, 1961) and their activated morphology during repair (Reznik, 1969; Snow, 1977; Snow, 1978). In the intact unstressed muscle, satellite cells lay wedged between the basal lamina and plasma membrane of the muscle cell. The quiescent satellite cell is transcriptionally and mitotically inactive and hence has a large nucleus to cytoplasm ratio, few organelles and condensed interphase chromatin (Mauro, 1961; Schultz, 1974).

More recently, reliable molecular markers for identifying satellite cells and myoblasts by optical methods have been established. Pax7 is a convenient satellite cell marker that is expressed by quiescent and proliferating satellite cells (Olguin and Olwin, 2004; Seale et al., 2000; Yablonka-Reuveni et al., 2008). Some satellite cells express Pax3 (Buckingham et al., 2003). Expression of LacZ in majority of the quiescent satellite cells in *Myf-LacZ* mice indicates that the Myf5 locus is active in most quiescent satellite cells (Beauchamp et al., 2000). All quiescent and early activated satellite cells also express the transmembrane heparin sulfate proteoglycans syndecans 3 and 4 (Cornelison et al., 2001). Some other markers of satellite cells include cell adhesion protein M-cadherin (Irintchev et al., 1994), tyrosine kinase receptor c-met (Cornelison and Wold., 1997), myocyte nuclear factor (Garry et al., 1997), nuclear envelope proteins lamin A/C and emerin, α7 integrin (Gnocchi et al., 2009), and cluster of differentiation CD34 (Beauchamp et al., 2000). In general, satellite cells could be heterogeneous for the expression of a particular marker or the marker is expressed by non-myogenic cells as well, in which case a satellite cell is identified on the basis of two or more characteristics, such as expression of more than one marker and by staining for the basal lamina.

Following activation, quiescent satellite cells often enter the cell cycle and begin to express muscle regulatory factors (MRFs) such as Myf5 or MyoD prior to proliferation while continuing to express Pax7, followed by expression of both Myf5 and MyoD in proliferating cells (Cornelison and Wold, 1997; Cooper et al., 1999; Grounds et al., 1992; Yablonka-Reuveni and Rivera., 1994; Yablonka-Reuveni et al., 2008). The onset of differentiation is marked by Myogenin expression along with downregulation of Pax7

expression (Olguin and Olwin, 2004). Activated satellite cells also express other markers depending on their stage following initial activation. For example, recently activated satellite cells continue to express syndecans 3 and 4 whereas activated satellite cells that have initiated the differentiation program will begin expressing MRF4 and other muscle specific proteins such as myosin (Cornelison et al., 2001; Yablonka-Reuveni and Rivera, 1994). Thus, the pattern of MRF expression in quiescent and activated satellite cells appears analogous to that during embryonic myogenesis.

1.4 Satellite cell activation

For satellite cells to contribute to homeostasis, growth and repair of skeletal muscle, they need to be activated. Activation during muscle repair involves the release of satellite cell from its location under the basal lamina, chemotaxis, proliferation followed by differentiation of majority of the activated satellite cells whereas a small population return to quiescence or self-renew. Activation is accompanied by changes in the appearance of quiescent satellite cells. The cells appear swollen, have irregular shape and may have cytoplasmic processes extending from their edges (Schultz and McCormick, 1994). Additionally, there is a reduction in heterochromatin likely due to the activation of transcriptional machinery and an increase in intracellular organelles such as Golgi and granular endoplasmic reticulum (Church et al., 1966; Ishikawa, 1966).

1.5 Factors involved in satellite cell activation

Satellite cells in unstimulated muscle are sheltered from activating agents such as growth factors, cytokines and other signaling molecules and are wedged in intimate contact with the basal lamina made up of extracellular matrix (ECM) molecules such as Type IV collagen, laminin, fibronectin and several glycoproteins (Sanes, 2003). Muscle injury can disturb the structure of basal lamina and expose satellite cells to growth factors, cytokines and enzymes tethered to the ECM or released from injured myofibres, immune cells such as macrophages or serum. These released substances can activate satellite cells and influence their proliferation and/or migration and/or differentiation. Some of the molecules implicated in activating satellite cells are described here.

Hepatocyte growth factor (HGF) acts via its receptor c-met and both are expressed in quiescent and activated satellite cells. HGF is also expressed by myotubes in vitro and

myofibres in vivo (Tatsumi et al., 1998). HGF is transcribed in levels proportional to injury and released from ECM (Tatsumi et al., 1998). HGF is tethered to heparan sulfate proteoglycans (HSPGs) and mechanical stretch can release it (Tatsumi et al., 2001). HGF release is proposed to involve nitric oxide synthesis since a nitric oxide donor could accelerate satellite cell activation via HGF whereas inhibition of nitric oxide synthesis did not accelerate satellite cell activation (Tatsumi et al., 2002; Tatsumi et al., 2006). Furthermore, nitric oxide in damaged muscle can activate matrix metalloproteinases which can release HGF from HSPGs (Yamada et al., 2006).). HGF has been shown to enhance satellite cell proliferation in vitro and in vivo (Allen et al., 1995; Tatsumi et al., 1998). Also, HGF inhibits differentiation and likely promotes chemotaxis of satellite cells in the early phase of regeneration (Bischoff, 1997; Miller et al., 2000). The mode of action of HGF in enhancing proliferation involves activation of mitogen activated protein kinase (MAPK)/ extracellular signal regulated kinase (ERK) signaling triggered by binding of Grb2 to phosphorylated c-met (Leshem et al., 2002). HGF inhibition of differentiation in vitro occurs by increasing the levels of Twist (suppressor of MyoD and MEF2) and decreasing the levels of cell cycle inhibitor p27 (Leshem et al., 2000).

Transcripts of several **fibroblast growth factors** (FGFs) in skeletal muscle have been reported in mouse muscle cell lines and some such as FGF1 and 2 have been proposed to initiate DNA synthesis and suppress differentiation (Hannon et al., 1996). Of these FGF6 is highly expressed in skeletal muscle in vivo and wild type mice upregulate FGF6 following injury. A knockout mouse model of FGF6 shows impaired regeneration due to reduced number of proliferating myoblasts suggesting deficit in satellite cell activation (Floss et al., 1997). Indeed injecting exogenous FGF2 increased the number of $BrdU^{+}$ myoblasts in injured muscle of mdx mice (Lefaucher and Sebille, 1995). FGFs signal via transmembrane tyrosine kinase FGF receptors (FGFR) of which there are four types. Receptor availability is important for skeletal muscle development (Scata et al., 1999). FGF2 is expressed in basement membrane surrounding myotubes whereas FGFR and syndecans 3 and 4 (HSPGs) which mediate FGF signaling are present on quiescent and activated satellite cells. In vitro, binding of FGF to its receptor and HSPG (Olwin et al., 1992) activates ERK1/2 via Ras/MAPK kinase (MAPKK) pathway leading to transition of satellite cells from G1 to S-phase (Fedorov et al., 2001; Jones et al., 2001). Inhibition

of signaling via MAPKK led to the removal of FGF2 mediated inhibition of differentiation in vitro (Weyman and Wolfman, 1998). Fibroblast growth factor (FGF) signaling in vivo can modulate the state of quiescence in satellite cells (Chakkalakal et al., 2012; Lagha et al., 2008). When levels of FGF were perturbed by manipulating levels of FGF inhibitor Sprouty, more $Pax7^{+}$ myoblasts compared to those lost to Myogenin expression were obtained, indicating that FGF pathway can influence the ratio of proliferating and differentiating myogenic precursors (Lagha et al., 2008). Similarly, increased levels of FGF2 and reduced levels of Sprouty in aged muscle drive aged satellite cells out of quiescence and into cycling. This can be restored by increasing Sprouty expression or reducing FGF2 availability. To summarize, FGFs mentioned here appear to promote proliferation and suppress differentiation of satellite cells.

Insulin-like growth factors (IGF) are involved in increasing both mitotic activity and differentiation and thus lead to muscle hypertrophy by increasing satellite cell proliferation and differentiation detected by increase in DNA as well as message for MyoD, myogenin and structural proteins (Chakravarthy et al., 2000; Coleman et al., 1995; Coolican et al., 1997; Musaro et al., 2004; Musaro et al., 2001). Mice mutant for IGF-I or IGF-II display muscle insufficiency (Liu et al., 1993), whereas overexpression in transgenic mice leads to increased size of muscle fibres (Coleman et al., 1995). IGF-I effects on proliferation and differentiation are mediated through tyrosine kinase IGFI receptor (IGFRI) to activate phosphatidyl inositol 3-kinase/AKT/mTOR or Ras/Raf/ERK cascade (Coolican et al., 1997). IGF availability is regulated through IGF binding proteins (IGFBP). Knockdown of IGFBP5 in vitro decreased myogenin and myosin heavy chain expression and impaired differentiation (Ren et al., 2008). To summarize thus far, IGF-I promotes satellite cells to proliferate and differentiate as opposed to promoting proliferation and suppressing differentiation by HGF and some FGF members mentioned previously. It is possible that HGF and FGF act early in the muscle repair process during the proliferative phase whereas IGF acts both early and late.

Transforming growth factor β (TGF-β) has been suggested to play a role in suppressing proliferation and differentiation of myoblasts in vitro, by silencing transcriptional activation of *Myf-5*, *MyoD* and *Myogenin* by signaling through the intracellular SMAD

family of proteins (Furutani et al., 2011; Martin et al., 1992). Conversely, TGF-β has also been proposed to support differentiation in a SMAD independent manner in vitro (Droguett et al., 2010). To summarize, the effect of TGF-β on satellite cell activation in vivo remains to be elucidated and might vary based on signaling mechanisms at play.

Matrix metalloproteinases (MMPs) are a family of zinc dependent enzymes that play an important role in mediating satellite cell chemotaxis likely by degrading ECM components (Chen and Li, 2009). MMP-2 and 9 are secreted by satellite cells soon after injury and function to degrade collagen allowing satellite cells to migrate to wound site (Kherif et al., 1999; Nishimura et al., 2008). Another mode of MMP action could be as follows: nitric oxide can upregulate MMP-2, leading to release of HGF from HSPG and ultimately lead to satellite cell activation via HGF (Yamada et al., 2006; Yamada et al., 2008). Thus, MMPs can be involved in satellite cell activation directly by cleaving components of extracellular matrix for increased satellite cell mobility and indirectly influence proliferation and perhaps differentiation by cleaving molecules involved in these processes directly or indirectly.

Several other growth factors and cytokines secreted by myoblasts and/or macrophages in injured muscle can influence satellite cell activation. For example, vascular endothelial growth factor (VEGF) significantly increased macrophage infiltration at injury site followed by significant increases in the number of myoblasts and regenerating myotubes at wound site (Lescaudron et al., 1999). Similarly, in a model of ischemic muscle injury, regions of VEGF and VEGF-receptor expression were correlated with increased macrophage infiltration and capillaries (Rissanen et al., 2002). To summarize, a number of different growth factors, cytokines and enzymes can activate satellite cells in a variety of ways. Whereas the effect of the growth factors/cytokines is sometimes known in vitro and in vivo, for many of the effecting molecules the exact mechanism remains to be elucidated in vivo and is likely to involve coordinated action of more than one effector. Determining how they influence the environment of the satellite cell and satellite cell activation in the intact animal during growth and repair would be critical for therapeutic applications.

1.6 Satellite cell self-renewal and the role of Notch signaling

Not all activated satellite cells progress through to differentiation and instead self-renew. Some downregulate MyoD, continue to express Pax7 and return to quiescence (Olguin and Olwin, 2004, Zammit et al., 2004). Another mode of self-renewal occurs following asymmetric cell division (Kuang et al., 2007). $Pax7^{+}Myf5^{-}$ satellite cells divide asymmetrically to generate basal $Pax7^{+}Myf5^{-}$ and apical $Pax7^{+}Myf5^{+}$ progeny. Upon transplantation, $Pax7^{+}Myf5^{+}$ cells largely differentiate whereas $Pax7^{+}Myf5^{-}$ cells expand the satellite cell pool considerably in addition to providing differentiating precursors (Kuang et al., 2007). The asymmetric division mode of self-renewal might be influenced by Notch signaling since the Notch ligand Delta-1 is expressed at higher levels in the differentiation-prone satellite cells, whereas receptor Notch3 is highly expressed in the quiescent satellite cell population (Kuang et al., 2007; Fukada et al., 2007). Moreover, treatment with the Notch inhibitor DAPT significantly increased the number of satellite cells committed to differentiation and reduced the number of quiescent $Pax7^{+}MyoD^{-}$ cells (Kuang et al., 2007). However, the mechanism underlying Notch regulation of $Myf5^{+}$ and $Myf5^{-}$ satellite cells remains to be elucidated. An alternate mechanism of Notch regulated asymmetric division has been demonstrated in vitro (Conboy and Rando, 2002). The authors found that the Notch inhibitor Numb was asymmetrically distributed between daughter cells in dividing myoblasts. $Numb^{+}$ cells expressed Pax7, Myf5 and desmin whereas $Numb^{-}$ cells expressed Pax3 but neither Myf5 nor desmin suggesting that $Numb^{+}$ cells are more committed to differentiation compared to $Numb^{-}$ cells. Moreover, constitutively active receptor Notch1 increased the rate of myoblast proliferation and reduced myosin expression whereas constitutively active Numb decreased proliferation rate and led to myotube formation. Thus, the level of Numb could influence satellite cell self-renewal. The authors obtained further evidence for this in aged muscle (Conboy et al., 2003). Myoblasts from aged muscle showed poor proliferative capacity with decreased levels of Delta-1 and increased levels of Numb compared to young muscle. Several other studies provide evidence for the role of Notch signaling in regulating cell fate. Ligand binding (Delta or Jagged) to Notch receptor leads to cleavage of the extracellular domain (Rand et al., 2000) and release of Notch intracellular domain (NICD) by a series of proteolytic events including cleavage by gamma secretase enzyme.

NICD translocates to the nucleus and converts the transcriptional repressor RBPj into an activator leading to the transcription of Notch target genes (De Strooper et al., 1999). Inhibition of Notch signaling via mutation in RBPj or by inhibiting ligand Delta-1 leads to decrease in $Pax3^+$ cells followed by absence of satellite cells. Notch inactivation by conditional knockout of the transcription factor RBP-J in mouse embryos led to uncontrolled differentiation and depletion of proliferating and quiescent satellite cells during fetal development (Vasyutina et al., 2007). Similarly, mouse mutants of Notch ligand Delta-1 showed a loss of progenitor cells due to excessive differentiation (Schuster-Gossler et al., 2007). In conclusion, the Notch signaling pathway appears to modulate both proliferation and differentiation and thereby could influence the fate of satellite cells towards differentiation or self-renewal.

1.7 Potential therapeutic role of satellite cells

Muscle is important for maintaining posture, mobility and metabolism. Muscle degeneration and loss of function can occur due to trauma/injury, muscle wasting or cachexia, age related muscle loss and muscular dystrophy. Muscle degeneration can be overcome by regenerating muscle via utilizing satellite cells. Hence, a major therapeutic focus is to deliver satellite cells in degenerating muscle to promote muscle repair and growth.

For satellite cell therapy to be effective in promoting muscle repair and growth upon transplanting into host tissue, donor myogenic cells should be able to migrate and expand their population prior to differentiation. Moreover, some of the transplanted cells should be capable of self-renewal, that is return to quiescence and repopulate the satellite cell niche as a reservoir for future repair and growth of the host muscle. Early research in dystrophic mice showed that injection of wildtype muscle precursor cells could lead to fusion of injected cells with host fibres (Partridge et al., 1989). However, success of satellite cell injections into dystrophic animals or patients has been limited by poor survival, migration, expansion and self-renewal (Fan et al., 1996; Partridge, 2003; Skuk et al., 2006). Grafting freshly isolated myofibres with as few as seven to eight $Pax7^+$ satellite cells generated many fibres in the host tissue (Collins et al., 2005), suggesting that less activated satellite cells were capable of efficient expansion. Indeed, when

prospectively isolated Pax3:GFP^{+}Pax7^{+}CD34^{+}CD45^{-} satellite cells (Montarras et al., 2005) or Pax7^{+}Myf5^{-} satellite cells (Kuang et al., 2007) were transplanted into host muscle, the transplanted cells gave rise to new fibres and donor derived satellite cell progeny, showing that prospectively freshly isolated satellite cells or less committed Pax7^{+} satellite cells might be more proliferative compared to culture expanded myoblasts expressing Pax7 and MRFs. Another limitation has been long-term efficacy of injected donor cells. The above mentioned studies (Collins et al., 2005; Kuang et al., 2007; Montarras et al., 2005) showed that donor satellite cells colonized the satellite cell compartment and gave rise to new progeny and regenerated myofibres upon injury or grafting into dystrophic mice (Montarras et al., 2005), indicating that freshly isolated or prospectively isolated less committed satellite cells are capable of self-renewal, a necessity for long term efficacy of satellite cell therapy to treat chronic degeneration. However, factors that maintain isolated satellite cells in a quiescent state outside of their niche for extended periods until transplanted into donor tissue are not well understood. Also following transplantation, enhancing donor cell expansion, migration and self-renewal within host tissue requires knowledge of the niche and signals regulating satellite cell behavior and function within the niche.

Recent studies have highlighted the therapeutic potential of adding growth factors or MMPs to satellite cells delivered into host tissue. For example delivery of satellite cells on scaffolds containing HGF and FGF2 promoted proliferation, differentiation, self-renewal of donor satellite cells and increased the number of regenerating myofibres and muscle mass of injured muscle (Hill et al., 2006). Another study found that addition of a splice variant of IGF-1 known as mechano growth factor (MGF) during donor cell delivery enhanced migration of muscle precursors by utilizing the fibrinolytic system and MMPs in host muscle of SCID (severe combined immunodeficiency) mice (Mills et al., 2007).

In order to convert the potential of satellite cell therapy into reality, a lot more needs to be understood about the satellite cell and it's niche. Better understanding of niche composition, niche interactions with satellite cells and niche regulation could lead to designing optimal satellite cell therapeutics for muscle diseases in humans and animals.

An ideal way to study satellite cell interactions with its niche would be to examine the satellite cell in vivo during growth and repair. Such studies are generally limited by the duration for which satellite cell behavior can be studied in vivo prior to niche destruction for removal of satellite cell into in vitro culture.

To study the in vivo behavior of $Pax7^+$ myogenic precursors in growing and regenerating muscle, work in this thesis describes the use of vertebrate zebrafish. Zebrafish embryos and larvae are small and amenable to live imaging. The zebrafish genome has been sequenced (Howe et al., 2013) and they are genetically tractable. The recent addition of Pax7:gfp fish makes it possible to image $Pax7:gfp^+$ cells in the larvae for extended periods. Thus, investigating Pax7 expressing muscle precursors in zebrafish could provide a platform to study niche composition, interactions and niche regulation in a living vertebrate. A better understanding in these areas could lead to improvements in the efficacy of stem cell based therapeutics

Satellite cells in amniotes expressing the transcription factors Pax7 and Pax3 arise in the dermomyotome during embryogenesis (Relaix et al., 2005). Studies in zebrafish show that cells marked by Pax7 and Pax3 are present in the zebrafish dermomyotome (Hammond et al., 2007). These dermomyotomal $Pax7^+$ myogenic precursors in zebrafish have been proposed but not demonstrated to be involved in muscle growth and repair. The work described in this thesis investigates the behavior of $Pax7^+$ cells as they translocate from the dermomyotome into the myotome and give rise to muscle fibres. Hence the following introduction sections briefly describe somite development in amniotes and zebrafish followed by the role of Pax3, Pax7 transcription factors and MRFs in amniote and zebrafish myogenesis. Importantly, the following sections highlight the unknowns regarding myogenesis in the zebrafish model before it can be utilized to study niche dynamics.

1.8 Amniote satellite cells arise in the dermomyotome

Skeletal muscle originally arises in transient epithelial structures called somites in the developing embryo (Christ and Ordahl, 1995). Somites form from unsegmented bilateral blocks of paraxial mesoderm aligned on either side of the neural tube and notochord. The unsegmented mesoderm progressively epithelializes to generate distinct segmented

blocks from the anterior to posterior of the animal such that rostral somites are older than caudal somites. At the center of epithelial somites called somatocoel, lies a loose meshwork of mesenchymal cells. The ventral portion of the somite undergoes epithelial to mesenchymal transition and along with the somatocoel form the mesenchymal sclerotome which acts as a source of progenitors for the development of skeleton, ribs, components of spinal cord and vertebrae (Brent et al., 2003; Christ et al., 2000; Christ et al., 2004). Dorsal portion of the somite forms dermomyotome which is a source of progenitors for all skeletal muscle of the trunk and limbs, dermis, endothelial cells, vascular smooth muscle and brown fat (Buckingham, 2006). Cells at the lips of the dermomyotome de-epithelialize and invade the underlying myotome (Gros et al., 2004) giving rise to distinct muscles. Progenitor cells from the dorsomedial lip migrate ventrolaterally to give rise to the epaxial deep back muscles (Denetclaw et al., 1997). Progenitors from the ventrolateral lip migrate to form hypaxial muscle (Denetclaw et al., 2001) or delaminate from somites at the level of limb and migrate to the limb buds as progenitors of limb muscle (Buckingham et al., 2003; Christ et al., 1977; Jacob et al., 1978; Jacob et al., 1979). The first wave of cells enter the myotome from the dorsomedial (epaxial) and ventrolateral lips, express *Myf5* and *Mrf4* and give rise to pioneer fibers in the primary myotome (Cinnamon et al., 1999; Huang and Christ, 2000; Kahane et al., 1998a). Following the first wave, myogenic cells delaminate from all four lips including rostral and caudal lips, intercalate between or fuse with the primary pioneer fibers or migrate to limb buds and lead to further myotome expansion (Denetclaw and Ordahl, 2000; Gros et al., 2004; Kahane et al., 1998b; Kahane et al., 2002). The cells of the second wave also express *Myf5* and *MyoD* in addition to prior expression of *Pax3* and other migratory markers specifically expressed by precursors migrating to limb buds. The third wave of cells in mouse and chick arise by central dermomyotome delamination to give rise to progenitors of the dermis as well as proliferative progenitors for future myotome growth by (Ben-Yair and Kalcheim, 2005; Gros et al., 2005; Kassar-Duchossoy et al., 2005; Relaix et al., 2005; Schienda et al., 2006). The different cell fates of the progenitors occurs via asymmetric cell divisions (Ben-Yair and Kalcheim, 2005) Cell lineage tracing experiments showed that mitotic myogenic cells, many of them expressing Pax3 and Pax7 migrate from the central dermomyotome to the myotome, are the majority of proliferating

cells in the myotome. Some of these proliferating $Pax3^+$ and $Pax7^+$ cells contribute to the myotome while others take up positions adjacent to fibres, become quiescent satellite cells and aid in postnatal growth (Ben-Yair and Kalcheim, 2005; Gros et al., 2005, Relaix et al., 2005). Interestingly, satellite cells in the limbs predominantly arise from the migratory $Pax3^+$ cells in the hypaxial dermomyotome (Kassar-Duchossoy et al., 2005; Schienda et al., 2006). These multipotent cells migrate from the ventro-lateral border of the dermomyotome and some give rise to various tissues in the limb (He et al., 2003; Hutcheson et al., 2009). From E11.5 onwards Pax7 is expressed in some progenitor cells in the anterior limb buds (Relaix et al., 2004) and these cells and other undifferentiated Pax3 expressing cells form the future quiescent satellite cells of the limbs (Hutcheson et al., 2009). To conclude, satellite cells for postnatal muscle growth arise from Pax3 and/or Pax7 marked cells in the dermomyotome in mice and chick.

In the amphibian *Xenopus*, majority of the $Pax7^+$ satellite cells were shown to arise from the dorsolateral mesoderm instead of the paraxial mesoderm (Daughters et al., 2011). These $Pax7^+$ progenitor cells were proliferative, some gave rise to fibres while others took up positions adjacent to myofibres and likely formed satellite cells that gave rise to new fibres upon injury (Daughters et al., 2011; Gargioli and Slack 2004). Pax3 expression increases in parallel with dermomyotome formation (Della Gaspera et al., 2012; Grimaldi et al., 2004) followed by presence of $Pax3^+$ cells within the myotome in the developing embryo (Grimaldi et al., 2004). Similar to amniotes, Pax3 expressing precursors migrate from the ventro-lateral region of somites and express Myf5 and MyoD prior to differentiation (Martin and Harland, 2001; Satoh et al., 2005).

1.9 Evidence of a dermomyotome in *Xenopus* and *Danio rerio* (Zebrafish)

Some early studies in *Xenopus* reported a one to two cell layer thick 'dermatome' lying superficial or external to the myotome of 18-23 stage embryos (Blackshaw and Warner, 1976; Hamilton, 1969). A more recent study refined the description of this external cell layer based on morphology and molecular characteristics (Grimaldi et al., 2004) of the cells lying external to the myotome in stage 22, 28 and 35 embryos. The authors showed that the layer of cells proposed to be the dermomyotome is myosin negative and located external but adjacent to the myosin positive myotome. Within the dermomyotome,

XMyf5^{+} cells are primarily located at the dorsal and ventral extremes whereas XMyod^{+} cells are located in a dorsoventral chevron across the somite. Pax3^{+} mononucleate cells were also found to be present in the Xenopus dermomyotome similar to that in amniote dermomyotome (Goulding et al., 1994). Further, similar to amniotes, dermal precursors have been reported in the Xenopus dermomyotome (Ben-Yair and Kalcheim, 2004; Grimaldi et al., 2004). Interestingly in the amphibian Xenopus, majority of the Pax7^{+} progenitor cells were shown to arise from the dorsolateral mesoderm instead of the paraxial mesoderm (Daughters et al., 2011). The Xenopus study was conducted at an earlier developmental time point compared to the studies in amniote embryos and the difference in location of where the embryonic Pax7^{+} progenitor cells arise from might be reflective of the different development time at sampling (Daughters et al., 2011).

In zebrafish and other teleosts, the external cell layer is proposed to be the dermomyotome based on morphological and molecular characteristics (Devoto et al., 2006; Feng et al., 2006; Groves et al., 2005; He et al., 2003; Waterman, 1969). Similar to amniotes and Xenopus, the external cell layer is myosin negative and lies adjacent and external to the myosin positive somitic muscle (Devoto et al., 2006; Groves et al., 2005; Hammond et al., 2006). Moreover, the external cell layer in zebrafish contains mononucleate myogenic (expressing Pax3/Pax7, Myod or Myogenin) and dermal progenitors (Barresi et al., 2001; Devoto et al., 2006; Groves et al., 2005; Hammond et al., 2007; Hollway et al., 2007; Stellabotte et al., 2007). Furthermore, a fraction of the mononucleate cells in the external cell layer of zebrafish were found to cycling (Barresi et al., 2001; Devoto et al., 2006; Hammond et al., 2007; Stellabotte et al., 2007) and thus are reminiscent of the proliferative myogenic precursors in amniote dermomyotome (Ben-Yair and Kalcheim, 2005; Gros et al., 2005; Kassar-Duchossoy et al., 2005; Relaix et al., 2005). Also, rhodamine labeled mononucleate cells from the dermomyotome were observed to give rise to muscle fibres in the myotome suggesting that addition of muscle fibres to the zebrafish myotome can occur from migration of dermomyotomal myogenic precursors into the myotome (Hollway et al., 2007; Stellabotte et al., 2007), similar to that shown in amniotes (Ben-Yair and Kalcheim, 2005; Gros et al., 2005; Kassar-Duchossoy et al., 2005; Relaix et al., 2005). To summarize, commonalities between the amniote dermomyotome and external cell layer in Xenopus and zebrafish have led to the proposal

in literature of the external cell layer as being the structural equivalent of the amniote dermomyotome. However, movement of myogenic precursors from the dermomyotome into the myotome and their fate have not been characterized in zebrafish and has been addressed in this thesis.

1.10 Role of Pax3 and Pax7 in early myogenesis and adult satellite cells of amniotes

In vertebrates, Pax3 and Pax7 are expressed in embryonic skeletal muscle progenitors and adult satellite cells. In the mouse embryo at E8.5, *Pax3* transcripts are found in the dorsolateral mesoderm prior to dermomyotome formation (Goulding et al., 1991). By E10, *Pax3* is found in the dermomyotome of the segmented mesoderm and around E11, *Pax3* expression in the dermomyotome starts to disappear with the disintegration of the central dermomyotome and appear in the myotome (Goulding et al., 1991; Relaix et al., 2005). Also, from E9.5 onwards *Pax3* expression can be observed in the muscle progenitor cells migrating from the ventrolateral dermomyotome to the limb buds (Goulding et al., 1991; Bober et al., 1994; Relaix et al., 2004). In chick, *Pax3* expression has been observed in stage 17HH embryos in regions of the somite that are part of the future dermomyotome (Marcelle et al., 1995; Williams and Ordahl, 1994). Later, *Pax3* expression is mostly in the lateral dermomyotome and excluded from regions of *MyoD* expression. As the primary myotome forms, *Pax3* expression is restricted to the dermomyotome distinct from *Myf5* expressing cells in the myotome. Further, around stage 18HH, *Pax3* expression is seen in muscle precursors migrating from lateral edge of the dermomyotome to limb buds. *Pax3* expression in the dermomyotome translocates to the myotome with disintegration of the dermomyotome around stages 18-21HH (Marcelle et al., 1995; Williams and Ordahl., 1994). *Pax7* expression is observed in more mature somites (from E9 onwards) than *Pax3*. *Pax7* expression is concentrated in the central and dorsomedial dermomyotome unlike *Pax3* which is expressed throughout the dermomyotome with strong expression at the epaxial and hypaxial extremes (Relaix et al., 2004; Jostes et al., 1990; Tajbakhsh et al., 1997). *Pax7* expression is observed in proximal and distal limb muscles at E11.5 and E12.5 respectively (Relaix et al., 2004). The number of *Pax7* expressing cells in myotome increases with the translocation of *Pax7* expressing cells from the disintegrating central dermomyotome into the myotome (Gros

et al., 2005; Relaix et al., 2005). As previously described in Section 1.8, satellite cells involved in postnatal growth and repair of trunk and limb muscle derive from the *Pax3* and *Pax7* expressing cells in the dermomyotome (Ben-Yair and Kalcheim, 2005; Gros et al., 2005; Kassar-Duchossoy et al., 2005; Relaix et al., 2005; Schienda et al., 2006). *Pax3* and *Pax7* expression is detected in satellite cells of mice, although *Pax3* expression in satellite cells varies in frequency between muscles (Conboy and Rando, 2002; Relaix et al., 2006; Seale et al., 2000).

Studies in knockout mice have revealed the importance of *Pax3* in generating embryonic trunk and limb muscle. *Pax3* is essential for segmentation of somite (Schubert et al., 2001) and formation of the dermomyotome especially the hypaxial (Relaix et al., 2004; Schubert et al., 2001). All limb muscles are lost in *Pax3*$^{-/-}$ mice (Relaix et al., 2004). Migratory muscle precursors involved in forming distant muscle masses such as those involved in forming limb muscles and some head muscles are adversely affected in the absence of *Pax3* (Borycki et al., 1999; Epstein et al., 1991; Kardon et al., 2002; Tajbakhsh and Buckingham 2000). *Pax3* modulates c-Met expression within migratory muscle precursors of the hypaxial dermomyotome and could thereby influence their delamination and migration (Epstein et al., 1996; Relaix et al., 2004; Yang et al., 1996). During early muscle development, *Pax3* acts as a transcriptional activator (Relaix et al., 2003) and is responsible for *Myf5* activation in the hypaxial dermomyotome (Bajard et al., 2006) as well as *MyoD* (Brunelli et al., 2007). Thus, *Pax3* has varied functions in early myogenesis including migration.

The migration of myogenic precursors from the dermomyotome to limbs was less efficient by *Pax7* expressing cells (Relaix et al., 2004), indicating that *Pax7* cannot fully compensate for *Pax3* functions in limb myogenesis. *Pax7* is required for the specification and survival of postnatal myogenic precursors in the embryo. *Pax7* appears to be required for the maintenance of satellite cells, as there is a reduction in the number of satellite cells (Oustanina et al., 2004; Relaix et al., 2006; Seale et al., 2000) as well as reduced number of regenerating myofibres (Kuang et al., 2006) in *Pax7* null mice. Interestingly, some *Pax3* positive cells which also positive for the MRF *MyoD* were found during regeneration in the adult *Pax7* $^{-/-}$ mice; suggesting their involvement in regenerating muscle (Kuang et al., 2006). However, lack of *Pax7* transcription factor beyond a certain

developmental stage did not affect satellite cell viability or function indicating that *Pax7* requirement in skeletal muscle progenitors is temporal (Lepper et al., 2009). To summarize, *Pax3* has functions in early skeletal muscle development that are not compensated by *Pax7*. Further in *Pax3*$^{-/-}$*Pax7*$^{-/-}$ mice muscle does not form beyond the primary myotome, which taken together with studies in mice mutant for either transcription factor alone, show the importance of *Pax3* and *Pax7* in maintenance and specification of myogenic precursors in myogenesis from early myogenesis to adult muscle progenitors (Relaix et al., 2004; Relaix et al., 2005).

Zebrafish have two *pax3* (*pax3a* and *3b*) and *pax7* (*pax7a* and *7b*) genes (Groves et al., 2005; Hammond et al., 2007; Minchin and Hughes, 2008; Minchin et al., 2013; Seo et al., 1998) and in muscle the transcripts appear to be restricted to the dermomyotome in 1 day old embryos. In *Xenopus* two Pax3 genes are predicted (3a: Gene ID: 496376; 3b: Gene ID: 496377), although not described in literature, whereas only one Pax7 gene is predicted and described (Chen et al., 2006; Grimaldi et al., 2004).

1.11 Progenitors with myogenic potential are located in the zebrafish dermomyotome

Zebrafish muscle development is similar to amniotes in that it arises in somitic structures and muscle precursors express *Myf5* and *Myod* but differs in other aspects from that in chick and mouse. During embryonic myogenesis in zebrafish the first somite arises from paraxial mesoderm at 10.5 hours post fertilization (hpf) and thereafter a somite forms every 30 minutes (Kimmel et al., 1995; Ochi and Westerfield, 2007; Stickney et al., 2000). The onset of myogenesis in zebrafish begins with expression of members of the Myod family of MRFs, committing cells of the presomitic mesoderm to myogenesis as in amniotes reviewed in (Buckingham, 2001). Specifically, *myod* (by 7.5 hpf, (Weinberg et al., 1996)) and *myf5* (8 hpf, (Coutelle et al., 2001)) are expressed in triangular patches of cells on either side of the embryonic shield. These cells elongate to form the adaxial cells on either side of the notochord and express both *myf5* and *myod* until their terminal differentiation into mononucleate superficial slow fibres (Kimmel et al., 1995). The twenty superficial slow muscle fibers get located at the outer edge of each somite surrounding the underlying deep layer of fast muscle fibers through radially outward

migration of the adaxial cells away from the notochord (Devoto et al., 1996; Fig. 1.3). About 2-3 adaxial cells per somite fail to fully migrate. They remain medially located between the superficial surface and notochord (Devoto et al., 1996). These specialized types of slow muscle fibers termed muscle pioneers (Felsenfeld et al., 1991) are present medially at the level of the future horizontal myoseptum and express Engrailed (Hatta et al., 1991). The development of superficial slow fibers and muscle pioneers from adaxial cells is dependent on hedgehog signaling (Barresi et al., 2000; Blagden et al., 1997; Currie and Ingham, 1996; Du et al., 1997). Cells lateral to the slow cells within the somite also express *myf5* and *myod* (Coutelle et al., 2001; Weinberg et al., 1996) and give rise to two kinds of multinucleate fast fibres: the Fgf8-dependent lateral fast fibres and the Fgf8-independent medial fast fibres (Groves et al., 2005), a subset of which become the fast Engrailed-expressing cells as a result of later Hh signalling (Wolff et al., 2003). Fin muscle precursors arise from somites two-four in the hypaxial domain and migratory fin precursors express *pax3* and *lbx1* similar to amniotes (Neyt et al., 2000). To summarize, primary myogenesis of zebrafish trunk muscle involves differentiation of muscle precursors located within the somite. Whether they have a dermomyotomal origin is unknown.

Future growth of the muscle has been proposed to be supported by progenitor cells translocating from the dermomyotome and giving rise to the secondary slow fibers at the dorsal and ventral extremes of each somite (Barresi et al., 2001) as well as medial and lateral fast fibers (Hollway et al., 2007; Stellabotte et al., 2007). The secondary slow fibers are hedgehog independent unlike the slow muscle formed during the first wave of myogenesis (Barresi et al., 2001), indicating that muscle precursors involved in myotome expansion of larval stages might be regulated differently compared to muscle precursors involved in embryonic muscle development. These precursors arise from the anterior border of somites (Hollway et al., 2007; Stellabotte et al., 2007). The anterior border cells are an epithelial layer of cuboidal cells present in the anterior part of every somite and express the zebrafish orthologues of the transcription factors *pax3* (*pax3a*) and *pax7* (*pax7a*, (Hollway et al., 2007)). Around 15 hours post fertilization (hpf), the anterior border cells begin to move laterally to come to lie in the external cell layer or dermomyotome of 24 hpf zebrafish (Hollway et al., 2007; Stellabotte et al., 2007).

Lineage tracing of cells within the anterior border domain of somites (Hollway et al., 2007; Stellabotte et al., 2007) has shown that they give rise to cells with dermal or myogenic fate similar to chick (Ben-Yair and Kalcheim, 2005). Further, $Pax7^{+}$ cells in zebrafish have been suggested to occupy satellite cell-like positions under the basal lamina from 3 dpf onwards (Hollway et al., 2007) similar to $Pax7^{+}$ cells arising in the dermomyotome in amniotes (Relaix et al., 2005).

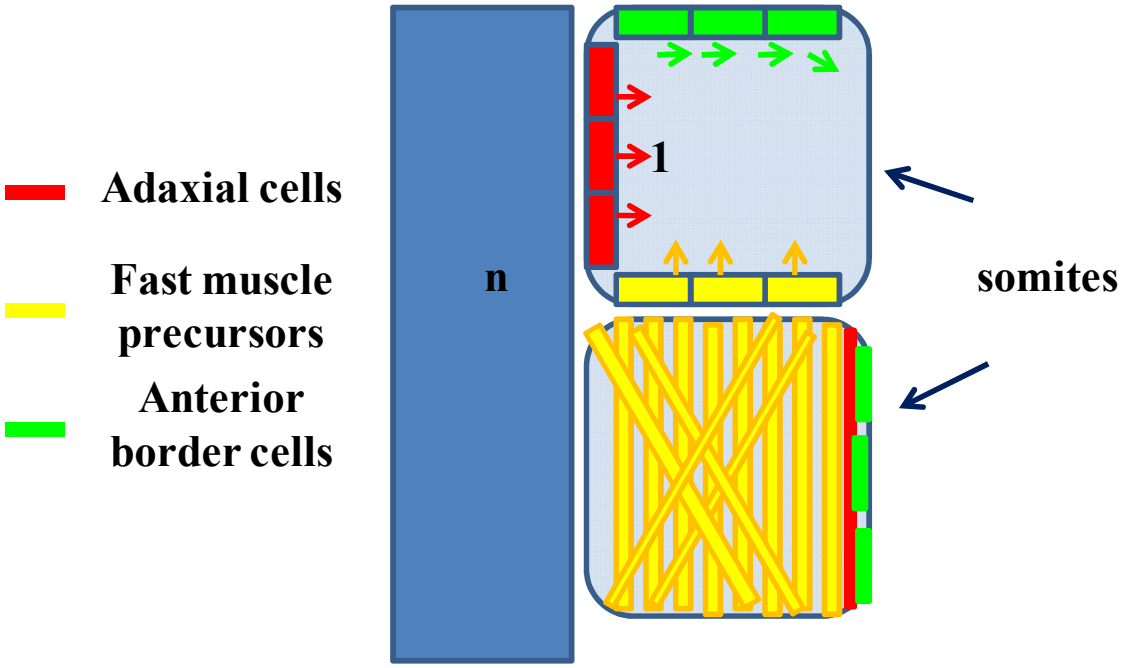


Fig. 1.3 Myogenesis in zebrafish embryos
Adaxial cells (red) migrate first and away from the notochord (n) to form the outer monolayer of layer of slow muscle (red) followed by fast muscle precursors (yellow) differentiation and anterior border cell (green) migration from the anterior of the somite to the lateral surface to come to lie superficial to slow muscle in the dermomyotome.

1.12 Role of MRFs Myf5 and MyoD in skeletal muscle growth and repair in amniotes

Two important components of myogenesis are the sequential action of myogenic regulatory factors (MRFs) on Pax3/7-expressing myogenic cells during muscle development (Garry and Olson, 2006; Sambasivan and Tajbakhsh, 2007). The muscle regulatory factors or MRFs include *Myf5*, *MyoD*, *Mrf4* and *myogenin* (Weintraub, 1993) and belong to the basic helix loop helix (BHLH) family of transcription factors. They act sequentially and sometimes redundantly to specify precursors towards a myogenic

lineage and differentiation into muscle fibers. Studies in the mouse embryo of null mutations of MRF genes have shown that these genes generally function hierarchically during myogenesis. Several lines of evidence indicate a role for *Myf5*/*MyoD* in specification and suggest that they work redundantly. *Myf5*-/- mice in general show a fairly normal musculature (Braun et al., 1992) although the intercostal and paraspinal muscle arising from the dorsomedial lip were delayed (Kablar et al., 1997). Moreover, *Myf5* expressing dorsomedial lip precursor cells did not migrate ventrally until later coincident with *MyoD* expression (Tajbakhsh et al., 1996). Further, some migrated aberrantly indicating a role for *Myf5* in specification and migration and suggesting compensation by *MyoD*. *Myf5* might act upstream of *MyoD* since *MyoD* activation in dorsomedial and ventrolateral progenitors and myotome differentiation is delayed in *Myf5*-/- mice (Tajbakhsh et al., 1997). *MyoD*-/-mice also have fairly normal musculature but show a delay in limb and abdominal wall muscles arising from the ventrolateral lip of dermomyotome (Kablar et al., 1997). *MyoD*-/-mice showed a 3.5 fold increase in Myf5 expression suggesting that *Myf5* might compensate for *MyoD*. Further evidence for a role of *Myf5* and *MyoD* in specification and that they might work redundantly comes from *Myf5*-/- *MyoD* -/- mice. Mice lacking both functional Myf5 and *MyoD* lacked myoblasts and muscle (Rudnicki et al., 1993). Moreover limb muscle progenitors in *Myf5*-/-*MyoD*-/- embryos become integrated into chondrogenic fates providing evidence of their role in specification. Further, tissue culture and regeneration studies indicated a role of *Myf5* and *MyoD* in influencing muscle precursor cell number, proliferation and differentiation (Cornelison et al., 2000; Megeney et al., 1996; Sabourin et al., 1999; White et al., 2000; Yablonka-Reuveni et al., 1999) (Montarras et al., 2000). Furthermore, mouse triple mutants in Myf5, MyoD and Mrf4 fail to make myoblasts and muscle (Kassar-Duchossoy et al., 2004; Rudnicki et al., 1993) whereas the presence of either Myf5/MyoD myoblasts are made, indicating a role for all three in myoblast formation or maintenance.

1.13 Role of Pax 3/7 and MRFs in skeletal muscle growth and regeneration in zebrafish

The role of myoblasts expressing Pax3/7 in growth and regeneration and the role of myoblasts expressing MRFs in regeneration has not been studied in zebrafish and some of these roles have been examined in this thesis. Specifically, the role of Pax7 and

Myogenin-marked cells in growth and regeneration of post-hatched zebrafish larvae has been addressed. The expression pattern of Pax3/7 in the early embryo has been described previously and relevant details are mentioned in chapter 3 introduction section.

In zebrafish similar to amniotes, *myf5/myod* expression generally precede that of *myogenin* (Weinberg et al., 1996). *Myogenin* expression was generally coincident with the expression of skeletal proteins such as tropomyosin and terminal differentiation, indicating a role for *myogenin* in muscle differentiation in zebrafish. Morpholino mediated knockdown of myogenin showed that slow muscle myogenesis was not adversely affected in morphants and only a small subset of fast muscle differentiation was affected (Hinits et al., 2009; Hinits et al., 2011). It could be speculated that this reflects the situation in the mouse mutant where primary myogenesis is not dramatically affected (Venuti et al., 1995). Currently, a null myogenin mutant is not available and the phenotype awaits description (Hinits et al., 2011).

Somitic myogenesis appears to be distinctly regulated in the medial versus lateral compartments of the somite such that either *myf5* or *myod* can drive medial myogenesis whereas lateral myogenesis appears to be *myod*-driven (Hinits et al., 2009). Similar to mouse MyoD-/-, knockdown of *myod* transcripts or in the zebrafish *myod*^{fh261} mutants, absence of Myod protein did not lead to absence of Myogenin although, in contrast to mouse, Myogenin levels were reduced in knockdown or mutant fish (Hinits et al., 2009; Hinits et al., 2011). Similarly muscle formation was reduced but not abrogated indicating that differentiation can occur in the absence of *myod*. Importantly, *myod*-driven *myogenin* expression was found to be required for lateral fast fibres specifically formed from the rostral posterior border cells of the somite (Hinits et al., 2009). To summarize *myf5* and or *myod* are sufficient to drive slow and fast myogenesis from the medial portion of somite whereas *myod* is required for driving a specific population of fast muscle precursors from the posterior border cells in the developing zebrafish. However, *myogenin* transcript accumulation was observed just prior to both medial and lateral fast myogenesis and knockdown of both *myod* and *myogenin* expression in *myf5*^{hu2022} mutants abrogated all muscle indicating that *myogenin* accumulation is required for fast fibre differentiation.

1.14 Role of Myogenin in myoblast fusion and differentiation in amniotes and zebrafish

Myogenin is proposed to play a later role in myogenesis since myogenin expression is generally detected after MyoD/Myf5 expression both in vitro and in vivo (Sassoon et al., 1989; Wright et al., 1989). Myogenin peaks in cell culture following induction of differentiation conditions and myogenin$^{-/-}$ mice have a fairly normal number of myoblasts in the correct positions but these fail to differentiate in vivo, indicating a role for myogenin in differentiation (Hasty et al., 1993; Nabeshima et al., 1993; Venuti et al., 1995). Myogenin was also shown to influence the expression of some proteins of the muscle contractile machinery suggesting that myogenin plays a role in fiber formation (Hasty et al., 1992; Myer et al., 1997). Further, myogenin expression was found to precede withdrawal of myoblasts from cell cycle which in turn preceded myosin expression and myotube formation (Andres and Walsh, 1996), suggesting that myogenin might be involved in cell cycle withdrawal and myoblast fusion. Some evidence for a role of myogenin in fusion comes from chimeric embryos of mice containing mixtures of myogenin-null and wild type cells. Whereas most of the myoblasts in myogenin$^{-/-}$ mice appear unfused in vivo (Hasty et al., 1993), in chimeric mice the myogenin-null myoblasts appear to fuse in vivo in the presence of wild type myoblasts (Myer et al., 1997) showing that myogenin plays an important role in fusion in vivo, although myogenin-null myoblasts differentiate and fuse in vitro (Nabeshima et al., 1993). However, other factors such as noggin and ski are likely involved in myoblast fusion since noggin-null embryos and a mutation in ski lead to poor myotube formation despite myogenin expression Colmenares et al., 1991; Tylzanowski et al., 2006).

1.15 Thesis proposal

Previous sections have discussed the ontogeny of satellite cells, importance of their role in stem cell therapeutics and the need to investigate the behavior of satellite cells in their niche in vivo. Zebrafish are a good model to study in vivo cell behavior. Due to their small size and transparency, they are amenable to non invasive imaging in the live animal. Importantly, Pax7 expressing cells in zebrafish arise in the dermomyotome similar to the Pax7 expressing cells which are precursors of satellite cells in amniotes. Indeed, the Pax7 expressing cells arising in zebrafish dermomyotome have been proposed to be myogenic

precursors with a role in muscle growth and repair but not demonstrated. Hence, prior to undertaking niche studies in zebrafish it is important to determine the role of (i) $Pax7^+$ cells and (ii) MRFs in muscle growth and repair.

To determine whether Pax7 expressing cells in zebrafish dermomyotome contributed to muscle growth, the spatiotemporal dynamics of $Pax7^+$ cells was quantitated in growing larvae in chapter 3 to explore the possible cell fates of $Pax7^+$ precursors in the myotome in a time frame during which their translocation from the dermomyotome into the myotome is occurring. The number of $Pax7^+$ cells was found to increase specifically at certain locations within the deep myotome whereas remaining similar elsewhere and especially in the dermomyotome/superficial myotome. Importantly, the regions associated with increase in $Pax7^+$ cells correlated with regions of fibre growth, strongly suggesting that Pax7 expressing precursors play a role in muscle formation, similar to other species.

To investigate the role of Myod and Myogenin in influencing the behavior of $Pax7^+$ cells, the spatiotemporal dynamics of Pax7 expressing precursors in *myod*^{fh261} mutants was investigated and revealed that *myod* influences the number and differentiation kinetics of $Pax7^+$ muscle precursors. Moreover, investigation of the spatiotemporal dynamics of Myogenin-expressing precursors in control, *myod*^{fh261} mutant and wild type fish revealed that the number of these precursors is elevated prior to differentiation, suggesting that as in post-natal and adult satellite cells of amniotes, Myogenin expression in muscle precursors of growing zebrafish precedes differentiation.

To determine the role of Pax7 expressing cells in muscle repair, zebrafish larvae were wounded and the spatiotemporal dynamics of Pax7 and Myogenin-expressing cells was investigated in wounded somites over the duration of muscle repair. The number of proliferating Pax7 expressing cells and differentiating Myogenin expressing cells peaked prior to muscle recovery supporting the role of Pax7 and Myogenin expressing cells in muscle repair in zebrafish. Investigation of the proliferation and differentiation dynamics revealed functional heterogeneity amongst the precursors as shown in other models (Collins et al., 2005; Ono et al., 2010). Moreover, the functional heterogeneity was found

to correlate with particular regions (niches) suggesting intrinsic and/or extrinsic differences in Pax7 expressing precursors at these locations.

In summary, investigations in this thesis of the spatiotemporal proliferation and differentiation dynamics of $Pax7^+$ cells during growth and repair, strongly support the role of $Pax7^+$ cells as promoters of muscle growth and repair in zebrafish. Among the MRFs, interestingly, Myod appears to influence certain aspects of $Pax7^+$ cell behavior whereas peak Myogenin expression precedes muscle growth and repair. Moreover, the study provides a map of the functionally heterogeneous myogenic precursors within the muscle and thereby helps to develop an in vivo model to study muscle precursor cell-niche dynamics.

Chapter 2: Materials and Methods

2.1 Fish maintenance

Wildtype and transgenic adult zebrafish were stocked in the fish facility at King's College London on a 14/10hr light to dark cycle at a 28.5°C. All fish lines were maintained on King's wild type background (*kwt*) and staging and husbandry were as described previously (Westerfield, 1995).

Table 2.1 Transgenic/mutant zebrafish lines used

Line	Usage	Reference
Tg(9.7kb smyhc1:eGFP)^{I104}	GFP expressed in slow muscle cells. This line was primarily used to image slow muscle before pre and post wounding.	(Elworthy et al., 2008)
Tg(-2.2mylz2:GFP)^{gz8}	GFP expressed in fast muscle cells. This line was primarily used to image fast muscle pre and post wounding.	(Gong et al., 2003)
Tg(lysC:EGFP)^{nz117}	GFP expressed in immune cells. This line was primarily used to image immune cell dynamics pre and post wounding.	(Hall and McDonnell, 2007)
Tg(mpo:GFP)^{i114}	GFP expressed in immune cells. This line was primarily used to image immune cell dynamics pre and post wounding.	(Renshaw et al., 2006)
mitfa$^{w2/w2}$;roy$^{a9/a9}$	Mutations in both mitfa and roy genes leading to a lack of melanocytes (mitfa) and iridophores (roy) in these fish.	(White et al., 2008)

	Thus the fish are completely transparent and were used in imaging experiments without the need for ptu treatment to suppress pigmentation	
myod^{fh261}	Mutant in myod with a stop codon at residue 126 generating a predicted null mutation. Carrier fish and mutant larvae were identified as described in section 2.1.1	(Hinits et al., 2011)
Tg(*pax7*:EGFP) ^{MPIEB}	GFP expressed in cells expressing the transcription factor Pax7. These fish were primarily used for live imaging of Pax7^{+} cells pre and post wounding.	(Alsheimer, S., unpublished)

2.1.1 Identification of adult myod^{fh261} carriers

Adult **myod**^{fh261} carrier fish were identified by genotyping tail clips. 1 month old fish were anaesthetized in fish water containing 1:15 dilution of tricaine. The fish were moved to a clean petri dish and a small piece from the end of the tail fin was cut with a scissor. Using forceps, the bit of tail fin was transferred to an eppendorf containing 100 µl of lysis buffer (DirectPCR Lysis Reagent Ear Peqlab Company, 31-401-E) and 1 µl proteinase K. The eppendorf containing the tissue and lysis buffer was kept overnight in a 55ºC waterbath. Next day, the eppendorf was kept at 85ºC for 45 minutes and spun down for 10 seconds at 13,000 rpm to pull down impurities. 2 µl of the supernatant was used for setting up the following 20µl PCR reaction:

Supernatant	2.0µl
GoTaq buffer x5	4.0µl

myod-exon1-fwd 10µM 0.8µl [**5' - GGA CCC CAG GCT TGT TC - 3']**

myod-exon1-rev 10µM 0.8µl [**5' - GTT GGA TCT CGG ACT GGA - 3']**

dNTP mix (10mM each) 0.5µl

GoTaq polymerase 0.2µl

ddH2O 12.7µl

The following program was used:

95°C 2mins

95°C 30sec

56°C 30sec (35 rounds)

72°C 30sec

72°C 5mins

4°C ∞

5µl of the PCR reaction was run on a 2% agarose gel to observe a PCR product of 397bp.

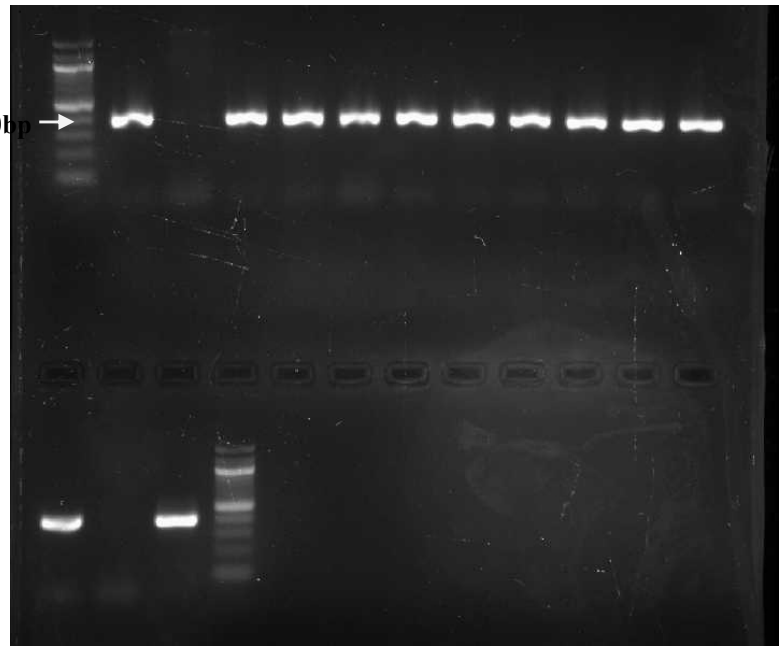


Fig. 2.1 Results of genotyping PCR from DNA extracted from fish fin clips (lanes 2-12), and from negative control (lane 13) and positive control (lane 14). 100bp ladder was run in lanes 1 and 15. A product of 397 bp is expected from the PCR reaction.

The remaining PCR reaction was cleaned using a PCR purification kit (Qiagen catalogue 28104) and sent for sequencing with myod-ex1-FWD primer. Below (Fig. 2.2) is the difference in peaks between the wildtype (+/+) genotype compared to the heterozygous carrier (+/-) due to an A -> T conversion in the heterozygous genome.

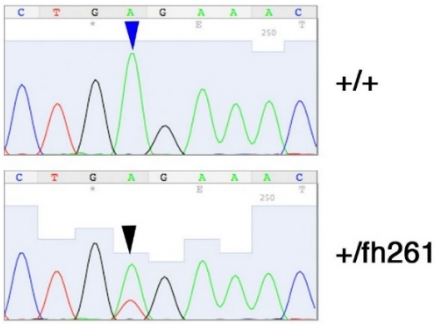


Fig. 2.2 Chromatograms from genotyping sequencing showing the difference in peaks (blue arrowhead in wt/homozygous genome vs. black arrowhead in heterozygote) due to an A-> T conversion within the sequence CTGAGAAAC at the GAG location.

2.1.2 Identification of myod^{fh261} mutant larvae

Live myod mutant larvae were identified from **4 dpf** onwards by the jaw phenotype (Fig. 2.3A) that originates from the lack of almost all head muscle except the sternohyoides and a few residual ones (Hinits et al., 2011). **Fixed** myod mutant larvae were identified from **3 dpf** onwards by staining for myosin using the A4.1025 antibody. Myod mutants show no stain for myosin in some head muscles compared to siblings (Fig. 2.3B).

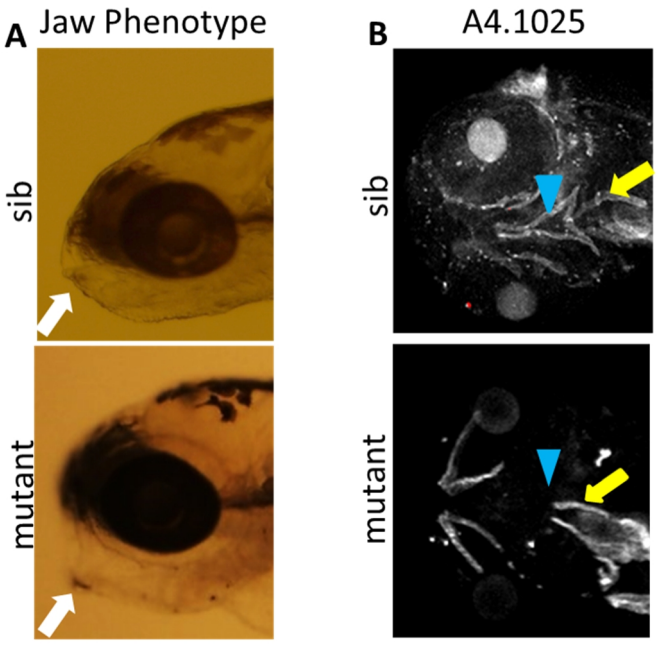


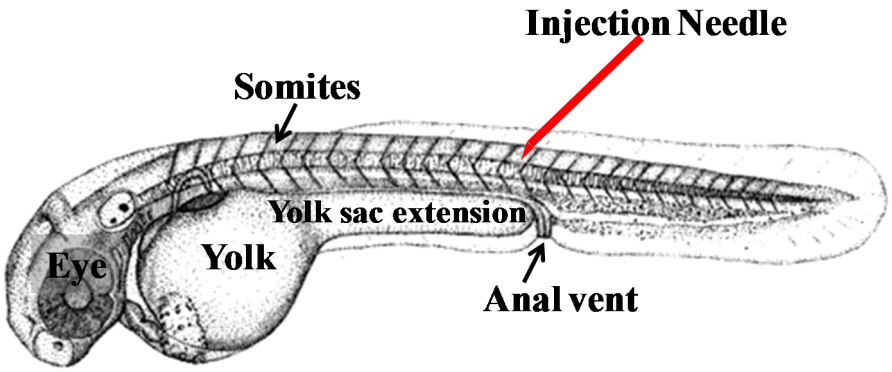
Fig. 2.3 Identifying live and fixed myod^{fh261} mutant larvae **A:** Bright field images of a live 4 dpf sibling and myod^{fh261} mutant (retrospectively sequence genotyped) showing difference in jaw phenotype (white arrows). **B:** Wholemount larvae at 3 dpf were fixed and stained for myosin using A4.1025 antibody. Confocal images are single slices in the head region of a sibling and myod^{fh261} mutant (retrospectively sequence genotyped. Some myosin positive head muscle is absent in the mutant (blue arrows) although some others are present (yellow arrows).

2.2 Zebrafish embryo manipulations

2.2.1 PTU treatment

Pigmentation was inhibited in embryos by keeping the embryos in system water (from the fish facility) containing 1-phenyl-2-Thiourea (PTU) from 12 hpf onwards until the end of experiment. 120 mg PTU was dissolved in 1 ml DMSO and this was diluted in 400 ml system water. 5ml of this was used for every 25 ml of system water giving a final concentration of 60 mg per ml.

2.2.2 Wounding



Dechorionated 2.5-3.5 dpf fish were anaesthetized with 0.02% Tricaine methanesulfonate or MS222 (3-amino benzoic acidethylester) prepared according to published methods (Westerfield, 2000) and mounted in 1% low melting agarose (LMA) in system water containing 0.008% MS222. Embryos were oriented laterally with their head to the left, tail to the right and dorsal up before the agarose solidified in five cm petri dishes. The solidified agarose was covered with system water containing 0.008% MS222. Two to four epaxial dorsal somites above the anal vent (in somite numbers as indicated in Results section/figure legends) were injured in anaesthetized fish mounted in 1% agarose with an injection needle using the microinjector Picospritzer II (Parker Hannifin). The needle was inserted five times into each epaxial somite at various angles to achieve maximum destruction of muscle tissue in the injured epaxial somite. The location and extent of wound was recorded in each fish after injury. Post wounding, embryos were released from the agarose individually and maintained in separate containers with system water for live imaging or fixing between 0 hour post wounding (hpw) up to 10 days post wounding (dpw). Unwounded fish from the same lay were also mounted and subsequently released from agarose without injury. They were imaged or fixed

concurrently with wounded embryos i.e. between 2.5 dpf up to 13.5 dpf. Larvae older than 5 dpf were given baby food (SDS-100, catalogue number: 824856) once per day.

2.2.3 Live imaging of embryos/larvae

Post wounding embryos were maintained in fresh system water containing 0.5% Penicillin-Streptomycin. They were anaesthetized with MS222 and mounted in 1% low melting agarose for fluorescence or confocal microscopy at the times indicated in Results section. For **fluorescence imaging** of live transgenic embryos/larvae, images were obtained using Olympus DP370 digital camera attached to Leica MZ-16F with GFP filter set and supporting software (DP Controller). For **DIC** (Differential Interference Contrast) imaging embryos were mounted in PBS on a depression slide and cover slipped and imaged with the Zeiss Axiophot with Axiocam using Nomarski optics and Openlab software.

Live imaging of anaesthetized transgenic embryos expressing GFP in muscle cells or muscle progenitors was done with 20x dipping objective whereas fixed wholemount embryo processed for immunohistochemistry were imaged using the 10x air or 40x water immersion objectives (Table 2.2) on a **confocal** Zeiss Exciter laser scanning microscope (LSM) fitted with a motorized stage. Embryos were viewed laterally, generally with their head to the left, tail to the right and dorsal at the top of the image. Live embryos/larvae were mounted in 1% low melting agarose containing anaesthetic MS222 and covered with system water also containing MS222, after the agarose solidified. Fixed fish were mounted on slides in Citifluor. Three to nine somites around the anal vent were imaged from lateral using the tile scan function. Often both sides of the fish were scanned. On other occasions, only down to the neural tube was scanned. Initial image processing was done using the Zen confocal software (2009+2012) or Zen lite (2009+2012) to select and export short stacks or tiff images of specific slices, cross sectional views and maximum intensity projections from wholemount confocal stacks.

Table 2.2. List of objectives utilized

Zeiss Objective	Usage
10x/0.3 DIC Plan-Neofluar	Orientation and overview images of fixed or live embryos/larvae
20x/1.0 W Plan-Apochromat DIC (UV) Vis-IR	Wholemount stack of live fish and XZ scans in live/fixed fish
40x/1.1 LD C-Apochromat	Wholemount scans of fixed fish

Tiff images were cropped and enhanced in brightness/contrast using Microsoft Office Picture Manager. Images were assembled using Microsoft PowerPoint 2007. Illustrations were made with Adobe Illustrator CS4 or Microsoft PowerPoint 2007. The Tiff images and edited images are stored in the same folder as the original images. Images are stored on Whitewhale server and an external hard drive.

2.2.4 Embryo fixation

Embryos older than 18 somite stage (ss) were manually dechorionated with a pair of watchmakers 5a forceps prior to short or long fixation. Short fix: Embryos were fixed in 2% paraformaldehyde (PFA) in PBS for 25 minutes at room temperature (RT). Long fix: Embryos were fixed in 4% PFA in PBS for 2 hours at RT or overnight at 4˚C.

2.2.5 Wholemount embryo and larval immunohistochemistry

Embryos for immunohistochemistry were subjected to a short/long fix depending on the age of the embryo and the primary antibody to be used subsequently. In general, embryos younger than 3 dpf could be fixed with 4% PFA or 2% PFA without loss in signal. However, in embryos 3 dpf and older immunolabeling appeared to be compromised on fixing with 4% PFA with many of the primary antibodies used. Embryos were washed three times in PBTx (Triton-100 in PBS, 0.25% Triton-100 for embryos 1 – 2.5 dpf; 0.5% Triton-100 for embryos 2.5-3.5 dpf; 1% Triton-100 for embryos older than 4dpf) and then incubated on a rotary shaker with primary antibody for 3-5 overnights at 4°C. Following incubation with primary antibody (Table 2.3), embryos were washed every 10 minutes for two hours in PBTx (0.25% Triton-100 for embryos 1 – 2.5 dpf; 0.5% Triton-100 for embryos younger than 3 - 4 dpf; 1% Triton-100 for embryos older than 4dpf). Embryos were then incubated with subclass specific secondary antibody overnight on a rotary

shaker at 4°C. Embryos were then washed every 10 minutes for two hours in PBTx (0.25% Triton-100 for embryos 1 – 2.5 dpf; 0.5% Triton-100 for embryos younger than 3 - 4 dpf; 1% Triton-100 for embryos older than 4dpf). Primary antibodies used are listed in Table. 2.3. Alexa-conjugated (488/564/688, Molecular Probes) secondary antibodies were used followed by Hoechst 33342 staining for two hours with a 1:2000 dilution of a 2 mM stock at room temperature. Embryos were washed several times and mounted under a cover slip on a glass slide with Citifluor AF1 (Citifluor Ltd.).

Table 2.3. Primary antibodies

Primary antibody	Specificity	Fixation (PFA)	Isoform	Dilution	Reference/Company
A4.1025	Anti-sarcomeric MyHC	4%	IgG2a	1:10	(Dan-Goor et al., 1990)
Anti-Pax7	Pax7	2%	IgG1	1:5	(Kawakami et al., 1997)
Anti-GFP	GFP	2% or 4%	IgY	1:500	Abcam ab13790
Anti-GFP	GFP	2% or 4%	Rabbit IgG	1:500	Sigma G1546
β-catenin	Membranes	2%	Rabbit IgG	1:500	Sigma 2206
DP312	Pax3/7	2% or 4%	IgG1	1:5	(Davis et al., 2005)
F59	Slow muscle	2% or 4%	IgG1	1:5	(Crow and Stockdale, 1986)
Myogenin	Myogenin	2%	Rabbit IgG	1:50	Santa Cruz (sc-576)

2.2.6 BrdU treatment and detection in 4 dpf wholemount zebrafish

Protocol was modified from (Barresi et al., 2001). Briefly, embryos were incubated in 10 mM BrdU in sterile system water and 15% DMSO at 6-8ºC for 20 minutes. Embryos were left in system water for an hour in 28.5°C incubator and fixed with 4% PFA for 2

hours. The embryos were washed twice with MeOH and left in fresh MeOH at -20ºC overnight. Embryos were rehydrated by washing once with 50% MeOH 50% 0.1%Tween-20) for 10 minutes and two washes with 100% PBSTx (0.5-1% - depending on embryo age) for 5 minutes each. Proteinase K treatment was done with 10 µg/ml for 60 minutes. The embryos were rinsed with PBSTw (0.1% Tween-20) thrice for 5 minutes each followed by refixing in 4% PFA for 20 minutes then rinsed with PBSTw (0.1% Tween-20) twice followed by a PBS rinse. Next, the embryos were rinsed with PBSTx-DMSO-1% thrice followed by treatment with 2N HCL for 1 hour at room temperature. Prior to incubation with primary antibody, the embryos were rinsed with (0.5-1%Tx) PBSTx-DMSO-1% thrice and blocked with 5% Goat serum in (0.5-1% Tx) PBSTx-DMSO-1% for up to 30 minutes. The embryos were incubated overnight with primaries (1:500 BrdU, 1:5 A4.1025) in 2%Goat serum-(0.5-1%Tx)PBSTx-DMSO-1% on rotary shaker at 4°C and rinsed with (0.5-1%Tx) PBSTx-DMSO-1%. Secondary incubation (1:1000 goat anti mouse IgG1; 1:1000 goat anti mouse IgG2a) was done in 2%Goat serum-(0.5-1%Tx)PBSTx-DMSO-1% - overnight on rotary shaker at 4°C. Following incubation with secondaries, the embryos were rinsed with (0.5-1%Tx) PBSTx-DMSO-1% and mounted in Citifluor.

2.2.7 EdU treatment and detection in wholemount zebrafish

Labeling and quantification of cells in the S-phase of the cell cycle was done using 5-ethynyl-2′-deoxyuridine (EdU) which is a nucleoside analog of thymidine that is incorporated into DNA during active DNA synthesis. The Invitrogen kit no. C10084 was used. 10 mg EdU was dissolved in 1 ml PBS (1%). 1:10 final concentration of EdU to system water was added and used to treat fish for 3 hours. Treated fish were fixed immediately with 2% PFA for 25 minutes. Staining was done according to manufacturer's instruction using the Click-iT EdU kit (Invitrogen). Staining of EdU treated larvae was done after antibody labeling and prior to EdU detection.

2.3 Wound area calculations

Image J software was used to calculate areas of the wound (black regions devoid of green fluorescence) selected by using the draw tool so as to as accurately as possible capture the black regions and exclude any green fluorescence in the field. In this manner it was possible to draw around or in between occasional cells in the wound site soon after

wounding as well as in between the increasing number of apparent regenerated fibers later. The epaxial somites containing the wound. %wound area was calculated for individual wounded somites in each embryo. % Average wound area was calculated for each wounded embryo by averaging the wound areas in individual somites over the number of wounded somites per embryo.

Any green fluorescence in the image resembling a cell or fibre regardless of density or intensity was regarded as muscle and excluded as wound region. Intensity of fluorescence was unhelpful in wound area calculations since, during development and regeneration the brightest fibres/cells are likely the new upcoming generation whereas older fibres and differentiating or quiescent cells generally appeared dimmer in the fish lines used in this thesis. Additionally, the threshold of fluorescent intensity varied during prolonged and repeated observations/scanning in the same transgenic fish as they continued to grow their muscle as well as repair wounded regions and undergo some level of bleaching.

2.4 Counting of nuclei labeled with EdU/Pax7/Myogenin antibodies

Nuclei were identified based on Hoechst 33342 staining. The number of nuclei was counted by stepping in z direction for a given co-ordinate of x. The number of nuclei in Myod siblings and mutants in chapter 3 was counted in one or three equi-spaced transverse images from somite 17 of each embryo at the ages mentioned and averaged for the number of embryos indicated in text. The somite length at the horizontal myoseptum and height were obtained from a single lateral image.

2.5 Statistics

Statistics was performed using Excel 2003 in the number of somites/embryos indicated in the Results section/figure legends. F-test was used determine whether the means being compared varied equally or unequally. Based on the outcome, Student's t-test for equal variance or unequal variance was used to determine the p-value. Error bars are standard error of the mean.

Chapter 3: Characterization of muscle progenitor cells during growth

3.1 Summary

Myod is a key muscle regulatory factor expressed by muscle precursors and has been proposed to play a role in establishing or maintaining myoblasts (Weintraub, 1993). In zebrafish, Myod is important for fast fibre differentiation (Hinits et al., 2011). Mutants lacking a functional Myod protein have reduced muscle mass (Hinits et al., 2011). However, the somitic muscle defect appears to be transient. The somitic trunk muscle is reduced at 1 and 3 dpf whereas by 5 dpf the muscle mass recovers. An excess number of $Pax7^+$ precursor cells are present superficial to the myotome in 1 dpf *myod*^{fh261} mutants (Hammond et al., 2007), suggesting de-regulation of precursor cell number. To understand the changes in muscle precursor behaviour and the mode of muscle mass recovery in the absence of Myod, initially the spatiotemporal distribution of $Pax7^+$ precursor cells was quantitated in growing wildtype fish between 3 and 6 dpf. In wildtype zebrafish between 3 and 6 dpf, the distribution of $Pax7^+$ cells was primarily at five regions encompassing the four borders: the anterior and posterior border (vertical septae), dorsal edge, horizontal myoseptum and the central body. Muscle fibres extend within the central body with their fibre ends at the anterior and posterior borders. Between 3 and 6 dpf, the total number of $Pax7^+$ cells increased significantly due to increases in the deep myotome at both the vertical borders and central body locations, suggesting migration of these cells from superficial to deep myotome. A combination of quantitation in fixed wholemounts at 4 dpf and time lapse imaging of *Tg(pax7:EGFP)*^{MPIEB} larvae at 3, 3.5 and 4 dpf suggested that the increment in the number of $Pax7^+$ cells in the deep central body occurs around 4 dpf. Whereas, the number of $Pax7^+$ muscle precursors significantly increased in the deep myotome, the number of superficial $Pax7^+$ cells between 3 and 6 dpf did not decrease significantly, suggesting a role for proliferation in maintaining cell numbers superficially. The small fraction of $Pax7^+$ cells in S-phase at the dorsal edge and horizontal myoseptum correlated with the lack of significant increase in the number of $Pax7^+$ cells observed at these locations. In contrast, a larger fraction of $Pax7^+$ cells in S-phase located at the vertical borders and central body correlated with the significant $Pax7^+$

cell number increase at these locations. If the Pax7^{+} cells at the five regions were synchronous, a hypothetical maximum and minimum number of additional Pax7^{+} cells could be postulated based on the number of cells in S-phase. The number of new Pax7^{+} cells at each location based on the postulation was generally more than the actual observed increases. While this might reflect the absolute number of Pax7^{+} cells arising from an asynchronous population, another possibility could be that Pax7^{+} cells are lost by differentiation. Myogenin expression was used to gauge the number of precursors likely to be lost by differentiation from the pool of Pax7^{+} precursor cells. Differentiating Pax7^{+} cells, i.e. Pax7^{+}Myogenin^{+} cells were observed at the vertical borders, dorsal edge and central body but significantly increased in the central body in growing fish, correlating with the location of muscle fibres. Myogenin^{+} cells were also primarily located amongst the muscle fibres in the central body, correlating with the location of muscle growth. Further, using *Tg(pax7:EGFP)*^{MPIEB}, we observed Pax7:gfp^{+} cells co-labeled with Myogenin and Myosin markers. Thus, it appears likely that extra Pax7^{+} cells in the central body are lost via differentiation and contribute to myotomal growth. In the *myod*^{fh261} mutants Pax7^{+}, differentiating Pax7^{+} and Myogenin^{+} cells were located in the deep central body at 3 dpf in contrast to the control situation where deep Pax7^{+} cells were predominantly observed from 4 dpf onwards. In addition to the location, the number of differentiating Pax7^{+} cells and Myogenin^{+} cells was significantly increased compared to controls. However, the extra precursors in the deep myotome reduced to 'control' levels by 5 dpf, coincident with a significant increase in myotomal nuclear number and myotome volume recovery, strongly suggesting the involvement of deep precursors in muscle growth recovery in *myod*^{fh261} mutants.

3.2 Introduction

Muscle precursor differentiation and fusion are central to muscle growth. Muscle precursors express a series of muscle regulatory factors (MRFs) such as *Myf5*/*MyoD*/*Mrf4* and *myogenin* prior to differentiation (Buckingham, 1994; Pownall et al., 2002; Rudnicki and Jaenisch, 1995; Weintraub et al., 1991). Differentiating muscle precursors lead to muscle growth by increasing the number of muscle fibres or the number of nuclei per fibre or both by fusing with each other or existing myofibres respectively. Myod is a key myogenic regulatory factor expressed by muscle precursors on their route to differentiation and Myod-driven Myogenin expression is important for a subset of fast fibre differentiation in zebrafish (Hinits et al., 2011). Zebrafish *myod*^{fh261} mutants display a delay in muscle development similar to the mouse model (Kablar et al., 1997), although the location and severity of this defect are altered in zebrafish. Specifically in zebrafish embryos the somitic trunk muscle growth is delayed in addition to severe head and jaw muscle defects (Hinits et al., 2011). Aberrantly high numbers of myogenic precursors are found in the dermomyotome (Hammond et al., 2007) and muscle mass is significantly reduced (Hinits et al., 2011), suggesting alterations in the differentiation kinetics of muscle precursors. Interestingly, the growth defect of the somitic muscle in *myod*^{fh261} mutants recovers, but the fate of the excess number of myogenic precursors is currently unknown. In the current study, the number and location of precursors prior to myotome recovery and the number of myonuclei at the time of post-recovery were examined with a view to understand how precursor dynamics (1) are altered in the absence of Myod and (2) might influence muscle growth.

To determine alterations in the behaviour of muscle precursor cells in the absence of Myod, it is useful to know the dynamics of these cells in a wildtype situation. Currently, there is limited quantitative characterization of the distribution of muscle precursors, their proliferative capacity and differentiation kinetics during a period of muscle growth in zebrafish. A better understanding of the spatio-temporal dynamics of muscle precursors during muscle growth can lead to new hypotheses regarding the regulation of myogenic cells. In this chapter a quantitative characterization of the *in vivo* behaviour of muscle precursors is provided, using the developing zebrafish as a vertebrate model.

Pax7 expression was utilized as a marker to identify a population of muscle precursors in the zebrafish embryo and larvae, because embryonic and post-embryonic muscle growth in vertebrates is proposed to arise from $Pax7^+$ muscle progenitor cells (Ben-Yair and Kalcheim, 2005; Gros et al., 2005; Kassar-Duchossoy et al., 2005; Relaix et al., 2005). In the 24 hpf embryo, *pax3a* and pax*7a* transcripts were detected by in situ hybridization and found to lie in the dermomyotome underlying the skin and superficial to slow muscle fibers expressing slow myosin heavy chain protein (Devoto et al., 2006; Groves et al., 2005; Hammond et al., 2007). The number of Pax7+ cells in the dermomyotome is reported to be between 40-50 per somite at 24 hpf (Hammond et al., 2007; Hollway, 2007; Stellabotte et al., 2007). A fraction of Pax7+ cells in the dermomyotome of 24 hpf fish are proliferative as determined by H3P stain marking cells in the M phase of mitosis (Hammond et al., 2007). In addition to *pax3a* and *pax7a*, zebrafish has duplicated genes, namely *pax3b* (Minchin et al., 2013) and pax*7b* (Minchin and Hughes, 2008), which like *pax3a* and *7a* in the somites appear to be restricted to the dermomyotome layer at 24 hpf. Outside of the somitic region, *pax3a*, *3b*, *7a*, and *7b* are also expressed in the various brain compartments and neuronal tissues during development (Hammond et al., 2007; Minchin and Hughes, 2008). Pax3a and 7a expression in the somites can be distinguished from the neural crest cells expressing the same by their shape, size and superficial location with respect to slow myosin staining and co-localization with neural crest specific marker foxd3 (Minchin and Hughes, 2008). To summarize the Pax3/7 expressing cells are located in the dermomyotome of 1 dpf fish. However, the location and number of these cells is unknown in the post hatched larvae from 3 dpf onwards and these have been quantitated in the current study. Moreover, $Pax7^+$ cells in the dermomyotome of zebrafish have been suggested but not demonstrated to contribute to muscle growth and repair. In this chapter, the role of dermomyotomal Pax7+ cells in muscle growth was assessed based on the distribution of $Pax7^+$ cells in epaxial somites of fish between 3 and 6 dpf, determined by utilizing a combination of *in vivo* confocal imaging in live and antibody-stained fixed wholemounts.

Myogenin expression was used to identify differentiating precursors (Hasty et al., 1992; Nabeshima et al., 1992; Sassoon et al., 1989) and to provide a quantitative account of the distribution of $Myogenin^+$ cells in fixed wholemounts of zebrafish between 3 and 6 dpf.

Somite growth was determined by the increase in somite width in 3 to 6 dpf fish whereas nuclear accretion in growing somites was determined by counting nuclei in optical transverse sections of myosin and Hoechst stained wholemount fish. The data show that Pax7 and Myogenin^{+} muscle precursors are enriched in the deep myotome of growing somites in wildtype fish correlating with the location of muscle fibre growth whereas in *myod*^{fh261} mutants, myotome growth is coincident with a reduction in the number of excess muscle precursors and nuclear accretion, strongly suggesting that recovery of muscle growth is Pax7+ and Myogenin+ precursor cell driven.

3.3 Results

3.3.1 Pax7^{+} cells are clustered at the borders and located close to muscle fibres in the central body of zebrafish somites

To determine the distribution of Pax7^{+} cells in somites of developing zebrafish, wholemount larvae/larvae between the ages of two and seven days post fertilization (dpf) were fixed and stained with markers detecting nuclei, muscle and Pax7^{+} cells. Bulk of the myotome of growing zebrafish is located within somites (Representative image at 4 dpf, Fig. 3.1A). The epaxial and hypaxial somite can be divided into four borders and a central portion (Fig. 3.1B). The four edges correspond to the two vertical septae or vertical borders (VB), horizontal myoseptum (HM) and dorsal edge (DE). The term central body is used to refer to the central portion of the epaxial/hypaxial somite. Muscle fibres lie within the central body region while fibre ends are located at the two vertical septae in each somite. In the central body, Pax7^{+} cells are nestled close to fibres (superficial slow fibres, Fig. 3.1C; deep fast fibres, Fig. 3.1D). The number of Pax7+ cells increased significantly between three and seven dpf (Fig. 3.4), specifically in the deep myotome (Fig. 3.8).

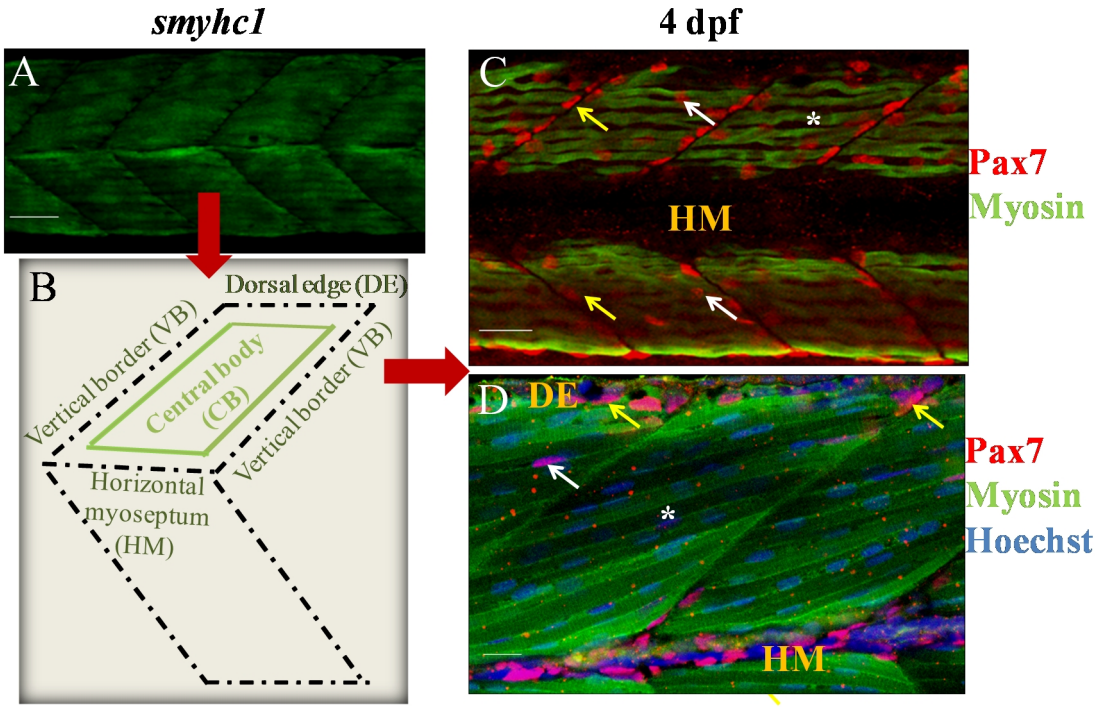


Fig. 3.1 Pax7^{+} cells are located at the borders and central body of somites.

Fig. 3.1 Pax7$^+$ cells are located at the borders and central body of somites.
Confocal images are single slices from stacks of 4 dpf wholemount larvae and are lateral views oriented with dorsal up and anterior to left. **A:** Representative somites in a live *Tg(9.7kb smyhc1:gfp)^{i104}* larvae expressing GFP in the slow fibres. **B:** Schematic of a zebrafish somite depicting borders and central body regions. **C:** Wild type larvae were stained with anti-Pax7 (red), A4.1025 (detecting myosin, green) and Hoechst 33342 (detecting nuclei), at 4 dpf. Lateral view of the myotome showing the superficial monolayer of slow muscle cells aligned parallel to the horizontal myoseptum (green, asterisk) in somites 15-18. Pax7$^+$ cells are present at borders (yellow arrows) and central body (white arrows) in the epaxial and hypaxial somite. The large gap in the region of horizontal myoseptum is an artefact created during flat-mounting. **D:** *Tg(-2.2mylz2:GFP)^{gz8}* were stained with Hoechst 33342 (blue), anti-Pax7 (red) and anti-GFP (detecting myosin, green). Lateral view of the epaxial deep myotome showing fast muscle fibres oriented at angles to the horizontal myoseptum (green, asterisk). Pax7$^+$ cells are located at the borders (yellow arrows) and central body (white arrows). Vertical border (VB), Dorsal edge (DE), Horizontal myoseptum (HM) and Central body (CB). Scale bar 50 μm.

3.3.2 The number of Pax7$^+$ cells increases in somites between day 3 and 6 of development

Based on confocal scans of wholemount larvae, the distribution of Pax7$^+$ cells appeared to be concentrated at the borders with some cells scattered in the central body. To determine whether the distribution of Pax7$^+$ cells at the various somitic locations changed during development, the number of Pax7$^+$ cells was determined in the epaxial somite of three to four fish at 3, 4 and 6 dpf. Quantitation was done mainly in the epaxial somites. However, the pattern of stained cells appeared to be similar in epaxial and hypaxial somite. For quantitation purposes, mononucleate Pax7$^+$ cells were assigned to a particular border based on their proximity to that border as follows: **a.** Pax7$^+$ nuclei were identified as being at the vertical borders if they were touching the border. This included two types of Pax7$^+$ nuclei: some whose long axis was parallel to the vertical border and others at an angle to the vertical border but still touching the border (Fig. 3.2A). **b.** Pax7$^+$ cells were classified as located at the horizontal myoseptum if they lay close to the muscle fibres in the horizontal myoseptum region where the epaxial and hypaxial parts of the somite fold inwards (Fig. 3.2B,C). **c.** Pax7$^+$ cells were included as part of the dorsal edge if they lay at the dorsal most extreme of the epaxial somite. This edge is further dorsal to the dorsal region of the central body and is part of the superficial myotome (Fig. 3.2D,E,F), although

to view the dorsal edge in a confocal stack, one must travel to the deeper myotome (Fig. 3.2E,F). $Pax7^+$ cells lying in the space encompassed by the four borders but not a part of the borders or touching them were grouped as belonging to the central body. $Pax7^+$ cells likely to be xanthophores were excluded from the counts based on their high fluorescence intensity (Fig.3.2G,H) or in some cases based on the irregular shape of the nuclei. On average five to eight xanthophores were observed in the superficial myotome of zebrafish between 3 and 6 dpf.

Confocal stacks of wholemount fish were used for counting the number of $Pax7^+$ cells. For imaging purposes, the somites in the region above the anal vent (somite numbers 15-20) are towards the end of the yolk extension making these somites easier to image compared to those closer to the yolk. However, it was unknown whether the number of $Pax7^+$ cells was similar between different somites in a fish. Based on the location parameters, the number of $Pax7^+$ cells was determined in several epaxial somites of individual fish to determine the variation in the number of $Pax7^+$ cells along the anterior-posterior axis of 4-4.5 dpf fish. The number of total $Pax7^+$ cells (i.e. sum of the number of $Pax7^+$ cells at the borders and central body) or $Pax7^+$ cells at the borders or in the central body alone, were not found to vary significantly with somite number (Fig. 3.3A-C). Hereafter, epaxial somites 15-20 in general were used for quantifying the number of $Pax7^+$ cells. The number of $Pax7^+$ cells was determined in the epaxial somites of 3, 4 and 6 dpf fish by counting in the XZ direction at each location from confocal stacks of wholemount fish. Somite width and the total number of $Pax7^+$ cells increased significantly between 3 and 6 dpf ($p=0.011$, Fig. 3.4A; $p=0.005$, Fig. 3.4B). The increase in the total number of $Pax7^+$ cells could be attributed to an increase in the number of $Pax7^+$ cells at the vertical borders ($p=0.001$, Fig. 3.4C) and central body ($p=0.011$, Fig. 3.4D), since the number of $Pax7^+$ cells at the remaining two locations - horizontal myoseptum and dorsal edge (Fig. 3.4E,F), remained similar between day 3 and 6 of development. The data indicate that the number of $Pax7^+$ cells increases at specific somitic locations during muscle growth between 3 and 6 dpf. The locations associated with the increase are the (i) vertical septae, the region where fibres ends are located and (ii) central body where $Pax7^+$ cells have been shown to take up satellite cell positions in adult zebrafish (Hollway et al., 2007).

To visualize the dynamics of Pax7^{+} cells in live growing fish, the transgenic Tg(*pax7:*EGFP)^{MPIEB} bred on pfeffer background was utilized. The pfeffer mutants (*pfe*^{tm236b}) carry a mutation in csf1rA/fmsA, one of two paralogs of the Csf1 receptor in teleosts. The mutation results in a defect in pigment cell formation and migration (Odenthal et al., 1996), likely contributing to a reduction in the number of xanthophores in the *pax7*:gfp fish. In order to examine the expression pattern and quantify Pax7:gfp^{+} cells versus the endogenous Pax7 expression in *pax7:*GFP *pfe/pfe*, transgenic larvae were immunolabeled for gfp and Pax7 at 3.25 dpf. At first glance, the staining pattern of gfp^{+} cells and Pax7 antibody stained nuclei appeared largely similar (Fig.3.5A-C). Upon closer examination, several differences became apparent. Occasionally, Pax7:gfp^{+} cells were labeled with faint Pax7 antibody stain and vice versa (Fig. 3.5D-G). The faint antibody stained cells could signify that Pax7 expression has been downregulated in these cells whereas the gfp fluorescence perdures. Faint gfp stain in Pax7^{+} cells could signify slower gfp translation compared to endogenous protein production. Rarely, gfp^{+} cells that were not detected by the Pax7 antibody could be observed (Fig. 3.5 H-K). These cells could also belong to the category of cells that have downregulated Pax7 expression but the gfp perdures. Some cells at the horizontal myoseptum and vertical borders close to the horizontal myoseptum region were detected by the Pax7 antibody but were not gfp positive (Fig. 3.5L-O). Quantification revealed that the total number of gfp^{+} cells was significantly less than the number of antibody stained nuclei (Fig. 3.6). The number of gfp^{+} cells was significantly reduced at the horizontal myoseptum and vertical borders but similar at the dorsal edge and central body. These differences could mean that the transgene does not faithfully recapitulate the endogenous expression or that the extra Pax7 antibody stained nuclei express Pax7b and hence are not targeted by the transgene targeted to Pax7a expressing cells. Pax7a is 94% similar to Pax7b and previous work in the lab has suggested that the Pax7 antibody targets both Pax7a and 7b expressing cells (Minchin and Hughes, 2008). I have used the Pax7:gfp fish primarily for tracking the behaviour of gfp^{+} cells whereas quantification was done mainly in Pax7 antibody stained wholemounts

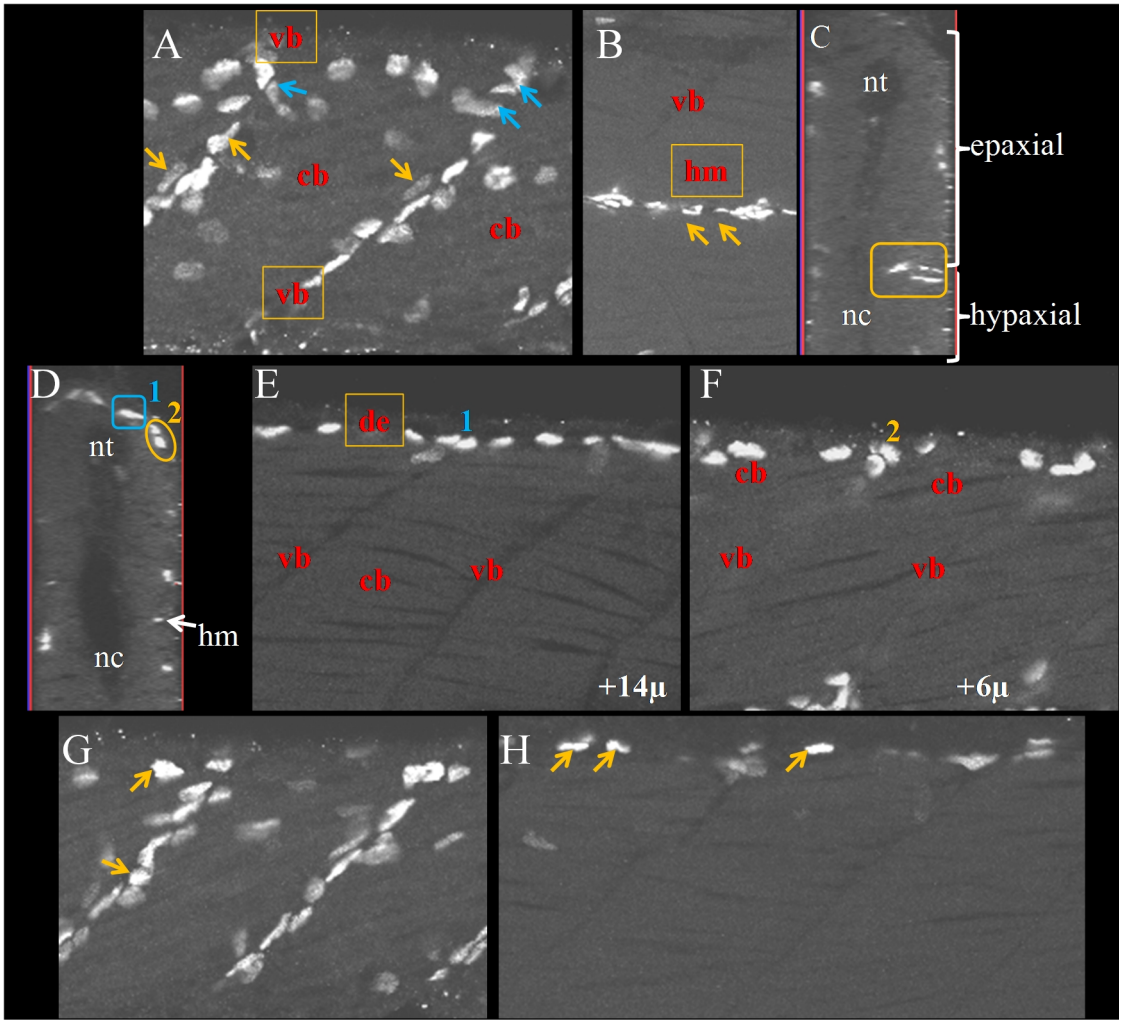


Fig. 3.2 Identification of Pax7^{+} cells at the borders.

Wholemount wild type larvae were stained with anti-Pax7 (white) and Hoechst 33342 (not shown) at 4 dpf. Confocal images are single slices from stacks and are lateral (A,B,E,F,G,H) or transverse (C,D) views of larvae oriented with dorsal up and anterior to left. **A:** Pax7^{+} cells at the vertical borders are parallel to the border (yellow arrows) or at various angles appearing to extend into the central body while still touching the vertical border (blue arrows). **B:** Pax7^{+} cells appear clustered in the horizontal myoseptum region. **C:** Transverse section shows that the Pax7^{+} cells are clustered in the crevice that forms as the epaxial and hypaxial portions of the somite folds inwards. **D:** Pax7^{+} cells at the dorsal edge (blue box) are dorsal to central body cells (yellow oval). **E,F:** The dorsal edge and Pax7^{+} cells at the dorsal edge can be seen in a slice at 14 microns depth (1, E) in the larvae, whereas the dorsal edge is not visible at 6 microns depth (2, F). **G,H:** Putative xanthophores were identified based on their higher fluorescence intensity (yellow arrows, G,H) and irregular shaped nuclei (yellow arrows, G). Vertical border (vb), central body (CB), horizontal myoseptum (hm), dorsal edge (de), neural tube (nt) and notochord (nc).

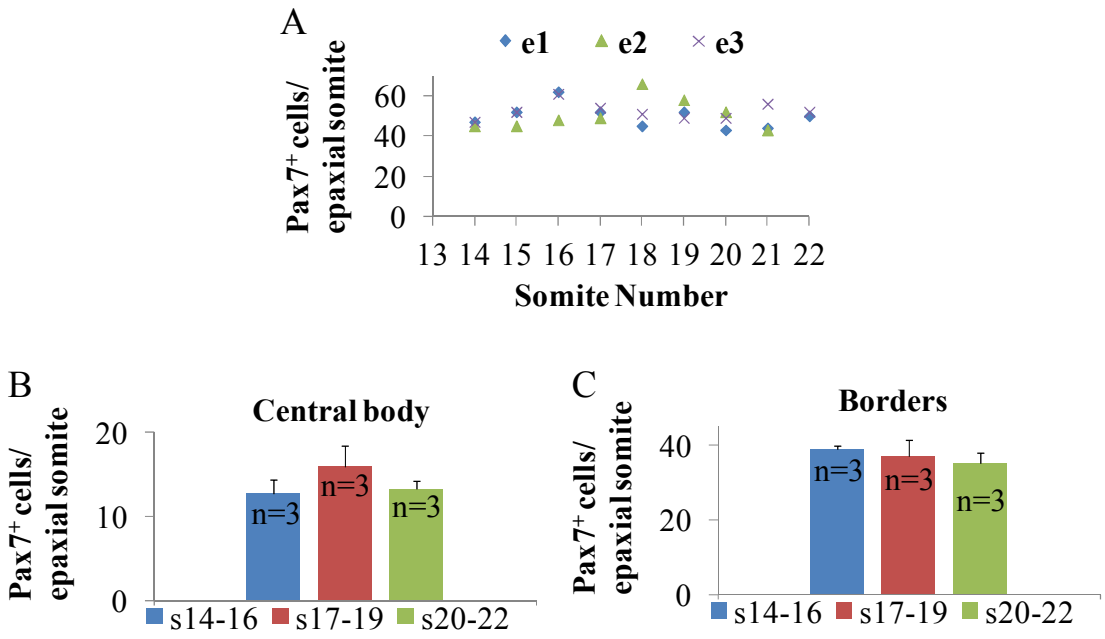


Fig. 3.3 Variation in the number of Pax7$^+$ cells in individual larvae.
The number of Pax7$^+$ cells in epaxial somites 14-22 for 4-4.5dpf zebrafish larvae shown in distinct colours. **A:** The total number of Pax7$^+$ cells varied within a similar range between somites 14-22 in individual larvae. **B:** The number of Pax7$^+$ cells in central body region did not differ significantly between the somite groups s14-16 and s17-19 [p=0.35] and between s17-19 and s20-22 [p=0.38]. **C:** The number of Pax7$^+$ cells at the borders was also similar between the somite groups s14-16 and s20-22 [p=0.39] and between s17-19 and s20-22 [p=0.77]. Error bars are standard error of the mean.

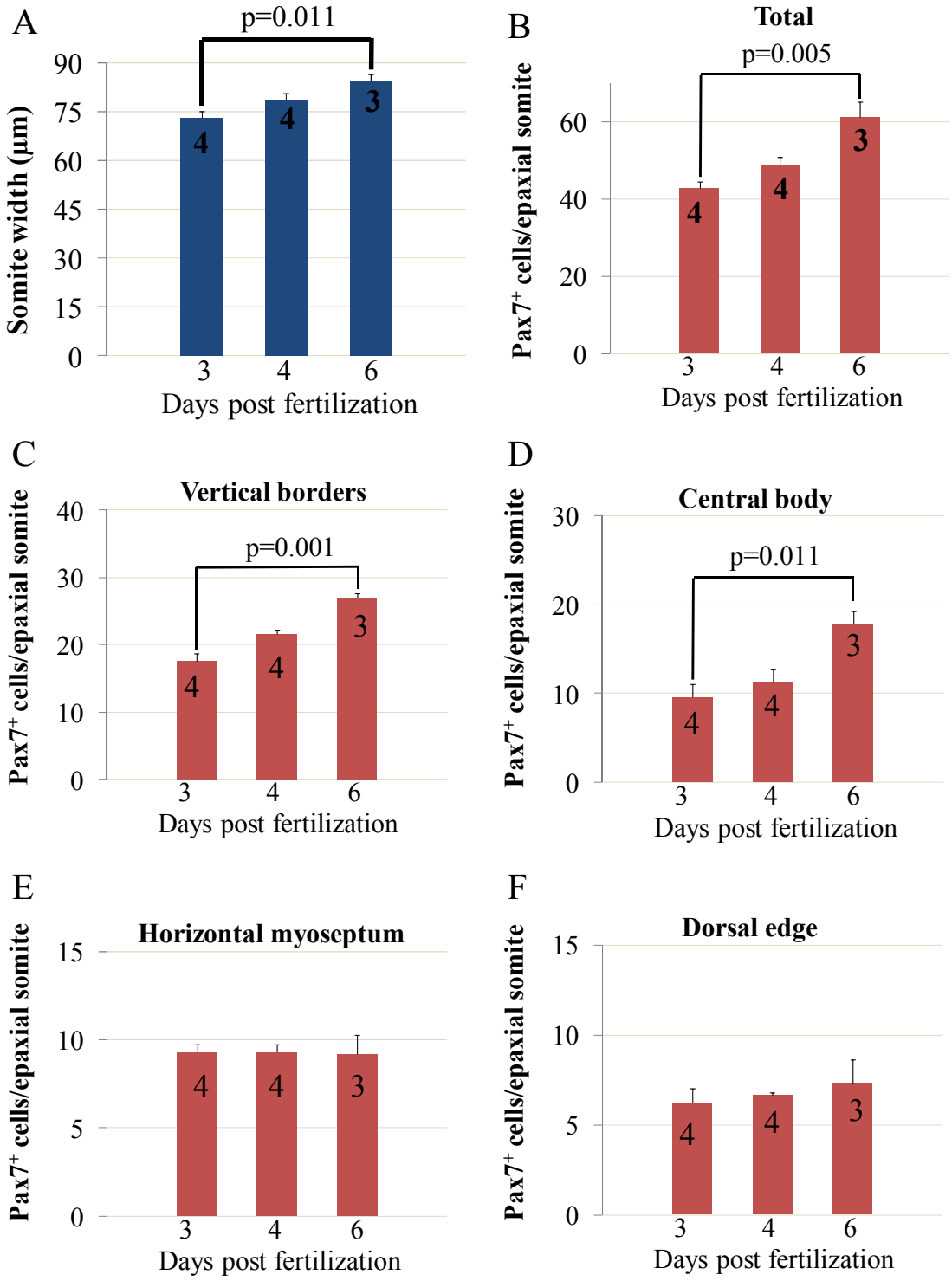


Fig. 3.4 Pax7$^+$ cells increase in epaxial somites at specific locations.

Fig. 3.4 Pax7$^+$ cells increase in epaxial somites at specific locations.
Plot of the number of Pax7$^+$ cells in epaxial somites of wholemount 3, 4 and 6 dpf larvae (A-E) stained with Hoechst 33342, Pax7 and Myogenin antibodies. The number of Pax7$^+$ cells was averaged from counts in somite number 16, 17 and 18 for sample number indicated within the bars at 3, 4 and 6 dpf. **A:** Somite width increased significantly between 3 and 6 days post fertilization. [p=0.011]. **B:** The total number of Pax7$^+$ cells increased significantly between 3 and 6 dpf in epaxial somites [p=0.005]. **C:** The number of Pax7$^+$ cells at the vertical borders increased significantly between 3 and 6 dpf in epaxial somites [p=0.001]. **D:** The number of Pax7$^+$ cells in the central body increased significantly between 3 and 6 dpf in epaxial somites [p=0.011]. **E:** The number of Pax7$^+$ cells at the horizontal myoseptum remained similar between 3 and 6 dpf in epaxial somites. **F:** The number of Pax7$^+$ cells at the dorsal edge did not change significantly between 3 and 4 dpf [p=0.051] and between 4 and 6 dpf [p=0.245]. Error bars are standard error of the mean.

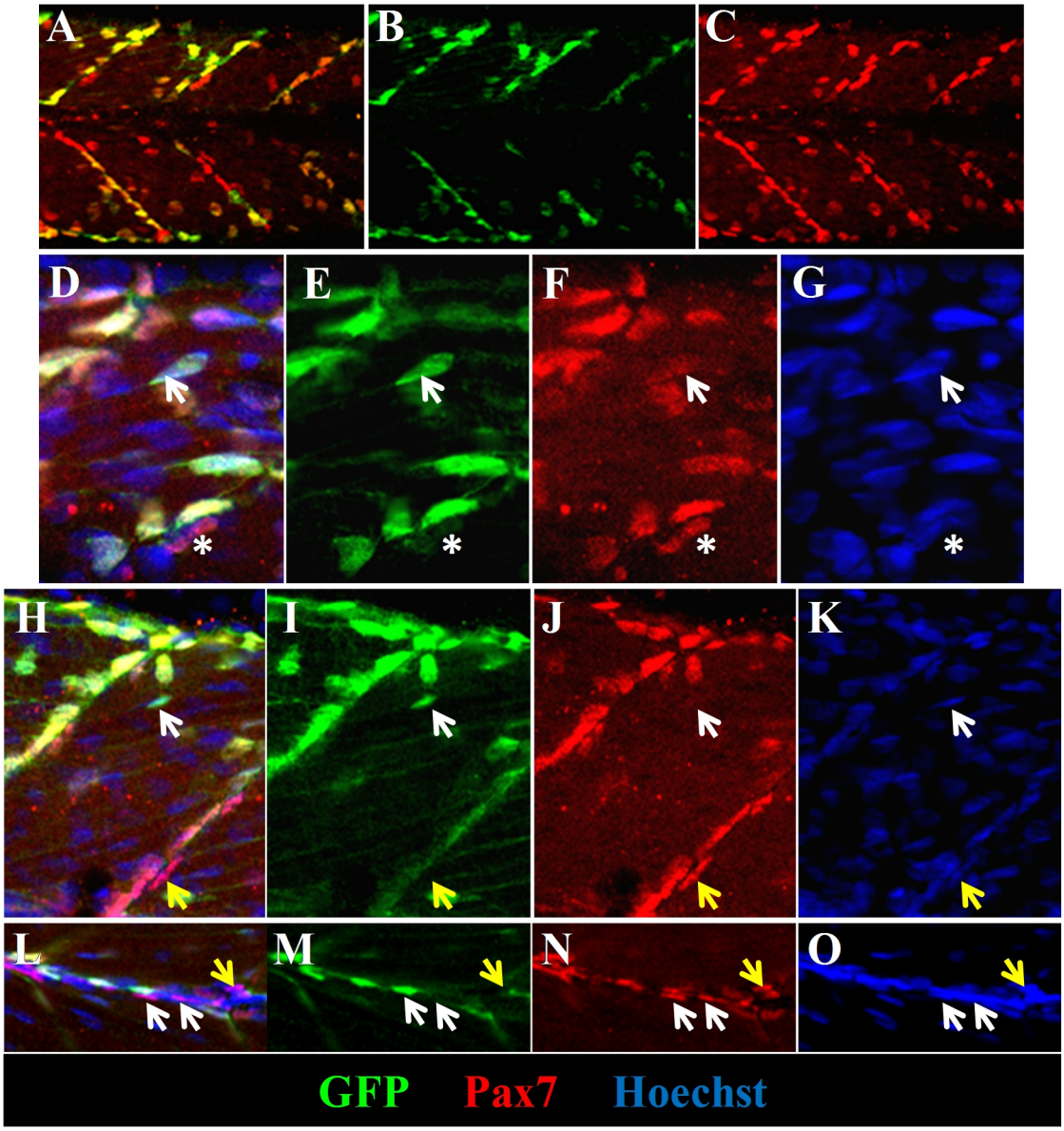


Fig. 3.5 Pax7:gfp$^+$ cells co-localize with Pax7 antibody stained nuclei
Wholemount 3.25 dpf *pax7:*gfp *pfe/pfe* transgenic larvae were stained with anti-gfp (green, A,B,D,E,H,I,L,M), anti-Pax7 (red, A,C,D,F,H,J,I,N) and Hoechst 33342 (blue, A,G,H,K,L,O). Confocal images are single slices from stacks and are lateral (A-O) views oriented with dorsal up and anterior to left. **A-C:** Gfp$^+$ and Pax7$^+$ cells in somites largely co-localize. **D-G:** A bright gfp$^+$ cell expressing low levels of Pax7 (arrows) and a dim gfp$^+$ expressing higher levels of Pax7 (asterisk). **H-K:** A gfp$^+$ cell that is not stained by Pax7 antibody. **L-O:** Some Pax7$^+$ cells at the horizontal myoseptum (white arrows) and vertical borders close to the horizontal myoseptum (yellow arrow) are not gfp$^+$.

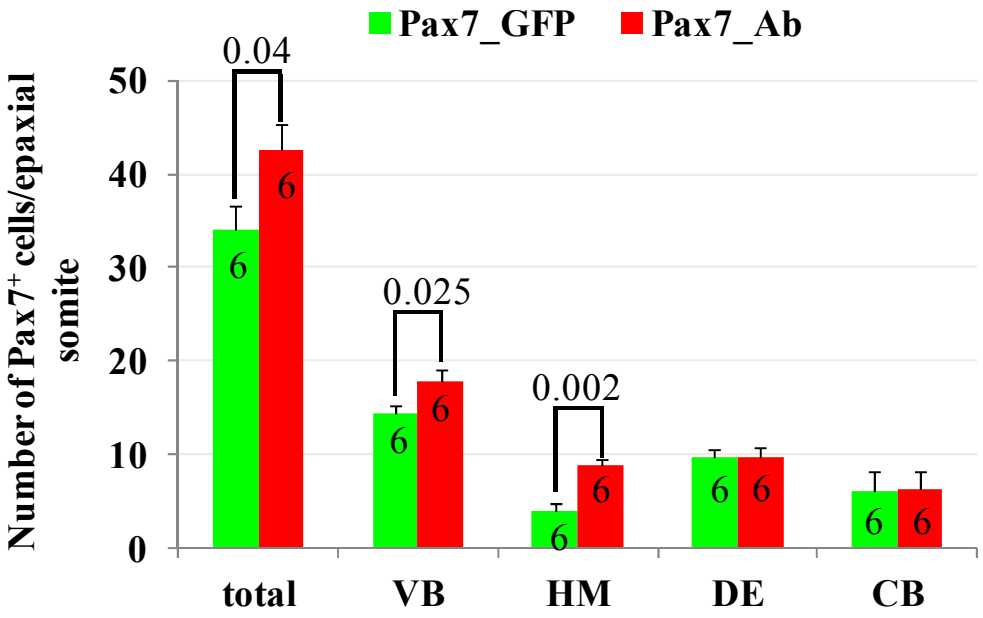


Fig. 3.6 Quantification of Pax7:gfp$^+$ cells versus Pax7 antibody stained nuclei
Plot of the number of Pax7$^+$ cells versus the number of gfp$^+$ cells in epaxial somites of wholemount 3.25 dpf *pax7::*GFP; *pfe/pfe* transgenic larvae, stained with Hoechst 33342, Pax7 and gfp antibodies. The number of stained cells (gfp$^+$ and Pax7 antibody$^+$) was counted in somite 17 for the sample number indicated within bars. The total number of cells stained by the Pax7 antibody is greater [p=0.04] compared to the total number of gfp$^+$ cells. The number of Pax7 antibody positive cells is significantly higher than the number of gfp$^+$ cells at the vertical borders (p=0.025) and horizontal myoseptum (p=0.002) whereas the number of Pax7 antibody positive cells is similar to the number of gfp$^+$ cells at the dorsal edge and central body locations. Error bars are standard error of the mean.

3.3.3 Pax7$^+$ cells increase in the deeper myotome during muscle growth

Pax7$^+$ cells at the horizontal myoseptum and in the deep central body have been shown to take up satellite cell-like positions underneath the basal lamina in 3 dpf and 7 dpf zebrafish respectively (Hollway et al., 2007). In 4 dpf larvae numerous Pax7$^+$ cells were observed to be oriented with their long axis parallel to the vertical border in the superficial region adjacent to the superficial monolayer of slow muscle cells (Fig. 3.1C) whereas few Pax7$^+$ cells adjacent to the deep fast fibres with their long axis oriented at angles to the vertical border and horizontal myoseptum were noticeable (Fig. 3.1D). Also, in live *pax7::*GFP; *pfe/pfe* transgenic larvae, parallely oriented Pax7:gfp$^+$ cells were

predominantly located in the superficial central body (excluding xanthophores with a large stellate cell body and a central irregular shaped nucleus) at 3 and 3.5 dpf (Fig. 3.7A,B), whereas numerous deep Pax7:gfp$^+$ cells oriented at angles were visible in the deep central body at 4 dpf (Fig. 3.7C). Further, during quantitation of Pax7$^+$ cells from wholemount scans of fish between 3 and 6 dpf, Pax7$^+$ cells in the deep myotome appeared to be rare at 3 dpf (Fig. 3.8A-D), contrary to numerous Pax7$^+$ cells at this location in 6 dpf fish (Fig. 3.8E-H). The latter observations with live and fixed fish suggest an increase in the number of Pax7$^+$ cells in the deep myotome during development.

To quantitate this phenomenon, Pax7$^+$ cells were counted in the superficial and deep myotome. The region chosen as superficial myotome included the dermomyotome, the first layer of muscle fibres which in zebrafish is the monolayer of slow muscle and up to the first layer of fast fibres that lies underneath the slow muscle layer. The dermomyotome is an external cell layer superficial to muscle and underlying the skin. Hence, Pax7$^+$ cells located between the skin and first layer of fast muscle were counted as part of superficial myotome whereas Pax7$^+$ cells located deeper than the first layer of fast muscle were classified as deep cells. Analysis of the distribution of Pax7$^+$ cells in the superficial versus deep domains of the epaxial myotome revealed that the number of Pax7$^+$ cells significantly increased between 3 and 6 dpf specifically in the deep myotome whereas remaining unchanged superficially (Fig. 3.8I). Pax7$^+$ cells could have arisen in the deep myotome through proliferation and/or migration from another location. Pax7:gfp$^+$ cells in the superficial myotome at the vertical borders, central body and dorsal edge are often seen extending into the deep myotome in 4 dpf and older larvae (Fig. 3.8J), suggesting that some deep Pax7$^+$ cells are likely to have arisen from migration of Pax7$^+$ cells from the superficial myotome.

Previous findings indicated that the number of Pax7$^+$ cells increase specifically at the vertical borders and central body between 3 and 6 dpf (Fig. 3.4B,C). To examine whether the location of deep Pax7$^+$ cells correlated with the location of increased Pax7$^+$ cells, location of the extra Pax7$^+$ cells in the deep myotome was determined with respect to the previously defined somitic regions: DE, VB, HM and CB. Applying the distinction of superficial versus deep to Pax7$^+$ cells located at the borders and central body revealed

that the number of Pax7^{+} cells significantly increased in the deep vertical septae and deep central body region at 6 dpf, but were not detectably changed superficially (Fig. 3.8K,L). Further, the number of Pax7^{+} cells remained unchanged at the horizontal myoseptum and dorsal edge (data not shown) at 3 and 6 dpf, reflecting the lack of significant increase seen between 3 and 6 dpf (Fig. 3.4D,E). Thus, the data indicate that the location of increased number of Pax7^{+} cells correlate with the deep Pax7^{+} cells, suggesting that migration of Pax7^{+} cells at the vertical borders and central body could have occurred from the superficial to deep myotome. However, migration of Pax7^{+} cells alone is not sufficient to explain maintenance of the population superficially while increasing in the deep. Consistent with such a possibility, cells at the vertical borders, central body and dorsal edge dorsal edge appear to extend into the central body, suggesting that Pax7^{+} cells at these locations could be lost by migration and differentiation. Nevertheless, the number of superficial Pax7^{+} cells was not diminished.

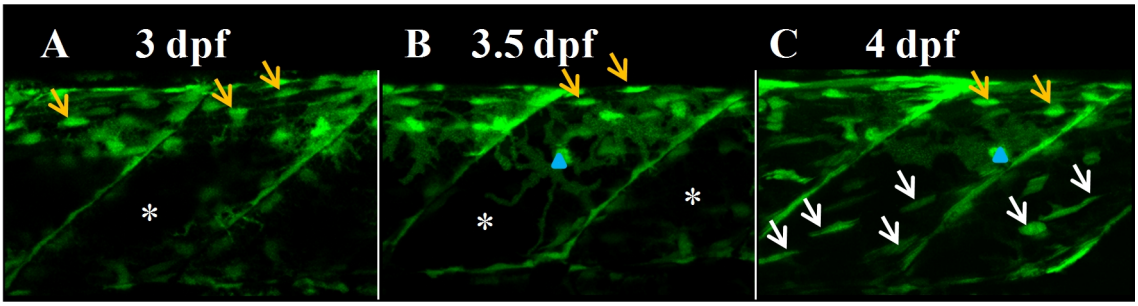


Fig. 3.7 Pax7:gfp^{+} cells increase in the deep central body
Live imaging of a *pax7::*GFP; *pfe/pfe* transgenic larvae at the ages indicated. Confocal images are maximum intensity projection of a short stack encompassing the superficial myotome and up to a depth of 26.78µm into the larvae. Images are lateral views (A-C) of larvae oriented with dorsal up and anterior to left. **A-C:** Parallely oriented superficial gfp^{+} cells in the epaxial somite (yellow arrows). The central portion of xanthophores are labelled with a blue triangle (B,C). Numerous Pax7:gfp^{+} cells in the deep myotome are seen oriented at angles in the central body at 4 dpf (white arrows, C) versus none at 3 and 3.5 dpf (asterisk, A-B).

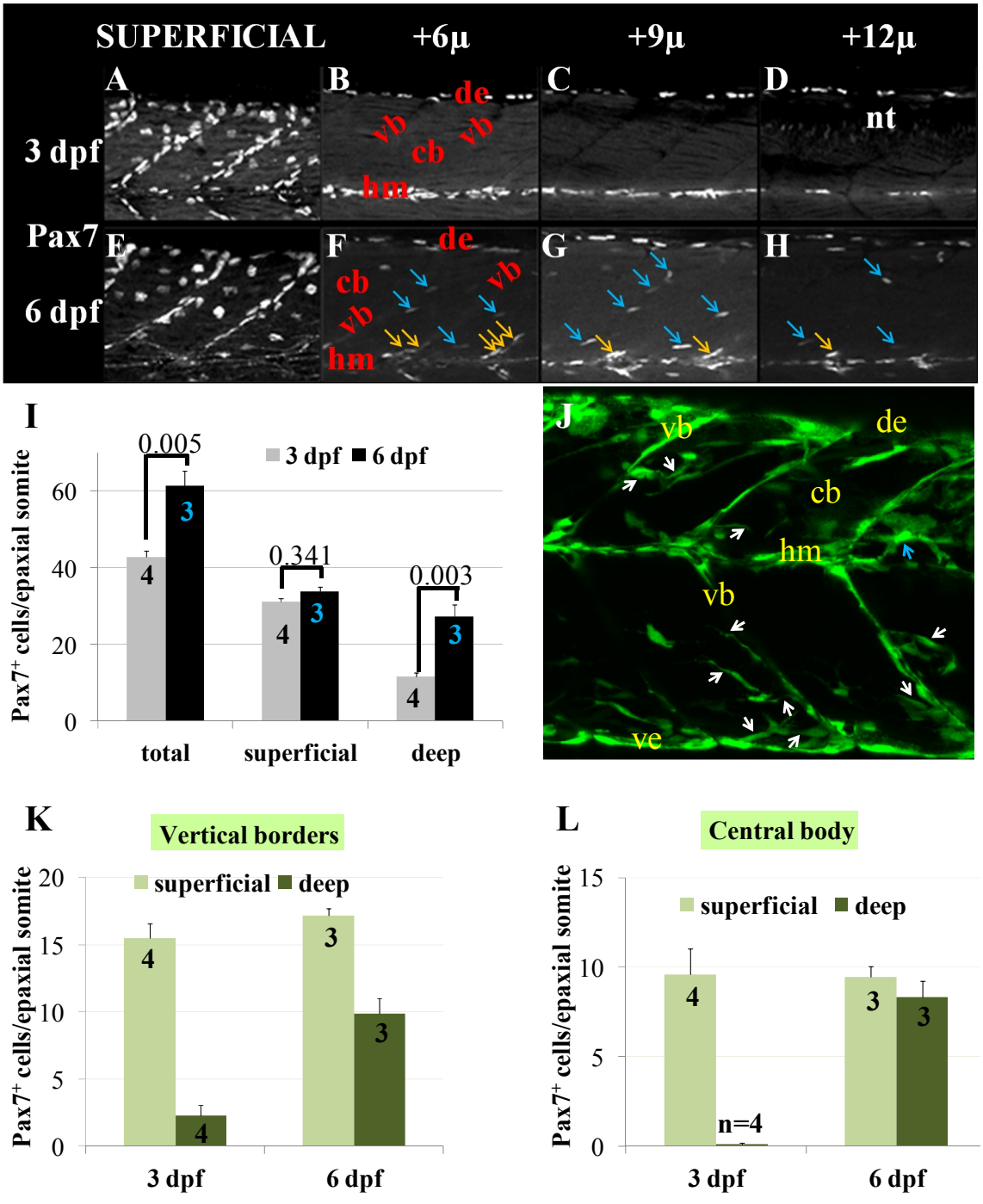


Fig. 3.8 Pax7^{+} cells increase in deep myotome.

Fig. 3.8 Pax7$^+$ cells increase in deep myotome.
Wholemount wild type larvae were stained with anti-Pax7 (white) and Hoechst 33342 (not shown) at 3 and 6 dpf (A-H). Lateral confocal images (A-H) are single slices oriented with dorsal up and anterior to the left. The single slices are in the superficial myotome (A,E), at a depth of 6 microns (B,F), 9 microns (C,G) and 12 microns (D,H) within the myotome from the superficial layer. Yellow arrows point to Pax7$^+$ cells at the vertical borders whereas blue arrows point to Pax7$^+$ cells in the central body (F-H). **A:** In a 3 dpf larva, Pax7$^+$ cells can be seen in the superficial myotome. **B-D:** In the same larva at a depth of 6 to 12 microns from the superficial layer, Pax7$^+$ cells can be seen at the dorsal edge and horizontal myoseptum, but not at the vertical borders and central body. **E:** In a 6 dpf larva, Pax7$^+$ cells can be seen in the superficial myotome. **F-H:** In the same larva at a depth of 6 to 12 microns from the superficial layer, Pax7$^+$ cells can be seen at the dorsal edge and horizontal myoseptum as well as at the vertical borders (yellow arrows) and central body (blue arrows). Pax7$^+$ cells were counted in the superficial and deep myotome at the vertical borders and central body in the same set of somites and larvae used in Fig. 3.4 (Sample number indicated within bars). **I:** The total number of Pax7$^+$ cells is significantly increased at 6 dpf compared to 3 dpf ($p=0.005$). The number of Pax7$^+$ cells in the deep myotome is also significantly increased at 6dpf ($p=0.003$) but did not change significantly in the superficial myotome ($p=0.341$). **J:** Live imaging of a *pax7::*GFP; *pfe/pfe* transgenic larva at 4 dpf. Confocal image is maximum intensity projection of a short stack of 30.48 μm of the deep myotome excluding the superficial myotome (depth of somite = 86 μm). Image is a lateral view of the larva oriented with dorsal up and anterior to left. Pax7:gfp$^+$ cells extend into the deep myotome from vertical borders and central body (white arrows). Blue arrow points to a xanthophore on superficial surface of myotome. **K:** The number of Pax7$^+$ cells is significantly increased in the deeper myotome at vertical borders in 6 dpf larvae ($p=0.001$), but remaining unchanged superficially ($p=0.302$). **L:** The number of Pax7$^+$ cells is significantly increased in the deeper myotome in the central body of 6 dpf larvae ($p=0.011$), but remaining unchanged superficially ($p=0.942$). Error bars are standard error of the mean. de: dorsal edge, ve: ventral edge, hm: horizontal myoseptum, vb: vertical borders, cb: central body.

3.3.4 The fraction of Pax7$^+$ cells in S-phase varies with the somitic location

To account for the lack of decrease and overall increase in the number of Pax7$^+$ cells, the incidence of Pax7$^+$ cells in the S-phase was investigated as an indication of their ability to proliferate in order to maintain and expand their numbers. Since the staining protocol for S-phase marker Bromodeoxyuridine (BrdU) was found to be incompatible with the staining technique for Pax7, EdU (analogue of BrdU) requiring a less harsh fixation and staining method was used. Zebrafish larvae (4 dpf) were treated with a short pulse of BrdU or EdU and stained for the respective marker. EdU was found to label cells at similar locations as BrdU such as in the somite, neural tube (Fig. 3.9A-D), gastrointestinal

tract, brain and skin (data not shown). Quantification of the number of S-phase positive cells in larvae treated with BrdU or EdU indicated that a similar number of mononucleate cells at the borders and central body of epaxial somites were labeled by either marker (Fig. 3.9E).

To assess the fraction of $Pax7^+$ cells in the S-phase, larvae were treated with a short pulse of EdU, fixed and stained for EdU and Pax7 (Fig. 3.9F-J). Approximately 17%-18.1% of the fraction of $Pax7^+$ cells co-labeled with EdU at all locations in the epaxial somite at 3 and 4 dpf respectively (total, Fig. 3.10A). The number of $Pax7^+$ cells in S-phase was found to be similar at 3 and 4 dpf (7.5 versus 8.7 respectively, p=0.69, Fig. 3.10B) The fraction of $Pax7^+$ cells in S-phase at vertical borders was found to be 20% at 3 dpf and 25% at 4 dpf (Fig. 3.10C). The number of $Pax7^+$ cells in S-phase at 3 dpf (3.9) and 4 dpf (4.7) was found to be similar (p=0.67, Fig.3.10D). The fraction of $Pax7^+$ cells in S-phase in the central body was found to be 18% at 3 dpf and 21% at 4 dpf (Fig. 3.10E). The number of $Pax7^+$ cells in S-phase in central body at 3 dpf (1.8) and 4 dpf (3.1) was also found to be similar (p=0.32, Fig. 3.10F). The data indicate that $Pax7^+EdU^+$ cells at the vertical borders and central body comprise majority of the total fraction of $Pax7^+$ cells in S-phase at 3 and 4 dpf. For example at 3dpf total 8 $Pax7^+EdU^+$ cells were found, of which 4 are at the vertical borders and 2 are at the central body. Remaining 1-2 cells likely arise by proliferation at the dorsal edge/horizontal myoseptum. Similarly at 4dpf total 9 $Pax7^+EdU^+$ cells were found of which 5 reside at the vertical borders and 3 are in the central body. Remaining 1 is likely generated at the horizontal myoseptum/dorsal edge. Thus, the data indicate that the vertical borders are the major source of proliferative Pax7+ cells compared to the other somitic locations in the zebrafish.

Since the larvae are growing, if Pax7+ cells are involved in muscle growth, they would be lost by differentiation. To test this hypothesis, larvae were stained for immunodetection of Myogenin to quantitate differentiating cells. $Pax7^+$ cell counts between 3 and 6 dpf revealed no significant change for $Pax7^+$ cells at the horizontal myoseptum and dorsal edge. Decreased proliferation or increased differentiation of $Pax7^+$ cells at these locations could account for the lack of significant increase. The fraction of $Pax7^+$ cells labeled with EdU at the horizontal myoseptum and dorsal edge were less than one and little over one respectively, supporting the decreased proliferation hypothesis.

Comparison of the fraction of $Pax7^{+}EdU^{+}$ co-labeled cells at the different borders and central body at 4 dpf revealed a significantly higher percentage of co-labeled cells at the vertical borders (25%) and central body (21%) compared to the horizontal myoseptum (5%, p=0.0007 and p=0.005 respectively) and dorsal edge (5%, p=0.021 and p=0.038 respectively) (Fig. 3.10G). The fraction of $Pax7^{+}$ cells in S-phase at the vertical borders was not found to be significantly different from that in the central body (p=0.45). Taking into consideration that in 4 dpf larvae, approximately 8-10 $Pax7^{+}$ cells are present at each of the two vertical borders as well as at the horizontal myoseptum (Fig. 3.4B-D), this result is interesting. The fraction of $Pax7^{+}$ cells labeled with EdU at the horizontal myoseptum indicates that less than one $Pax7^{+}$ cell at the horizontal myoseptum is in S-phase compared to more than two $Pax7^{+}$ cells per vertical border and more than three $Pax7^{+}$ cells at the central body. Thus, the reduced fraction of $Pax7^{+}$ cells at the horizontal myoseptum is not due to fewer $Pax7^{+}$ cells at this location and could signify niche differences. To summarize, the low incidence of $Pax7^{+}$ cells in S-phase at the horizontal myoseptum and dorsal edge correlate with the lack of significant increase in $Pax7^{+}$ cell number at these two locations, whereas the higher fraction of $Pax7^{+}$ cells in S-phase at the vertical borders and central body correlate with the increase in $Pax7^{+}$ cell number at these latter locations.

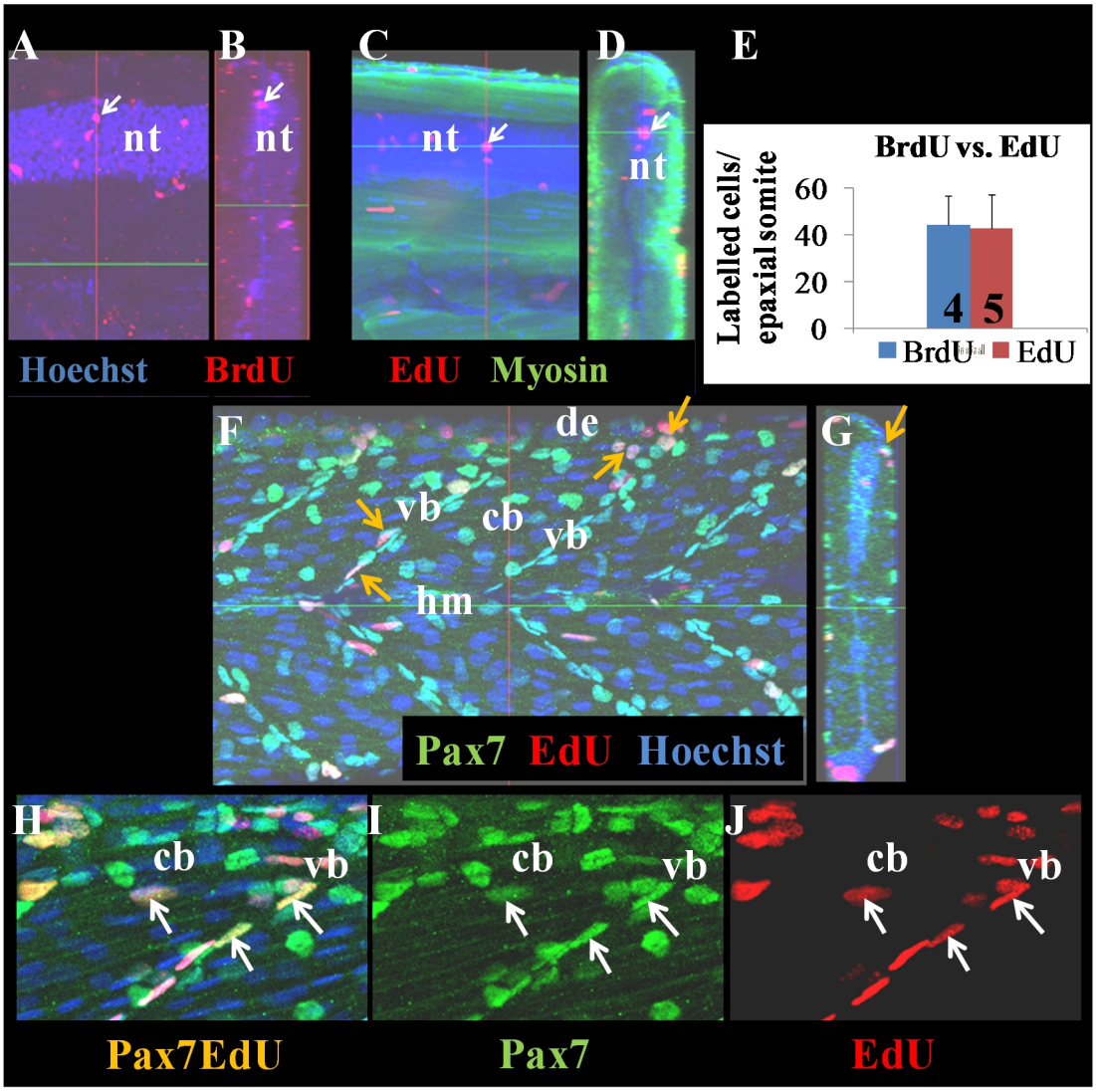


Fig. 3.9 Somitic Pax7^{+} cells are proliferative.
Wholemount wild type larvae at 4 dpf were either stained with Hoechst (blue) and anti-BrdU antibody (red) in panels A and B, or Hoechst (blue), anti-GFP (detecting myosin, green) and EdU (red) in panels C and D, or Hoechst (blue), anti-Pax7 antibody (green) and S-phase marker EdU (red) in panels E-J. Confocal images are single slices. Lateral (A,C,F,H,I,J) and transverse sections (B,D,G) are oriented with dorsal up and anterior to the left. **A-D:** BrdU^{+} and EdU^{+} cells are found at similar locations in the somite such as in the myotome (yellow arrows) and neural tube (white arrows). **E:** Quantitation of cells in the epaxial somite labelled with BrdU or EdU markers shows that a similar number of mononucleate cells are labeled with either marker. **F,G:** Mononucleate cells stained with Pax7 antibody and EdU cells are visible in the myotome (yellow arrows). **H-J:** Magnified view of the epaxial somite of a 4 dpf larvae stained with Hoechst, Pax7 and EdU showing several Pax7^{+} cells labeled by EdU (arrows) at the borders and central body. Error bars are standard error of the mean. nt neural tube, de dorsal edge, hm horizontal myoseptum, vb vertical borders, cb central body.

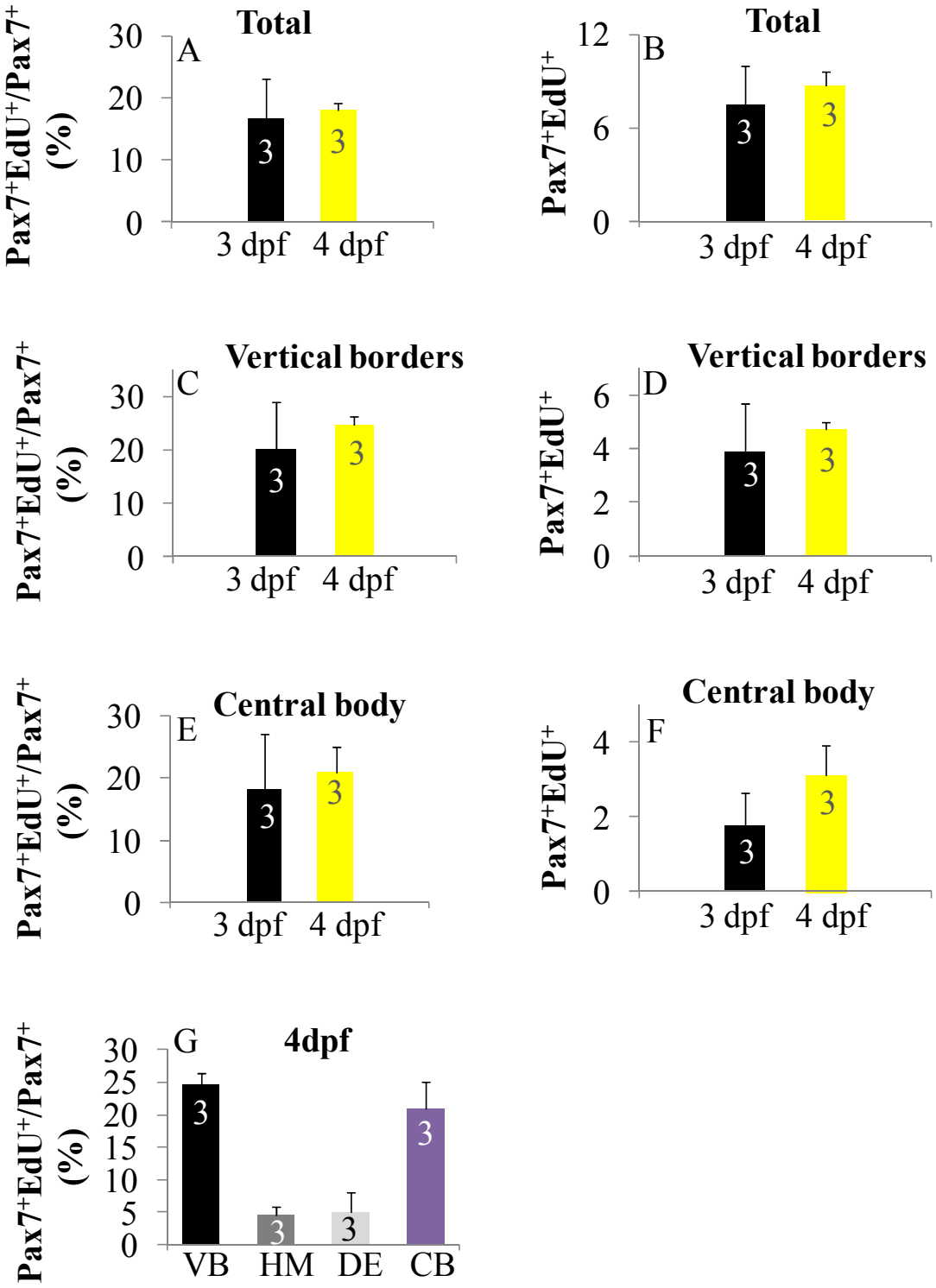


Fig. 3.10 The fraction of Pax7$^+$ cells in S-phase varies based on somitic location

Fig. 3.10 The fraction of Pax7$^+$ cells in S-phase varies based on somitic location. Wholemount wild type larvae were treated with S-phase marker EdU for three hours and then fixed and stained for EdU and anti-Pax7 antibody at 3 and 4 dpf. Quantitation of the fraction of Pax7$^+$ cells in S-phase (%, A,C,E,G) or number of dual labeled Pax7$^+$EdU$^+$ cells (B,D,F) in epaxial somites. Somites 16, 17 and 18 were analyzed in 3 larvae at 3dpf and 4 dpf (sample numbers are denoted within bars). **A,C,E:** The total fraction of Pax7$^+$EdU$^+$ cells (A) in epaxial somites as well as that at the vertical borders (C) and central body (E) are similar at 3 and 4 dpf. **B,D,F:** The total number of Pax7$^+$EdU$^+$ co-labeled cells (B, p=0.69) in epaxial somites as well as at the vertical borders (D, p=0.67) and central body (F, p=0.32) are similar at 3 and 4 dpf. **G:** At 4 dpf, a significantly greater fraction of Pax7$^+$EdU$^+$ cells are located at the vertical borders compared to horizontal myoseptum (p=0.0007) and dorsal edge (p=0.005) as well as in the central body compared to the horizontal myoseptum (p=0.021) and dorsal edge (p=0.038). The fraction of Pax7$^+$EdU$^+$ cells located at the vertical borders was not significantly different from that in the central body (p=0.45). Error bars are standard error of the mean.

3.3.5 Spatio-temporal distribution of putative myogenic precursors expressing differentiation marker Myogenin

In lineage tracing experiments, labeled cells giving rise to muscle fibres in the myotome of zebrafish larvae arose from the anterior portion of the somite to come to lie in the dermomyotome (Hollway et al., 2007; Stellabotte et al., 2007). Pax7 expression follows a similar pattern of being expressed earlier in the anterior border of somites and then in cells in the dermomyotome. Also, Pax7$^+$ cells in the superficial myotome can be observed extending into the deep central body in wholemount scans of live Pax7:*gfp* fish (Fig. 3.8J), suggesting that Pax7$^+$ cells migrate into the central body from borders and differentiate into muscle fibres. Indeed, elongated fibre-like structures with gfp perdurance (from Pax7:gfp cell) and positive for myosin stain can be observed. Also, gfp$^+$ cells positive for myogenin expression indicating differentiating precursors can be detected in the myotome of Pax7:*gfp* fish (Fig. 3.11). In such a scenario, the number of Pax7$^+$ cells in the central body and at the borders would reduce through differentiation. To examine whether the extra Pax7$^+$ cells proposed to arise from proliferation could be lost by differentiation, the spatiotemporal distribution of Pax7$^+$ cells expressing the differentiation marker Myogenin and the distribution of mononucleate cells expressing Myogenin only were examined in epaxial somites of 3 to 6 dpf fish. Myogenin$^+$ Pax7$^+$ cells were observed at the vertical borders (Fig. 3.12A-E), dorsal edge (Fig. 3.12F-J) and central body (Fig. 3.12A-E and K-O). The fluorescence intensity of Myogenin$^+$ Pax7$^+$

cells fell into three categories: dim Myogenin bright Pax7, dim Pax7 bright Myogenin, and Myogenin and Pax7 of similar intensity (Fig. 3.12C,E). Such a range of intensities could suggest that initially a bright $Pax7^+$ cell begins to express low levels of Myogenin, followed by increased expression of Myogenin and waning expression of Pax7. Cells expressing only Myogenin and not Pax7 could be seen at the dorsal edge (data not shown) but were predominantly found in the central body amongst muscle fibres (Fig. 3.12A-E and K-O). Thus, the distribution data indicate that differentiating $Pax7^+$ cells in the zebrafish myotome can be observed at the vertical borders, dorsal edge and central body whereas $Myogenin^+$ cells are largely located in the central body.

To determine the frequency of $Pax7^+$ cells likely to differentiate, the number of $Myogenin^+Pax7^+$ cells was determined between 3 and 6 dpf. $Myogenin^+Pax7^+$ cells at the vertical borders were cells with dim Myogenin and in conjunction with significant non-specific background at the vertical borders, accurate quantification of $Myogenin^+Pax7^+$ cells at this location became difficult. Further, $Myogenin^+Pax7^+$ cells were not observed at the vertical borders at 3 dpf. On an average, two to three $Myogenin^+Pax7^+$ cells were observed at each vertical border of somite 17 at 4 dpf. Quantification of $Myogenin^+Pax7^+$ cells at 3, 4 and 6 dpf is reported for the dorsal edge and central body (Fig. 3.13A). Quantification revealed that the total number of $Myogenin^+Pax7^+$ cells remained similar between 3 and 4 dpf ($p=0.2$) as well as between 4 and 6 dpf ($p=0.67$), but increased significantly between 3 and 6 dpf ($p=0.02$). The significant increase in the total number of $Pax7^+Myogenin^+$ cells was due to a significant increase in the number of these cells in the central body ($p=0.001$) whereas there was no significant change at the dorsal edge ($p=0.08$). Thus, the data indicate that on an average, a small fraction of $Pax7^+$ cells representing one-fifth of the $Pax7^+$ cells in the central body (3.44 out of 17.78 $Pax7^+$ cells) and $1/16^{th}$ of the $Pax7^+$ cells at the dorsal edge, express Myogenin and are likely to be lost from the Pax7 pool by differentiation.

To determine the differentiation kinetics between 3 and 6 dpf, cells expressing Myogenin only were quantified at the dorsal edge and central body (Fig. 3.13B). The total number of $Myogenin^+$ cells appeared to increase between 3 and 4 dpf before reducing close to 3 dpf levels by 6 dpf. However, the changes in the number of total $Myogenin^+$ cells were not significant between 3 and 4 dpf ($p=0.18$) and between 4 and 6 dpf ($p=0.13$),

suggesting that the number of Myogenin$^+$ cells remains similar between 3 and 6 dpf. Similarly, the number of Myogenin$^+$ cells at the dorsal edge did not change significantly between 3 and 4 dpf (p=0.79), although showing a tendency for decrease between 4 and 6 dpf (p=0.04) and overall between 3 and 6 dpf (p=0.07). The number of Myogenin$^+$ cells in the central body was not changed significantly between 3 and 4 dpf (p=0.19), 4 and 6 dpf (p=0.42) as well as between 3 and 6 dpf (p=0.36). Thus, the data indicate that on average between 2 and 9 Myogenin+ cells in the central body location per epaxial somite are available for terminal differentiation suggesting a slow rate of myofibre addition to the myotome. To summarize thus far, in growing fish between 3 and 6 dpf, the number of somitic Pax7$^+$ cells increases specifically at the vertical borders and central body, especially in the deep myotome. The number of differentiating Pax7$^+$ cells, i.e. Pax7$^+$Myogenin$^+$ cells, increase significantly in the central body, and Myogenin$^+$ cells are also found predominantly in the central body amongst muscle fibres in the growing fish, correlating with the region where myogenic cells from dermomyotome were observed to give rise to new fibres (Hollway, 2007; Stellabotte et al., 2007). Thus, the data is suggestive of a model in which enrichment of Pax7$^+$, Pax7$^+$Myogenin$^+$ and Myogenin$^+$ cells in the central body correlates with muscle growth.

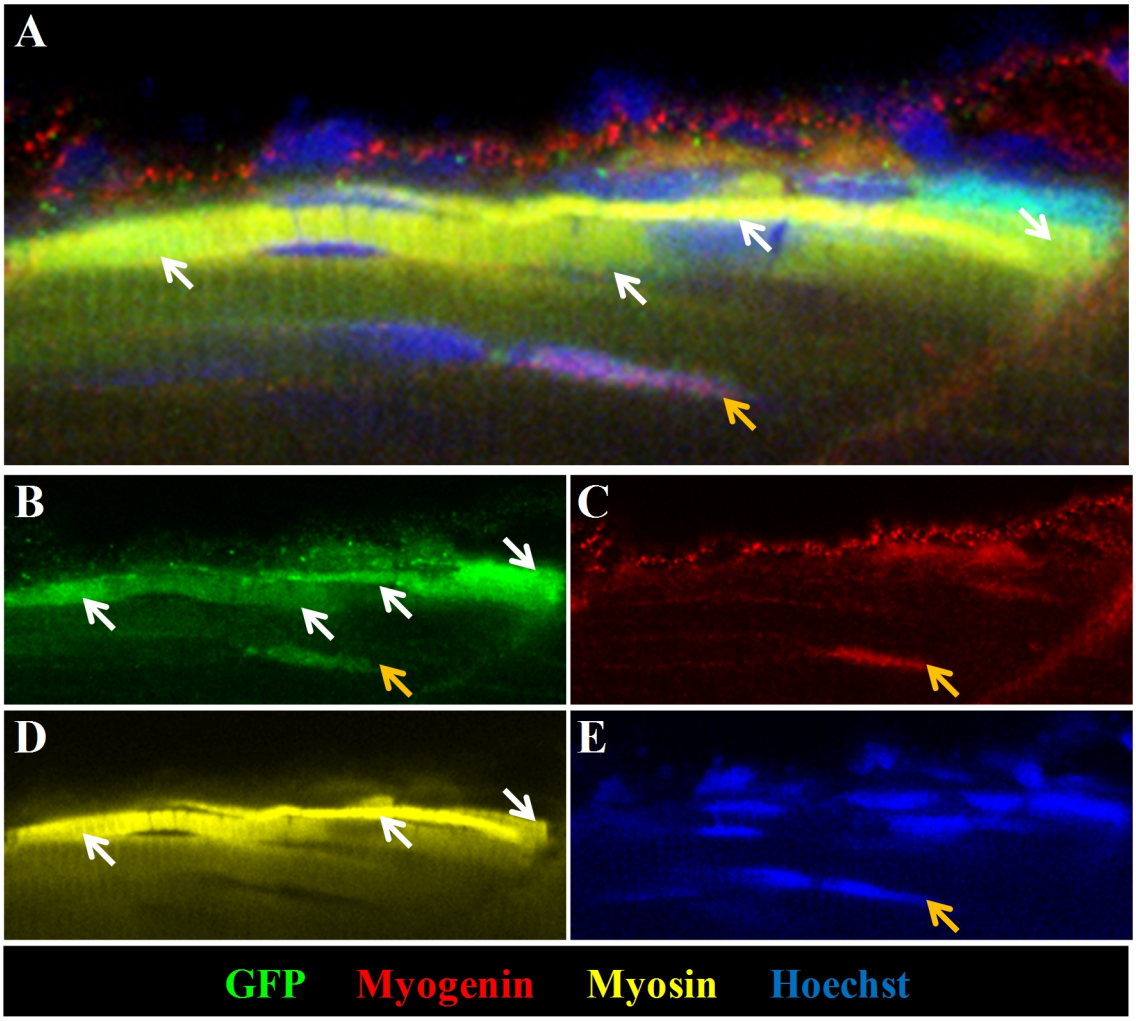


Fig. 3.11 Pax7:gfp^{+} cells differentiate into muscle fibres
Wholemount *pax7:*gfp; *pfe/pfe* transgenic larvae at 4 dpf were stained with Hoechst (blue), anti-gfp antibody (green), anti-Myogenin antibody (red) and A4.1025 (detecting myosin). Confocal images are single slices. Lateral views (A-E) are oriented with dorsal up and anterior to the left. **A,B,D:** Gfp perdurance can be seen in several myosin stained fibres (white arrows). **A,B,C,E:** A gfp^{+} cell co-labels with Myogenin (gold arrow).

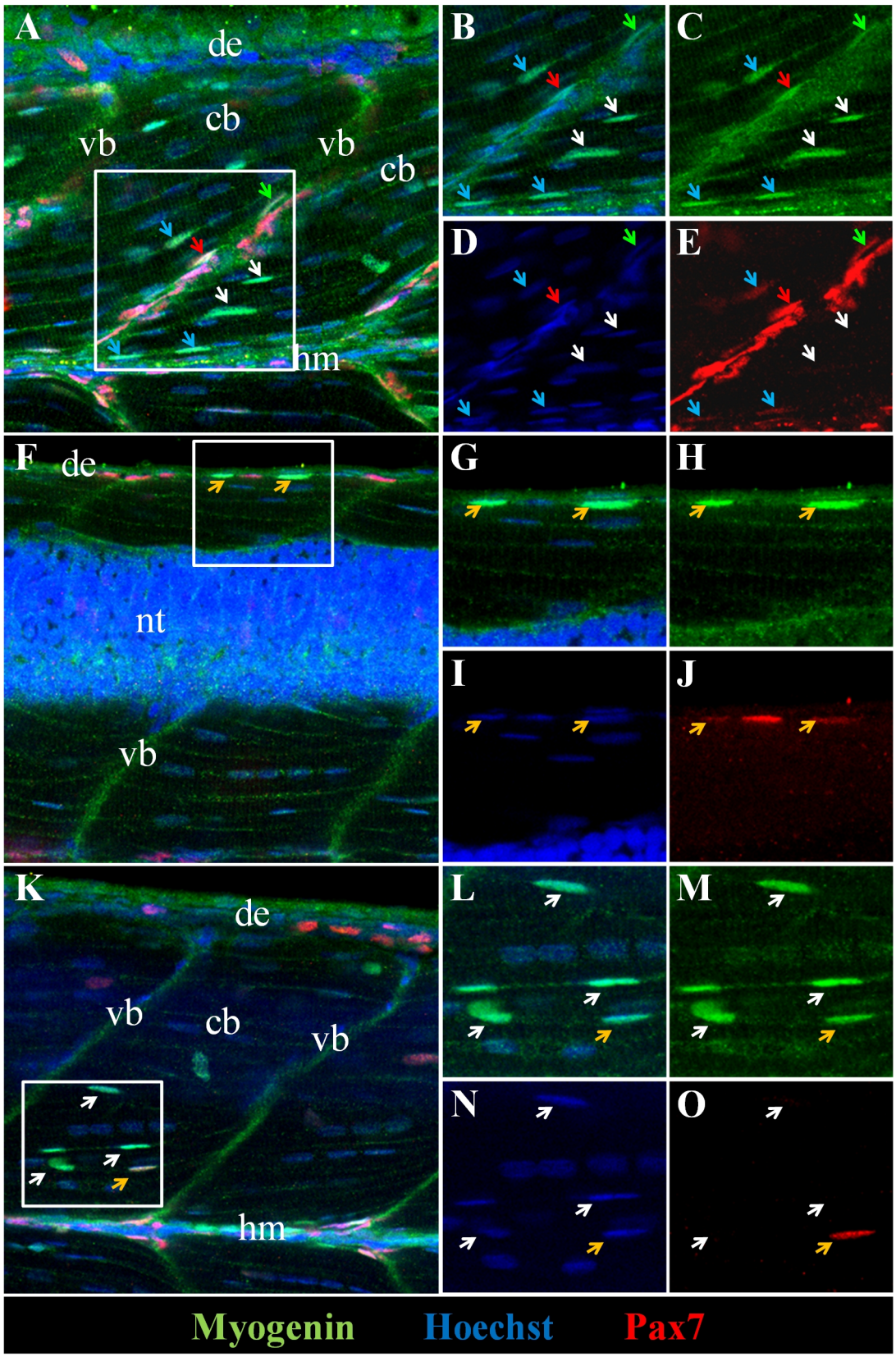


Fig. 3.12 Myogenin^{+} cells are located at the dorsal edge and central body.

Fig. 3.12 Myogenin$^+$ cells are located at the dorsal edge and central body.
Wholemount wild type larvae at 4 dpf were stained with Hoechst (blue), anti-Pax7 antibody (red) and anti-Myogenin antibody (green). Confocal images are single slices. Lateral views (A-O) are oriented with dorsal up and anterior to the left. Boxed region in A magnified in insets B-E, boxed region in F magnified in insets G-J and boxed region in K magnified in L-O. **A-E:** Myogenin$^+$ Pax7$^+$ cells at the vertical border and central body and Myogenin$^+$ cells in the central body of an epaxial somite. Green arrow points to a dim Myogenin$^+$ bright Pax7$^+$ cell at the vertical border. Red arrow points to a bright Myogenin$^+$ brightPax7$^+$ cell at the vertical border. In the central body, blue arrows point to bright Myogenin$^+$ dim Pax7$^+$ cells whereas white arrows point to Myogenin$^+$ cells. **F-J:** Myogenin$^+$Pax7$^+$ cells at the dorsal edge of an epaxial somite (gold arrows). **K-O:** Several Myogenin$^+$ cells in the central body of an epaxial somite (white arrows). Gold arrow points to a Myogenin$^+$Pax7$^+$ cell with bright Myogenin and dim Pax7 expression. cb central body, vb ventral border, de dorsal edge, hm horizontal myoseptum.

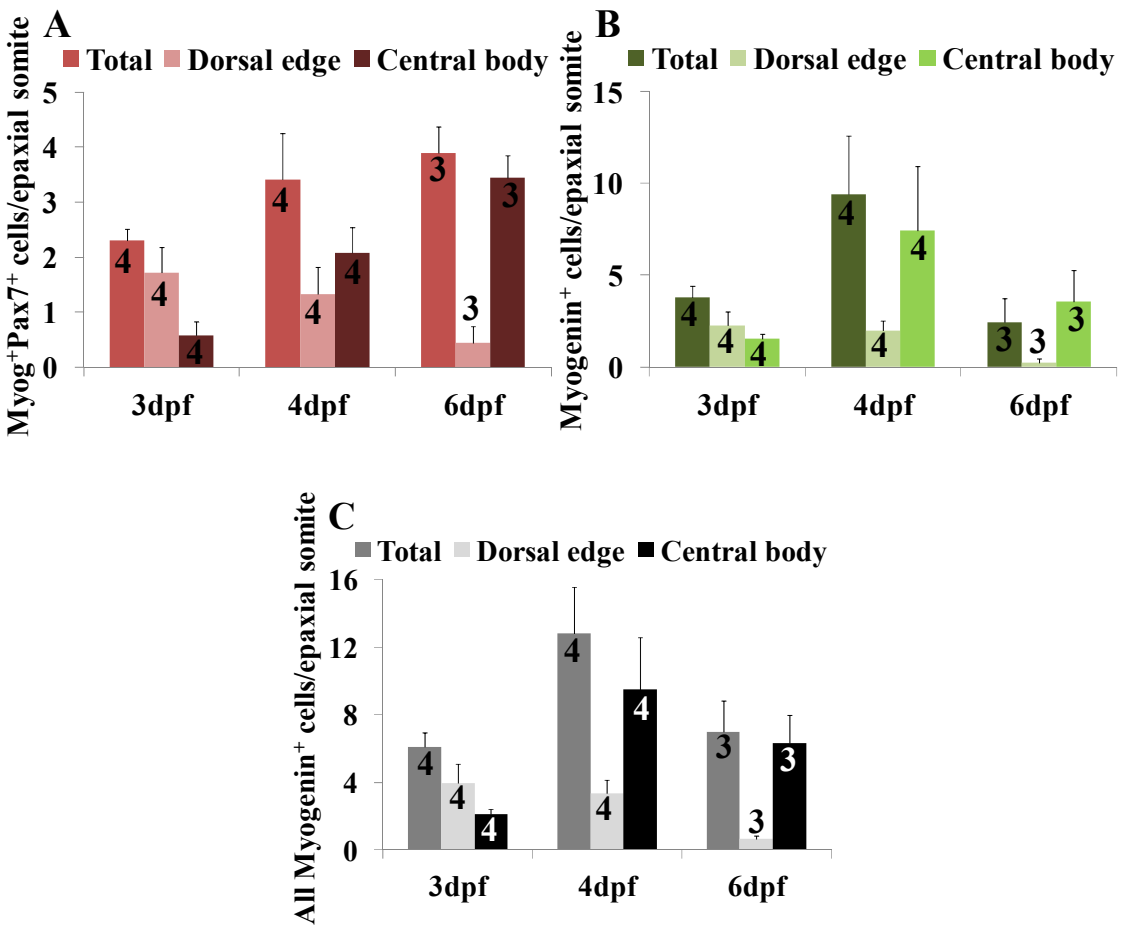


Fig. 3.13 Differentiating Pax7$^+$ cells increase significantly in the central body between 3 and 6 dpf. Wholemount wild type larvae (Fig. 3.4) were stained with Hoechst, anti-Pax7 and anti-Myogenin antibodies at 3, 4 and 6 dpf. Quantitation of Myogenin$^+$Pax7$^+$cells and Myogenin$^+$ cells was done by averaging the counts of three epaxial somites s16, s17 and s18 from confocal scans of the number of larvae indicated within bars. **A:** The number of total Myogenin$^+$ Pax7$^+$ (Myog$^+$Pax7$^+$) cells increases significantly between 3 and 6 dpf (p=0.02). The number of Myogenin$^+$Pax7$^+$ cells between 3 and 4 dpf (p=0.2) and between 4 and 6 dpf (p=0.67) is not significantly changed. The number of Myogenin$^+$Pax7$^+$ cells at the dorsal edge does not change significantly between 3 and 4 dpf (p=0.5), 4 and 6 dpf (p=0.2), as well as between 3 and 6 dpf (p=0.08). The number of Myogenin$^+$Pax7$^+$ cells in the central body significantly increases between 3 and 6 dpf (p=0.001). The number of Myogenin$^+$Pax7$^+$ cells significantly increases between 3 and 4 dpf (p=0.028) whereas no significant increase was seen between 4 and 6 dpf (p=0.086). **B:** The number of total Myogenin$^+$ cells does not change significantly between 3 and 4 dpf (p=0.08) as well as between 4 and 6 dpf (p=0.22). Similarly, the number of Myogenin$^+$ cells at the dorsal edge does not change significantly between 3 and 4 dpf (p=0.66) but shows a tendency towards decrease between 4 and 6 dpf (p=0.039). The number of Myogenin$^+$ cells in the central body does not change significantly between 3 and 4 dpf (p=0.09), 4 and 6 dpf (p=0.56) as well as between 3 and 6 dpf (p=0.12). **C:** Plot of all Myogenin$^+$ cells (cells expressing both

Myogenin and Pax as well as cells expressing Myogenin only) in epaxial somites. The total number of all Myogenin$^+$ cells does not change significantly between 3 and 4 dpf (p=0.08) as well as between 4 and 6 dpf (p=0.13). The number of all Myogenin$^+$ cells at the dorsal edge does not change significantly between 3 and 4 dpf (p=0.66) and shows a tendency for decrease between 4 and 6 dpf (p=0.039) and overall between 3 and 6 dpf (p=0.06). The number of all Myogenin$^+$ cells in the central body does not change significantly between 3 and 4 dpf (p=0.09), between 4 and 6 dpf (p=0.56) as well as overall between 3 and 6 dpf (p=0.12). Error bars are standard error of the mean.

3.3.6 Spatio-temporal dynamics of putative myogenic precursors is altered in *myod*^{fh261} mutants

To test the hypothesis that an enrichment of precursors expressing Pax7 and Myogenin correlates with muscle growth, *myod*^{fh261} mutants with perturbed growth were examined. Zebrafish *myod*^{fh261} mutants have a significantly reduced somitic muscle mass at 1 and 3 days post fertilization (Fig. 3.14-adapted from (Hinits et al., 2011)) and a greater than two-fold excess of precursor cells expressing Pax3/7 in the dermomyotome at 1 dpf (Hammond et al., 2007), suggesting altered precursor cell dynamics in the absence of a functional Myod. Interestingly, growth defect of the somitic muscle in *myod*^{fh261} mutants recovers by 5 dpf (Hinits et al., 2011). However, the fate of excess precursor cells in the dermomyotome of mutants reported at 1 dpf and the mode of growth recovery were unknown. Hence, the number and locations of Pax7$^+$ and Myogenin$^+$ cells in *myod*^{fh261} mutants were determined at 3 and 5 dpf with the aim to determine whether precursor cell dynamics in mutants reverts to *sibling* levels and, whether this reversal correlates with their growth recovery. Similar to previous findings at 1 dpf, the total number of Pax7$^+$ cells in *myod*^{fh261} mutants was elevated at 3 dpf compared to siblings (Fig. 3.15A,B). Moreover, the number of Pax+ cells in siblings was similar to that seen for wild type fish (Fig. 3.4B). However, unlike the greater than two-fold increase in Pax7$^+$ cells in 1 dpf larvae (Hammond et al., 2007), the Pax7$^+$ cells in mutants were elevated approximately 1.3 times that of siblings at 3 dpf (p=0.025, Fig. 3.15B). Further, by 5 dpf the number of Pax7$^+$ cells in the epaxial somite of mutants was similar to that in siblings, indicating that the number of Pax7$^+$ cells revert to normal levels correlating with growth recovery. The extra Pax7$^+$ cells in mutants at 3 dpf were predominantly in the deep myotome (p=0.019, Fig. 3.15C), at the central body location (p=0.003, Fig. 3.15D), specifically in the deep central body (p=9.24E-05, Fig. 3.15E), indicating that Pax7$^+$ cells in *myod*^{fh261} mutants

are located in the deep myotome earlier compared to siblings and wildtype fish (4 dpf, Fig. 3.7C). Thus, an enrichment of precursors expressing Pax7 and Myogenin correlates with the location of muscle growth in *myod*^{fh261} mutants.

If extra Pax7^{+} cells are differentiating in 3 dpf myod mutants, the location and number of Pax7^{+} cells expressing Myogenin should be increased in mutants compared to siblings. In siblings, the number of Pax7+Myogenin+ cells was similar to that seen in wildtype fish (Fig. 3.13A). In mutants, many more Pax7^{+}Myogenin^{+} cells could be observed in the central body at 3 dpf (Fig. 3.16A) and quantification in the central body region revealed that the total number of Pax7^{+}Myogenin^{+} cells and the number of Pax7^{+}Myogenin^{+} cells in the deep central body were significantly increased compared to siblings (p=4.9E-06 and p=4.6E-05 respectively, Fig. 3.16B). Also, a significantly higher percentage of Pax7^{+} cells in mutants expressed Myogenin (p=0.015, Fig.3.16C) suggesting that more Pax7^{+} cells in mutants were progressing towards differentiation.

Similar to the finding for the number of Pax7^{+} cells in mutants, the number of Pax7^{+} Myogenin^{+} cells also reverted to sibling levels by 5 dpf, correlating with recovery of myotome volume in mutants. At 3 dpf, the six fold increase in total number of Pax7^{+}Myogenin^{+} cells in *myod*^{fh261} mutants compared to siblings could indicate increased or stalled differentiation, in the absence of functional MyoD. This issue was addressed by quantitating the number of Myogenin expressing cells in the myotome of 3 dpf siblings and mutants with the expectation that an increased number of Myogenin alone expressing cells in mutants would suggest increased differentiation. Many more Myogenin^{+} cells were located in the deep myotome of mutants compared to siblings (Fig. 3.17A). In the central body, the total number of Myogenin expressing cells was increased by approximately five-fold in *myod*^{fh261} mutants compared to siblings at 3 dpf (p=0.0001, Fig. 3.17B), whereas at 5 dpf the total number of Myogenin expressing cells was similar between mutants and siblings (Fig. 3.17B). Similar to the extra Pax7^{+} and Pax7^{+}Myogenin^{+} cells, cells expressing Myogenin were specifically increased in the deep CB adjacent to muscle fibres (p=6.244E-05, Fig. 3.17B). Thus, the data indicate that at 3 dpf, extra Myogenin^{+} cells are present within the deep myotome of mutants and could give rise to new fibres by 5 dpf, leading to myotome volume recovery as well as a reduction in the number of extra precursors in *myod*^{fh261} mutants at 5 dpf.

To determine if extra precursors aid in myotome recovery, the number of myonuclei in transverse sections of epaxial somite 17 was examined in siblings and mutants at 3 and 5 dpf (Fig. 3.18). The number of nuclei per transverse section in mutants was approximately 1.6 fold lower than that in siblings (p=0.0006). At 5 dpf, the number of nuclei in siblings was greater by 1.21 fold compared to 3 dpf siblings (p=0.09) whereas in mutants the fold increase was 1.54 (p=0.0016). Co-incident with the nuclear increase, the myotome volume of 5 dpf siblings was 1.27 fold greater than 3 dpf siblings whereas the myotome volume of mutants was greater by 1.56 fold at 5 dpf compared to 3 dpf (Fig. 3.14). Further, at 5 dpf, the number of nuclei per transverse section of epaxial somite is similar between siblings and mutants (p=0.13). Thus the recovery of myotome volume in 5 dpf *myod*^{fh261} mutants is also reflected in the recovery of nuclear number in mutants.

To summarize, the data show that an increased number of Pax7^{+} and Myogenin^{+} precursor cells are present in *myod*^{fh261} mutants at 3 dpf. Further the number of precursors is significantly increased within the deep myotome compared to siblings. Myotome growth and nuclear number recover in 5 dpf *myod*^{fh261} mutants by a similar fold change coincident with a reduction in the elevated number of precursors and a significant increase in the number of myonuclei, strongly suggesting that the excess number of precursors contribute to muscle growth in the mutants.

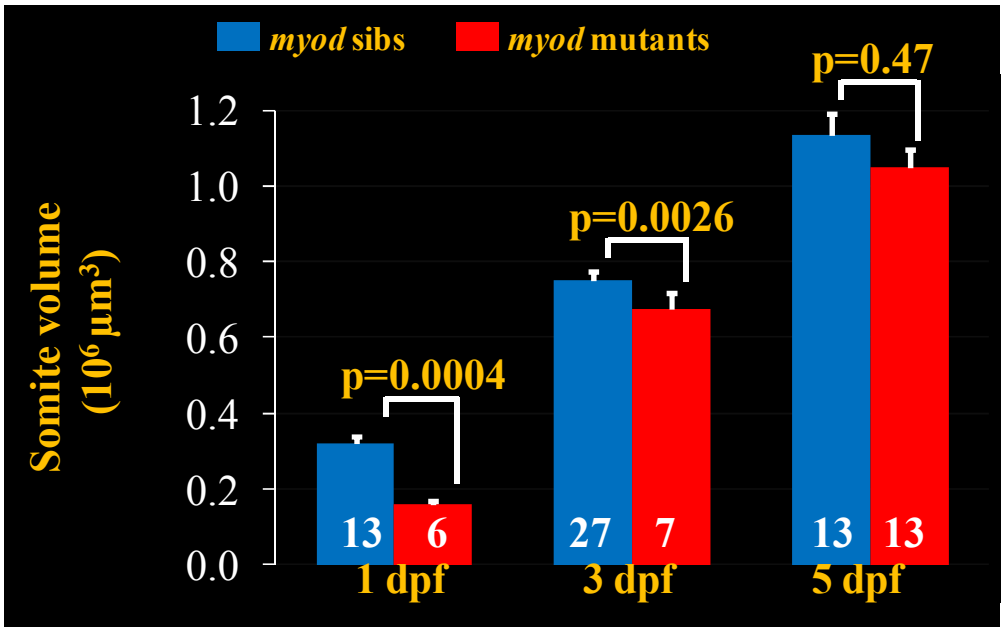


Fig. 3.14 Myotome growth recovers in 5 dpf *myod*^{fh261} mutants. ((Hinits et al., 2011) Experimental work in this graph was not performed by the candidate. The data from the authors was replotted by the candidate and is presented here for clarity. Myotome volume of somite 17 was measured in individual larvae at 1 dpf (n=13,6), 3 dpf (n=27,7) and 5 dpf (n=13,13). Myotome volume was significantly decreased in mutants compared to siblings at 1 dpf (p=0.0004) and 3 dpf (p=0.0026), but recovered at 5 dpf (p=0.47). Error bars are standard error of the mean.

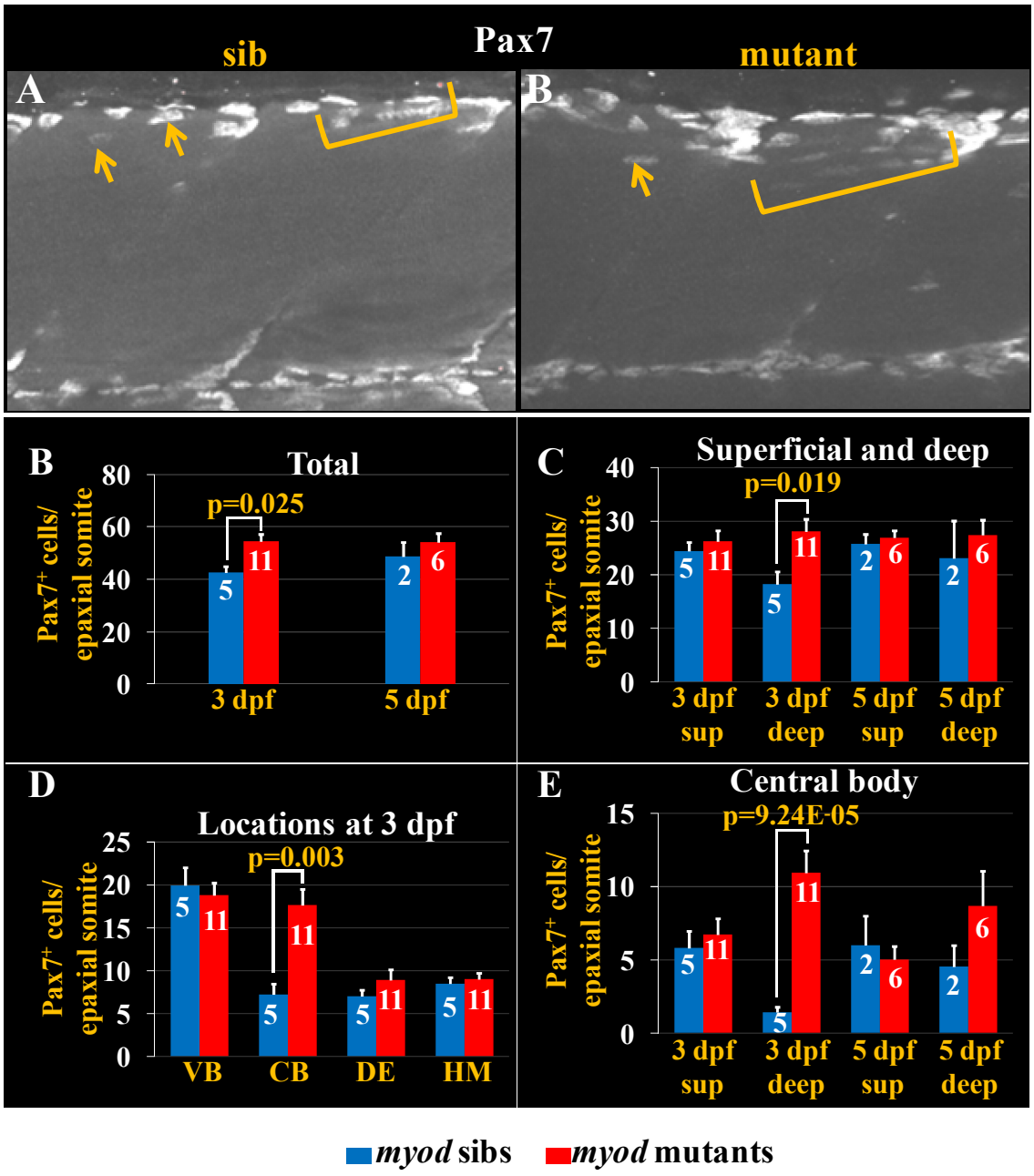


Fig. 3.15 Pax7^{+} cells revert to normal levels by 5 dpf in *myod*^{fh261} mutants.

Fig. 3.15 Pax7^{+} cells revert to normal levels by 5 dpf in *myod*^{fh261} mutants.
Wholemount siblings and *myod*^{fh261} mutants were stained with Pax7 antibody (white), A4.1025 (detecting myosin, not shown) and Hoechst33342 (detecting nuclei, not shown) at 3 dpf and 5 dpf. Confocal images (A,B) are short stacks of 9µm in the deep myotome of a sibling and mutant at 3 dpf showing Pax7 (white) expressing nuclei. Images are lateral views oriented with dorsal up and anterior to left. Quantitation of Pax7^{+} cells was done in siblings and *myod*^{fh261} mutants in the epaxial half of somite s17 from confocal scans of the number of larvae indicated within bars (B-E). **A:** Pax7 antibody stained cells in the deep central body of 3 dpf larvae appear more numerous in mutant myotome compared to siblings (arrows and bracketed region). **B:** The total number of Pax7^{+} cells is significantly increased in mutants compared to siblings at 3 dpf (p=0.025). The total number of Pax7^{+} cells at 5 dpf is similar between mutants and siblings. **C:** At 3 dpf, the number of Pax7^{+} cells in the superficial myotome is similar between siblings and mutants but significantly increased in the deep myotome in mutants compared to siblings (p=0.019). At 5 dpf, the number of Pax7^{+} cells in the superficial and deep myotome is similar between siblings and mutants. **D:** At 3 dpf, the number of Pax7^{+} cells in the central body (CB) is significantly increased in mutants compared to siblings (p=0.003). **E:** At 3 dpf, the number of Pax7^{+} cells is significantly increased in the deep central body in mutants compared to siblings (p=9.24E-05), whereas at 5 dpf, the number of Pax7^{+} cells is similar between siblings and mutants in both superficial and deep central body. VB: vertical borders, CB: central body, DE: dorsal edge, HM: horizontal myoseptum. Error bars are standard error of the mean.

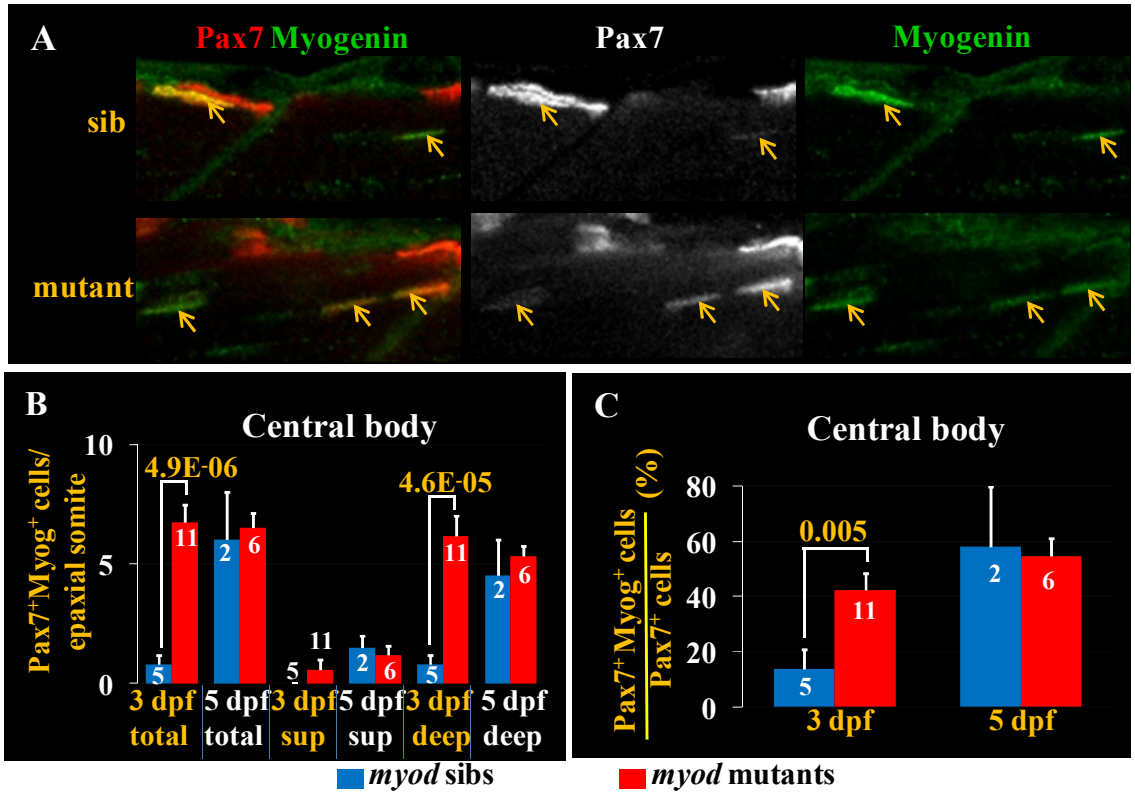


Fig. 3.16 Pax7^{+}Myogenin^{+} cells revert to normal levels by 5 dpf in *myod*^{fh261} mutants. Wholemount siblings and *myod*^{fh261} mutants were stained with Pax7 (red), Myogenin (green), A4.1025 (not shown) and Hoechst 33342 (not shown) at 3 and 5 dpf. Confocal images are single slices from a confocal stack of 3 dpf larvae. Images are single optical parasagittal sections oriented with dorsal up and anterior to left in the deep myotome. **A:** Pax7^{+}Myogenin^{+} cells appear more numerous in mutants compared to siblings at 3 dpf. **B,C:** Quantitation of Pax7^{+}Myogenin^{+} and Pax7^{+} cells was done in siblings and *myod*^{fh261} mutants in the epaxial half of somite s17 from confocal scans of the number of larvae indicated within bars (B,C). **B:** The total number of Pax7^{+}Myogenin^{+} cells in the central body is significantly increased at 3 dpf (p=4.9E-06), but similar to siblings at 5 dpf. The number of Pax7^{+}Myogenin^{+} cells in the superficial central body of siblings and mutants is similar at 3 dpf as well at 5 dpf. The number of Pax7^{+}Myogenin^{+} cells in the deep central body is significantly increased in mutants compared to siblings at 3 dpf (p=4.6E-05), but similar at 5 dpf. **C:** The fraction of Pax7^{+} cells expressing Myogenin is significantly greater in mutants compared to siblings at 3 dpf (p=0.005), but similar at 5 dpf. Error bars are standard error of the mean.

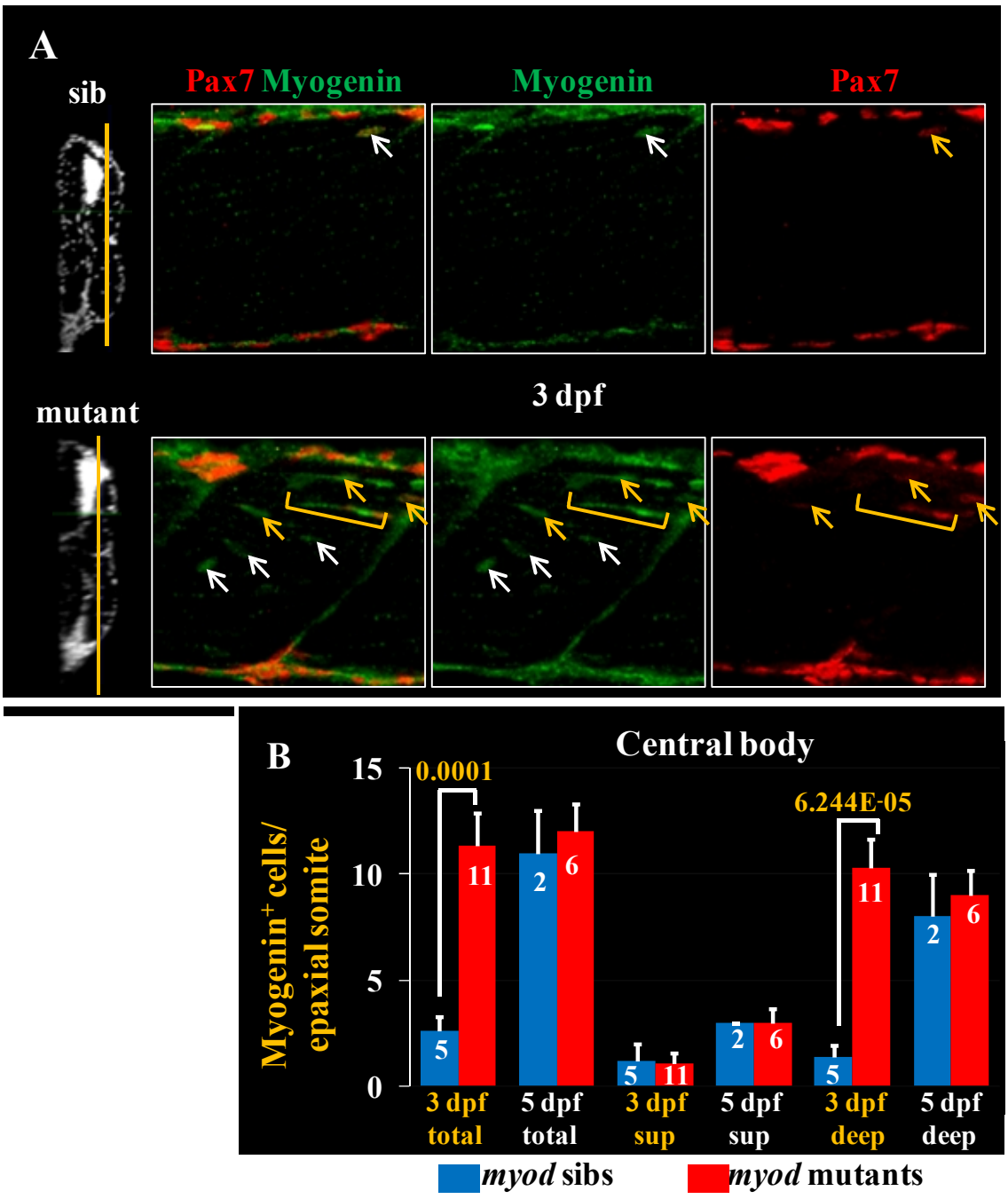


Fig. 3.17 Myogenin^{+} cells revert to normal levels by 5 dpf in *myod*^{fh261} mutants.

Fig. 3.17 Myogenin$^+$ cells revert to normal levels by 5 dpf in *myod*^{fh261} mutants. Wholemount siblings and *myod*^{fh261} mutants were stained with Pax7 (red), Myogenin (green) antibodies, A41025 (not shown) and Hoechst 33342(not shown) at 3 and 5 dpf. Confocal images are single slices from a confocal stack of 3 dpf larvae. Images are lateral sections oriented with dorsal up and anterior to left taken at the location indicated by the white line on transverse cross-sections. The slices are at a depth of 13.4µm in each larvae. Quantitation of all Myogenin$^+$ cells was done in siblings and *myod*^{fh261} mutants in the epaxial half of somite s17 from confocal scans of the number of larvae indicated within bars (C). **A:** Myogenin$^+$ cells appear more numerous in mutants compared to siblings at 3 dpf (white arrows). Some of these Myogenin$^+$ cells are also Pax7$^+$ (gold arrows). **B:** The total number of Myogenin$^+$ cells in the central body is significantly increased at 3 dpf ($p=0.0001$), but similar to siblings at 5 dpf. The number of Myogenin$^+$ cells in the superficial central body of siblings and mutants is similar at 3 dpf as well at 5 dpf. The number of Myogenin$^+$ cells in the deep central body is significantly increased in mutants compared to siblings at 3 dpf ($p=6.244E-05$), but similar at 5 dpf. Error bars are standard error of the mean. nt neural tube; nc notochord.

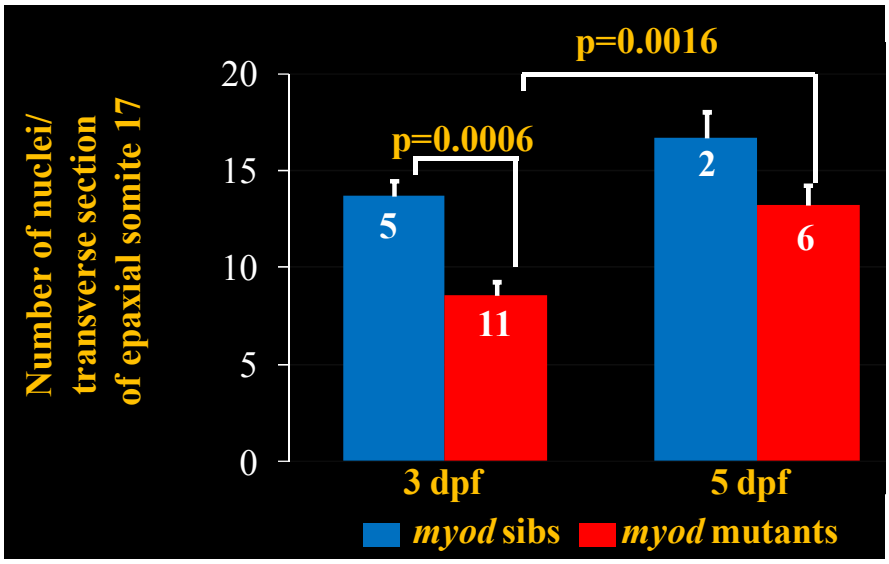


Fig. 3.18 Number of myonuclei in *myod*^{fh261} mutants increases by 1.5 fold between 3 and 5 dpf.

Wholemount siblings and *myod*^{fh261} mutants were stained with antibodies against Pax7, Myogenin, A4.1025 (detecting myosin) and Hoechst33342 (detecting nuclei) at 3 dpf and 5 dpf. Nuclei within the myosin stained region of the epaxial portion of somite 17 were counted and averaged from three transverse sections per larvae for the number of larvae indicated within bars. The number of nuclei is significantly decreased in mutants compared to siblings at 3 dpf (p=0.0006) but not at 5 dpf (p=0.12). The number of nuclei significantly increases in mutants between 3 and 5 dpf (p=0.0016). Error bars are standard error of the mean.

3.4 Discussion

3.4.1 Origin of Pax7$^+$ muscle progenitors in zebrafish muscle

The distribution of Pax7$^+$ cells in zebrafish somites can be categorized into five regions: the four borders and in the central portion of somites. At 3 dpf, majority of the Pax7$^+$ cells lie at the five regions superficially in the dermomyotome with increasing numbers observed within the myotome in the growing larva. There are similarities in the distribution of Pax7$^+$ cells in the zebrafish dermomyotome with that of the chick/mouse dermomyotome such that the dorsal edge in the former is a location similar to the dorsomedial lip in the latter, the horizontal myoseptum correlates with the ventrolateral lip, the anterior and posterior vertical borders in the fish correlate with the rostral and caudal dermomyotome lips respectively and the central body correlates with the central dermomyotome location. However, Pax7$^+$ progenitors that are involved in postnatal growth are primarily located in the central portion of the dermomyotome in mouse/chick and migrate into the myotome contributing to dermomyotome disintegration (Buckingham et al., 2006; Gros et al., 2005). They infiltrate the myotome and become progenitors for future muscle growth of the trunk. On the contrary, in zebrafish, the location of Pax7$^+$ cells at the borders and central body of the somites, suggests that the myotomal Pax7$^+$ cells do not exclusively arise from the central portion of the dermomyotome as in the mouse/chick (Ben-Yair and Kalcheim, 2005; Gros et al., 2005; Relaix et al., 2005). In other words, Pax7$^+$ progenitors in zebrafish muscle appear to arise from the borders/lips as well as the central portion of the dermomyotome. Lineage tracing studies using the transgenic Pax7:gfp fish should clarify the fate of Pax7$^+$ cells at each of the borders and central body.

3.4.2 The stem cell niche

A recent study using satellite cells isolated from mouse EDL muscle demonstrated that slowly dividing Pax7$^+$ cells are able to self-renew and maintain the precursor pool for a longer term compared to fast dividing Pax7$^+$ cells (Ono et al., 2012). Our data indicate that the frequency of Pax7$^+$ cells in S-phase varies with their somitic location in the zebrafish. A significantly greater proportion of Pax7$^+$ cells at the vertical borders are in S-phase, whereas the cells at the horizontal myoseptum are rarely in the S-phase. The low frequency of S-phase labeling in Pax7$^+$cells at the horizontal myoseptum suggests that

this location harbors a more slowly dividing population of Pax7$^+$ cells. Time-lapse imaging of cells at the horizontal myoseptum could provide clues to their self-renewal capacity while wounding studies could be used to determine their behavior during regeneration. As the self-renewal function of stem cells has been associated with the slowly dividing stem cells (Ono et al., 2012; Wagner et al., 2004), one possible view is that Pax7$^+$ cells at the horizontal myoseptum are more 'stem'-like.

Variation in the frequency of Pax7$^+$ cells in S-phase with location also suggests differential signaling or altered sensitivity to signals at the different borders and central body. Altered sensitivity to signals based on location is a common theme during development. For example, regionalization can influence cell fate during gastrulation (Parameswaran and Tam, 1995; Tam and Beddington, 1987). More recently, it was demonstrated that *fss/tbx6* is required to keep Pax7$^+$ cells in the central dermomyotome specifically from differentiating prematurely. Thus, investigation of signals that control proliferation kinetics at the borders could provide clues about the regulation and maintenance of niches at each location.

3.4.3 Number of somitic Pax7$^+$ cells in zebrafish larvae and larvae

The number of Pax7$^+$ cells in epaxial somites increases gradually from approximately 40 cells at 3 dpf to 60 cells at 6 dpf (Fig. 3.4). While the frequency of Pax7$^+$ cells in the S-phase could explain the increase in the number of cells between 3 and 4 dpf (approx. 8 cells), many Pax7$^+$ cells express myogenin, suggesting that they are primed for differentiation. Further, in the Pax7:gfp fish, gfp$^+$myogenin$^+$ as well as gfp$^+$myosin$^+$ cells are apparent indicating that Pax7$^+$ cells are likely lost by giving rise to muscle fibres. Hence, the apparent lack of decrease in the number of Pax7$^+$ cells between 3 and 6 dpf, suggests that Pax7$^+$ cells are be replenished by proliferation. Time lapse imaging of labeled Pax7$^+$ cells in the dermomyotome could clarify this issue.

Another study reported the number of Pax7 (antibody positive) and Pax7a:gfp (transgenic line) cells per somite of 1 to 5 dpf larvae (Seger et al., 2011). According to the data presented the number of Pax7$^+$ cells decrease to less than five by 5 dpf. This is in contrast to our observations with antibody labeled or Pax7:gfp cells using a distinct transgenic line. The difference between the counts could have arisen from the difference in method of antibody staining and counting. Initially, several different staining protocols were tried

to optimize the staining quality with DP312 (Fig. 3.19), Pax7 and Myogenin antibodies. Using high fixation (4% paraformaldehyde fix), one of the steps in the protocol used by Seger et al., 2011, I was able to obtain satisfactorily stained fish at 2 dpf (Fig. 3.19), but not at 3 dpf and older (data not shown). On the other hand, using a long-low fixation protocol (2% paraformaldehyde for 25 minutes) as I have done in my experiments, ensured labeling with dp312, Pax7 and Myogenin antibodies. Hence, differences in staining method are a likely reason behind the difference in the number of Pax7 antibody labeled cells between the two studies (approximately 3-10 in their studies versus 40-60 in mine). However, the number of gfp labeled $Pax7^{+}$ cells is also different between the two studies. The transgenic lines used are different in each study. As acknowledged by the authors (Seger et al., 2011), Pax7:gfp^{+} cells were not visible till 3 dpf with the transgenic line used in their study, lending credence to the idea that the line does not faithfully replicate the pattern of endogenous Pax7 expression. Further, the other study ignored all intensely gfp labeled cells on the premise that these were xanthophores. The transgenic line that I have used has a reduced number of xanthophores ranging from 3 to 5 per somite. Also, many of the $Pax7^{+}$ cells, especially those elongating to become fibres can be very bright. Hence, by eliminating all bright cells from $Pax7^{+}$ cell count, it is possible to arrive at a very low count of $Pax7^{+}$ cells

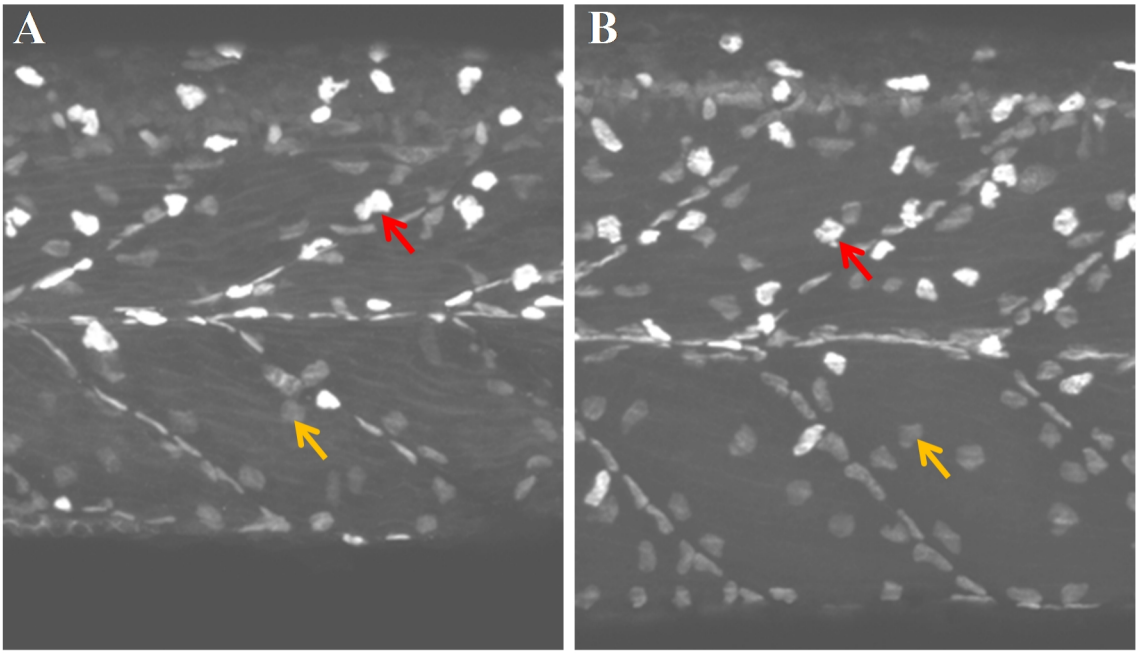


Fig. 3.19 Staining regimens tested for DP312 antibody staining
Zebrafish embryos at 2 dpf were fixed with 4% paraformaldehyde and incubated with primary antibody DP312 (detecting Pax3/7^{+} cells) overnight (A) or fixed with 2% paraformaldehyde and incubated with primary antibody for three overnights (B). Shrinkage is apparent in the 4% paraformaldehyde fixed tissue (A) compared to 2% (B). Images are short stacks showing the superficial myotome of larvae whole wholemount confocal stacks. Lateral images (A,B) are of larvae oriented with dorsal up and anterior to left. **A,B:** DP312 labeled cells (false coloured white) are apparent at locations where Pax7^{+} cells are found in the superficial myotome. Bright cells are xanthophores (red arrows) whereas dim cells are the Pax3/7^{+} myogenic cells (gold arrows).

3.4.4 A model of myotomal myogenesis

To assess the contribution of Pax7^{+} and Myogenin^{+} precursors to myotomal growth, a model of myotomal myogenesis is proposed based on the data from S-phase and Myogenin labeling. The data thus far indicate that the number of Pax7^{+} cells gradually increases in the central body and vertical borders of growing fish between 3 and 6 dpf. Approximately one-fifth of the Pax7^{+} cells at the vertical borders are in S-phase during at 3 dpf, suggesting an increase of approximately eight Pax7^{+} cells at this location. However, only four additional Pax7^{+} cells were found at this location at 4 dpf, suggesting a loss by some mechanism. In the central body, one-fifth of the fraction of Pax7^{+} cells are in S-phase and one-fifth express Myogenin, indicating a similar rate of generation of new

$Pax7^+$ and loss of $Pax7^+$ cells by differentiation, assuming the time taken by the cell to divide is similar to the time taken by a $Pax7^+Myogenin^+$ cell to become a muscle fibre. However, assuming that $Myogenin^+$ cells in the central body arose from $Pax7^+$ cells, the number of $Pax7^+$ cells proposed to be lost via differentiation further increases such that the fraction differentiating in the central body exceeds that dividing, which would create a net decrease in the number of $Pax7^+$ cells in the central body. Since $Pax7^+$ cells in the central body are seen to increase while and $Pax7^+$ cells at the vertical borders appear to be lost by some mechanism, the model predicts that extra $Pax7^+$ cells in the central body arise from the vertical borders.

The migration hypothesis is supported by the observations that superficial $Pax7^+$ cells at the vertical borders are seen extending into the superficial central body (Fig. 3.2A) as well as deep central body in live *pax7::*GFP; *pfe/pfe* transgenic larvae (Fig. 3.8J), suggesting that $Pax7^+$ cells or differentiating $Pax7^+$ cells ($Pax7^+Myogenin^+$) migrate from the vertical borders into the central body. However, since the duration for which a cell is in S-phase versus the length of time a cell expresses Myogenin prior to differentiating into a muscle fibre is unknown in our model. By crossing two lines of fish currently at our facility, *Myogenin:RFP* and *Pax7:GFP* the model can be tested by **a.** examining the dynamics of $Pax7^+Myogenin^+$ cells at the vertical borders **b.** following the transition time of a $Pax7^+Myogenin^+$ cell to $Myogenin^+$ cell **c.** Tracking and quantitating $Pax7^+$ and/or $Pax7^+Myogenin^+$ cells that migrate into the central body and differentiate into $Myogenin^+$ cells and **d.** examine the average transition time of $Myogenin^+$ cells to differentiate into muscle fibres.

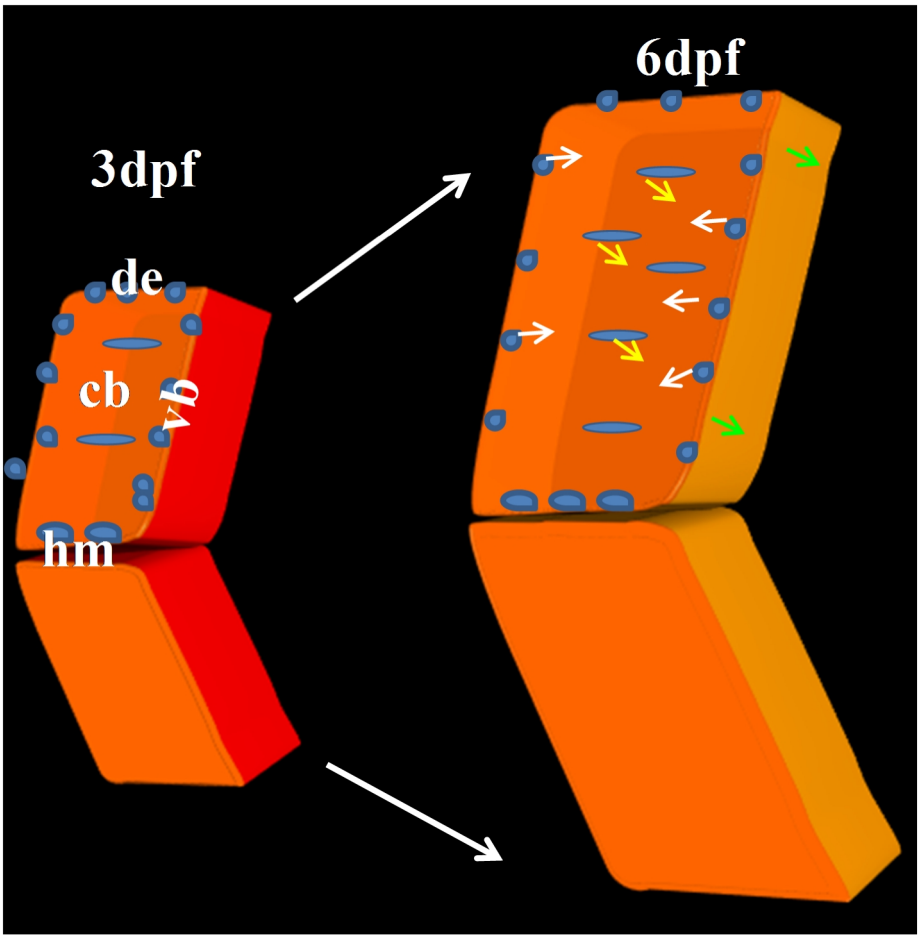


Fig. 3.20 Model of muscle growth and movement of Pax7^{+} precursor in 3-6 dpf zebrafish larvae.
In 3 dpf larvae, Pax7^{+} muscle precursors (blue cells) are found at the five locations in the epaxial somite: horizontal myoseptum (hm), dorsal edge (de), vertical borders (vb) and central body (cb). The somite grows between 3 and 6 dpf. Pax7^{+} cells at the vertical borders and central body of larvae older than 4 dpf migrate into the deeper myotome (yellow and green arrows). The model also predicts movement of Pax7^{+} cells located at the vertical borders into the superficial and deep central body (white arrows), acting as a source of myogenic cells for further growth of the myotome.

3.4.5 Regional variation in the proliferation behaviour of muscle precursors in growing zebrafish

Previous studies in mice, chick and zebrafish have quantified the fraction of $Pax7^+$ cells that are proliferating based on co-labeling with Ki67, BrdU or H3P (Gros et al., 2005; Hammond et al., 2007; Relaix et al., 2005; Seger et al., 2011). Of the two studies that quantified proliferative cells in zebrafish myotome, one was in 1 dpf larvae (Hammond et al., 2007) and the other in 4 dpf larvae (Seger et al., 2011). The study in 1 dpf larvae used an antibody (DP312) that detects Pax3 as well as Pax7 and detected the percentage of mitotic nuclei to be 4% of $Pax3/7^+$ cells per somite with phosphohistone H3. This translates to approximately 1.6 $Pax3/7^+$ mitotically active nuclei out of 40 $Pax3/7^+$ cells in a somite at 1 dpf. Since, phosphohistone H3 labels nuclei in the mitotic phase which itself is a small part of the cell cycle, it is likely that many more $Pax3/7^+$ proliferative cells are present in 1 dpf which are somewhere between in S-phase and M-phase in the cell cycle. The study in 4 dpf larvae (Seger et al., 2011) labeled transgenic $Pax7a:gfp^+$ fish with a 15 minute pulse of BrdU prior to fixation. Their data shows approximately 1 $BrdU^+$ $Pax7a:gfp^+$ cell per three $Pax7a:gfp^+$ cells per somite in 4 dpf fish using a 15 minute BrdU pulse. This translates to 33% $Pax7a:gfp^+$ cells per somite in 4 dpf fish. Our data indicate that 8.65 $Pax7^+$ cells out of 47.42 $Pax7^+$ cells in epaxial somite co-label with BrdU after a one hour BrdU pulse. In other words, about 18% of $Pax7^+$ (antibody-labeled) cells are also $BrdU^+$ in the epaxial somite. The difference in percentages between the two studies is likely the number of $Pax7^+$ cells in each case. The data presented in this thesis show that Pax7+ cells in the myotome divide less frequently than that reported in a previous study (Seger et al., 2011), consistent with the finding that Pax7 is co expressed with Myogenin in some precursors en route to terminal differentiation.

Our study indicates that few $Pax7^+$ cells at the horizontal myoseptum are in S-phase versus those in the central body. Interestingly, in juvenile and adult zebrafish, more mitotically active $Pax7^+$ cells (detected by phosphohistone H3) were reported at the horizontal myoseptum in contrast to $Pax7^+$ cells in the central body (Hollway et al., 2007). They reported that $Pax7^+$ cells in the deep myotome situated adjacent to muscle fibres were located under the basal lamina from 7 dpf onwards. Since the study did not quantitate these observations; it is difficult to draw comparisons based on percentages

and number of proliferating cells. Qualitatively, the data is suggestive of a shift of the $Pax7^+$ cells into quiescent satellite–cell like positions in the deep myotome of the growing juvenile.

3.4.6 Myogenin expression in Myod mutants

In zebrafish *myod*^{fh261} mutants the number of $Myogenin^+$ cells is significantly increased. This is in contrast to studies that showed a delay or reduction in Myogenin expression in the absence of MyoD (Cornelison et al., 2000; Hinits et al., 2009; Kablar et al., 1997; Pannese et al., 1995; Sabourin et al., 1999; Sabourin and Rudnicki, 1999; Yablonka-Reuveni et al., 1999). However, concurrent with other studies, muscle differentiation and growth is delayed suggesting that transition of precursors to myotubes is delayed. Moreover, my data indicate that an increase in the number of Myogenin+ precursors does not correlate with faster differentiation but correlates with muscle growth.

It is not clear from my studies as to what drives Myogenin expression in Myod mutants in the absence of functional Myod. Myf-5 expression was four-fold higher in mouse mutants of Myod (Rudnicki et al., 1992), suggesting that Myf-5 might compensate for Myod loss. Similarly in fish, both myf5 and myod knockdown were required to ablate mef2d, indicating a compensatory role of myf5 (Hinits et al., 2009). However, the significant increase in the number of precursors expressing Myogenin is not clear. Among many molecules proposed to interact with myod to transcriptionally reduce myogenin levels, mitogen activated protein kinase p38gamma was found to alter the number of myogenin positive precursors. Mitogen-activated protein kinase p38gamma temporally regulates Myogenin expression via Myod (Gillespie et al., 2009). Specifically, it was shown that when p38gamma phosphorylates Myod, a repressor Myod complex occupies Myogenin transcription site, thereby blocking Myogenin expression. Satellite cell from mutant mice lacking p38gamma showed a 40% increase in the number of Myogenin expressing precursor cells. Also, mutating the phosphorylation sites on Myod markedly reduced repressor complex binding to myogenin promoter, leading to increased activation of myogenin. Thus it is plausible that in the absence of Myod, the p38gamma-regulated repressor complex is not formed, allowing for excess Myogenin expression.

I have found significantly increased number of $Pax7^+$/$Myogenin^+$ cells in the deep myotome at a time when these cells are not common at that location. This could be

interpreted in two ways (a) the cells are more migratory (b) an excess of these cells is present in the dermomyotome at 1 dpf and the excess in the deep myotome at 3 dpf is simply a function of the increased number of cells in mutants (c) contact inhibition in the dermomyotome due to overcrowding by an excess number of cells causes a translocation of $Pax7^{+}$ and $Myogenin^{+}$ cells into the myotome. It is interesting to note that PEA3 transcription factor, correlated with metastatic potential of mammary adenocarcinomas (Trimble et al., 1993) was found to be increased 6-fold in Myod deficient myoblasts (Sabourin and Rudnicki, 1999), suggesting that Myod deficient myoblasts are likely to be more migratory. While it remains unknown whether PEA3 expression is increased in zebrafish *myod*^{fh261}mutants *in vivo*, time-lapse imaging of precursors in zebrafish Myod mutants could be used to investigate their migratory behaviour.

3.5 Conclusion

In conclusion, Pax7+ cells appear to be involved in muscle growth in growing zebrafish between 3 and 6 dpf likely by differentiating into Myogenin+ cells. The horizontal myoseptum and dorsal edge appear to harbour slowly dividing Pax7+ cells compared to the vertical borders and central body regions, suggesting differences in their functional role. A manner to test the correlation between proliferation kinetics and precursor cell function is to observe the behaviour of precursor cells during regeneration. Thus, in the following chapter, the spatiotemporal dynamics of muscle precursors is investigated following acute mechanical muscle injury in 3 to 6 dpf fish.

Chapter 4: Characterization of muscle regeneration in zebrafish

4.1 Summary

The spatiotemporal dynamics of muscle precursors and immune cells was investigated following acute mechanical muscle injury in 3 to 6 dpf fish. Specifically, the dynamics of $Pax7^+$ cells, $Myogenin^+$ cells, neutrophils and macrophages was examined during muscle regeneration in zebrafish larvae. Wounds were created by mechanical lesions using a fine needle. The earliest immune cells in wounds were found within an hour post injury whereas $Pax7^+$ myogenic cells were found within 18 hours following injury, time by which immune cells had exited the wound. Distinct muscle fibres arose within 48 hours post injury and were preceded by a significant increase in the number of $Pax7^+$ and $Myogenin^+$ cells in the wound. Proliferating $Pax7^+$ cells were predominantly located at the vertical borders of wounded and adjacent unwounded muscle whereas differentiating cells were predominantly located in the central body similar to that found in Chapter 3. Thus, destroying the niche at the various locations did not alter the functional behavior of $Pax7^+$ cells observed in the intact niches pre-wounding. The number of Myogenin expressing cells returned to normal levels by 3 dpw whereas the number of $Pax7^+$ cells in S-phase remained elevated in wounded muscle, likely leading to the persistence of $Pax7^+$ cells within the regenerated muscle at three days post injury although bulk of the muscle was repaired by this time. We propose that the vertical borders harbour $Pax7^+$ cells involved in muscle regeneration and muscle precursors express Myogenin on their way to terminal differentiation, in the growing zebrafish.

4.2 Introduction

Skeletal muscle injury in humans and animals can occur from exercise, trauma, diseases and disuse. Repair occurs by the fusion of muscle progenitor cells (satellite cells in adults) to damaged fibres, thereby repairing them, or to each other to form new fibres (Bintliff and Walker, 1960; Konigsberg et al., 1960; Cooper and Konigsberg, 1961; Mintz and Baker, 1967; Snow, 1978; Partridge et al., 1978; Lipton and Schultz, 1979; Grounds et al., 1980; Watt et al., 1982; Capers, 1960). Tritiated thymidine labeling studies suggested that myoblasts involved in muscle repair largely arise from resident muscle stem cells known as satellite cells in adults (Reznik, 1969; Snow, 1977; Snow, 1978) while in the developing embryo, myoblasts that aid in muscle growth are likely the precursors of the satellite cells in adults (Church, 1969; Relaix et al., 2005; Reznik, 1976). Studying muscle stem cells during muscle repair can provide therapeutic insights for many instances of muscle degeneration. Hence, numerous studies have characterized the process of muscle regeneration in different animal models with an aim to improve our understanding of the behaviour and regulation of satellite cells during muscle repair. Following muscle injury, there is a degenerative phase during which macrophages and neutrophils invade muscle wounds and clear out debris (Lescaudron et al., 1999). During this degenerative phase the wound is characterized by a lack of healthy muscle and a reduction in the number of myonuclei (Snow, 1978). This phase is followed by the proliferative phase during which activated satellite cells or myoblasts increase in number and some of them differentiate to give rise to regenerated muscle fibres. Some myoblasts do not differentiate and return to quiescence (Collins et al., 2005; Zammit et al., 2004). Electron microscopy was the key method used to identify satellite cells by their location under the basal lamina (Mauro, 1961) and their activated morphology during repair (Reznik, 1969; Snow, 1977; Snow, 1978), until reliable molecular markers for identifying satellite cells and myoblasts by optical methods were established. **Pax7**, **Myf5, Myod and Myogenin** (and others such as Mrf4, Mef2, c-met, m-cadherin) are some of the commonly used molecular markers in wounding studies to identify muscle progenitor cells. Myogenin is especially useful as an early marker of myoblasts that are likely to differentiate (Devoto et al., 2006; Grounds, 1992). To summarize, muscle wounds are invaded by different types of cells, initially

immune cells followed by myogenic cells. Moreover, molecular markers can be used to follow the behaviour of muscle precursors during muscle repair.

Current understanding of muscle repair comes from studies in adult vertebrate models of muscle repair, based on *in vitro* or *ex vivo* observations. The difficulty of imaging the muscle repair process in the live animal has hampered efforts to analyse muscle stem cell regulation within the niche. With this in mind, a number of groups have turned to the zebrafish, in which optical clarity permits lineage tracing and monitoring of individual identified cells in vivo over long periods (Seger et al., 2011; Stellabotte et al., 2007). Zebrafish models of a number of muscle-degenerative diseases have been generated (Bassett, 2004; Hall and McDonnell, 2007). Satellite cells marked by Pax7 have been reported in a variety of teleost species, including zebrafish (Hollway et al., 2007). Teleost fish including zebrafish have been reported to efficiently repair muscle wounds (Camargo, 2004; Erazo-Pagador, 2001; Rowlerson et al., 1997). The study on adult zebrafish muscle wounds described the muscle repair process to be similar to mammalian models with respect to the cascade of events (Rowlerson et al., 1997). However, to date, studies in fish have been hampered by the inability to follow individual live fish through the repair process. A key advantage of using the embryonic and larval zebrafish to study muscle regeneration is the ability to follow the recovery process in live individuals at the microscopic level, complementing data obtained from fixed specimens at certain time points. Using a combination of live *in vivo* imaging and fixed wholemounts, the dynamics of individual muscle progenitor cells can be studied in a spatiotemporal manner, allowing a deeper understanding of their behaviour during regeneration. Increased understanding can then be used to formulate and test hypotheses regarding the regulation of progenitor cell behaviour.

Currently, little is known about the process of muscle repair and behaviour of muscle progenitor cells during repair in vertebrate embryos/fetuses. **Wound repair in embryos/fetuses** came to be studied to understand the wound healing process in fetuses post reconstructive surgery in the womb. In fetal wound healing models involving the skin/epithelial tissues, scarring was found to be variable (Adzick and Longaker, 1991), depending on the animal model, day of fetus at wound, extent of wound (Cass et al., 1997) and also the extent of inflammation (Armstrong, 1995; Hurley, 1994). A few studies that

have wounded striated muscle tissue in addition to epithelial and other tissues in fetuses have generally reported muscle tissue healing in fetal rat cheek (Robinson, 1981), fetal rat and mouse upper lip (Rowsell, 1984; Whitby, 1991) and fetal mouse naso-labial (Nakasone et al., 2007) wounds, but not in the diaphragmatic wounds of fetal sheep (Longaker, 1991). A number of the above mentioned studies reported observing tissue loss and the absence of normal looking muscle at 1 day post wounding (dpw) (Nakasone et al., 2007; Rowsell, 1984; Whitby, 1991) followed by the appearance of striated myotubes by 2 dpw (Nakasone et al., 2007; Rowsell, 1984) and muscle tissue appearing healed between 3-5 dpw (Nakasone et al., 2007; Rowsell, 1984; Whitby, 1991). However, it was unclear whether healed muscle arose due to muscle regeneration linked to myoblast proliferation and differentiation. Further, these studies did not stain for myosin to detect the time course of myofibre recovery. A recent but limited study on skeletal muscle wound repair in *Pax7a:gfp* zebrafish larvae reported an increase in Pax7:gfp^{+}BrdU^{+} myoblasts within 1 dpw (Seger et al., 2011). However, this study did not provide a time line of appearance of muscle fibres followed by muscle recovery. Further, this study did not investigate the spatiotemporal dynamics of myoblasts expressing Pax7 and an early differentiation marker Myogenin during muscle regeneration.

In order to obtain evidence that Pax7-marked myogenic cells are involved in fibre regeneration in zebrafish, in this chapter, using various markers in live and fixed embryos/larvae, I have characterized a timeline of muscle repair in zebrafish larvae in addition to providing a spatiotemporal relationship of the myoblasts involved in muscle regeneration. Demonstrating that Pax7 and Myogenin marked cells are involved in muscle regeneration would justify further studies to follow the behavior of these cells in order to understand their cellular behavior and regulation *in vivo*. Immune cells play a role in modulating the behavior of myogenic precursors at various stages of myogenesis (Chazaud et al., 2009; Sonnet et al., 2006).

To date, a description of the spatiotemporal dynamics of immune cells in embryonic/larval muscle repair is lacking. Using two zebrafish transgenic lines expressing GFP in macrophages or neutrophils, I provide a characterization of the acute inflammatory response to muscle wounding.

4.3 Results

4.3.1 Muscle wounds repair within 7 days post injury

To determine the timeline of muscle wound repair in zebrafish larvae, 2.5-3.5 day old zebrafish were wounded in epaxial somites and the wounded and adjacent unwounded somites were imaged by Differential Interference Contrast (DIC) microscopy between two and six days post wounding (dpw). The wounded regions showed a reduction in birefringence and appeared as a dark region compared to unwounded areas which reflected regular birefringence pattern and showed striations in the muscle (Fig. 4.1). Since muscle fibres aligned in their regular pattern are highly birefringent, the absence of striations in the wounded regions indicates structural changes in muscle fibres at the wound site leading to an interruption in the regular alignment of fibres.

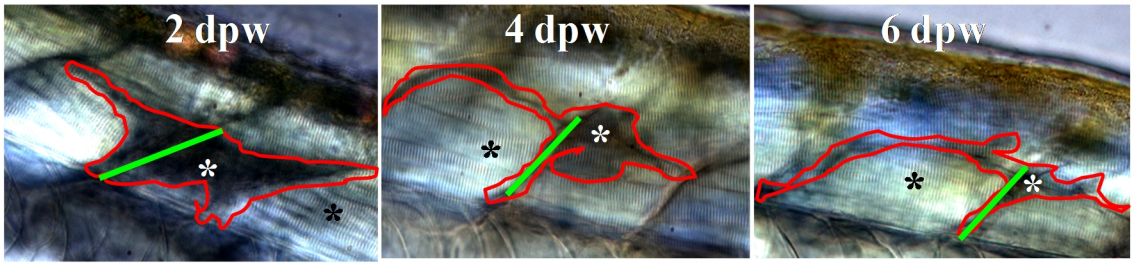


Fig. 4.1 Reduction of non-birefringent area in muscle wounds.
DIC images of an embryo wounded in somites 15-16 with a fine needle at 2.5 dpf and imaged at two, four and six days post wounding. Images are lateral views with dorsal up and anterior to left. Wound region is outlined in red. Green line highlights the somite boundary. The striated pattern of muscle in the unwounded region marked by black asterisks is absent in the wounded region (white asterisks). The non-birefringent region appears to reduce between two and six days post wounding. dpf: days post fertilization; dpw: days post wounding.

To examine the rate of muscle recovery, reduction in the area of the dark region in wounded somites was estimated from DIC images (Fig. 4.2) using Image J software. The dark region representing the wound occupied on an average 20% of the wounded epaxial somites at two days post wounding, reducing below 10% by four days post wounding and was close to 5% by six days post wounding. The rate of disappearance of the dark area between two and four days post wound appeared to be similar to that between four and six days post wound. Since, a larger dark region was present at two days post wound the data suggests that rate of muscle repair is similar for smaller and bigger wounds. This

was a counter-intuitive result since a smaller wound might require less repair and hence be expected to heal faster.

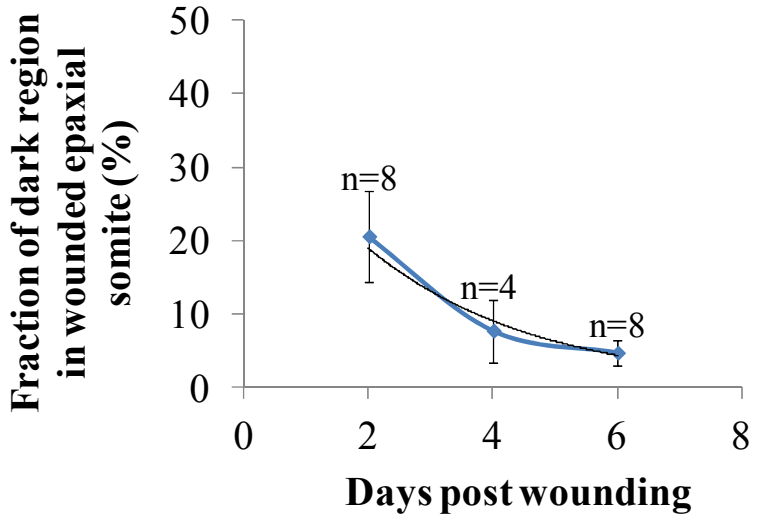


Fig. 4.2 Average wound area reduction with time.
Quantification of the reduction in the non-birefringent area in wounded epaxial somites of the indicated numbers of fish. Two to four epaxial somites within somites 5-12 were wounded in 2.5 dpf embryos and the same eight fish were imaged on two and six days post wounding. On day four post wounding four out of the eight fish were imaged. The area of wounded somites was calculated using Image J. Reduction in wound area was averaged for the indicated number of fish on days two, four and six post wounding and plotted against time. The grey line in the graphs is the exponential curve fitted to the data. Error bars are standard error of the mean.

To confirm the DIC result by another imaging technique, wounds in fish expressing green fluorescent protein (gfp) in their slow fibres were imaged by confocal microscopy (Fig. 4.3). Area of the dark wound region lacking gfp was calculated by using Image J software as described in Section 2.3. A significant loss of gfp^+ fibres was observed in the wounded somites at 1 dpw whereas adjacent somites appeared unaffected. By 2 dpw, small fibres containing GFP were observed extending into the wound. The wound area appeared largely covered with green fibres at 3.5 dpw and the wound region appeared similar to the adjacent unwounded somites except minor patterning defects at 4.5 dpw.

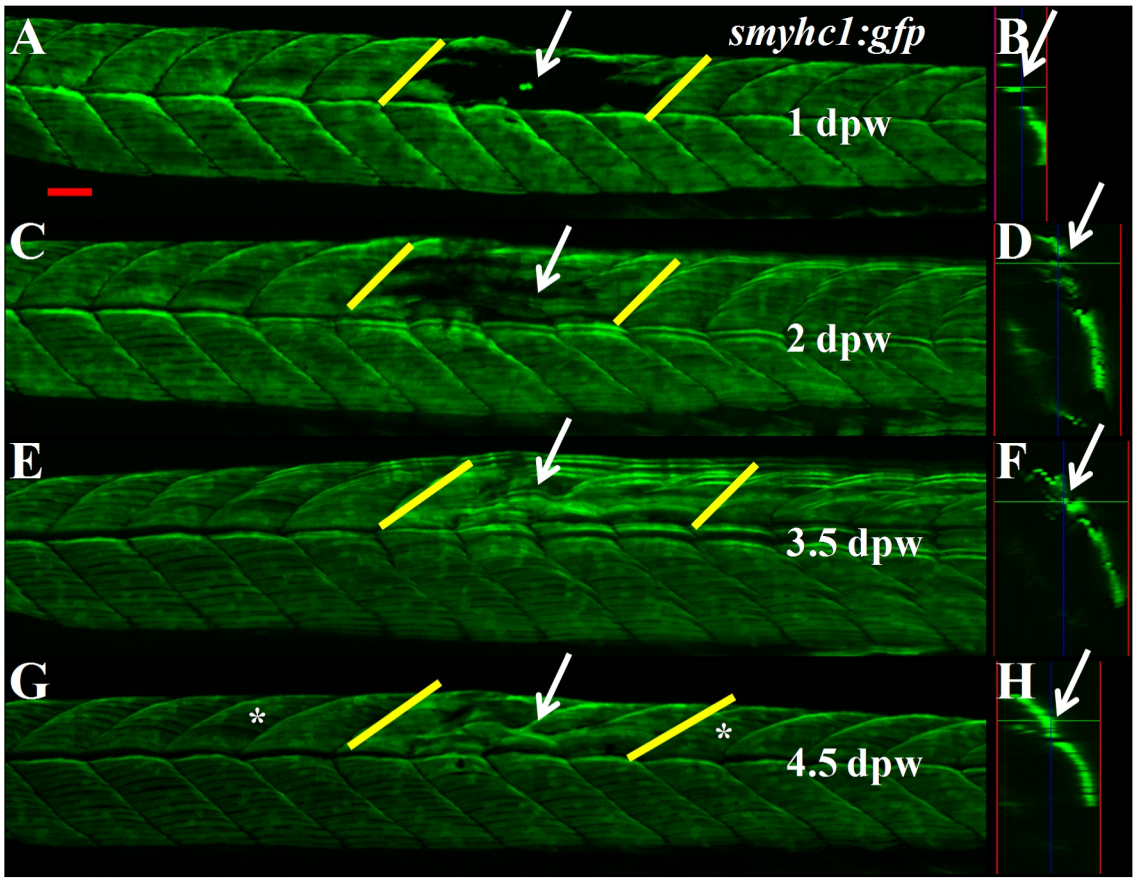


Fig. 4.3 Confocal imaging of wound repair in live embryos.
Slow muscle repair in a transgenic zebrafish expressing gfp in slow fibres [Tg(9.7kb smyhc1:gfp)^{i104}]. The fish was mechanically wounded in epaxial somites 15-18 at 3 dpf and imaged at 1, 2, 3.5 and 4.5 dpw by confocal fluorescence microscopy. Images are maximum intensity projections of confocal stacks of the wholemount fish. Lateral (A,C,E,G) and transverse (B,D,F,H) views are with anterior to left, dorsal up. Crossbars in transverse sections correspond to the region pointed to by arrows in lateral sections. Yellow bars in panels A,C,E,G demarcate the wounded epaxial somites from the adjacent unwounded somites. **A,B:** Wounded epaxial somites (arrows) lack gfp$^+$ fibres at 1 dpw. **C,D.** Gfp$^+$ fibres are visible at 2 dpw (arrows). **E,F:** Majority of the dark region in A is filled with gfp$^+$ fibres by 3.5 dpw. **G,H:** The wound region filled with gfp$^+$ fibres (arrows) appears less regularly patterned compared with adjacent unwounded somites at 4.5 dpw (asterisks, G). Scale bar 50 µm.

To examine the rate of muscle recovery, reduction in the area of the dark region in wounded somites was estimated from confocal images of the wounded embryo in Fig. 4.3 using Image J software (Fig. 4.4). At 1 dpw, approximately 70% of the wounded epaxial somites lacked slow muscle fibres. By 2 dpw, only 30% of the wounded epaxial somites lacked fibres, suggesting that more than half of the wound area was filled by

muscle fibres between 1 and 2 days post wound. By 3.5 dpw, 10% of the wound remained unfilled with fluorescent fibres whereas by 4.5 dpw, the entire wounded region appeared to be filled with fibres. Thus, regenerating fibres in zebrafish larvae muscle wounds appear to arise by 2 dpw and the rate of repair appears to be independent of wound size.

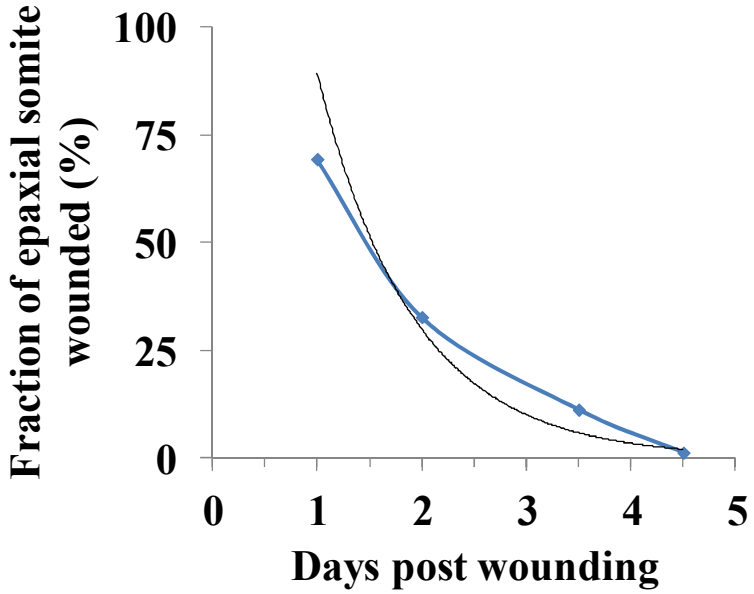


Fig. 4.4 Rate of wound resolution is independent of projected wound area. Quantification of reduction in the dark region of wounded epaxial somites of fish in Fig. 4.3. The area of the wounded region was calculated using Image J. Reduction in wound area was plotted against time. The grey line in the graphs is the exponential curve fitted to the data.

Comparison of the wound region at 6 dpw in DIC image (Fig. 4.1) and that at 4.5 dpw in confocal image (Fig. 4.3), suggests that the minor patterning defects visible in the confocal image are likely viewed as the non-birefringent area in the DIC image. Hence, the 5% dark region in muscle wounds at 6 dpw (Fig. 4.2) is likely a reflection of patterning defects as observed in Fig. 4.3, instead of a region devoid of regenerating muscle fibres.

Slow muscle in zebrafish larvae constitutes a tiny fraction of the somitic trunk muscle whereas bulk of the trunk muscle is composed of fast fibres. It is not known whether the fast muscle repairs at a similar rate as the slow muscle. Hence, 8-20 fish expressing gfp in slow or fast fibres were wounded and repair was examined by confocal microscopy.

4.3.2 Slow and fast muscle fibres regenerate at a similar rate

To compare the rate of appearance of regenerating slow and fast fibres, large numbers of *smyhc1:gfp* and *mylz2:gfp* zebrafish were wounded at 3.5 dpf. GFP labelled slow and fast fibres were lost at the wound site at 1 dpw (Fig. 4.5A). Potential regenerating fibres could be seen in the wound site by 2 dpw and more than half of the dark region lacking muscle was covered with fluorescent fibres by 3 dpw. Emergence of muscle fibres in the wound region appeared to reach a plateau between 5 and 7 dpw, although remodeling appeared to be ongoing such that at 7 dpw the wounded muscle appeared less disarrayed compared to 5 dpw. The data indicate that both slow and fast fibres arise within 2 dpw in zebrafish larvae muscle wounds. Quantitative comparison of muscle recovery by fibre type across a population of wounded fish unexpectedly showed that slow and fast fibre wounds recovered at a similar rate (Fig. 4.5B) and moreover that fast fibres repair better compared to slow fibres. Since there are only 8 to 12 slow fibres versus more than a hundred fast fibres in an epaxial somite (Devoto et al., 1996), the finding that fewer defects are apparent in repaired fast muscle compared to slow muscle could arise due to a similar number but a smaller fraction of fibres showing defects in fast muscle.

In addition to minor defects in the orientation of some slow fibres in the repaired muscle slow muscle was also seen at ectopic locations in wounded somites, where it is normally not present. The slow muscle layer in zebrafish embryos/larvae is organized in a monolayer beneath the skin and superficial to fast muscle. Surprisingly, slow muscle fibres could be detected in the deep fast fibre region of wounded larvae fixed and stained for immunodetection of F59 antibody at 2 dpw (Fig. 4.6A), 3 dpw (Fig. 4.6B) and 7 dpw (Fig. 4.6C). Slow muscle fibres can be distinguished from fast muscle fibres as F59 strongly stains the slow muscle whereas fast muscle is weakly stained. Slow muscle fibres in the deep fast muscle region were also observed in live and fixed *smyhc1:gfp* embryos (Fig. 4.6D-G). Some of the myotube like structures expressing slow myosin within the deep fast muscle were associated with multiple nuclei (Fig. 4.6G,H) suggesting that either slow myosin is expressed in the early regenerating fast fibres in zebrafish which later change to the fast form or that slow fibres regenerating within an area of fast fibres begin to shift from slow to fast phenotype. Quantification revealed that deep slow fibres were present in the majority of wounded embryos between 2 and 7 dpw (Table 1, Fig. 4.6).

Moreover, quantification of the number of wounded embryos with deep slow fibres by following the same set of live embryos between 2 and 7 dpw suggested a reduction in the number of embryos with deep slow fibres at 7 dpw. Such a reduction could occur due to a shift in the phenotype of deep slow fibres to the fast form. To summarize, the data indicate that wound region is devoid of healthy muscle at 1 dpw and new fibres arise by 2 dpw. To examine the changes in muscle wounds at the molecular level wounded embryos were stained for the immunodetection of structural proteins.

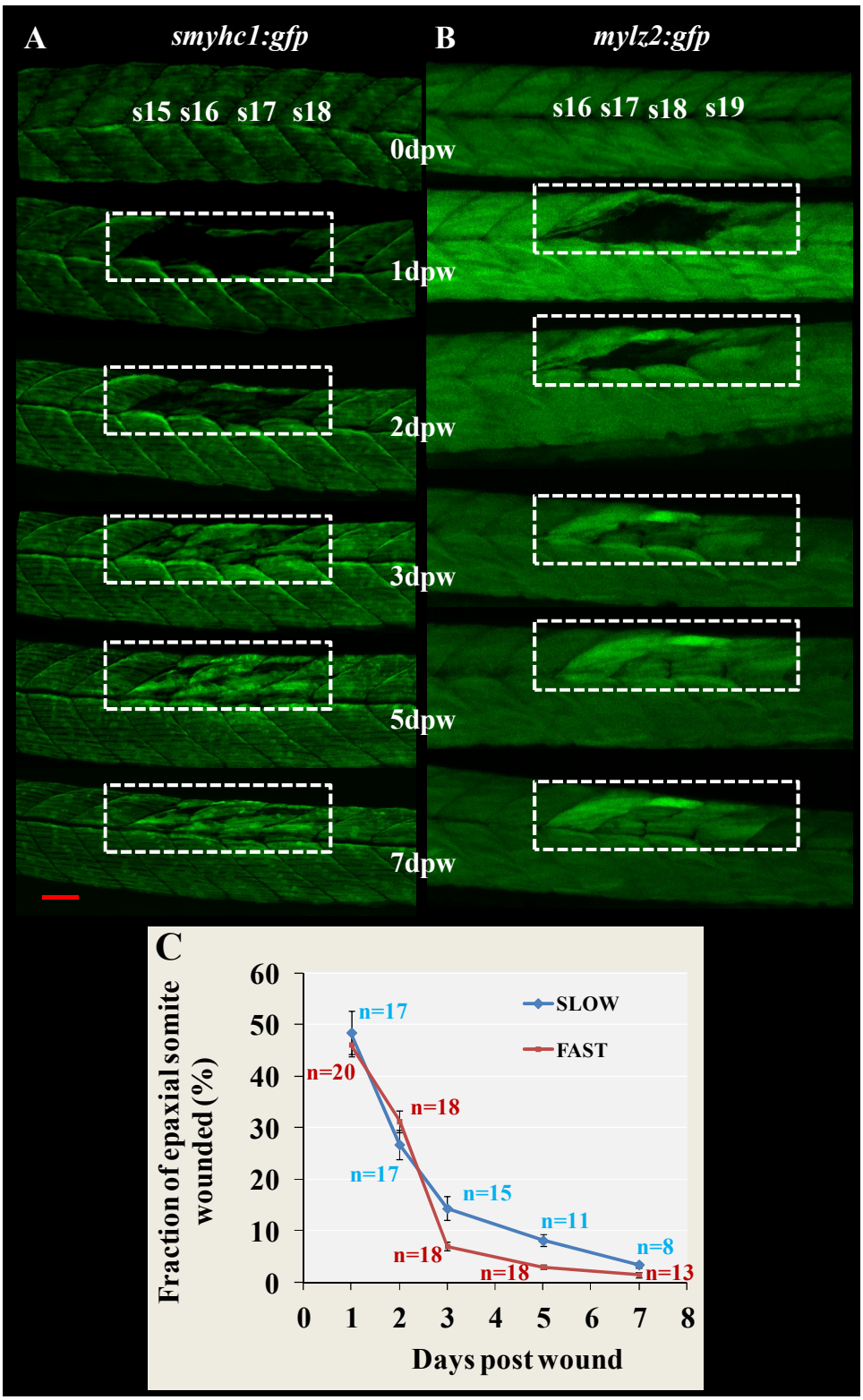


Fig. 4.5 Slow and fast muscle in zebrafish larvae muscle wounds repair at a similar rate.

Fig. 4.5 Slow and fast muscle in zebrafish larvae muscle wounds repair at a similar rate.

Mechanical wounds in epaxial somites of 3.5 dpf zebrafish larvae carrying transgenes expressed in slow (A) or fast fibres (B) were repeatedly imaged over 7 days by confocal fluorescence microscopy. Live embryos are shown anterior to left, dorsal up. A single embryo each of **A:** Tg(9.7kb smyhc1:gfp)^{i104} and **B:** Tg(-2.2mylz2:GFP)^{i135} , show slow and fast muscle repair (boxed regions) respectively. Somites 15-18 in slow:gfp fish and somites 16-19 in fast:gfp fish were wounded with a fine needle. **C:** Graph shows that wound recovery is similar in slow and fast muscle for the indicated numbers of fish. Error bars are standard error of the mean. Scale bar 50 μm.

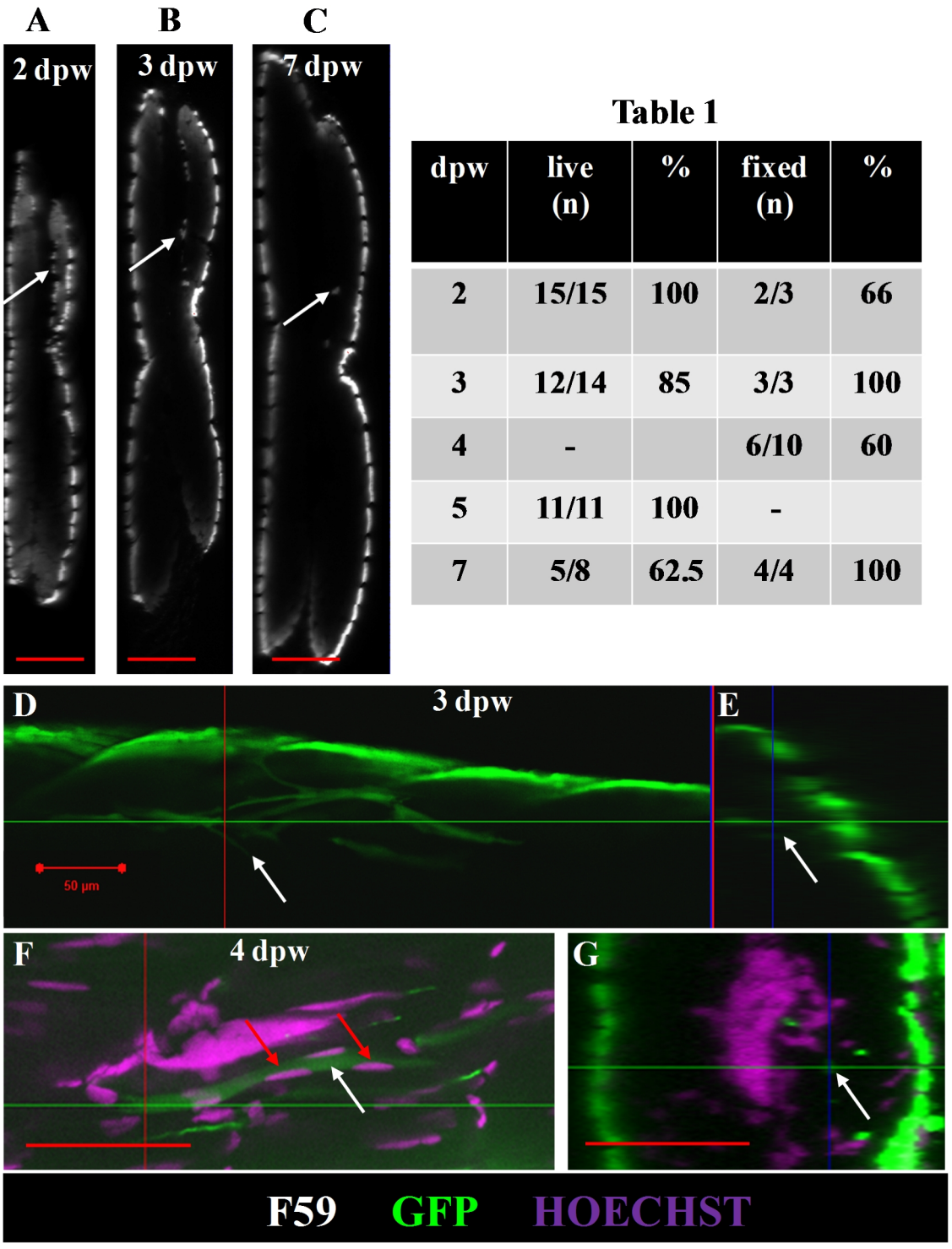


Table 1

dpw	live (n)	%	fixed (n)	%
2	15/15	100	2/3	66
3	12/14	85	3/3	100
4	-		6/10	60
5	11/11	100	-	
7	5/8	62.5	4/4	100

Fig. 4.6 Slow fibres are detected in the fast muscle layer in wounded muscle.

Fig. 4.6 Slow fibres are detected in the fast muscle layer in wounded muscle. Zebrafish larvae wounded at 3.25 dpf (A-C) or 3.5 dpf (D-G) were fixed and stained for immunodetection of F59 antibody (A-C) or gfp antibody (F-G) or imaged live (D). Images are optical transverse sections (A,B,C,E,G) or single lateral slices (D,F) from confocal slices of wholemount fish oriented with dorsal up and anterior to left. **A-C:** Slow fibres in wildtype stained intensely by F59 antibody are visible within the deep fast muscle region (arrows) of wounded epaxial somites in 2, 3 and 7 dpw fish. Note that fast muscle stains weakly by F59 antibody. **D,E:** Deep gfp^{+} slow fibres (arrows) in a live *smyhc1:gfp* fish at 3 dpw. **F,G:** Immunodetection of slow fibres with GFP antibody (green) in a wounded and fixed *smyhc1:gfp* fish shows a deep slow fibre (white arrow) at 4 dpw associated with multiple nuclei stained with Hoechst 33342 false colored magenta (red arrows). **Table 1:** Quantification of the number of wounded fish that were imaged live or fixed and stained for immunodetection of slow muscle fibres and were positive for the presence of deep slow fibres. Scale bars 25μm (A-C); 50 μm (D-G).

4.3.3 Structural proteins are lost and recover during muscle regeneration asynchronously

To examine whether the dark regions in DIC and confocal images of wounds in live fish (Fig. 4.1, 4.3 and 4.5A) correlated with a loss of structural proteins, wounded fish were stained for myosin heavy chain, F-actin and cell membrane protein ß-catenin. The ß-catenin antibody appeared to decorate Z line striations in the unwounded muscle in my experiments. The antibody appeared to detect an antigen that was lost upon muscle damage and begin to reappear over the course of muscle regeneration. It is possible that the striated staining pattern arises from the localization of ß-catenin to costameres which function to anchor Z-discs in cardiomyocytes (Wu et al., 2002). Also, ß-catenin has been detected by microscopy in places coinciding with Z-discs of striated skeletal muscle and the dense bodies of smooth muscle (Kurth et al., 1996). Disarrayed nuclei and loss of myosin was apparent at 1 dpw in muscle wounds stained with an anti-myosin heavy chain antibody (A4.1025) and Hoechst 33342 (Fig. 4.7 A-C). In contrast, adjacent unwounded regions were primarily filled with myosin-positive fibres and well-aligned nuclei (Fig. 4.7 A-C). By 2 dpw, numerous nuclei surrounded by myosin positive tubular structures were visible in the wounds (Fig. 4.7D-F). Some of the tubular structures detected by myosin antibody appeared to be small caliber fibres (Fig. 4.7F). The data suggest that myosin is adversely affected in wounded muscle at 1 dpw and appears in fibre-like structures in wounds at 2 dpw.

To determine the changes in muscle fibre integrity at wound site, wounded fish were stained with phalloidin (detecting F-actin), anti-ß-catenin antibodies and Hoechst 33342 (detecting nuclei). Wound regions were filled with numerous nuclei (Fig. 4.8 A-B), a mass of membrane-like structures (Fig. 4.8C) and non-striated actin at 4 hpw (Fig. 4.8D). The membranous mass at the wound site lacked the striated pattern of ß-catenin antibody staining as seen in the adjacent unwounded muscle (Fig. 4.8C), indicating that the antigen was adversely affected and suggesting a loss of ß-catenin in the membranes of wounded fibres. Similarly wound regions were largely devoid of muscle fibres containing striated actin (Fig. 4.8D) indicating that sarcomeric protein actin was also adversely affected by wounding. At 1 dpw, numerous nuclei are seen concentrated at certain locations within the wound (Fig. 4.9A,B). The regions packed with nuclei coincide with brightly stained ß-catenin positive membranous structures (Fig. 4.9C) and weakly labelled unstriated actin filaments (Fig. 4.9D), suggesting nuclei and membrane assembly and the absence of contractile actin in wounds at 1 dpw. By 2 dpw, the wound region is filled with numerous nuclei (Fig. 4.10A,B) and striated material that is primarily positive for ß-catenin stain (Fig. 4.10C) but also for actin within sturctures resembling muscle fibres (Fig. 4.10D) suggesting recovery of the structural components of muscle fibres in wounds. The absence of nuclei with Hoechst staining and lack of myosin stained tissue strongly provided an indirect evidence of damage to cells although direct evidence of necrosis or apoptosis was not obtained. To summarize, the data show a loss of nuclei and muscle fibre integrity by four hours post wounding followed by the emergence of nuclei and cell membranes by 1 dpw and an increase in the number of nuclei and recovery of contractile proteins in wounded muscle at 2 dpw. The recovery of contractile proteins in wounded muscle coincides with the emergence of regenerating gfp^{+} fibres observed in live transgenic embryos (Fig. 4.5A).

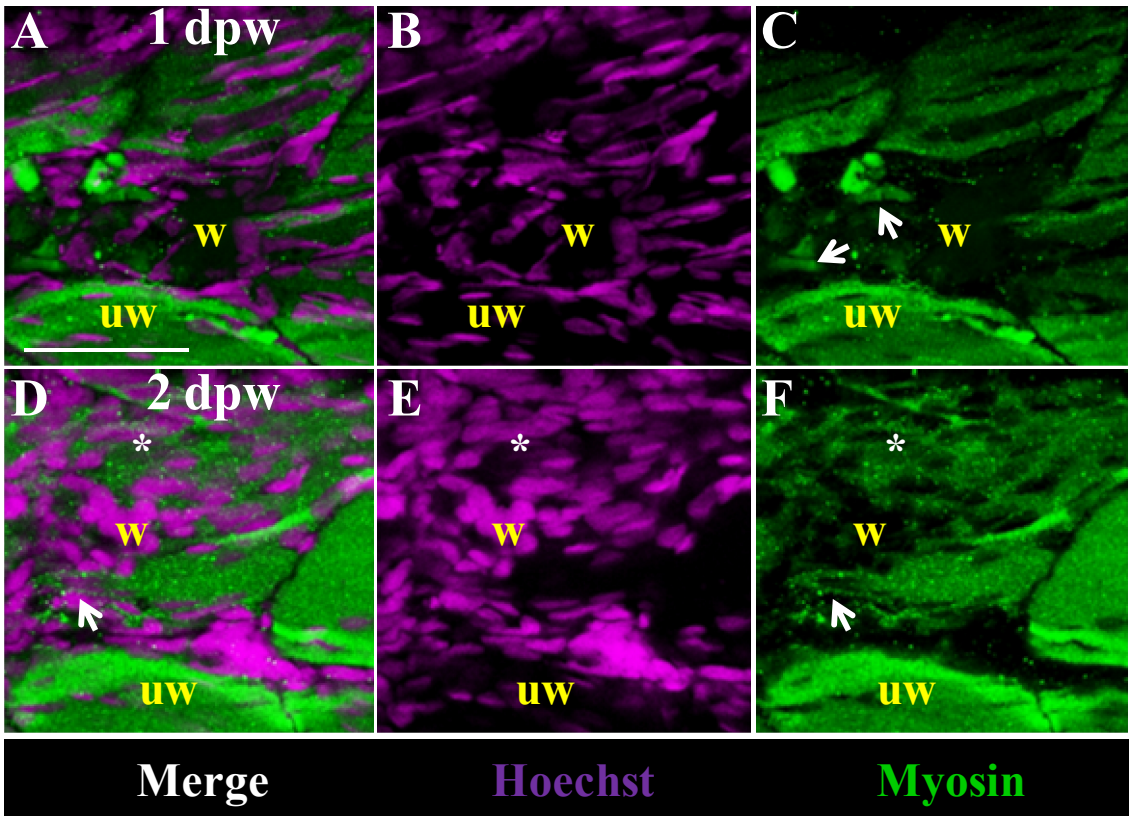


Fig. 4.7 Loss and recovery of myosin heavy chain positive muscle fibres in wounded epaxial somites.
Wild type larvae at 3 dpf were wounded and stained with Hoechst (false coloured magenta) and A4.1025 antibody (green, detecting myosin heavy chain) at 1 dpw (A-C) and 2 dpw (D-F). Confocal images are single slices from confocal stack of wholemount embryo. Images are lateral views (A-F) of embryo oriented with dorsal up and anterior to the left. Wounded epaxial region is marked w and adjacent unwounded regions are marked uw on individual images. **A-C:** Wound site appears to contain many nuclei (B) whereas myosin stained fibres are absent or irregular in appearance in the wound site (arrows, C). **D-E:** An increased number of nuclei appear to be in wound site at 2 dpw (E). **F:** Myosin reactivity increases in wound site at 2 dpw compared to 1 dpw. The wound region filled with nuclei coincides with myosin positive material (asterisks). Some small caliber myosin positive fibres become apparent at 2 dpw. Scale bar 50 µm.

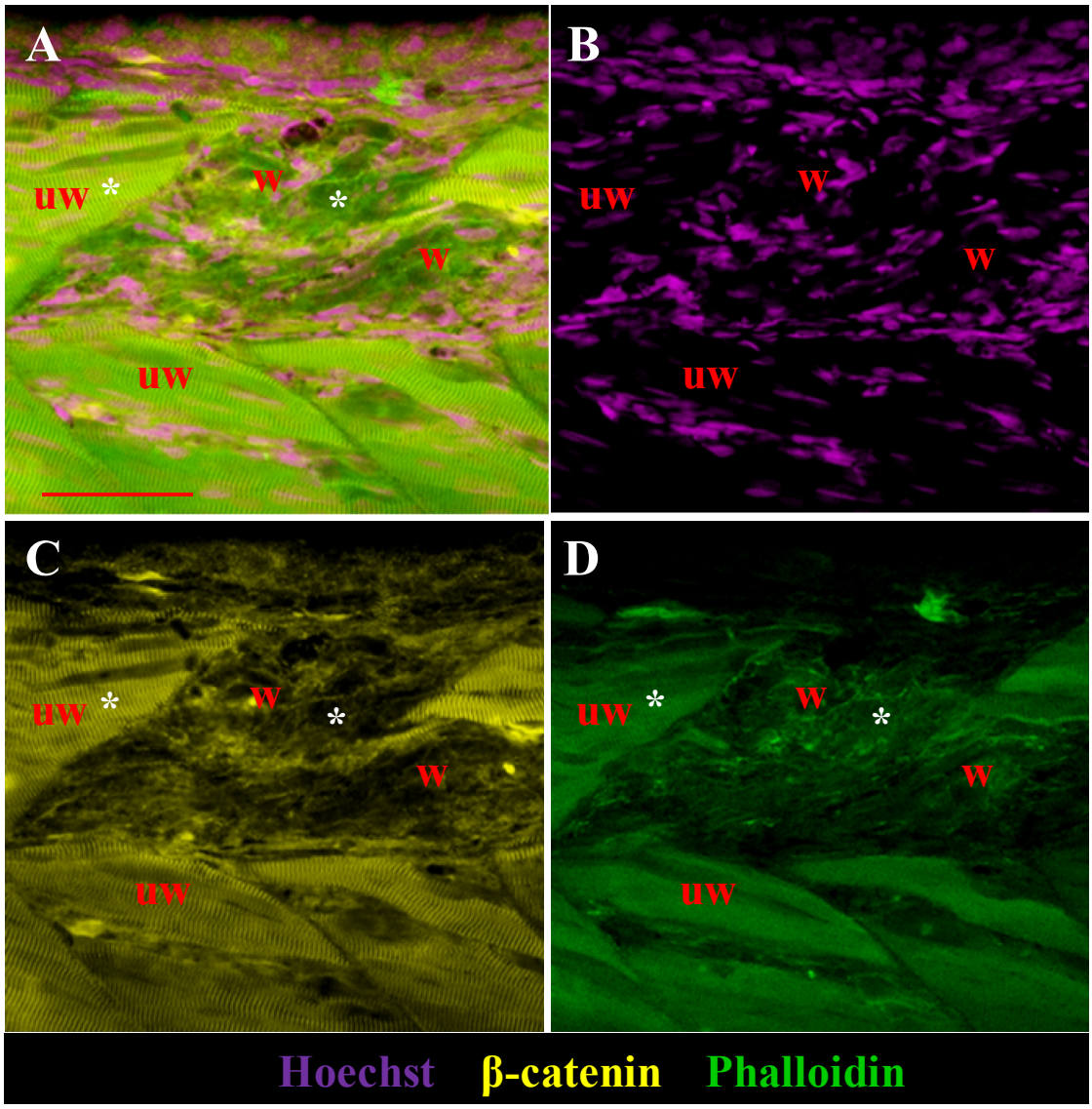


Fig. 4.8 Loss of ß-catenin and striated actin positive muscle fibres in wounded muscle at 4 hpw.

Wild type larvae at 3 dpf were wounded and stained with Hoechst (false coloured magenta), ß-catenin antibody (yellow, detecting cell membranes) and Phalloidin (green, detecting F-actin) at 4 hpw. Confocal images are single slices from confocal stack of wholemount embryo. Images are lateral views (A-D) of embryo oriented with dorsal up and anterior to left. Wounded epaxial region is marked w and adjacent unwounded regions are marked uw on individual images. **A,B:** Wound site appears to contain disarrayed nuclei compared to unwounded regions (B). **C:** Striated fibres detected by ß-catenin antibody are lost at wound site compared to unwounded regions (asterisks, A,C). **D:** Striated actin positive fibres are lost at wound site (asterisks, A,D). Scale bar 50 µm.

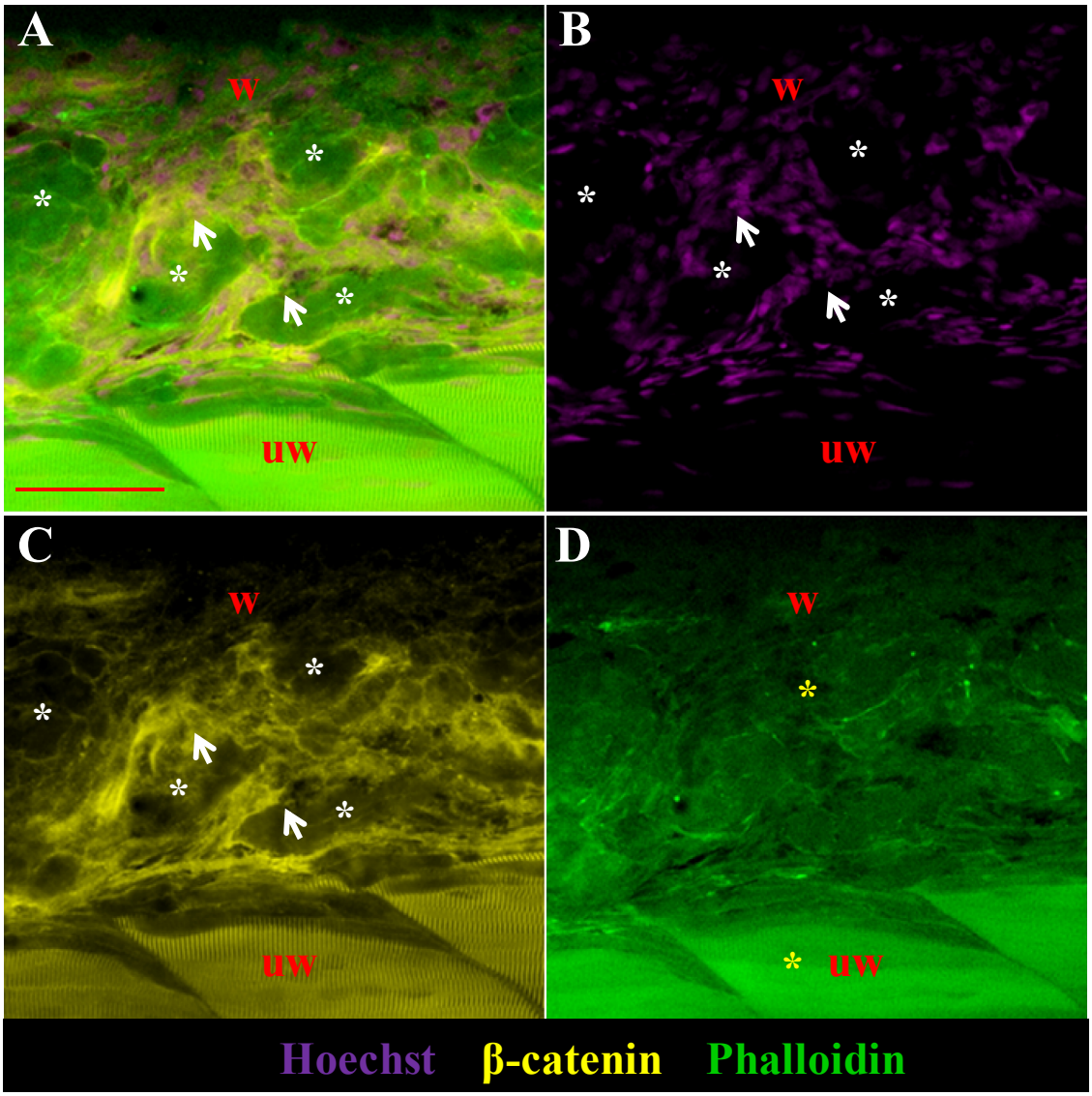


Fig. 4.9 Brightly stained ß-catenin material in wounds coincide with a concentration of nuclei but not striated actin.
Wild type larvae at 3 dpf were wounded and stained with Hoechst (false coloured magenta), ß-catenin antibody (yellow, detecting cell membranes) and Phalloidin (green, detecting F-actin) at 1 dpw. Confocal images are single slices from confocal stack of wholemount embryo. Images are lateral views (A-D) of embryo oriented with dorsal up and anterior to left. Wounded epaxial region is marked w and adjacent unwounded regions are marked uw on individual images. **A,B:** Wound site appears to contain masses of nuclei concentrated at certain locations in the wound (compare empty spaces at wound site marked by asterisks versus clumps of nuclei marked by arrows in A, B). **C:** Intensely stained ß-catenin positive material at wound site are at similar locations as the clumps of nuclei (arrows, A-C). **D:** Striated actin positive fibres are absent at wound site in wounded tissue compared to unwounded tissue (asterisks). Scale bar 50 µm.

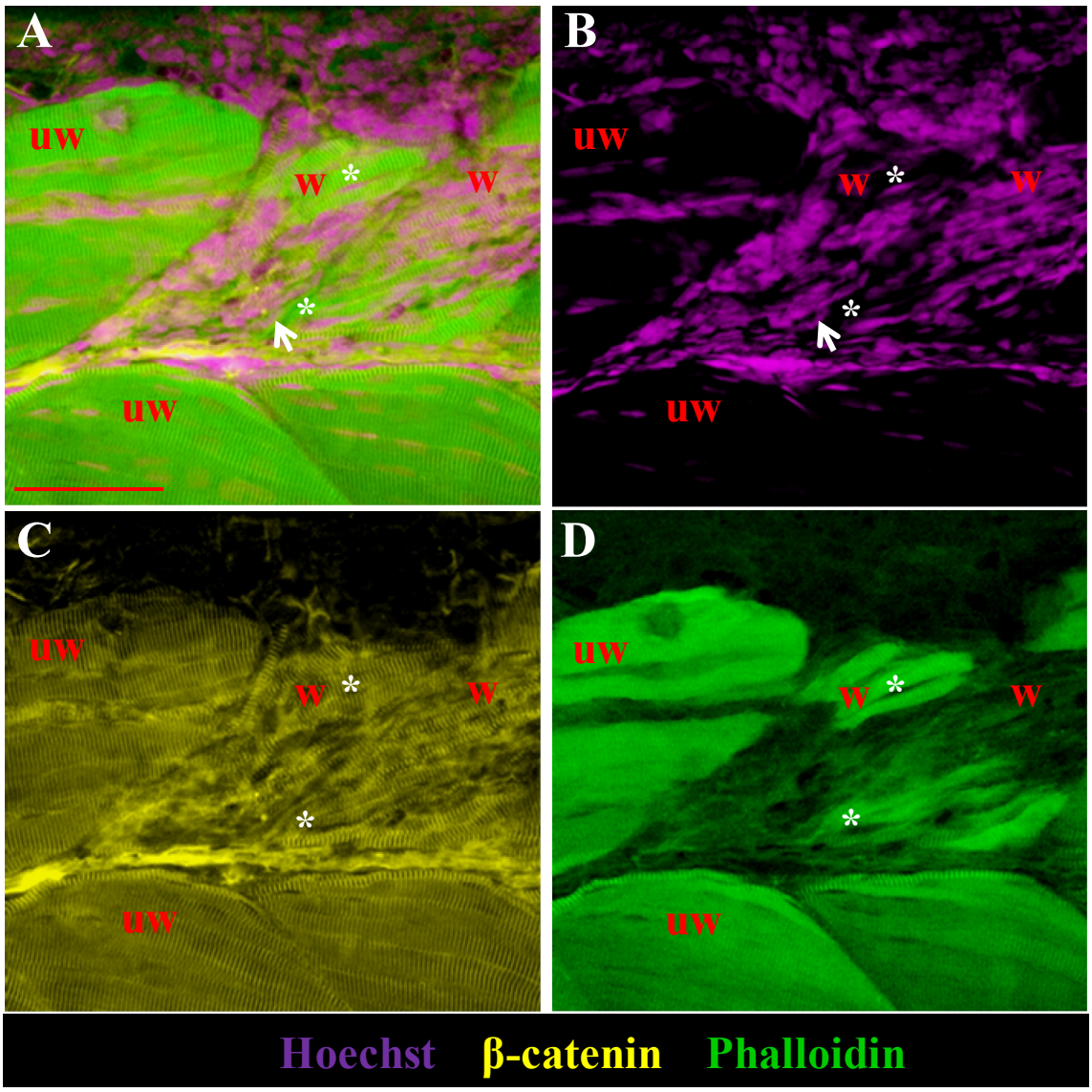


Fig. 4.10 Wound site is filled with striated material at 2 dpw.
Wild type larvae at 3 dpf were wounded and stained with Hoechst (false coloured magenta), ß-catenin antibody (yellow, detecting cell membranes) and Phalloidin (green, detecting F-actin) at 2 dpw. Confocal images are single slices from confocal stack of wholemount embryo. Images are lateral views (A-D) of embryo oriented with dorsal up and anterior to left. Wounded epaxial region is marked w and adjacent unwounded regions are marked uw on individual images. **A,B:** Wound site appears to contain an increased number of nuclei compared to unwounded tissue (compare w with uw in A, B). **C:** ß-catenin positive striated material at wound site appears to be at a similar intensity as that in unwounded tissue (compare w with uw). **D:** Striated actin positive fibres also positive for ß-catenin are present at wound site in wounded tissue (asterisks in A,C,D). Nuclei appear less dense in actin^{+}ß-catenin^{+} fibres (asterisks, B) similar to unwounded tissue. Scale bar 50 µm.

4.3.4 Nuclear recovery in wounded somites occurs by 2 days post wound

The apparent loss and recovery of nuclei was investigated in muscle wounds. Larvae between the ages of 3 and 3.5 dpf were mechanically wounded with a fine needle or left uninjured (control). Wounded and control fish were fixed and stained with Hoechst and antibodies detecting myosin between 1 and 7 dpw. The frequency of nuclei was compared to myosin content in optical transverse sections at 1 and 2 dpw (Fig. 4.11). Sections from unwounded muscle adjacent to wound site showed an even staining pattern between somites on either side of the neural tube with antibody detecting myosin heavy chain (Fig. 4.11A,B) and Hoechst (detecting nuclei, Fig. 4.11C) or F59 antibody (primarily detecting slow muscle, Fig. 4.11D) and Hoechst (Fig. 4.11E). In contrast wounded muscle at 1 dpw, lacked myosin stain (Fig. 4.11F,G) and reduced tissue containing nuclei (Fig. 4.11H) compared to contralateral. Strongly F59 stained slow muscle was similarly absent in wounded muscle compared to contralateral (Fig. 4.11I) as was tissue containing nuclei (Fig. 4.11J). The data indicates that loss of tissue at wound site lead to a reduction in myosin stained area and nuclei at 1 dpw. Sections from unwounded muscle adjacent to wound site at 2 dpw also showed an even staining pattern between somites on either side of the neural tube with antibody detecting myosin heavy chain (Fig. 4.12A,B) and Hoechst (detecting nuclei, Fig. 4.12C) or F59 antibody (primarily detecting slow muscle, Fig. 4.21D) and Hoechst (Fig. 4.12E). In contrast wounded muscle at 2 dpw, showed uneven myosin stain with some unstained regions compared to contralateral (Fig. 4.12F,G). Moreover, brightly stained nuclei appeared to be packed into reduced tissue space (Fig. 4.12H) compared to contralateral. Strongly F59 stained slow muscle was present to some extent in wounded muscle compared to contralateral (Fig. 4.12I) as was tissue containing nuclei (Fig. 4.12J). The data indicate recovering tissue at 2 dpw albeit reduced, leading to some myosin stained regions and brightly packed nuclei in wounds.

Whereas the loss of myosin was apparent in transverse sections at 1 dpw, the extent of loss and recovery of nuclei at 2 dpw in transverse sections was difficult to determine. A loss in clarity arose from extensive loss of epaxial somite volume leading to contact between dermal and densely packed neural tube nuclei. This made quantitation of muscle nuclei at 1 dpw difficult as muscle nuclei could not all be distinguished from neural and epidermal nuclei. Patches of bright nuclei adjacent to myosin stained tissue were apparent

in wounded muscle at 2 dpw, suggesting an increase in the number of nuclei between 1 and 2 dpw. However, the brightness of these patches also made it difficult to accurately count the number of nuclei. The number of nuclei in the bright patches was estimated based on the approximate area one nucleus would normally occupy.

To compare the number of nuclei in control, unwounded and wounded somites, fish were wounded between 3 and 3.5 dpf. Initially, the number of nuclei was counted in three evenly spaced transverse sections (Fig. 4.13A) through somite 17 in control fish and in adjacent unwounded somites (between somite 12-14) and somite 17 (wounded) in wounded fish at 1 and 2 dpw. The number of nuclei was computed by the formula shown in Fig. 4.13B. The number of nuclei in unwounded epaxial somites adjacent to wounded somites was similar compared to controls ($p=0.07$), whereas the number of nuclei in wounded somites significantly decreased compared to both controls ($p=0.0049$) and adjacent unwounded somites ($p=3.08E-05$, Fig. 4.13C). The number of nuclei in epaxial somites of control fish increased though not significantly between 1 and 2 dpw ($p=0.1$) whereas the number of nuclei in unwounded and wounded somites increased significantly between 1 and 2 dpw ($p=0.001$ and $p=0.001$ respectively). At 2 dpw, the number of nuclei is similar between control, adjacent unwounded and wounded somites. The data indicate that wounding is associated with a loss of nuclei in wounded somites at 1 dpw and an increase in the number of nuclei in both wounded and unwounded somites in wounded fish at 2 dpw, suggesting that wounding elicits a system wide response that is not restricted to the wound.

To quantify more rapidly, the number of nuclei in three transverse sections through the somite were averaged from the fish used in Fig. 4.13C and plotted at 1 and 2 dpw (Fig. 4.13D). Similar results were obtained such that sections from wounded somites showed a significant decrease in nuclear number compared to control and adjacent unwounded sections at 1 dpw ($p=0.009$ and $p=0.0009$ respectively). Moreover, the number of nuclei significantly increased in wounded somites between 1 and 2 dpw ($p=0.0014$), such that the number of nuclei in control, unwounded and wounded sections is similar at 2 dpw. This method of rapid quantification was used to analyze the number of nuclei in fish from three separate wounding experiments (Fig. 4.13E). Similar results were obtained such

that sections from wounded somites showed a significant decrease in nuclear number compared to adjacent unwounded sections at 1 dpw ($p=0.01$) and a significant increase between 1 and 2 dpw ($p=0.02$). However, the significant increase seen in the number of nuclei in adjacent unwounded somites (Fig. 4.13C) was not obtained by quantitation using transverse sections (Fig. 4.13D,E), although a trend could be observed when data from three separate experiments was used ($p=0.08$, Fig. 4.13E). The difference could arise from a difference in the way the number of nuclei is computed for somites and for transverse sections. The quantitation for somites takes into account the width of the somite and the length of a nucleus. Since the fish increase in length between 1 and 2 dpw, quantitation based on the number of nuclei in transverse sections alone without accounting for the increased space covered by the somite could mask the projected increase in the number of nuclei.

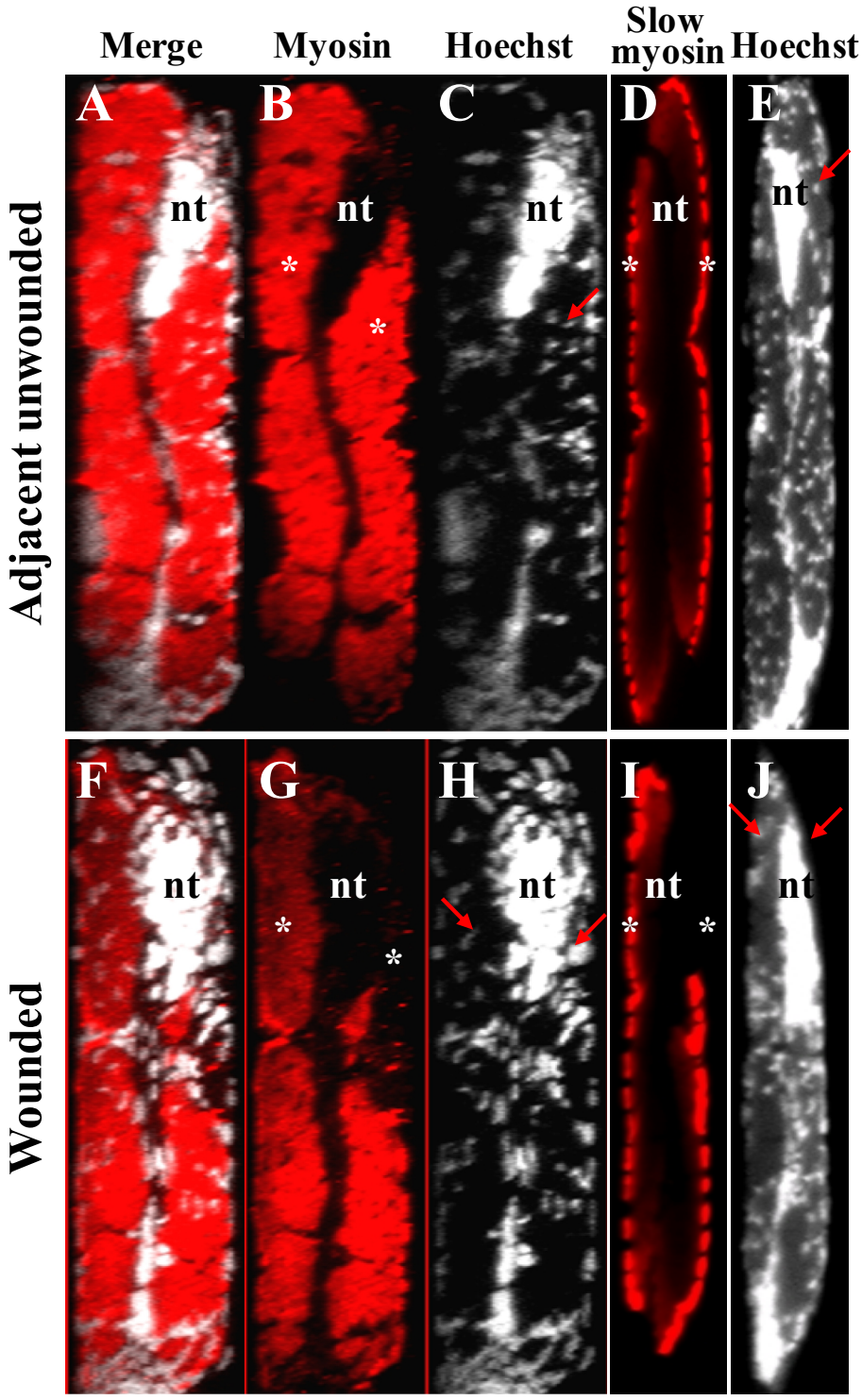


Fig. 4.11 Changes in the distribution of myosin and nuclei in wounded sections at 1 dpw.

Fig. 4.11 Changes in the distribution of myosin and nuclei in wounded sections at 1 dpw.

Wild type larvae between 3 and 3.5 dpf were wounded and stained with Hoechst (false colored white) and A4.1025 antibody (red, detecting myosin heavy chain) or F59 antibody (red, primarily detecting slow myosin) at 1 dpw. Confocal images are optical transverse sections from confocal stacks of wholemount larvae oriented with dorsal up and anterior to left. Transverse sections are from adjacent unwounded (A-E) and wounded somites (F-J) in wounded fish. **A,B:** Similar levels of myosin stain are apparent on either side of the neural tube (asterisks). **C:** Hoechst stained nuclei are apparent throughout the section and brightest in the neural tube. **D:** Slow muscle is apparent on either side of neural tube to a similar extent (asterisks). **E:** Hoechst stained nuclei are apparent throughout the section and brightest in the neural tube. **F,G:** Tissue stained with myosin is mostly absent on the wounded side of the section (asterisks). **H:** The space covered by Hoechst stained nuclei is reduced on the wounded side of section (compare regions with arrows in C and H). **I:** Slow muscle is absent on the wounded side of the transverse section (asterisks). **J:** Tissue containing Hoechst stained nuclei is absent on the wounded side (compare arrows in E and J). nt neural tube.

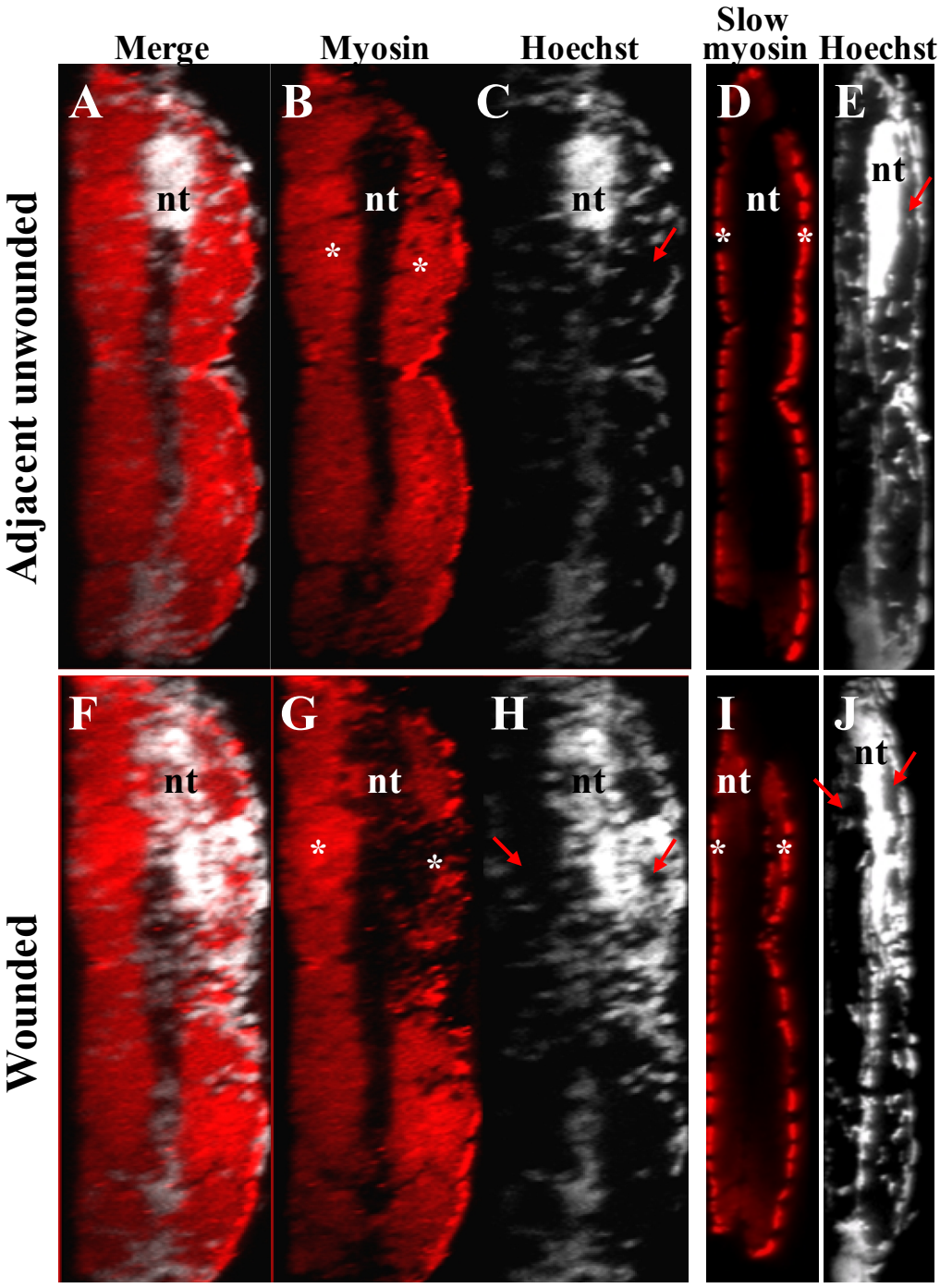


Fig. 4.12 Changes in the distribution of nuclei in wounded sections at 2 dpw.

Fig. 4.12 Changes in the distribution of nuclei in wounded sections at 2 dpw.
Wild type larvae between 3 and 3.5 dpf were wounded and stained with Hoechst (false colored white) and A4.1025 antibody (red, detecting myosin heavy chain) or F59 antibody (red, primarily detecting slow myosin) at 1 dpw. Confocal images are optical transverse sections from confocal stacks of wholemount larvae oriented with dorsal up and anterior to left. Transverse sections are from adjacent unwounded (A-E) and wounded somites (F-J) in wounded fish. **A,B:** Similar levels of myosin stain are apparent on either side of the neural tube (asterisks). **C:** Hoechst stained nuclei are apparent throughout the section and brightest in the neural tube. **D:** Slow muscle is apparent on either side of neural tube to a similar extent (asterisks). **E:** Hoechst stained nuclei are apparent throughout the section and brightest in the neural tube. **F,G:** Tissue stained with myosin is present but reduced on the wounded side of the section (asterisks). **H:** Bright Hoechst stained are apparent on the wounded side of section (compare regions with arrows in C and H). **I:** Slow muscle is apparent in the wounded side of the transverse section (asterisks). **J:** Tissue containing Hoechst stained nuclei is reduced on the wounded side but contains brighter nuclei compared to control and unwounded (compare arrows in E and J). nt neural tube.

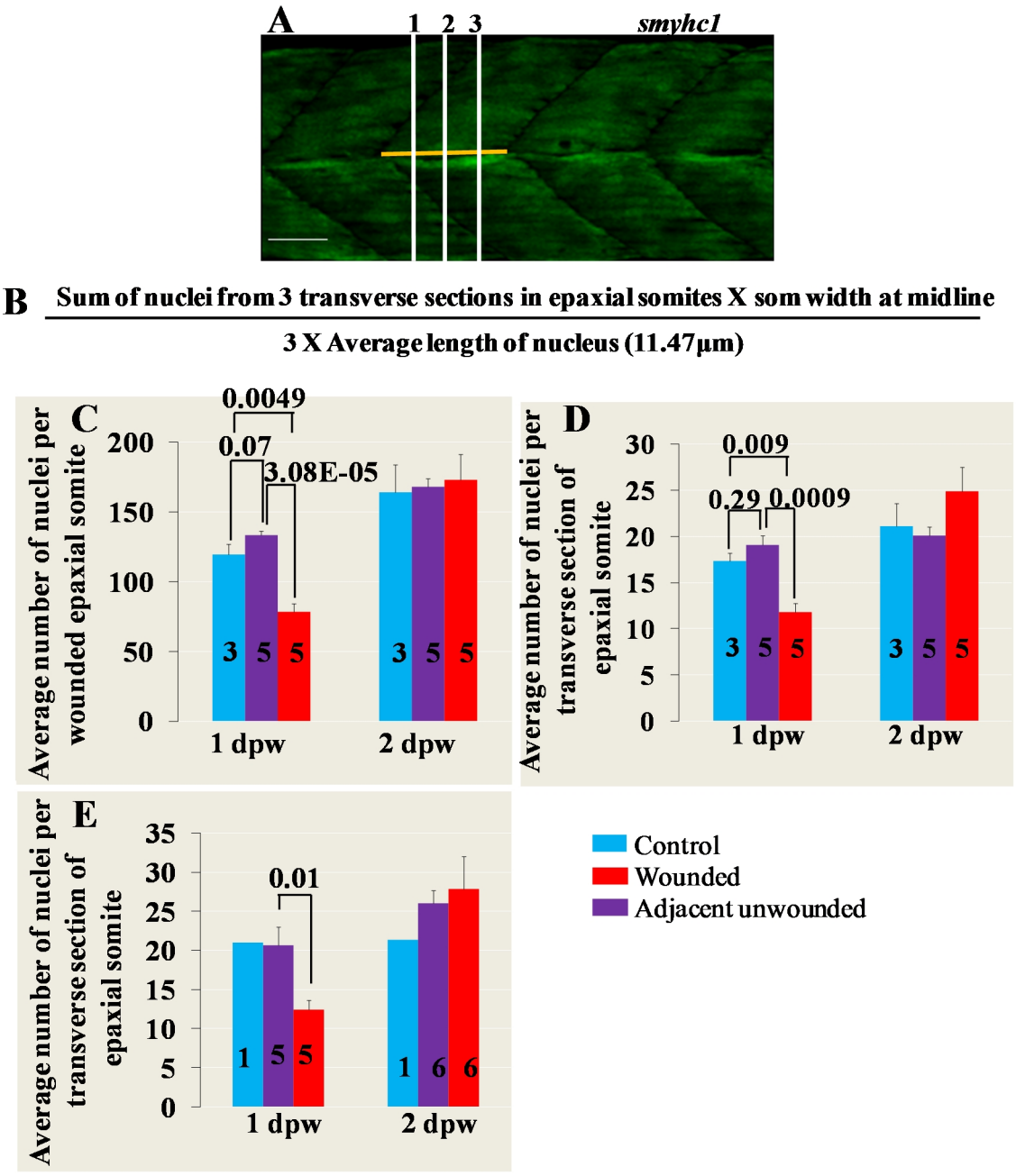


Fig. 4.13 Quantification of myonuclei in wounds at 2 dpw.

Fig. 4.13 Quantification of myonuclei in wounds at 1 and 2 dpw.
Epaxial somites of 3-3.5 dpf zebrafish larvae were wounded and fixed at 1 and 2 dpw for immunodetection of myosin heavy chain or slow myosin and Hoechst 33342. Hoechst stained nuclei were counted in three sections of epaxial somites in control and wounded larvae at 1 and 2 dpw. The number of nuclei in transverse sections of somite number 17 was counted for wounds and control whereas adjacent unwounded was usually somite 12-14. The number of larvae are indicated within bars. **A:** Three equispaced transverse sections (white bars) in a representative somite. Midline width of somite is represented by the orange bar. **B:** The equation used for calculating the number of nuclei in epaxial somites plotted in graph C. **C:** The number of nuclei per epaxial somite is similar between control and adjacent unwounded somites at 1 dpw. The number of nuclei per wounded epaxial somite is significantly reduced compared to control (p=0.0049) and adjacent unwounded epaxial somites (p=3.08E-05). The number of nuclei in controls remains similar between 1 and 2 dpw whereas significant increases occur in adjacent unwounded (p=0.001) and wounded epaxial somites (p=0.001). The number of nuclei is similar between control, unwounded and wounded epaxial somites at 2 dpw. **D:** The number of nuclei in three equispaced transverse sections was averaged and plotted for control, unwounded and wounded epaxial somites from fish used in C. The number of nuclei per transverse section decreased significantly in wounds compared to that from control (p=0.009) and adjacent unwounded (p=0009) epaxial somites. The number of nuclei per transverse section increased significantly in wounded epaxial somites between 1 and 2 dpw (p=0.0014) whereas the number of nuclei per transverse section from control and adjacent unwounded epaxial somites remained similar. The average number of nuclei per transverse section was similar between control, adjacent unwounded and wounded epaxial somites at 2 dpw. **E:** The average number of nuclei per transverse section in adjacent unwounded and wounded epaxial somites was computed for wounded fish from three separate experiments. The number of nuclei in transverse sections from wounded epaxial somites decreased significantly compared to that from adjacent unwounded epaxial somites (p=0.01). The number of nuclei in wounded sections increased significantly between 1 and 2 dpw (p=0.02) whereas the number of nuclei in sections from adjacent unwounded epaxial somites did not change significantly (p=0.08). Error bars are standard error of the mean. Scale bar 50 μm.

4.3.5 Rapid response of immune cells post muscle injury

The number of nuclei in wounds is significantly reduced at 1 dpw although not decimated. To examine the type of cells that are in the wound at 1 dpw, we assayed muscle wounds for the presence of inflammatory cells. The spatiotemporal dynamics of cells involved in the acute inflammatory response of muscle wounds in zebrafish is unknown. Taking advantage of two zebrafish transgenic lines *Tg(lysc:gfp)* and *Tg(mpo:gfp)* the spatio-temporal dynamics of immune cells in embryonic muscle wounds was characterized. GFP-labeled immune cells in *Tg(lysc:gfp)* line are thought to mark macrophage

precursors in zebrafish developing zebrafish embryos due to their expression of the transcription factor PU.1, leukocyte marker *leukocyte specific plastin* (L-plastin) and *draculin* (Herbomel et al., 1999) as well as by morphology and cell behaviour (Hall et al., 2007., Guyader et al., 2008). Further in zebrafish, embryonic macrophages have also been identified by their expression of *fms* (Herbomel et al., 2001) and *lysC* (Liu et al., 2002). On the other hand, embryonic neutrophils in zebrafish are identified by *mpo* expression (Lieschke et al., 2001; Renshaw et al., 2006). As the precursors mature, some remain macrophages whereas many of them give rise to neutrophils and are stained by Sudan black unlike macrophages (Guyader et al., 2008). Thus, the *lysC:gfp* line marks precursors for both macrophages and neutrophils.

In control larvae, majority of the gfp^+ cells are located ventrally in the caudal hematopoietic tissue and rarely observed in the epaxial somitic region in the absence of injury (Fig. 4.14A,B). Muscle wounds in larvae from both transgenic lines, elicited a rapid invasion of wounds by gfp^-marked cells between 1-2 hpw compared to none in control larvae (Fig. 4.14C,D). In some wounded larvae, gfp^+ cells were detected as early as 45 minutes post wounding (data not shown). By 5 hpw, gfp^+ cells in the control larvae were located similar to the previous time point (Fig. 4.14E) whereas in wounded larvae, gfp^+ cells were dispersing away from the wound site (Fig. 4.14F). By 24 hpw or 1 dpw, the gfp^+ cells had exited the wound site and were mainly observed in the ventral tail region in the caudal hematopoietic tissue, similar to control larvae (Fig. 4.14G,H).

The number of gfp^+ cells were quantitated in wounded *LysC:gfp* (Fig. 4.15) and *MPO:gfp* fish (data not shown) to determine the contribution of immune cell numbers to the number of nuclei in wounds at 1 dpw. The number of gfp^+ cells steadily increased at the wound site within the first two hours post wound and peaked at 3.3 hpw. The number of gfp^+ cells began to decrease by 5 hpw and reduced significantly between 21-26 hpw compared to 3.3 hpw ($p=5.53E-10$). The number of gfp^+ cells again increased significantly at the wound site at 48 hpw ($p=0.0142$) before reducing at 96 hpw. The data indicate that immune cells arrive at the wound site within two hours after injury and are rarely observed at 1 dpw. The data also suggests that some immune cells visit the wound at 2 dpw. Comparison of the number of gfp^+ cells in muscle wounds of *MPO:gfp* and

LysC:gfp fish (Fig. 4.16) showed that more putative neutrophils (in *MPO:gfp* fish) are at the wound site compared to macrophages (in *LysC:gfp* fish) at the time points assayed. The data show that the maximum number of gfp^+ cells (macrophages and neutrophils) present in muscle wounds appears to be approximately 20, indicating that immune cells are a tiny fraction of the number of nuclei present in wounds.

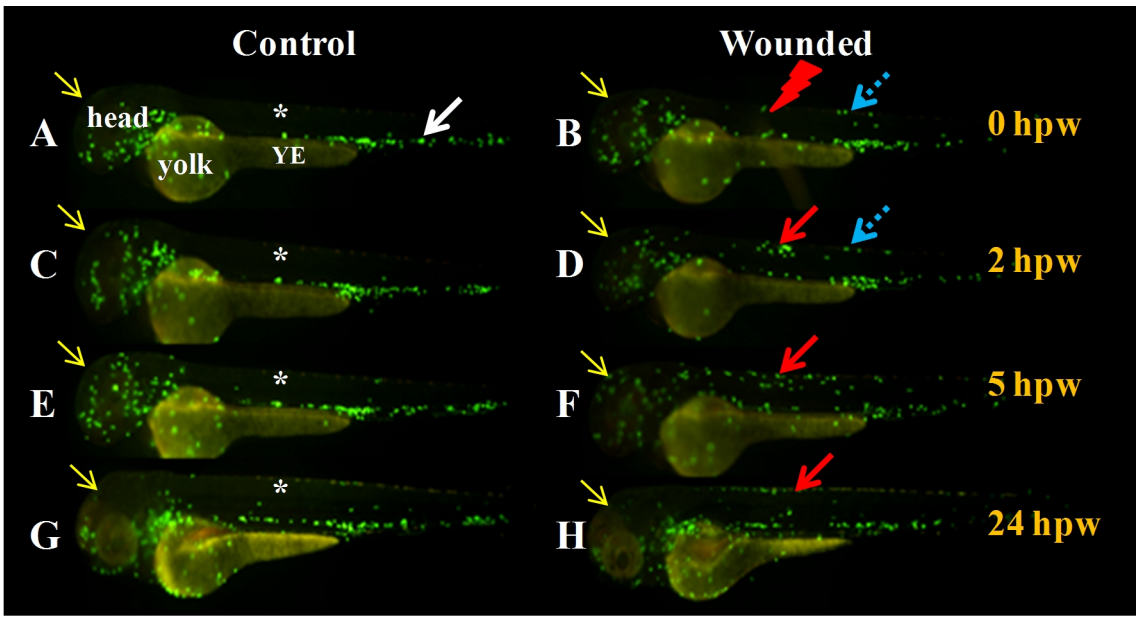


Fig. 4.14: **Dynamics of macrophages in zebrafish muscle wounds**.
LysC:gfp fish were mechanically wounded at 2.5 dpf and repeatedly imaged at 1, 2, 5 and 24 hpw. Live fluorescence imaging of control (uninjured, A,C,E,G) and wounded larvae (B,D,F,H). Images are lateral views of larvae mounted with dorsal up and anterior to left. Asterisks in control larvae highlight the region occupied by wounds in wounded larvae. **A,B,C:** Majority of Gfp^+ cells in uninjured larva are located ventrally, in the caudal hematopoietic tissue in uninjured larvae (white arrow). Few gfp^+ cells are located underneath the dorsal fin external to the muscle (blue arrow, B). **D:** Gfp^+ cells are present at wound site 2 hours post wound (red arrow). The gfp^+ cells located underneath the dorsal fin have not moved at this time in response to injury (blue arrows, B,D). **E,F:** Gfp^+ cells in control larva are not observed in the epaxial somitic region (asterisk, E) at 5 hpw whereas in wounded larva gfp^+ cells appear to be dispersing away from the wound (red arrow, F). **G,H:** Majority of gfp^+ cells are not observed in the epaxial somitic region in both control (asterisk, G) and wounded larvae (red arrow, H) at 24 hpw. Note the movement of gfp^+ cells in the head region (yellow arrows). YE yolk extension.

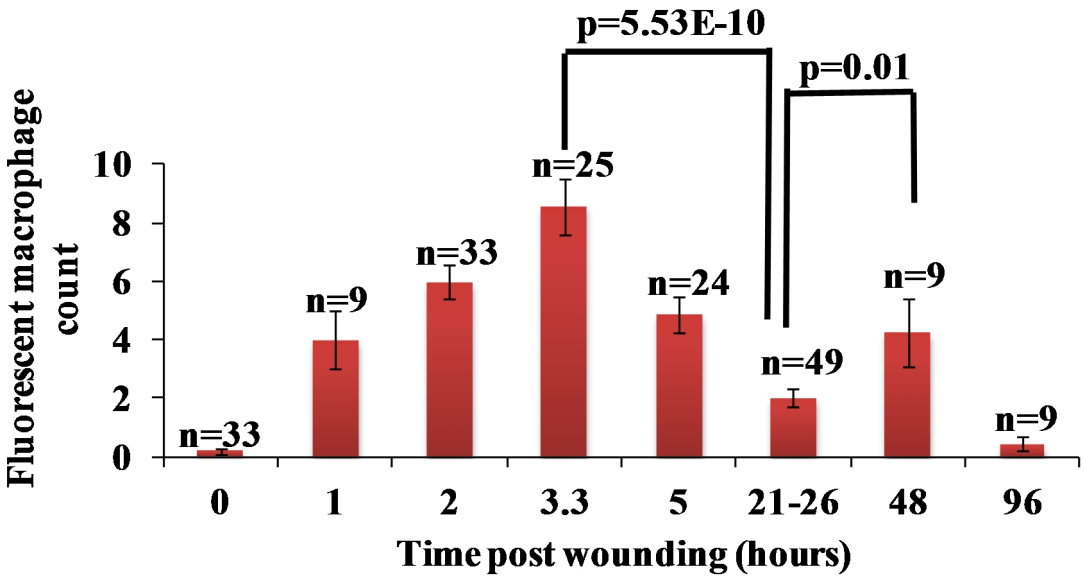


Fig. 4.15 Quantification of macrophage dynamics in muscle wounds.
LysC:gfp fish were wounded at 2.5 dpf in two to four somites between epaxial somites 5 and 12. The fish were repeatedly imaged by fluorescence microscopy at the intervals indicated in the figure. Green fluorescent cells were counted at the wound site in the number of wounded embryos indicated as n in the figure and plotted vs. time after injury. Data are from three separate wounding experiments. Error bars are standard error of the mean.

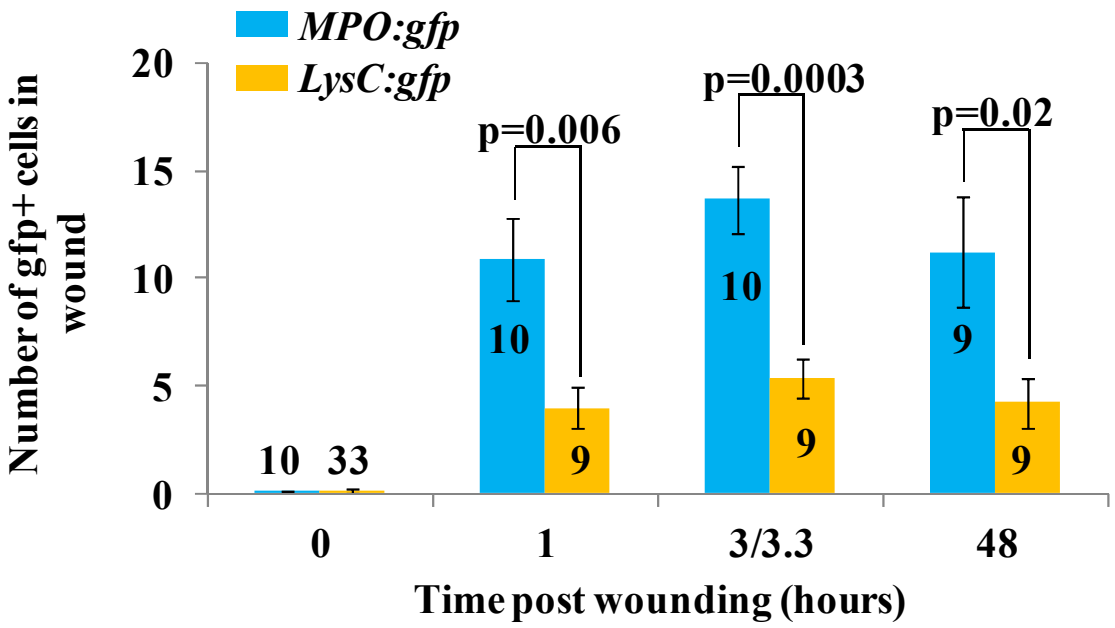


Fig. 4.16 Neutrophils are more numerous in muscle wounds compared to macrophages.
MPO:gfp and *LysC:gfp* fish were wounded in two to four somites between epaxial somites 5 and 12 at 2.5 dpf. The fish were repeatedly imaged by fluorescence microscopy at the intervals indicated in the figure. Green fluorescent cells were counted at the wound site of wounded embryos in the number of fish indicated above/within bars and plotted versus time after injury. Significantly more *MPO:gfp*$^{+}$ cells compared to the number of *LysC:gfp*$^{+}$ cells were present in wounds at 1, 3-3.3 and 48 hpw. Error bars are standard error of the mean.

4.3.6 Pax7:gfp^{+} cells contribute to muscle regeneration

Increase in the number of nuclei at the wound site between 1 and 2 dpw preceding the emergence of new fibres at 2 dpw suggested that the nuclei might belong to myogenic precursor cells. To test this hypothesis, myogenic precursor cells marked by Pax7 expression were examined during muscle repair in zebrafish larvae by imaging eight live wounded transgenic larvae (Pax7:gfp) between 0 and 6 dpw (aged 4 dpf to 10 dpf, Fig. 4.17A). At **two hours post wounding**, majority of the Pax7:gfp^{+} cells were absent in wounded somites, although they were visible in adjacent unwounded somites. Some of the fish were also imaged at 3 and 7 hpw and the wound site appeared to be similar to 2 hours post wounding such that new Pax7:gfp^{+} cells were not observed between 2 and 7

hpw. By **24 hpw**, many Pax7:gfp$^+$ cells were present in the wounded epaxial somites indicating that Pax7$^+$ myogenic cells could account for a portion of the nuclei seen in wounds at 1 dpw. Some Pax7:gfp$^+$ cells could be seen extending into the wounded somites from the adjacent unwounded somites. Many bright Pax7:gfp$^+$ cells appeared to be extending into the wound from the dorsal edge of wounded somites but not from the horizontal myoseptum side of the wound. Pax7:gfp$^+$ cells at the wound site were of variable morphology including elongated, rounded and irregular shaped cells (Fig. 4.17A,B). By **53 hpw**, the wounded somites are filled with Pax7:gfp$^+$ cells that have elongated into fibre like structures suggesting that Pax7:gfp$^+$ cells are involved in fibre regeneration in zebrafish muscle wounds. Disarray in fibre arrangement is noticeable at 53 hpw and later. By **76 hpw**, fibre arrangement at the wound site appears less chaotic and many Pax7:gfp$^+$ cells appear to be aligned adjacent to elongated Pax7:gfp$^+$ cells resembling muscle precursors lying adjacent to muscle fibres. Pax7:gfp$^+$ cells appear more numerous in wounds compared to adjacent unwounded epaxial somites at 76 hpw and also at 6 dpw. Many bright Pax7:gfp$^+$ cells appear to be aligned alongside gfp$^+$ fibres. Adjacent unwounded somites lack these bright myogenic gfp$^+$ cells (excluding xanthophores at 6 dpw, Fig. 4.17A,C), suggesting a specific increase in gfp$^+$ cells in the wounded somites. The fish were also imaged at 25 hpw to follow the fates of cells with variable morphology observed at 24 hpw. Cells appeared to be elongating and touching each other (Fig. 4.18) suggesting that the variable morphology of cells at wound site could signify cells involved in activities required for fibre generation.

To test the hypothesis that Pax7:gfp$^+$ cells give rise to muscle fibres seen at the wound site by 53 hpw, wounded Pax7:gfp larvae were fixed at 2 dpw and stained with antibodies detecting GFP and myosin heavy chain. Several striated fibres at the wound site were positive for both myosin expression and perduring gfp (Fig. 4.19) suggesting that myosin positive fibres arise from Pax7:gfp$^+$ cells.

Live imaging data indicated many Pax7:gfp$^+$ cells extending into wounds from adjacent unwounded somites at 24 hpw. Moreover cells of variable morphology were seen elongating and fusing between 24 and 25 hpw; events that likely gave rise to muscle fibres by 53 hpw. Hence, two fish were imaged frequently between 18 and 26 hpw with an aim

to quantitate the number of cells entering the wounds versus the number of new cells arising at wound site from cell division. In wounded fish, wounded somites largely lacked gfp^+ cells at 1 hpw (Fig. 4.20). Pax7:gfp^+ cells could be observed extending into the wound from the rostral (Fig. 4.21A) and caudal edges (Fig. 4.21B) of the wounded, suggesting that migrating Pax7:gfp^+ cells contribute to the number of gfp^+ cells at wound site. Between 20 and 26 hpw (Fig. 4.21B) the frequency of cells extending from the dorsal edge increased compared to few cells observed extending into the wound site from horizontal myoseptum (Fig. 4.22). Many more Pax7:gfp^+ cells could be seen extending into the wounds from the horizontal myoseptum at 43 hpw (Figs. 4.20 and 4.22) whereas by this time point the dorsal edge had many regenerated fibres (Fig. 4.20), suggesting a differential response of gfp^+ cells based on location. Cell dividing or poised to divide were frequently observed in the epaxial somites (Fig. 4.23A) and hypaxial somites (Fig. 4.23B,C) adjacent to the wound site between 18 and 26 hpw. However, due to the variable morphology and crowding of Pax7:gfp^+ cells in the wound site, it is was difficult to ascertain and quantify the frequency of cell division in wounds. To summarize, frequent time lapse imaging suggests that Pax7:gfp^+ cells in the wound site at 1 dpw could have entered from the rostral and caudal edges of the wound as well as the dorsal edge. To quantify the number of $Pax7^+$ cells, their differentiation rate and the frequency of $Pax7^+$ cells in S-phase, wild type embryos were fixed for immunodetection of Pax7 and Myogenin or S-phase marker EdU.

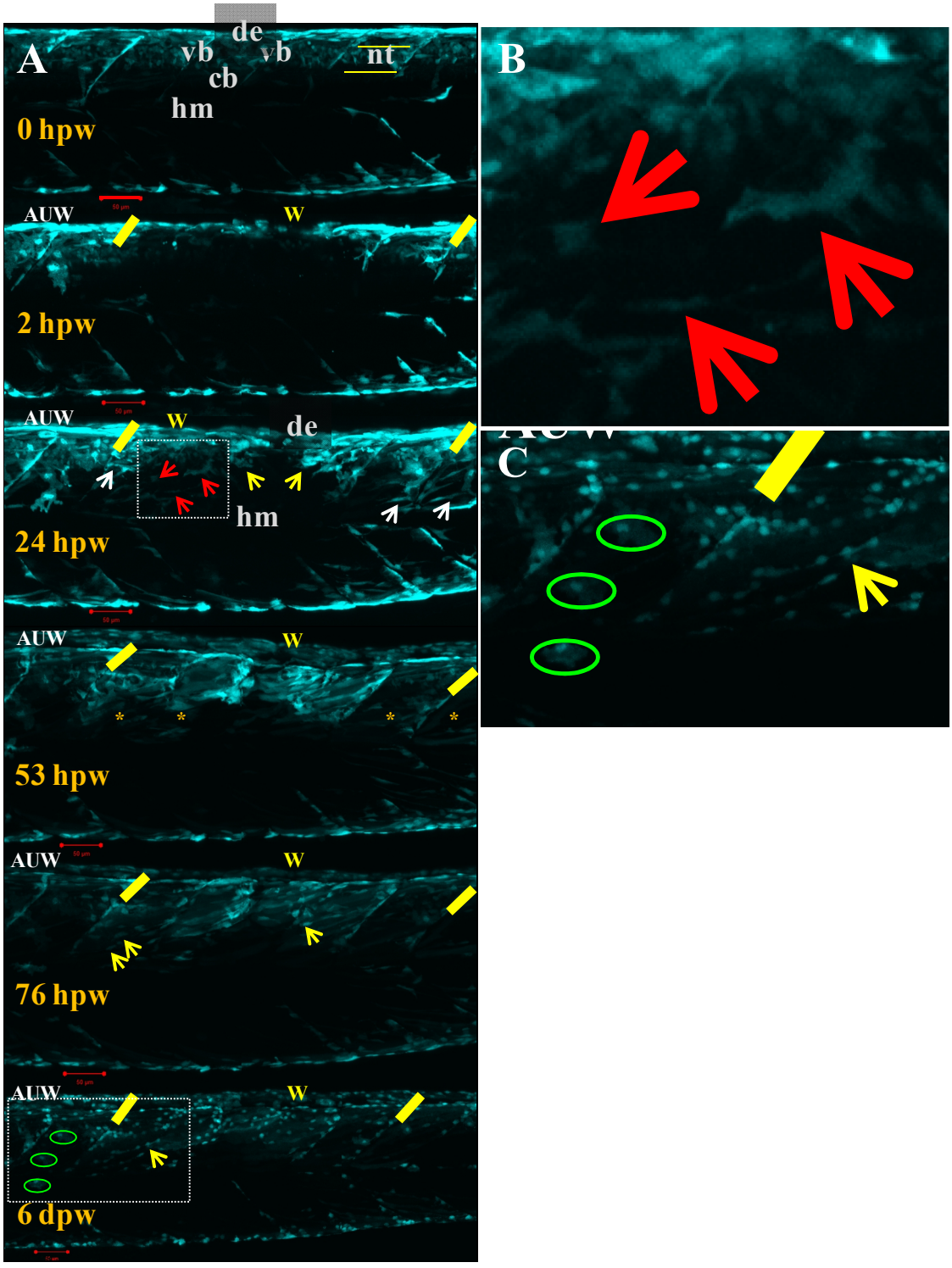


Fig. 4.17 Pax7:gfp^{+} cells contribute to muscle regeneration.

Fig. 4.17 Pax7:gfp$^+$ cells contribute to muscle regeneration.
Pax7:gfp fish were mechanically wounded at 4 dpf and imaged at 0, 2, 24, 25, 53, 76 hpw and 6 dpw. Live confocal images of a wounded larva (A-C). Images are maximum intensity projections of confocal stacks and are lateral views of the larva mounted with dorsal up and anterior to left. Vertical yellow bars in images demarcate the wounded epaxial somites (W) from adjacent unwounded somites (AUW). **A:** Majority of gfp$^+$ cells in uninjured larva at **0 hpw** are located at the dorsal edge and vertical borders at 4 dpf. Pax7:gfp$^+$ cells are visible in the neural tube (horizontal yellow bars). Gfp$^+$ cells are mostly absent in the wound site at **2 hpw**. **At 24 hpw**, many gfp$^+$ cells are seen extending into the wound from adjacent healthy epaxial somites (white arrows) and the dorsal edge of wounded somites (yellow arrows). Cells of variable morphology are seen in wounds (red arrows, also magnified in **B**). At **53 hpw** the wounded somites are filled with elongated Pax7:gfp$^+$ cells (asterisks). By **76 hpw** Pax7**:**gfp$^+$ cells are seen aligned adjacent to elongated Pax7:gfp$^+$ cells (arrows). At 76 hpw and **6 dpw** Pax7:gfp$^+$ cells excluding xanthophores appear more numerous in wounds compared to adjacent unwounded somites (arrow). Many Pax7:gfp$^+$ cells in adjacent unwounded are xanthophores (green ovals, also magnified in **C**).

B: Magnified view of boxed region at 24 hpw in panel A. Rounded, elongated and irregular shaped cells are visible in the wound.

C: Magnified view of boxed region at 6 dpw in panel A. Wound region has numerous Pax7:gfp$^+$ cells in contrast to unwounded somite (demarcated by yellow bar) which has many Pax7:gfp$^+$ xanthophores.

nt neural tube, vb vertical borders, de dorsal edge, cb central body, hm horizontal myoseptum. Scale bars 50 μm.

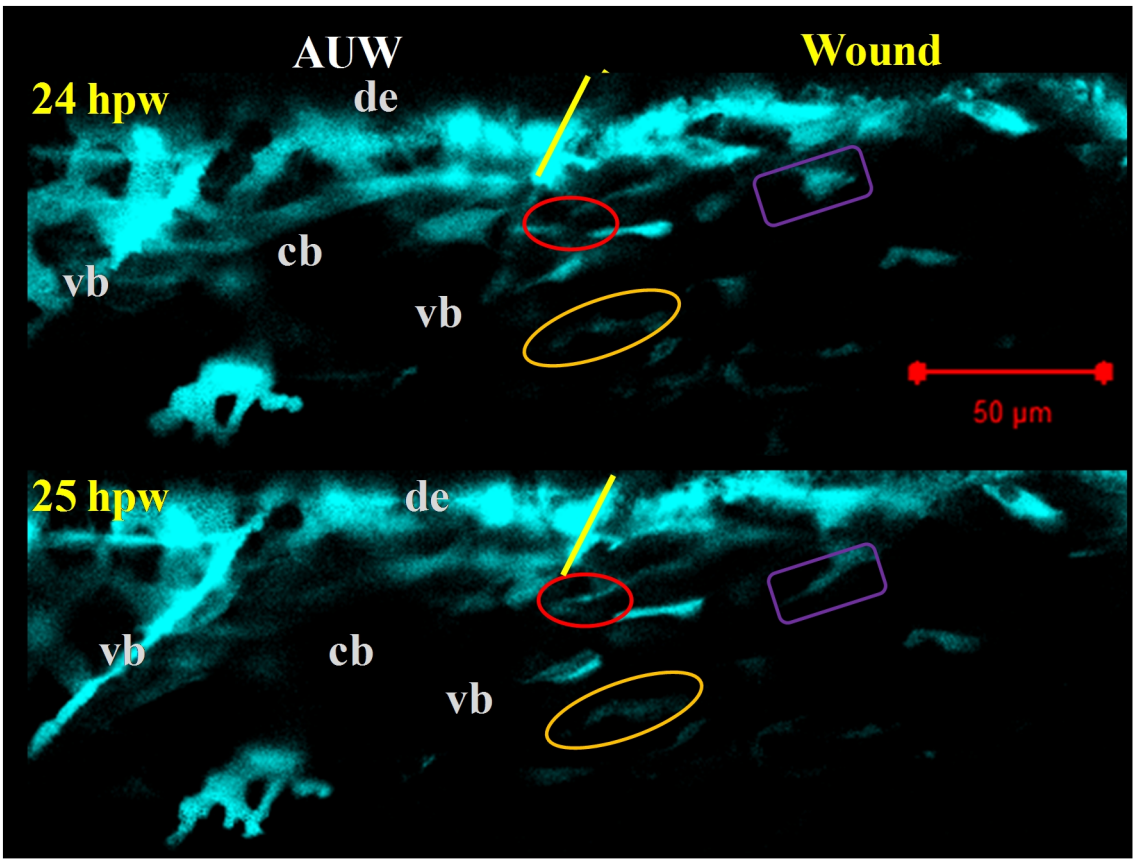


Fig. 4.18 Pax7:gfp$^+$ cells communicate with each other.
Pax7:gfp fish mechanically wounded at 4 dpf (Fig. 4.17) was imaged live by confocal microscopy at 24 and 25 hpw. Images are single slices from confocal stacks and are lateral views of larva mounted with dorsal up and anterior to left. Vertical yellow bars in images demarcate the wounded epaxial somites (W) from adjacent unwounded somites (AUW). Pax7:gfp$^+$ cells appear to elongate (purple rectangles) and come in contact with each other (red and yellow ovals at 24 and 25 hpw). vb vertical border, cb central body, de dorsal edge. Scale bar 50 µm.

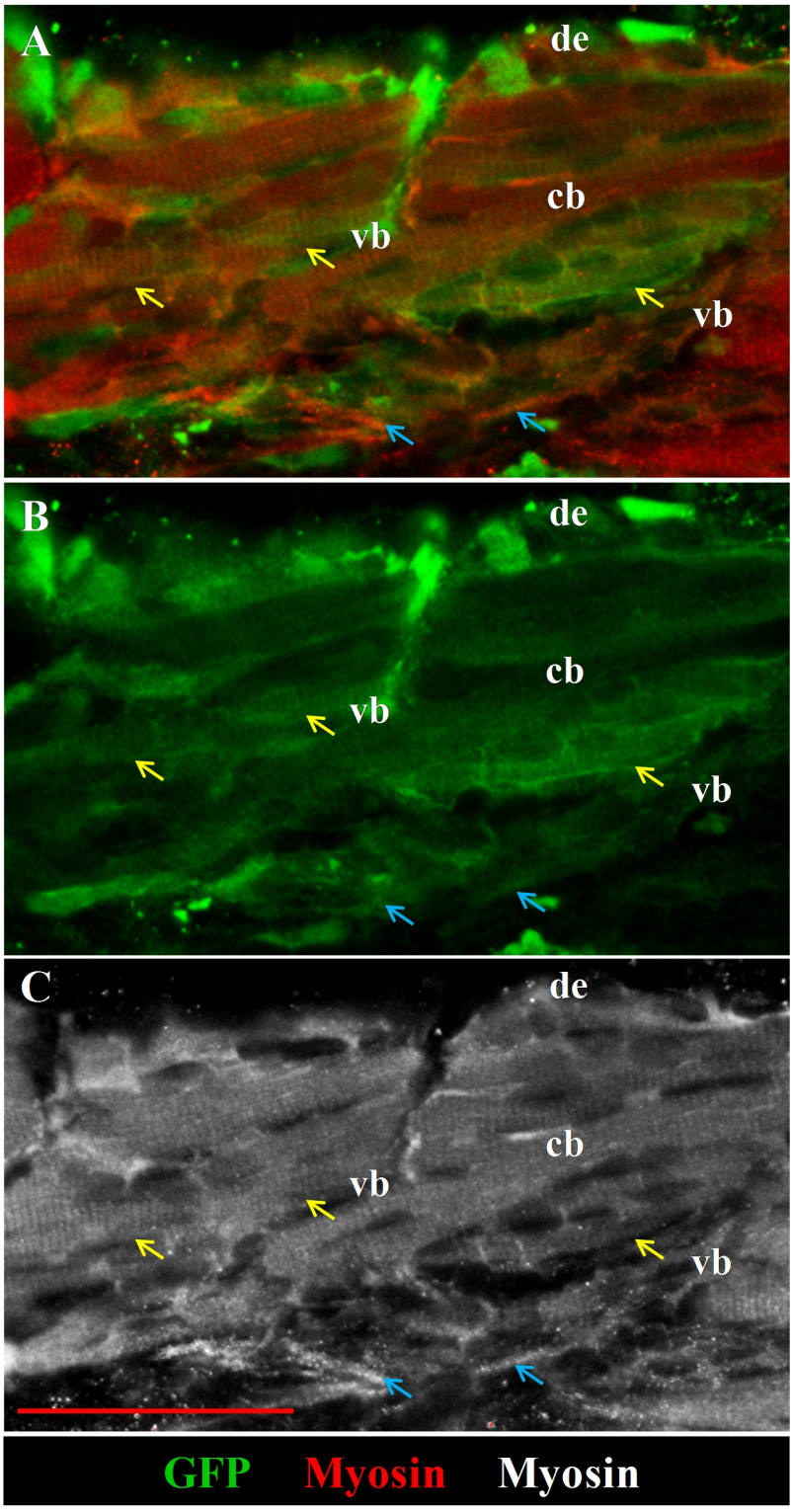


Fig. 4.19 GFP perdurance of Pax7:gfp^{+} cells coincides with large caliber myosin positive fibres

Fig. 4.19 GFP perdurance of Pax7:gfp$^+$ cells coincides with large caliber myosin positive fibres

Wholemount *Pax7:gfp* larvae at 3.25 dpf were wounded and fixed at 2 dpw for immunodetection of GFP (green, anti-GFP antibody) and myosin heavy chain (red, also false coloured white, A4.1025 antibody). Immunostained larvae were stained with Hoechst 33342 to detect nuclei. Confocal images are single slices from a confocal stack. Lateral views (A-C) are oriented with dorsal up and anterior to the left. Yellow arrows point to large caliber fibres whereas blue arrows point to small caliber fibres (A-C). **A:** Many large and small caliber gfp$^+$myosin$^+$ fibres are seen spanning the central body in the wounded muscle. **B:** Large caliber and small caliber fibres stain weakly for gfp. Gfp stain in large caliber fibres appears striated whereas the weak stain in small caliber fibres does not appear to be specific to the fibre. **C:** Large and small caliber striated myosin fibres are visible in the wounded muscle. Scale bar 50 μm.

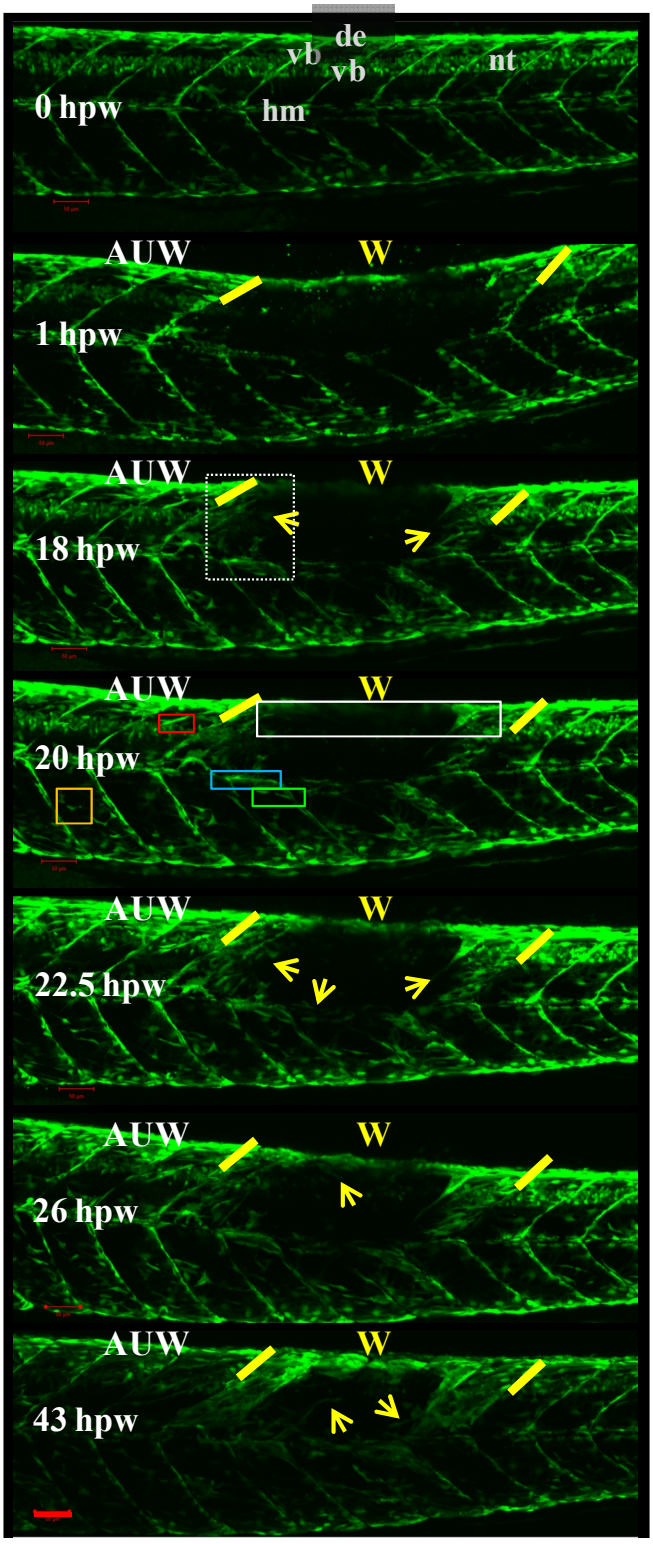


Fig. 4.20 Pax7:gfp^{+} cells enter the wounds primarily from vertical borders and dorsal edge

Fig. 4.20 Pax7:gfp$^+$ cells enter the wounds primarily from vertical borders and dorsal edge

Pax7:gfp fish were mechanically wounded at 4 dpf and imaged at 0, 1, 18, 20, 22.5, 26, 43 and 69 hpw. Confocal images of a live wounded larva is shown from 0-43 hpw. Images are maximum intensity projections of confocal stacks and are lateral views of the larva mounted with dorsal up and anterior to left. Vertical yellow bars in images demarcate the wounded epaxial somites (W) from adjacent unwounded somites (AUW).

Gfp$^+$ cells in uninjured larva at **0 hpw** are seen at the dorsal edge, vertical borders and horizontal myoseptum. Pax7:gfp$^+$ cells are visible in the neural tube (nt).

At **1 hpw** Gfp$^+$ cells are mostly absent in the wound site.

At **18 hpw**, many gfp$^+$ cells are seen extending into the wound from the vertical borders adjacent to the healthy epaxial somites rostral and caudal to the wound (arrows). Boxed region magnified in Fig. 4.21A

Between **20** and **26 hpw**, many Pax7:gfp$^+$ cells extend into the wound from the dorsal edge and the vertical borders in contrast to a few from the horizontal myoseptum (arrows in 20-26 hpw). Close-up views of boxed regions at 20 hpw are presented in Figs. 4.21 - 4.23.

At **43 hpw,** many elongated Pax7:gfp$^+$ cells are seen in the dorsal portion of the wounded somites in contrast to few Pax7:gfp$^+$ cells extending into the wound from the horizontal myoseptum and the vertical border close to the horizontal myoseptum (arrows).

nt neural tube, vb vertical borders, de dorsal edge, cb central body, hm horizontal myoseptum. Scale bars 50 μm.

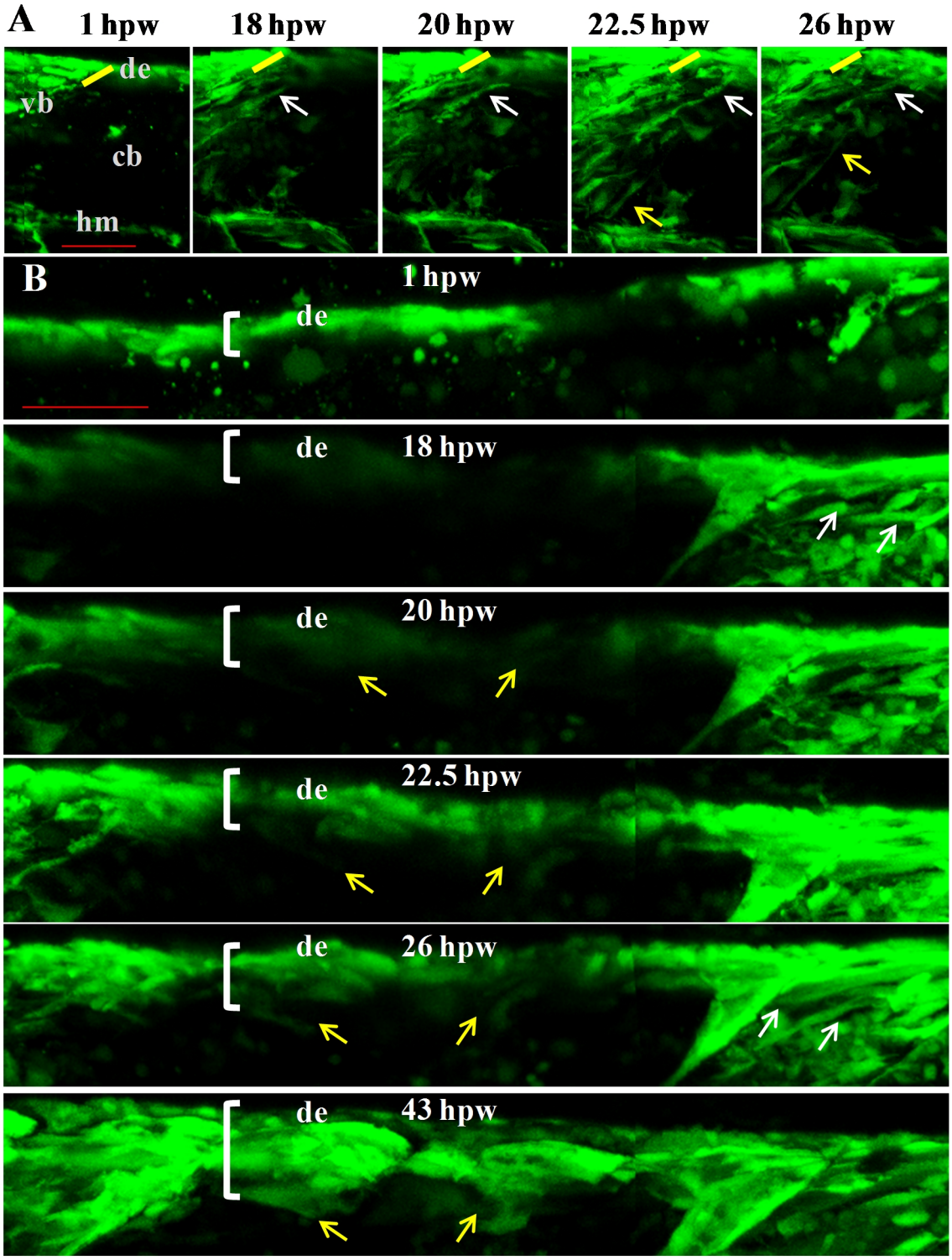


Fig. 4.21 Entry route of Pax7:gfp^{+} cells in wounds.

Fig. 4.21 Entry route of Pax7:gfp$^+$ cells in wounds.
Pax7:gfp fish were mechanically wounded at 4 dpf and imaged at 0, 1, 18, 20, 22.5, 26, 43 and 69 hpw. Close-up views of two of the boxed regions (white boxes) in confocal images of the wounded larva in Fig. 4.20 are shown here from 1-26 hpw (A) and 1-43 hpw (B). Images are maximum intensity projections of confocal stacks and are lateral views of the larva mounted with dorsal up and anterior to left. Vertical yellow bars in images demarcate the wounded epaxial somites from adjacent unwounded somites.

A: Gfp$^+$ cells in uninjured larva at **1 hpw** are absent in the central body of a wounded epaxial somite. Pax7:gfp$^+$ cells are visible in the adjacent unwounded epaxial somite separated by the vertical border. Between **18** and **26 hpw**, several Pax7:gfp$^+$ cells extend and elongate in the wounded somite adjacent to the vertical border (arrows). Between **18** and **22.5 hpw**, a Pax7:gfp$^+$ cell appears to elongate by cell division (white arrows).

B: Some gfp$^+$ cells survive at the dorsal edge of wounded somites at **1 hpw**. Between **1** and **43 hpw**, the number and intensity of Pax7:gfp$^+$ cells in the dorsal portion of the wounded somites increases (brackets). Some cells appear to extend into the wounded somites from the dorsal edge between **20** and **26 hpw** (arrows). By **43 hpw** many intense gfp$^+$ elongated cells occupy the dorsal portion of the wound. The caudal portion of wound is primarily filled with mononucleate Pax:gfp$^+$ cells at **18 hpw** (white arrows) and by elongated cells later (white arrows at 26 hpw).

nt neural tube, vb vertical borders, de dorsal edge, cb central body, hm horizontal myoseptum. Scale bars 50 μm.

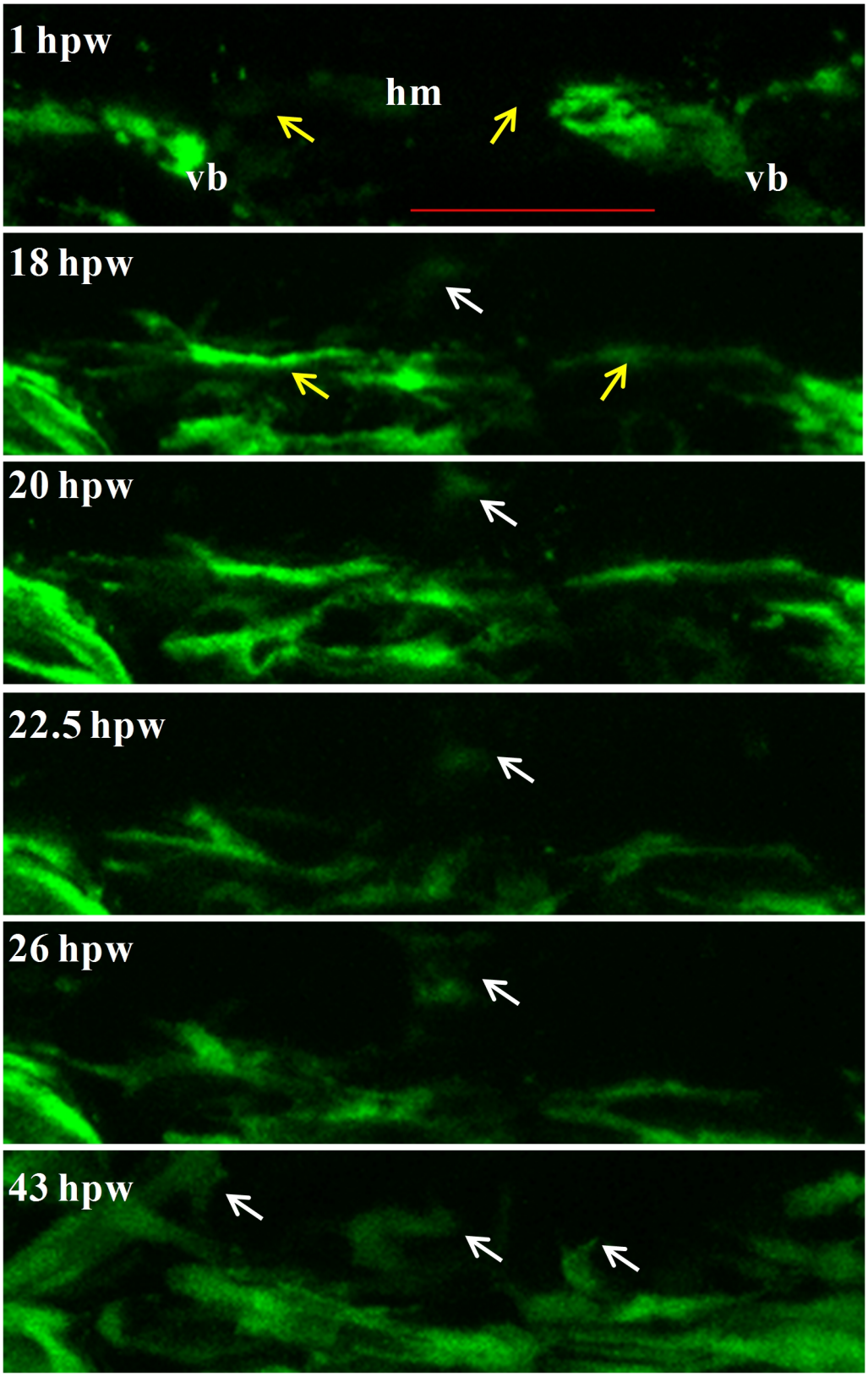


Fig. 4.22 Pax7:gfp^{+} cells loss and recovery at the horizontal myoseptum

Fig. 4.22 Pax7:gfp$^+$ cells loss and recovery at the horizontal myoseptum
Pax7:gfp fish were mechanically wounded at 4 dpf and imaged between 0 and 69 hpw. Close-up views of the blue boxed region in Fig. 4.20 are shown here from 1 - 43 hpw. Images are maximum intensity projections of confocal stacks and are lateral views of the larva mounted with dorsal up and anterior to left.

Gfp$^+$ cells are largely absent at the horizontal myoseptum of wounded somites in the injured larva at **1 hpw (**arrows**).** Pax7:gfp$^+$ cells are visible at the vertical borders of adjacent hypaxial unwounded somites. By **18 hpw**, several Pax7:gfp$^+$ cells are located at the horizontal myoseptum (yellow arrows) whereas few dim Pax7:gfp$^+$ cells extend into the wound region. Similarly between **20 and 26 hpw** few dim Pax7:gfp$^+$ cells appear to extend into the wound. By **43 hpw** the Pax7:gfp$^+$ cells at the horizontal myoseptum have grown in size and appear to extend larger sized protrusions into the wound.

vb vertical borders, hm horizontal myoseptum. Scale bar 50 μm.

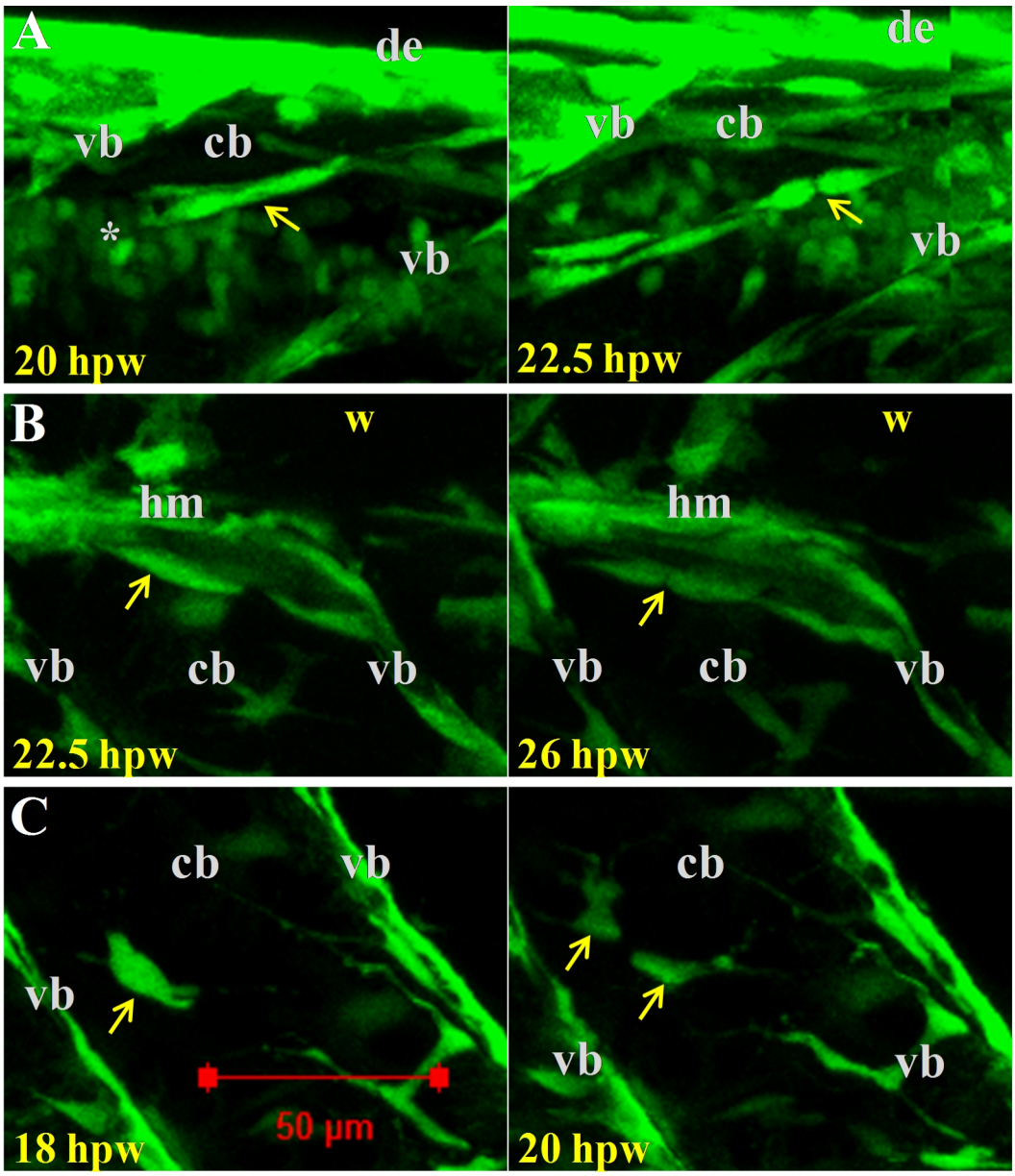


Fig. 4.23 Pax7:gfp$^+$ cells adjacent to wounds are mitotic.
Pax7:gfp fish were mechanically wounded at 4 dpf and imaged between 0 and 69 hpw. Close-up views of the red (A), green (B) and yellow (C) boxed regions in Fig. 4.20 are shown here at the time points indicated on images. Images are maximum intensity projections of confocal stacks and are lateral views of the larva mounted with dorsal up and anterior to left. **A:** A Pax7:gfp$^+$ cell in adjacent unwounded epaxial somite rostral to wound site divides between 20 and 22.5 hpw (arrows). Pax7:gfp$^+$ cells are apparent in the neural tube (asterisk). **B:** A Pax7:gfp$^+$ cell (arrows) in adjacent unwounded hypaxial somite ventral to the wound site appears to be in the process of division between 22.5 and 26 hpw. **C:** A Pax7:gfp$^+$ cell in adjacent unwounded hypaxial somite ventral to the wound site divides between 18 and 20 hpw (arrows). vb vertical borders, hm horizontal myoseptum. Scale bar 50 µm.

4.3.7 The number of Pax7$^+$ cells and Myogenin$^+$ cells in wounded somites increases during muscle regeneration

To quantify the number of myogenic cells in muscle wounds, Pax7 and Myogenin expression were used as markers of myogenic precursors in wounded fish. As described in Chapter 3, Pax7$^+$ cells in two to seven day old fish are found at the vertical septae, horizontal myoseptum, dorsal edge and in the central body. Moreover, the total number of Pax7$^+$ cells increases between 3 and 6 dpf due to specific increases at the vertical borders and central body. In this chapter, the changes in the population of myogenic cells expressing Pax7 and/or Myogenin in wounded epaxial somites were compared with adjacent unwounded epaxial somites in wounded fish. At **4 hpw**, few Pax7$^+$ cells could be seen at the wound site in contrast to the usual frequency of Pax7$^+$ cells in adjacent unwounded epaxial somites (Fig. 4.24A-C) suggesting that myogenic cells in the wounded muscle were adversely affected by wounding. Many more Myogenin$^+$ cells were apparent in the adjacent unwounded somites compared to the wound site within presumed fibres (Fig. 4.24D,E), suggesting a system wide response towards differentiation created by a lack of muscle in a small region. Myogenin$^+$Pax7$^+$ cells were rarely observed in wounds (data not shown), suggesting that shortly after wounding the few Pax7$^+$ cells remaining at the wound site do not show an increased propensity towards differentiation. To summarize the data suggest that shortly after wounding (4 hpw), myogenic cells in the wounded muscle are largely absent. Moreover, the propensity to differentiate appears unchanged in wounds but appears to be elevated elsewhere in unwounded regions.

At **1 dpw**, the wound site had many myogenic cells labelled by Pax7 and Myogenin antibodies (Fig. 4.25A), suggesting an increase in the number of myogenic cells in wounds at 1 dpw. Cells labeled by Pax7 appeared more frequently in wounded muscle especially in the central body (Fig. 4.25B,C). Moreover, the fraction of Pax7$^+$ cells in the central body also expressing Myogenin were more frequently observed in wounded muscle (Fig. 4.25D,E), suggesting an increase in the progression of Pax7$^+$ cells towards differentiation, also reflected by the increased frequency of Myogenin$^+$ cells at the wound site compared to unwounded muscle (4.25F,G). To summarize the data suggest that, by

1 dpw, the number of myogenic cells and differentiation increases in wounded muscle compared to adjacent unwounded muscle.

At **3 dpw**, wounded epaxial somites appear to contain an increased number of $Pax7^+$ cells (Fig. 4.26A) at the borders and in the central body compared to adjacent unwounded epaxial somites (Fig. 4.26B,C). The fraction of $Myogenin^+Pax7^+$ cells (Fig. 4.26D,E) and the number $Myogenin^+$ cells (Fig. 4.26F,G) appear to be similar between adjacent unwounded and wounded epaxial somites. The data suggests a further increase in the number of $Pax7^+$ cells at 3 dpw in wounded muscle whereas the fraction differentiating is similar to adjacent unwounded muscle.

To quantitate the observations in wounds, the number of $Pax7^+$ cells was counted from confocal images of immunostained fish at 4 hpw, 1 dpw and 3 dpw. Upon wounding, the number of $Pax7^+$ cells in the wounded epaxial somites decreased significantly at **4 hpw** in total ($p=1.71E-05$, Fig. 4.27A), at the borders ($p=0.003$) and in the central body ($p=5.42E-05$) compared to adjacent unwounded epaxial somites. The data indicate that $Pax7^+$ cells are decimated in wounded muscle shortly after wounding. By **1 dpw**, the total number of Pax7 cells in wounded somites recovered and is similar to that in the adjacent unwounded somites. Moreover, the total number of $Pax7^+$ cells significantly increased between 4 hpw and 1 dpw ($p=0.03$). Region-wise comparison revealed that the number of $Pax7^+$ cells in wounds is elevated in the central body compared to adjacent unwounded ($p=0.04$), but significantly increased compared to wounded 4 hpw ($p=0.03$). However, the number of $Pax7^+$ cells was significantly decreased when all the borders were compared to adjacent unwounded ($p=0.002$) but significantly elevated compared to vertical borders in wounds at 4 hpw ($p=0.0006$). The data indicate that $Pax7^+$ cells are present in the wound site at 1 dpw, likely accounting for a sizeable fraction of the nuclei in wounds at 1 dpw. Furthermore, majority of the $Pax7^+$ cells in wounds at 1 dpw appear to be at the site of future fibre generation i.e. the central body. At **3 dpw**, the total number of Pax7 cells in wounded muscle is significantly increased compared to adjacent unwounded muscle ($p=0.01$) due to increases at the borders ($p=0.007$) and in the central body ($p=0.01$). By 3 dpw, majority of the wound site is covered with muscle fibres. The data indicate that at this time point the number of $Pax7^+$ cells is further increased in

wounded somites at the borders and central body, confirming observations with live imaging at 76 hpw (Fig. 4.17). To summarize, the data indicate that the number of $Pax7^+$ cells decreased significantly shortly after wounding and recovered by 1 dpw, preceding the emergence of new fibres at 2 dpw. Moreover, the number of $Pax7^+$ cells further increased after bulk of fibre regeneration at 3 dpw.

To determine the likely contribution of $Pax7^+$ cells to regenerated muscle fibres, wounded larvae were co-labelled with Myogenin and the dual labeled cells in the central body were compared between wounded and unwounded epaxial somites. Differentiating Pax7 cells **(MyogeninPax7**, Fig. 4.27B) were decimated at **4 hpw** ($p=0.02$) but significantly increased in the central body at **1 dpw** ($p=0.0006$) and were similar to adjacent unwounded muscle at **3 dpw** ($p=0.05$). The data signifies that shortly after wounding at 4 hpw when the number of $Pax7^+$ cells in the wounded central body is significantly decreased, the tendency to differentiate is not altered. At 1 dpw the number of $Pax7^+$ cells in the central body of wounded somites is similar to that of unwounded somites whereas the fraction expressing Myogenin is significantly increased, indicating that more $Pax7^+$ cells are progressing to differentiation prior to the emergence of new fibres at 2 dpw. At 3 dpw, the number of $Pax7^+$ cells is significantly elevated in the central body of wounded somites whereas the fraction expressing Myogenin is similar to unwounded indicating that fewer $Pax7^+$ cells are progressing to differentiation after bulk of regeneration has occurred at this time point. Comparison of the percentage of $Pax7^+$ cells that are $Myogenin^+$ in the central body (Fig. 4.27C) confirmed that the rate of differentiation of $Pax7^+$ cells was similar between wounded and unwounded epaxial somites shortly after wounding at 4 hpw. At 1 dpw, the fraction of $Pax7^+$ cells expressing Myogenin significantly increased in the central body of wounded somites compared to unwounded somites. However, the number of $Pax7^+$ cells expressing Myogenin as a fraction of $Pax7^+$ cells was not changed significantly ($p=0.08$), suggesting that the increased number of $Pax7^+$ $Myogenin^+$ cells in the central body at 1 dpw is due to the increased number of $Pax7^+$ cells at this location and indicating that rate of differentiation is similar in wounds compared to unwounded. At 3 dpw, the number of $Pax7^+$ cells expressing Myogenin as a fraction of $Pax7^+$ cells was also similar between wounded and unwound ($p=0.3$), indicating that rate of differentiation of $Pax7^+$ cells is similar at this

time point. To summarize, the data indicate that rate of differentiation does not change significantly in wounds, although the fraction differentiating changes significantly through the time course of wound repair.

Myogenin expression was used to obtain a more direct readout of differentiating myogenic precursors in the central body of wounded and unwounded somites (Fig. 4.27D). Myogenin cells in the central body of wounded somites were decimated at **4 hpw** ($p=0.017$), significantly increased at **1 dpw** ($p=0.009$) and were not significantly different from adjacent unwounded muscle ($p=0.05$) at **3 dpw**. The data indicate that the number of differentiating precursors increased significantly at 1 dpw prior to the emergence of new fibres at 2 dpw and is similar to unwounded somites at 3 dpw, the time point by which more than 75% of the wounded region is covered with fibres.

To summarize, the data indicate that $Pax7^+$ and $Myogenin^+$ myogenic precursors are present in sufficient number at wound site at 1 dpw to account for the nuclear number estimated at this time point (approximately 75). However, since there are likely to be other cell types in the wound such as those belonging to blood vessels or neurons, the number of nuclei counted from transverse sections might represent an underestimated number of nuclei in wounds. Increase in the number of myogenic cells in wounds between 4 hpw and 3 dpw suggests is likely by proliferation and migration during muscle repair. To determine the role of proliferation in the increase in number of $Pax7^+$ cells during muscle repair, the number of $Pax7^+$ cells in S-phase was quantified.

.

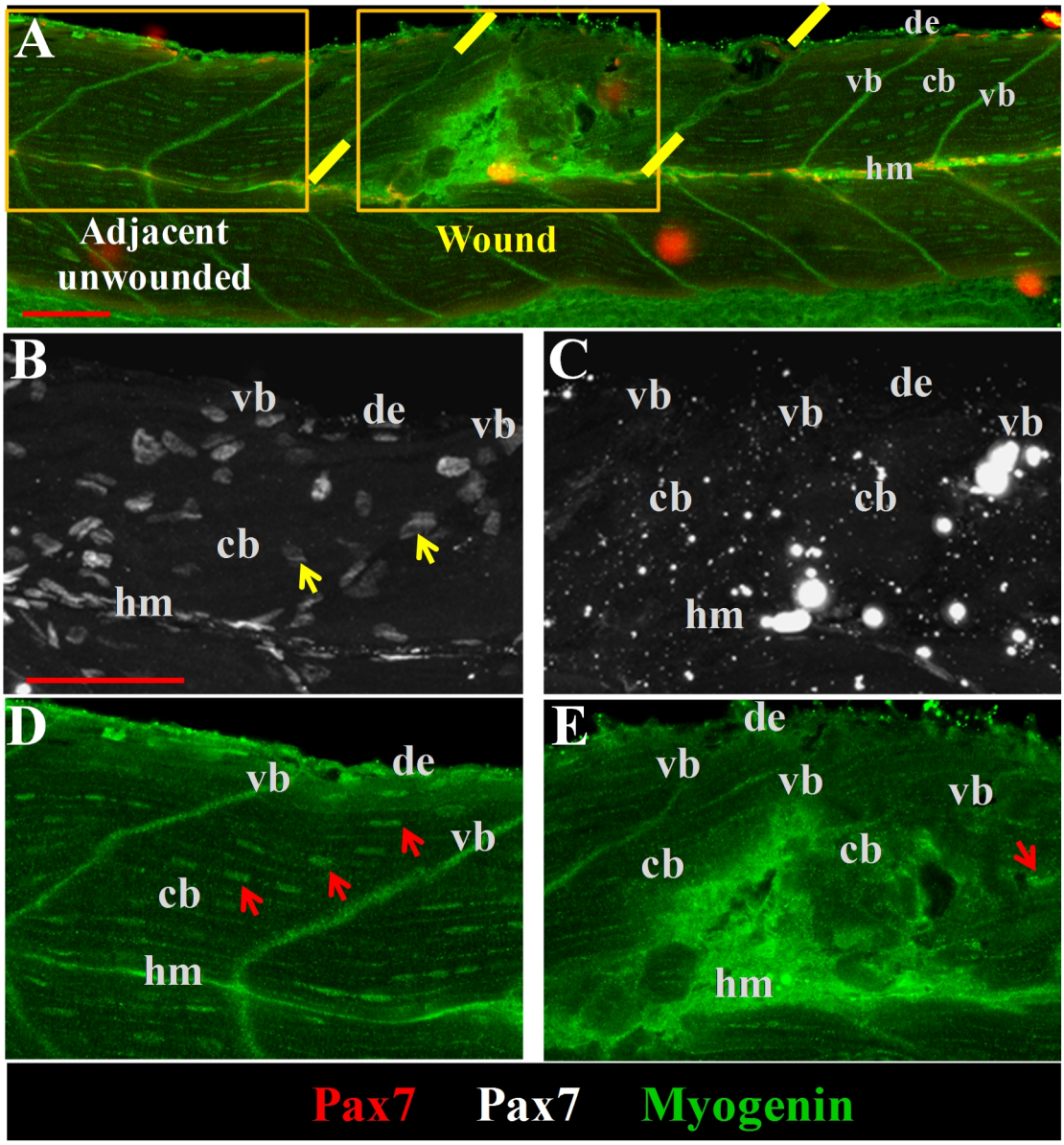


Fig. 4.24 Pax7$^+$ and Myogenin$^+$ cells are decimated in wounds at 4 hpw.
Wholemount wild type larvae at 3 dpf were mechanically wounded and fixed at 4 hours post wounding for immunostaining to detect Pax7 (red (A), also false colored white in panels B,C) and Myogenin (green, A,D,E). Larvae were also stained with Hoechst 33342 to detect nuclei. Confocal images are short stacks from a confocal stack of the wholemount larva with stacks in A,D,E from the deep myotome whereas stacks in B,C are from the superficial myotome. Lateral views (A-E) are oriented with dorsal up and anterior to left. Boxed regions in A are magnified in insets B-E. Vertical yellow bars demarcate wound region from adjacent unwounded **A-E:** Pax7$^+$ cells (arrows, B) and Myogenin$^+$ cells (arrows, D) in presumed fibers in the adjacent unwounded are frequently observed in contrast to rare Pax7$^+$ cells (C) and Myogenin$^+$ cells (E, arrow) in wounded epaxial somites. The dots in C are secondary antibody sticking to debris in wounded

tissue. vb vertical borders, cb central body, de dorsal edge, hm horizontal myoseptum. Scale bars 50 μm.

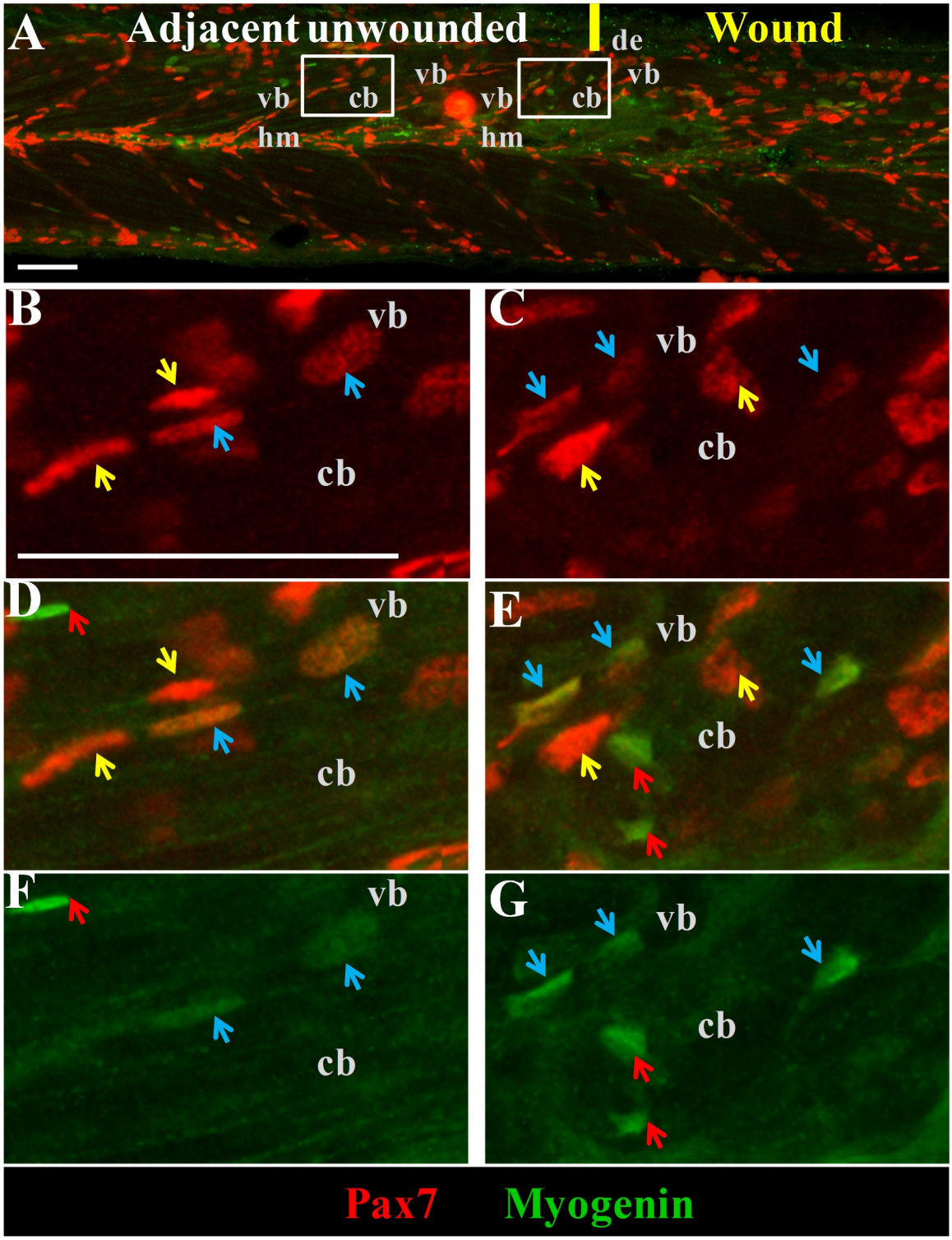


Fig. 4.25 Numerous Pax7^{+} and Myogenin^{+} cells are present in wounds at 1 dpw

Fig. 4.25 Numerous Pax7$^+$ and Myogenin$^+$ cells are present in wounds at 1 dpw. Wholemount wild type larvae at 3 dpf were mechanically wounded and fixed at one day post wounding for immunostaining to detect Pax7 (red, A-E), and Myogenin (green, A,D-G). Larvae were also stained with Hoechst 33342 to detect nuclei. Confocal images are a short stack from a confocal stack of the wholemount larva. Lateral views (A-G) are oriented with dorsal up and anterior to left. Boxed regions in A are magnified in insets B-G such that insets B,D,F are from adjacent unwounded, whereas C,E,G are from wounded region. Vertical yellow bar demarcates wound region from adjacent unwounded. Pax7$^+$ cells are denoted by yellow arrows, Pax7$^+$Myogenin$^+$ cells are denoted by blue arrows and Myogenin$^+$ cells are denoted by red arrows. **A:** Numerous Pax7$^+$ and Myogenin$^+$ cells are apparent in wounded epaxial somites. **B,C:** Pax7$^+$ cells are apparent at the vertical border and central body of adjacent unwounded (B) and wounded (C) epaxial somites (arrows). **D,E:** Pax7$^+$Myogenin$^+$ cells are apparent in the vertical border and central body of adjacent unwounded (D) and wounded (E) epaxial somites (arrows). Pax7$^+$Myogenin$^+$ cells appear more numerous in wounds. **F,G:** Myogenin$^+$ cells are apparent in the central body of adjacent unwounded (F) and wounded (G) epaxial somites (arrows). Myogenin$^+$ cells appear more numerous in wounds (arrows). vb vertical borders, cb central body, de dorsal edge, hm horizontal myoseptum. Scale bars 50 μm.

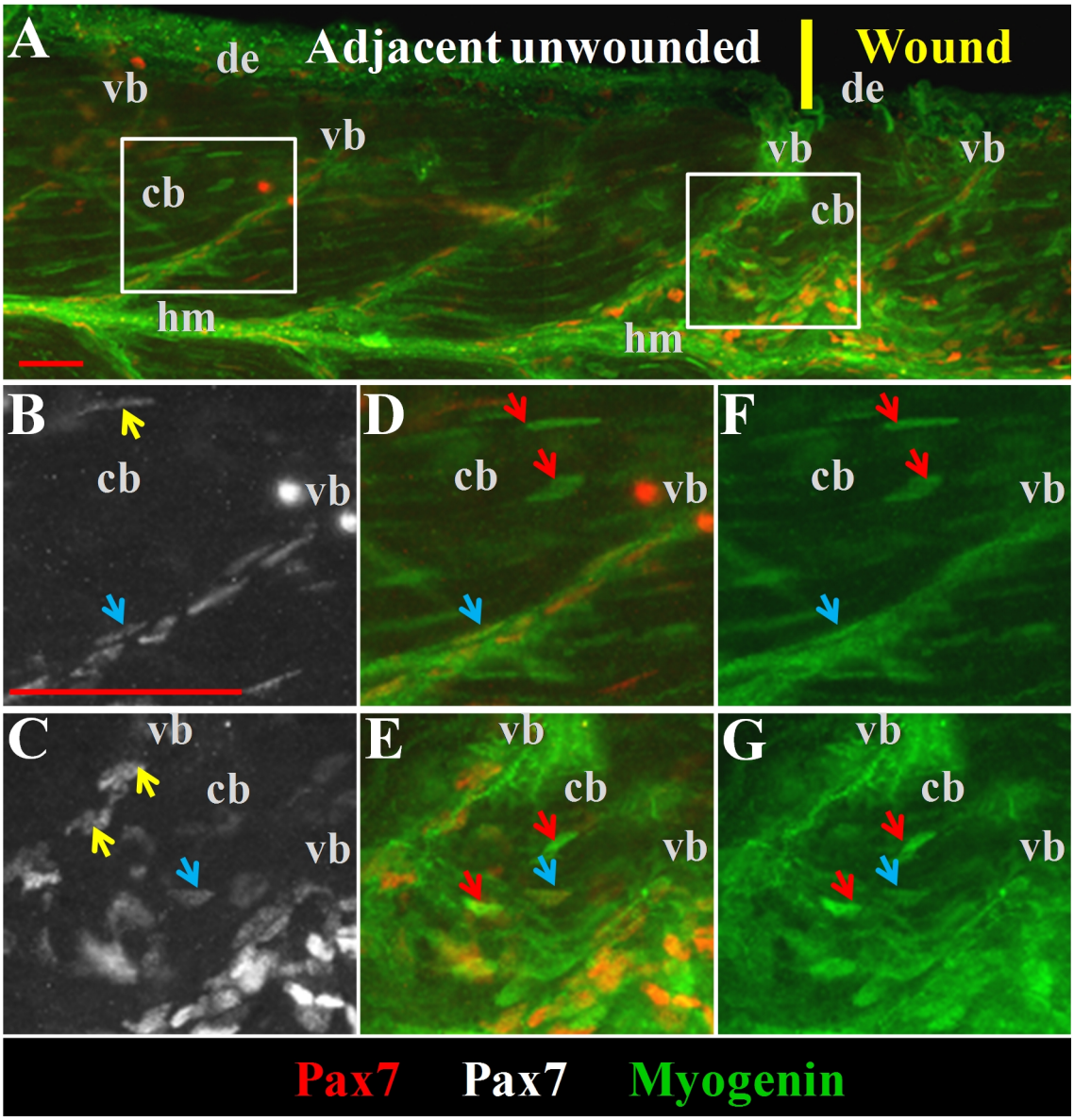


Fig. 4.26 Pax7^{+} and Myogenin^{+} cells appear more numerous in wounds compared to adjacent unwounded at 3 dpw.

Fig. 4.26 Pax7$^+$ and Myogenin$^+$ cells appear more numerous in wounds compared to adjacent unwounded at 3 dpw.
Wholemount wild type larvae at 3 dpf were mechanically wounded and fixed at three days post wounding for immunostaining to detect Pax7 (red, A-E), and Myogenin (green, A,D-G). Larvae were also stained with Hoechst 33342 to detect nuclei. Confocal images are a short stack from a confocal stack of the wholemount larva. Lateral views (A-G) are oriented with dorsal up and anterior to left. Boxed regions in A are magnified in insets B-G such that insets B,D,F are from adjacent unwounded, whereas C,E,G are from wounded region. Vertical yellow bar demarcates wound region from adjacent unwounded. Pax7$^+$ cells are denoted by yellow arrows, Pax7$^+$Myogenin$^+$ cells are denoted by blue arrows and Myogenin$^+$ cells are denoted by red arrows. **A,B,C:** Pax7$^+$ cells are apparent at the vertical border (arrow, B) and central body (arrow, B) of adjacent unwounded epaxial somites. Pax7$^+$ cells in wounded region (arrows, C) appear more numerous compared to unwounded region (B). **D,E:** Pax7$^+$Myogenin$^+$ cells are apparent in the vertical border and central body of adjacent unwounded (D) and wounded (E) epaxial somites (arrows). Pax7$^+$Myogenin$^+$ cells appear more numerous in wounds. **F,G:** Myogenin$^+$ cells are apparent in the central body of adjacent unwounded (F) and wounded (G) epaxial somites (arrows) and appear more numerous in wounds (arrows). vb vertical borders, cb central body, de dorsal edge, hm horizontal myoseptum. Scale bars 50 μm.

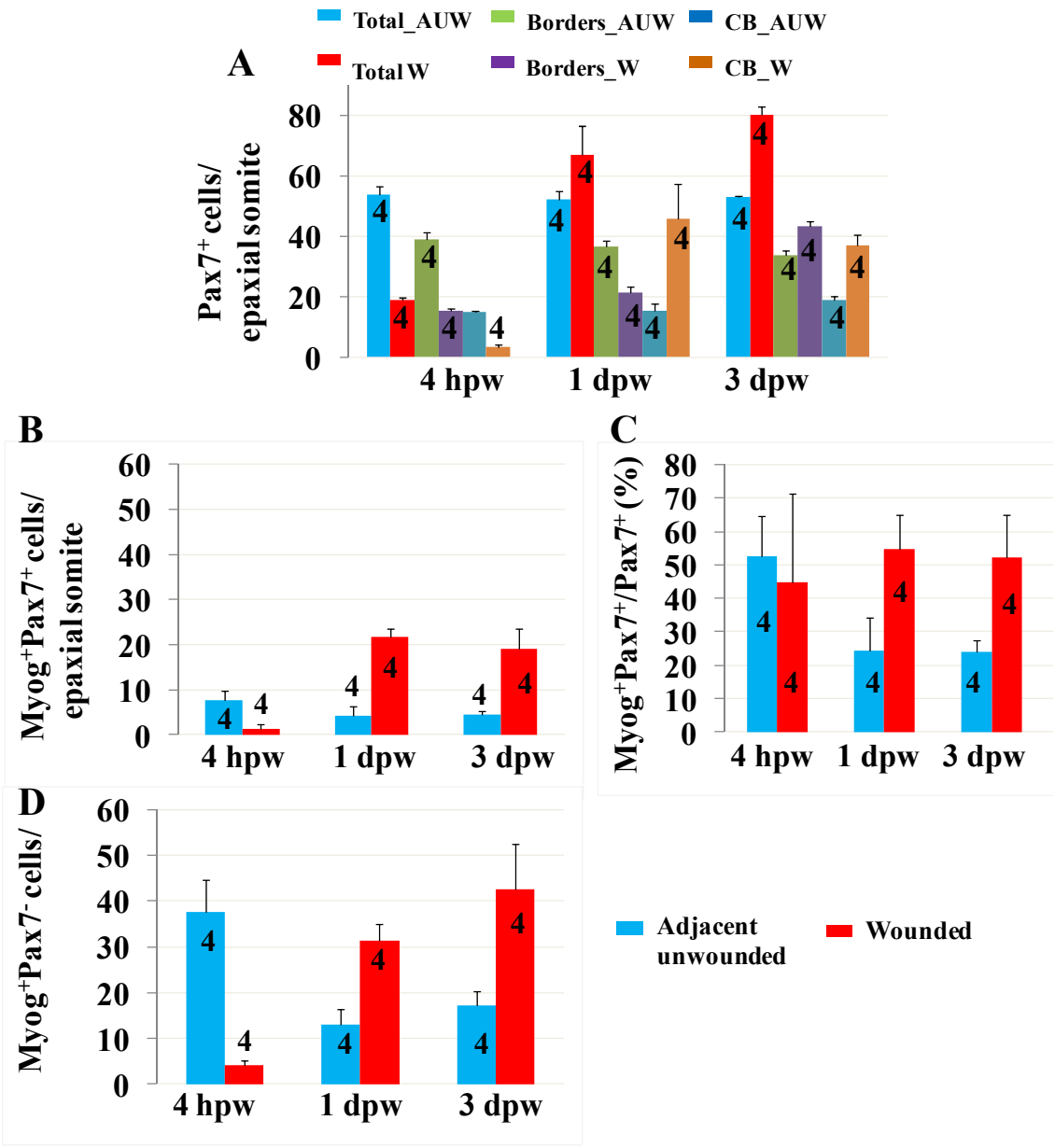


Fig. 4.27 Pax7$^+$ cells increase spatiotemporally in wounded muscle.

Fig. 4.27 Pax7$^+$ cells increase spatiotemporally in wounded muscle.
Wholemount wild type larvae at 3 dpf were mechanically wounded and fixed at four hours, one day and three days post wounding for immunostaining to detect Pax7$^+$, Pax7$^+$Myogenin$^+$ and Myogenin$^+$ cells. Quantification of mononucleate Pax7$^+$ cells (A), Myogenin$^+$ Pax7$^+$ cells (B,C) and Myogenin$^+$Pax7$^-$ cells (D) in adjacent unwounded (blue columns) wounded (red columns) epaxial somites at 4 hours post wound (4 hpw), 1 dpw and 3 dpw in the number of fish indicated within bars from two separate experiments. **A:** The number of Pax7$^+$ cells in total (p=1.71E-05) and specifically at the borders (p=0.003) and central body (p=5.24E-05) are significantly reduced at 4 hpw compared to adjacent unwounded. At 1dpw the number of Pax7$^+$ cells in total (p=0.03), at the borders (p=0.0006) and in the central body (p=0.03) are significantly increased compared to the respective Pax7$^+$ levels at 4 hpw in wounded epaxial somites. Moreover, the total number of Pax7$^+$ cells is similar between adjacent unwounded and wounded epaxial somites at 1 dpw although elevated in wounded central body (p=0.04) and significantly reduced when all the borders (p=0.002) are compared to adjacent unwounded. The number of Pax7$^+$ cells at 3 dpw is significantly increased in wounded epaxial somites in total (p=0.01), at the borders (p=0.007), and in the central body (p=0.01) compared to adjacent unwounded epaxial somites. **B:** The number of Myogenin$^+$Pax7$^+$ cells in the central body are significantly reduced at 4 hpw (p=0.02), significantly increased at 1 dpw (p=0.0006) and similar at 3 dpw (p=0.05) compared to adjacent unwounded epaxial somites. **C:** The number of Myogenin$^+$Pax7$^+$ cells as a fraction of Pax7$^+$ cells is similar between adjacent unwounded and wounded epaxial somites at 4 hpw, 1 dpw and 3 dpw. **D:** The number of Myogenin$^+$Pax7$^-$ cells in the central body are significantly reduced at 4 hpw (p=0.017), significantly increased at 1 dpw (p=0.009) and similar at 3 dpw (p=0.05) compared to adjacent unwounded epaxial somites. Error bars are standard error of the mean. AUW Adjacent unwounded, W Wounded.

4.3.8 The fraction of Pax7$^+$ cells in the S-phase increases at the borders and central body during muscle regeneration

The number of Pax7$^+$ cells significantly increased between 4 hpw and 3 dpw in wounded somites, suggesting an increase in Pax7$^+$ cell number by proliferation. To examine the dynamics of proliferating Pax7$^+$ cells during wound repair, wounded larvae were labeled with anti-Pax7 antibody and S-phase marker EdU at 5 hpw (Fig. 4.28), 1 dpw (Fig. 4.29) and 2 dpw (Fig. 4.30). At **5 hpw**, Pax7$^+$ cells at wound site appeared reduced confirming results obtained in the previous sections (Fig. 4.28A,C). In adjacent unwounded muscle, Pax7$^+$ nuclei co-labeling with EdU were generally bright and elongated and located at the borders and central body (Fig. 4.28B,C,D). In contrast, dim and rounded Pax7$^+$ nuclei in the central body and bright rounded nuclei at the borders in the wounded muscle appeared co-labeled with EdU. The data shows that the morphology of Pax7$^+$EdU$^+$ nuclei is altered in wounded muscle shortly after wounding such that the cells are predominantly rounded

suggesting that they are apoptotic cells. At **1 dpw**, many $Pax7^+$ cells are noticeable in wounds. Many of the $Pax7^+$ cells in the central body and few at the borders of wounded somites co-label with EdU (Fig. 4.29A-D). The data suggests an increase in the number of $Pax7^+$ and $Pax7^+$ cells in S-phase in wounds at 1 dpw. At **2 dpw**, numerous $Pax7^+EdU^+$ cells are visible in wounded muscle compared to adjacent unwounded (Fig. 4.30A-D). Thus, the data suggest an increasing number of $Pax7^+$ EdU^+ cells in wounds between 5 hpw and 3 dpw.

The number of $Pax7^+$ cells increased at specific locations during muscle repair between 4 hpw and 3 dpw suggesting changes in proliferation specific to these locations. To examine the dynamics of proliferating $Pax7^+$ cells in a region-wise manner during wound repair, the number of $Pax7^+$ cells, dual labeled cells ($Pax7^+EdU^+$) and the number of $Pax7^+EdU^+$ cells as a fraction of $Pax7^+$ cells was compared at the various somitic locations between control (unwounded embryos), wounded and unwounded somites (wounded embryos) at 5 hpw (Fig. 4.31), 1 dpw (Fig. 4.32) and 2 dpw (Fig. 4.33). Quantification of the number showed that $Pax7^+$ cells in wounds were significantly decreased at **5 hpw** compared to both controls (p=6.54719E-05) and adjacent unwounded (p=0.02), confirming previous results. The number of total $Pax7^+EdU^+$ cells was reduced compared to controls (0.025). The fraction of $Pax7^+$cells in S-phase was similar between wounded, adjacent unwounded and control epaxial somites.

Region-wise comparison indicated that the number of $Pax7^+$ cells at the vertical borders of wounded epaxial somites was significantly reduced in wounded epaxial somites compared to adjacent unwounded (p=0.008) and controls (p=1.22E-05). The number of $Pax7^+EdU^+$ cells was also significantly reduced at the vertical borders of wounded epaxial somites compared to adjacent unwounded (p=0.03). The fraction of $Pax7^+$ cells in S-phase was significantly increased at the vertical borders of both adjacent unwounded (p=0.01) and wounded (p=0.005) epaxial somites compared to controls indicating that more $Pax7^+$ cells at the vertical borders are ready for proliferation. Similar analysis at the horizontal myoseptum revealed that the number of $Pax7^+$ cells decreased significantly at this location in wounded epaxial somites compared to controls (p=0.0002) and adjacent unwounded (p=0.0006). However, the number of $Pax7^+EdU^+$ cells and the fraction of

$Pax7^+$ cells in S-phase remained unchanged. The number of $Pax7^+$ cells at the dorsal edge appeared to reduce, though not significantly (p=0.07). Moreover, the number of $Pax7^+EdU^+$ cells and the fraction of $Pax7^+$ cells in S-phase remained unchanged. The data indicate that amongst the borders, the vertical border appears to harbour a population of $Pax7^+$ cells that are first responders to the loss of $Pax7^+$ cells. In contrast to the borders, in the central body both $Pax7^+EdU^+$ cells and the fraction in S-phase were significantly reduced compared to controls (p=0.03 and 0.03 respectively) and adjacent unwounded (p=0.01 and 0.01 respectively), indicating that the $Pax7^+$ cells in the central body were not getting ready to proliferate unlike the vertical borders. To summarize, the data indicate that shortly after wounding the frequency of $Pax7^+$ cells in S-phase increases significantly in wounded embryos in a system-wide manner and could lead to an increase in the number of $Pax7^+$ cells in both wounded and unwounded somites of wounded larvae at 1 dpw. However at **1 dpw**, the total number of $Pax7^+$ cells was found to be similar between control, unwounded and wounded epaxial somites confirming previous results (Section 4.7) and indicating a significant increase in the number of $Pax7^+$ cells in wounds by 1 dpw (p=0.03), but not in the adjacent unwounded somites (Fig. 4.32). A possibility is that the extra $Pax7^+$ cells in adjacent unwounded somites differentiate to Myogenin expressing cells or migrate into wounds. Since, the number of $Myogenin^+$ cells in adjacent unwounded somites is not significantly increased at 1 dpw, the latter hypothesis is likely. Taking this scenario into account, the data suggests that proliferation of $Pax7^+$ cells at the vertical borders at 5 hpw leads to increases in the number of $Pax7^+$ cells in wounds by 1 dpw. The total number of $Pax7^+EdU^+$ cells was found to be similar between control and adjacent unwounded epaxial somites, but significantly increased in wounded epaxial somites compared to controls (p=0.03) and adjacent unwounded (p=0.02), indicating that more $Pax7^+$ cells in S-phase are present in wounds at 1 dpw. However, the number of $Pax7^+EdU^+$ cells as a fraction of $Pax7^+$ cells was found to be similar between the three groups, indicating that the fraction of $Pax7^+$ cells entering S-phase are similar in wounded and healthy tissue at 1 dpw, in contrast to the increased fraction in wounded tissue at 5 hpw. Region-wise comparison revealed that the number of $Pax7^+$ cells and $Pax7^+EdU^+$ cells was similar at the vertical borders between control, adjacent unwounded and wounded epaxial somites. However, the number of $Pax7^+$ EdU^+ cells as a fraction of

Pax7$^+$ cells was still significantly increased at the vertical borders in adjacent unwounded and wounded compared to controls (p=0.019 and p=0.012) respectively, indicating that more Pax7$^+$ cells at the vertical borders were in S-phase in wounded embryos compared to controls. Since time-lapse showed many Pax7:gfp$^+$ cells extending into the wounds via vertical borders, it is possible that proliferating Pax7$^+$ cells at the vertical borders provide many of the Pax7$^+$ cells in wounded muscle. The number of Pax7$^+$ cells, Pax7$^+$EdU$^+$ cells and the fraction of Pax7$^+$ cells in S-phase at the horizontal myoseptum and dorsal edge were similar in wounds compared to adjacent unwounded and controls, indicating that cells at these locations in the wound were proliferating similar to unwounded/controls. The number of Pax7$^+$ cells in the central body was found to be similar between control, adjacent unwounded and wounded whereas the number of Pax7$^+$EdU$^+$ cells was significantly increased in the central body of wounded epaxial somites compared to control (0.018) and adjacent unwounded (p=0.003) epaxial somites, indicating an increase in the number of Pax7$^+$ cells in S-phase in the central body at 1 dpw. However, the number of Pax7$^+$EdU$^+$ as a fraction of Pax7$^+$ cells was found to be similar between control and wounded (p=0.16) at the central body and with a tendency towards increase between adjacent unwounded and wounded (p=0.049), indicating that the frequency of Pax7$^+$ cells in S-phase was similar between the three groups with respect to central body location. To summarize, the data at 1 dpw show that the increase in the fraction of Pax7$^+$ cells in S-phase at 5 hpw persists at the vertical borders at 1 dpw. Moreover, the number proliferative Pax7$^+$ cells in the central body increased at 1 dpw but not at the dorsal edge and horizontal myoseptum. Moreover, the frequency of Pax7$^+$ cells to be in S-phase is increased in a system wide manner at the vertical borders in contrast to the horizontal myoseptum, dorsal edge and central body where it is similar between the three groups. The increase in proliferative Pax7$^+$ cells in wounds at 1 dpw could give rise to an increased number of Pax7$^+$ cells observed at later time points during muscle repair.

At 3 dpw the number of Pax7$^+$ cells is significantly increased in wounded epaxial somites compared to unwounded. To determine the role of proliferation in this increase, the number of Pax7$^+$EdU$^+$ cells was compared between adjacent unwounded and wounded epaxial somites from wounded embryos at **2 dpw**. The total number of Pax7$^+$ cells was

found to be similar between wounded, adjacent unwounded and age-matched controls (Fig. 4.33). However, both the total number of $Pax7^{+}EdU^{+}$ cells and the fraction of $Pax7^{+}$ cells in S-phase were significantly increased in wounded epaxial somites compared to adjacent unwounded ($p=0.0009$ and $p=0.001$ respectively), indicating that more $Pax7^{+}$ cells in wounds were proliferating and possibly leading to the increased number of $Pax7^{+}$ cells in wounds at 3 dpw.

The number of $Pax7^{+}$ cells increased at the borders and central body at 3 dpw. Region-wise comparison at all the borders and vertical borders alone unexpectedly revealed that the number of $Pax7^{+}$ cells, $Pax7^{+}EdU^{+}$ cells and the fraction of $Pax7^{+}$ cells in S-phase was similar between adjacent unwounded and wounded somites. It is plausible that proliferating $Pax7^{+}$ cells from adjacent healthy muscle translocate to the borders at 2 dpw thereby increasing the number of $Pax7^{+}$ cells at the borders at 3 dpw without an increase in the number of $Pax7^{+}$ cells in S-phase at this location. In the central body, the number of $Pax7^{+}$, $Pax7^{+}EdU^{+}$ and $Pax7^{+}$ cells in S-phase significantly increased ($p=0.006$, $p=0.005$ and $p=0.02$ respectively), supporting the hypothesis that $Pax7^{+}$ cells proliferating in the central body at 2 dpw led to an increased number of $Pax7^{+}$ cells at this location by 3 dpw.

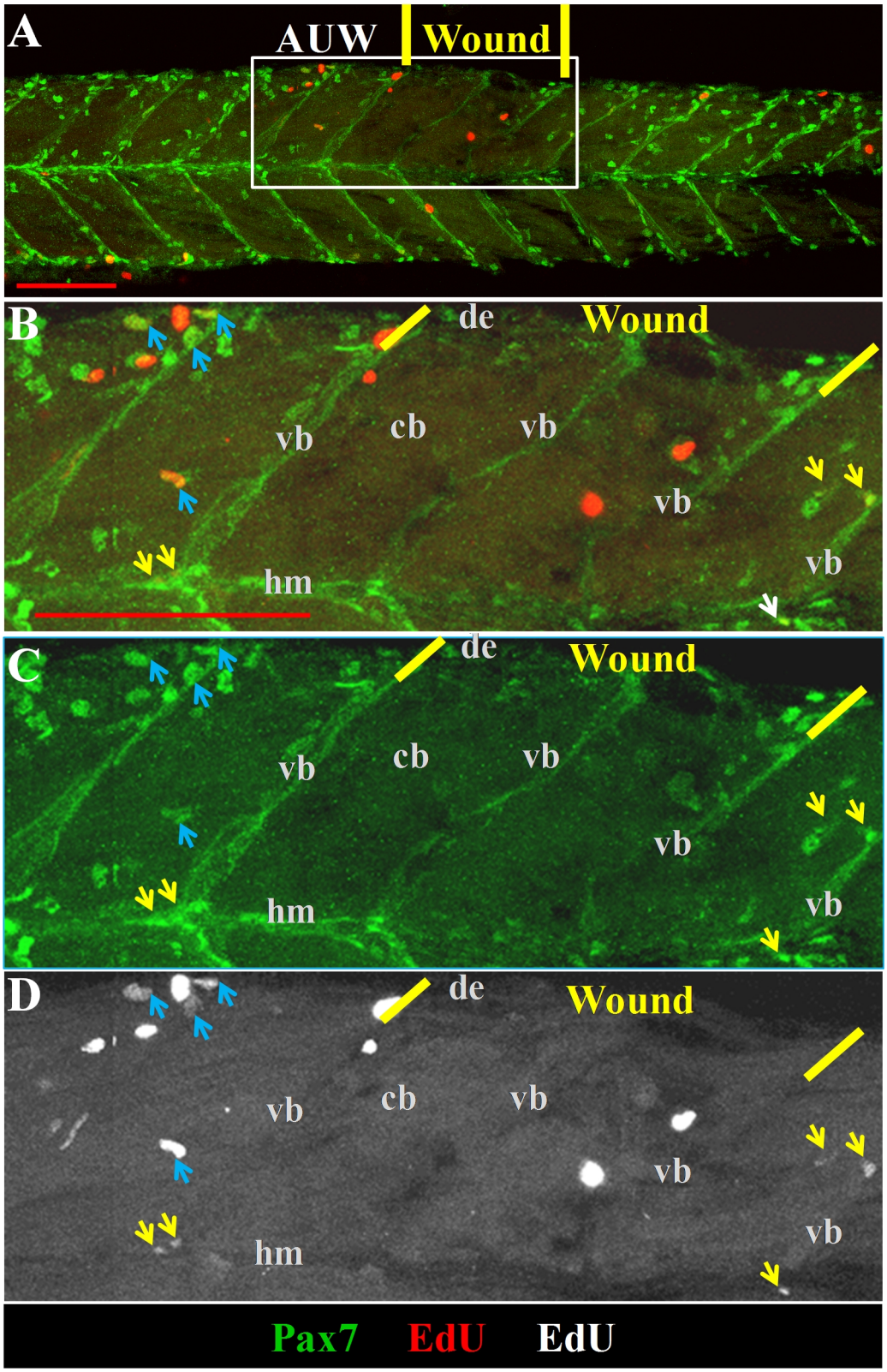


Fig. 4.28 Pax7^{+}EdU^{+} nuclei in wounded and unwounded epaxial somites at 5 hpw.

Fig. 4.28 $Pax7^{+}EdU^{+}$ nuclei in wounded and unwounded epaxial somites at 5 hpw. Wholemount wild type larvae at 3 dpf were mechanically wounded and fixed at 5 hours post wounding for immunostaining to detect Pax7 (green (A,B,C) and EdU (red, A,B, also false colored white in D). Larvae were also stained with Hoechst 33342 to detect nuclei. Confocal images are short stacks from a confocal stack of the wholemount larva. Lateral views (A-D) are oriented with dorsal up and anterior to left. Boxed region in A is magnified in B-D. Vertical yellow bars demarcate wound region from adjacent unwounded. Blue arrows denote cells in adjacent unwounded epaxial somites whereas yellow arrows denote cells in the wounded epaxial somites. **A,B:** $Pax7^{+}EdU^{+}$ cells are apparent in adjacent unwounded and wounded epaxial somites (arrows). **C,D:** In adjacent unwounded region, $Pax7^{+}$ cells (blue arrows, C) co-labeling with EdU (blue arrows, D) appear larger compared to those in wounded region (yellow arrows, C,D). vb vertical borders, cb central body, de dorsal edge, hm horizontal myoseptum. Scale bars 50 μm.

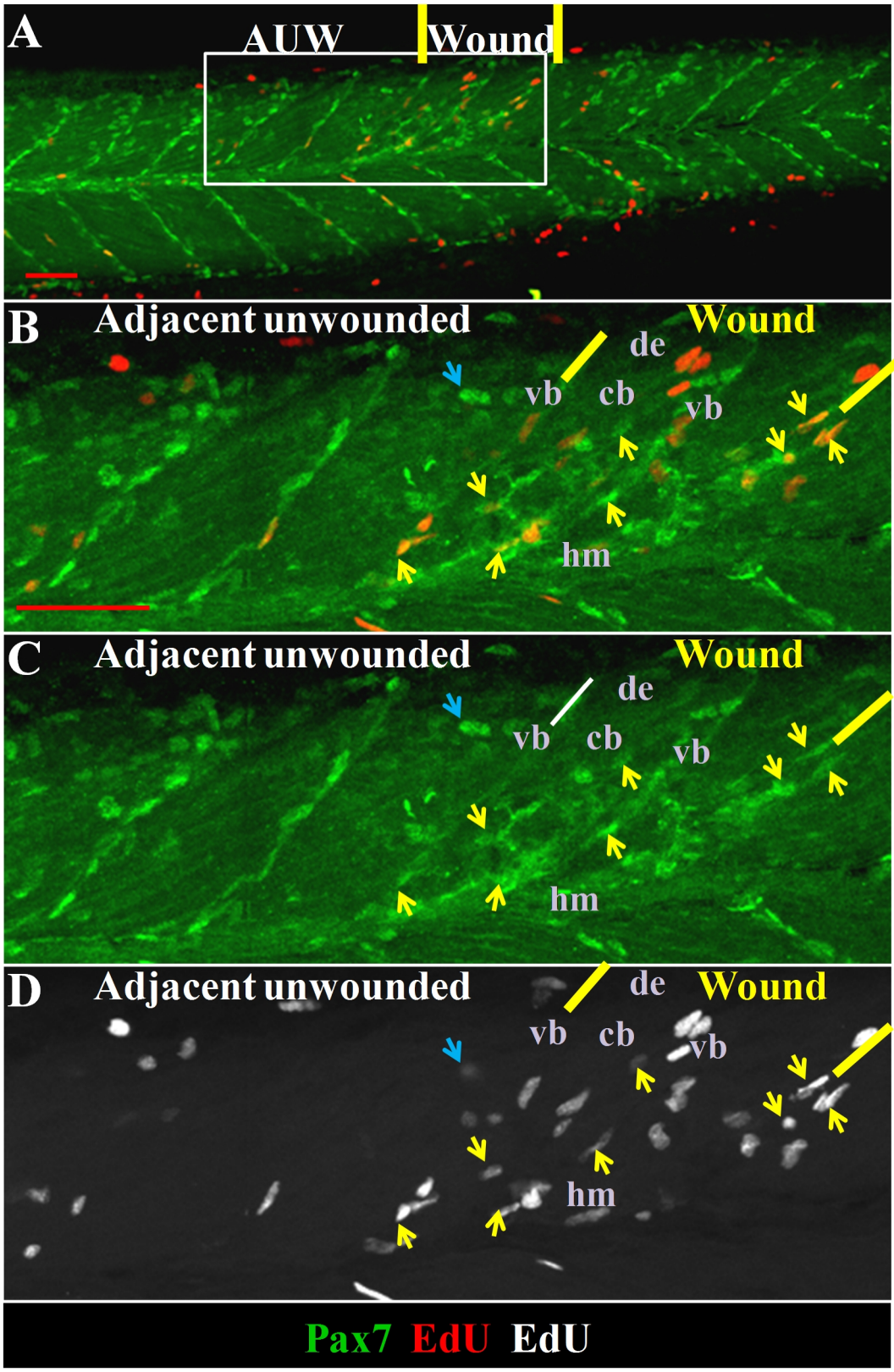


Fig. 4.29 Numerous Pax7^{+}EdU^{+} nuclei appear in wounds by 1 dpw.

Fig. 4.29 Numerous $Pax7^{+}EdU^{+}$ nuclei appear in wounds by 1 dpw.
Wholemount wild type larvae at 3 dpf were mechanically wounded and fixed at one day post wounding for immunostaining to detect Pax7 (green (A,B,C) and EdU (red, A,B, also false colored white in D). Larvae were also stained with Hoechst 33342 to detect nuclei. Confocal images are short stacks from a confocal stack of the wholemount larva. Lateral views (A-D) are oriented with dorsal up and anterior to left. Boxed region in A is magnified in B-D. Vertical yellow bars demarcate wound region from adjacent unwounded. Blue arrow denotes a cell in adjacent unwounded epaxial somite whereas yellow arrows denote cells in the wounded epaxial somites. **A-D:** $Pax7^{+}EdU^{+}$ cells are apparent in adjacent unwounded and wounded epaxial somites (arrows), although appearing more numerous in wounds. vb vertical borders, cb central body, de dorsal edge, hm horizontal myoseptum. Scale bars 50 μm.

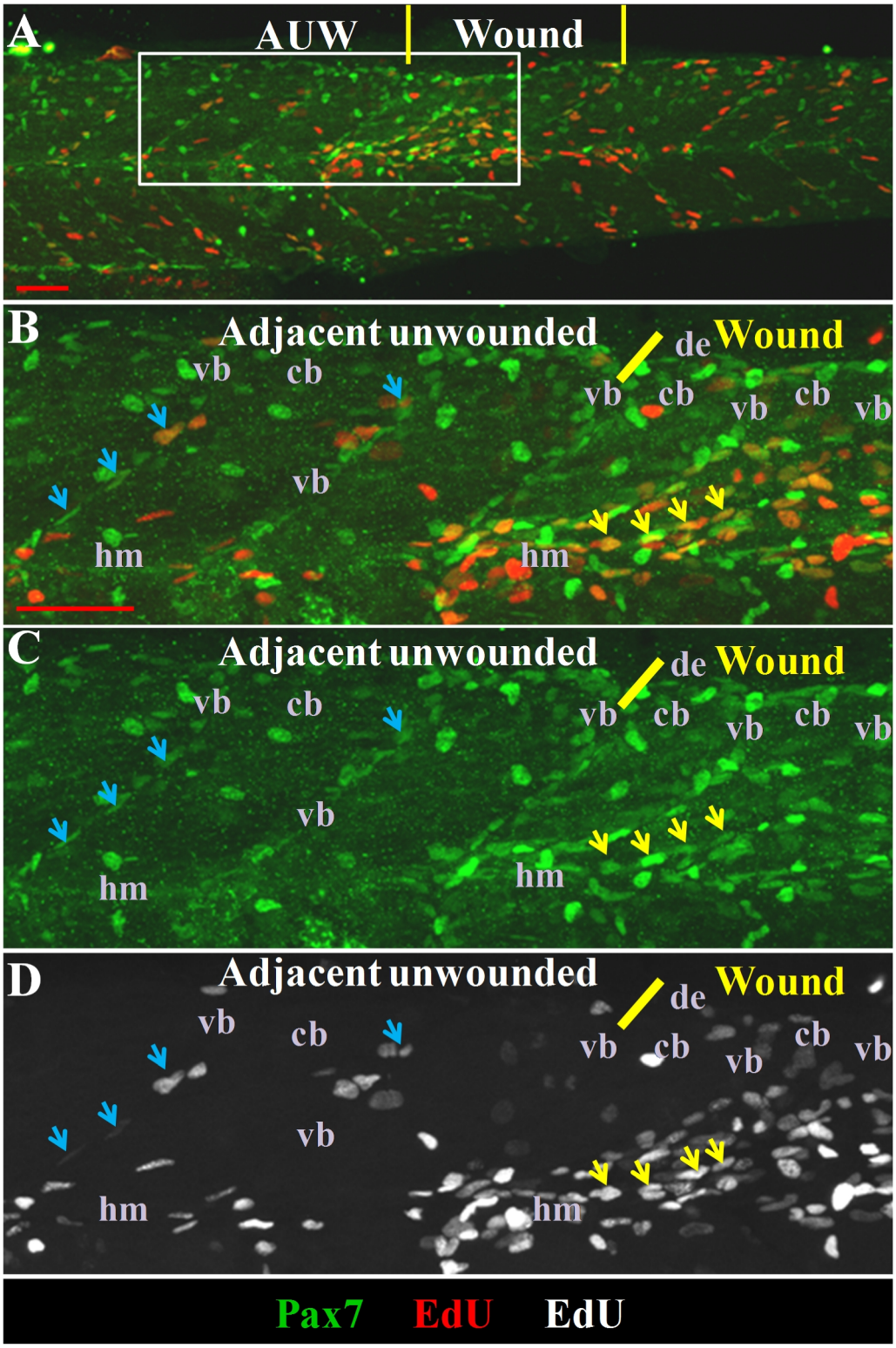


Fig. 4.30 Pax7^{+}EdU^{+} nuclei in the central body of wounds compared to adjacent unwounded at 2 dpw.

Fig. 4.30 $Pax7^{+}EdU^{+}$ nuclei in the central body of wounds compared to adjacent unwounded at 2 dpw.

Wholemount wild type larvae at 3 dpf were mechanically wounded and fixed at three days post wounding for immunostaining to detect Pax7 (green (A,B,C) and EdU (red, A,B, also false colored white in D). Larvae were also stained with Hoechst 33342 to detect nuclei. Confocal images are short stacks from a confocal stack of the wholemount larva. Lateral views (A-D) are oriented with dorsal up and anterior to left. Boxed region in A is magnified in B-D. Vertical yellow bars demarcate wound region from adjacent unwounded. Blue arrow denotes cells in adjacent unwounded epaxial somite whereas yellow arrows denote cells in the wounded epaxial somites. **A-D:** $Pax7^{+}EdU^{+}$ cells are apparent in adjacent unwounded and wounded epaxial somites (arrows), and appear more numerous in wounds, especially in the central body region. vb vertical borders, cb central body, de dorsal edge, hm horizontal myoseptum. Scale bars 50 μm.

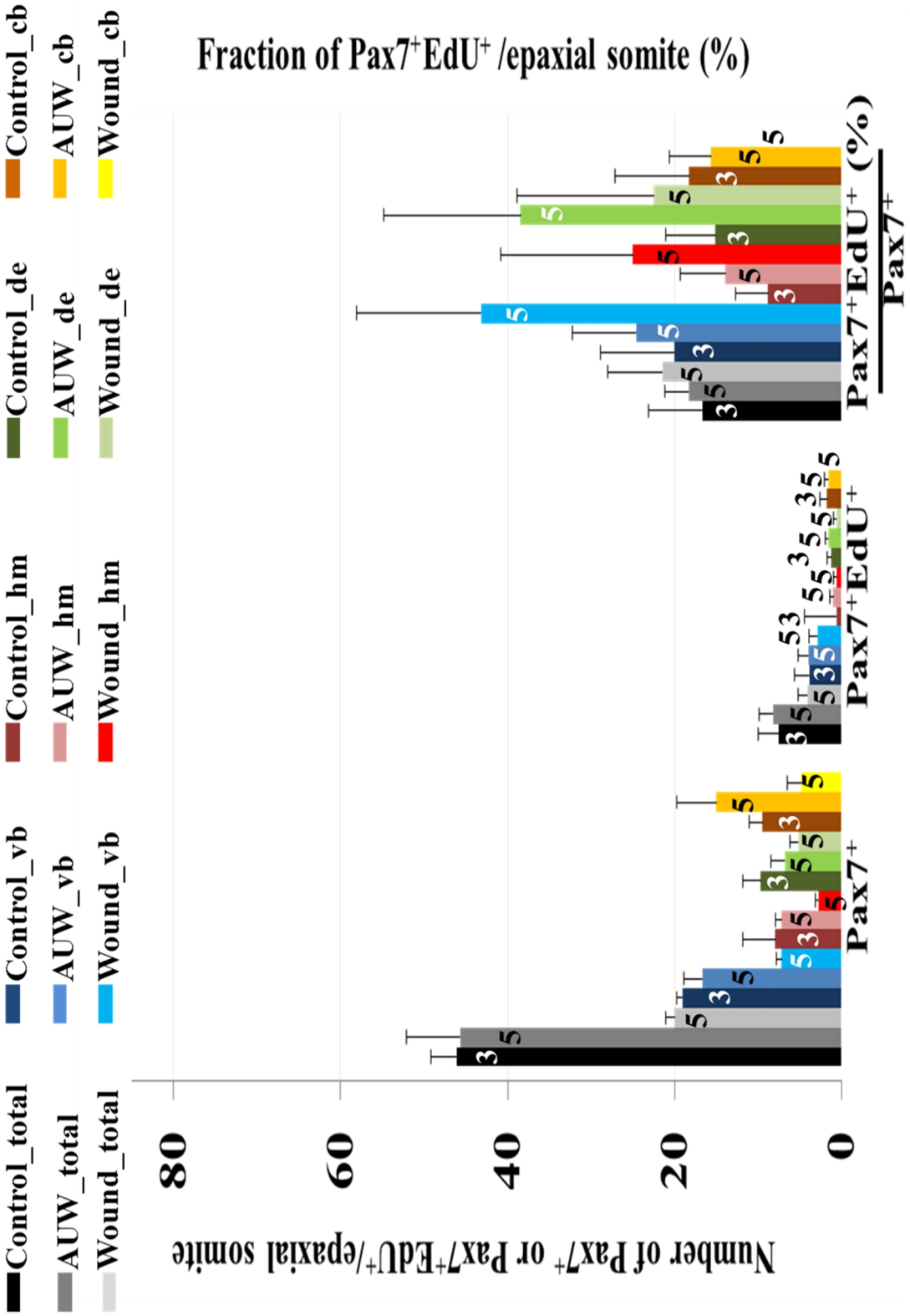


Fig. 4.31 At 5 hpw Pax7^{+} cells in S-phase are located at the vertical borders of both wounded and adjacent unwounded somites.

Fig. 4.31 At 5 hpw Pax7$^+$ cells in S-phase are located at the vertical borders of both wounded and adjacent unwounded somites.

Wholemount wild type larvae at 3 dpf were mechanically wounded and fixed at five hours post wounding for immunostaining to detect Pax7$^+$EdU$^+$ cells. Quantification of mononucleate Pax7$^+$, Pax7$^+$EdU$^+$ cells and the number of Pax7$^+$EdU$^+$ cells as a fraction of Pax7$^+$ cells in control, adjacent unwounded and wounded epaxial somites at 5 hours post wound in the number of fish indicated within bars from two separate experiments. The number of total Pax7$^+$ cells was significantly reduced in wounds compared to controls (p=6.55E-05) and adjacent unwounded (p=0.02). Total Pax7$^+$EdU$^+$ cells was significantly reduced in wounded epaxial somites compared to controls (p=0.025). The fraction of Pax7$^+$ cells that were in S-phase was similar between control, adjacent unwounded, and wounded epaxial somites. The number of Pax7$^+$ cells at the vertical borders was significantly reduced in wounded compared to controls (p=1.22E-05) and adjacent unwounded (p=0.008). The number of Pax7$^+$EdU$^+$ cells was also significantly reduced at the vertical borders in wounded epaxial somites compared to adjacent unwounded (p=0.03). The fraction of Pax7$^+$ cells in S-phase was also significantly increased at the vertical borders of both adjacent unwounded (p=0.01) and wounded (p=0.005) epaxial somites compared to controls. The number of Pax7$^+$ cells at the horizontal myoseptum was significantly reduced in wounded epaxial somites compared to controls (p=0.0002) and adjacent unwounded (p=0.0006). The number of Pax7$^+$ EdU$^+$ cells and the fraction in S-phase were similar at the horizontal myoseptum between the three groups. The number of Pax7$^+$ cells at the dorsal edge and central body were reduced but not significantly (p=0.07 and p=0.08 respectively). The number of Pax7$^+$EdU$^+$ cells in the wounded central body was significantly reduced compared to adjacent unwounded (p=0.014) and controls (p=0.03). The fraction of Pax7$^+$ cells in S-phase in the central body was also significantly reduced in wounded compared to adjacent unwounded (p=0.01) and controls (p=0.03).

Error bars are standard error of the mean. AUW Adjacent unwounded, W Wounded.

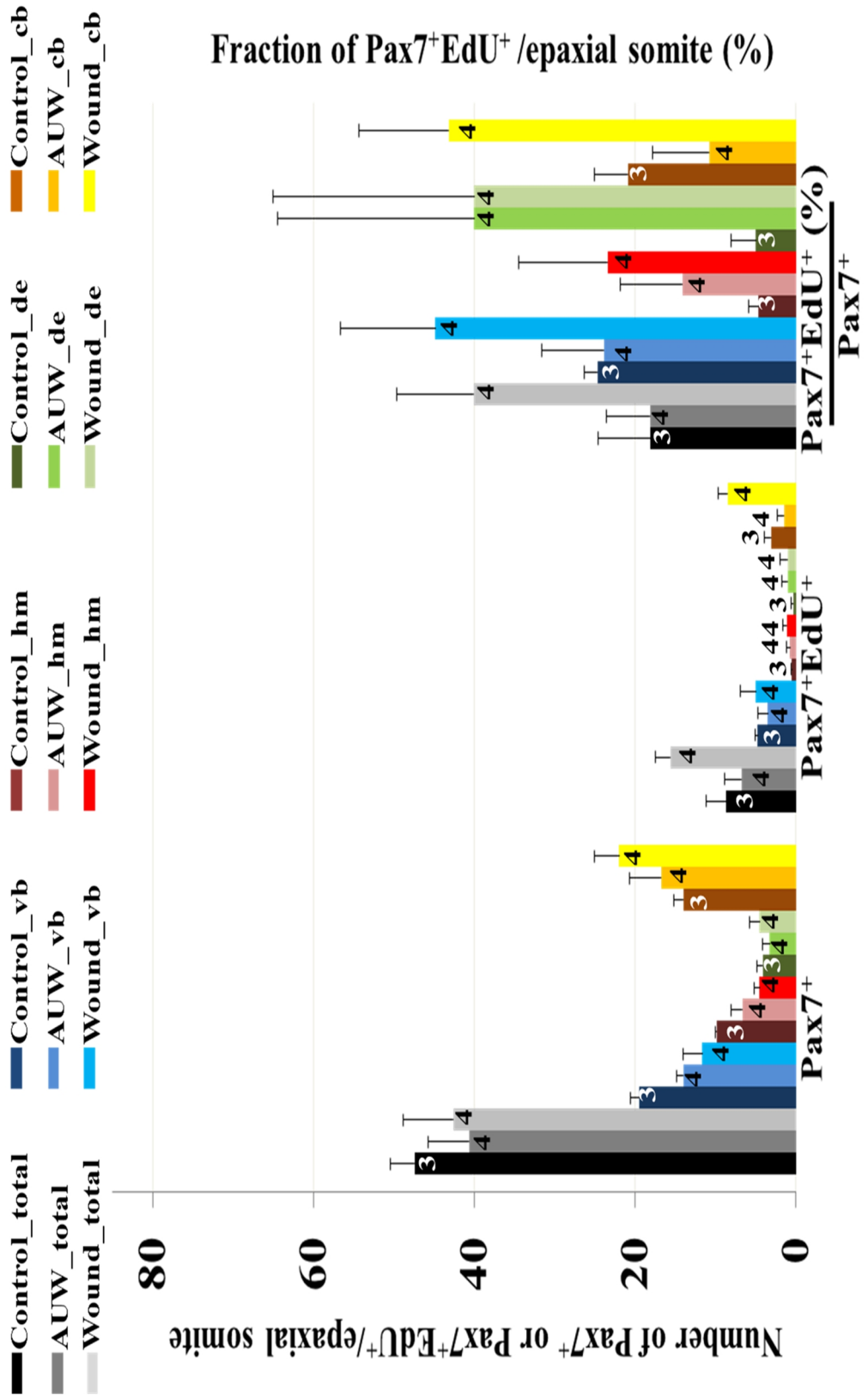


Fig. 4.32 Pax7^{+}EdU^{+} cells increase significantly in a spatiotemporal manner in wounded muscle

Fig. 4.32 At 1 dpw Pax7$^+$ cells in S-phase are located at the vertical borders and in the wounded central body.

Wholemount wild type larvae at 3 dpf were mechanically wounded and fixed at one day post wounding for immunostaining to detect Pax7$^+$EdU$^+$ cells. Quantification of mononucleate Pax7$^+$, Pax7$^+$EdU$^+$ cells and the percentage of Pax7$^+$EdU$^+$ cells as a fraction of Pax7$^+$ cells was done in control, adjacent unwounded and wounded epaxial somites at one day post wound in the number of fish indicated within bars from two separate experiments. The number of total Pax7$^+$ cells was similar in wounds compared to controls and adjacent unwounded. Total Pax7$^+$EdU$^+$ cells was significantly increased in wounded epaxial somites compared to adjacent unwounded ($p=0.02$) and controls ($p=0.03$). The fraction of Pax7$^+$ cells that were in S-phase was similar between control, adjacent unwounded, and wounded epaxial somites. The number of Pax7$^+$ cells at the vertical borders was similar in wounded compared to controls and adjacent unwounded. The fraction of Pax7$^+$ cells in S-phase was significantly increased at the vertical borders in wounded epaxial somites ($p=0.01$) as well as adjacent unwounded ($p=0.02$) compared to controls. The number of Pax7$^+$ cells at the horizontal myoseptum was significantly reduced in wounded epaxial somites compared to controls ($p=0.002$). The number of Pax7$^+$ cells at the dorsal edge was similar to controls and adjacent unwounded. The number of Pax7$^+$ cells in the wounded central body was similar to adjacent unwounded and controls. The number of Pax7$^+$EdU$^+$ cells in the central body of wounded epaxial somites was significantly increased compared to adjacent unwounded (0.003) and controls (0.02). The fraction of Pax7$^+$ cells in S-phase in the central body was similar between wounded, adjacent unwounded and controls. Error bars are standard error of the mean. AUW Adjacent unwounded, W Wounded.

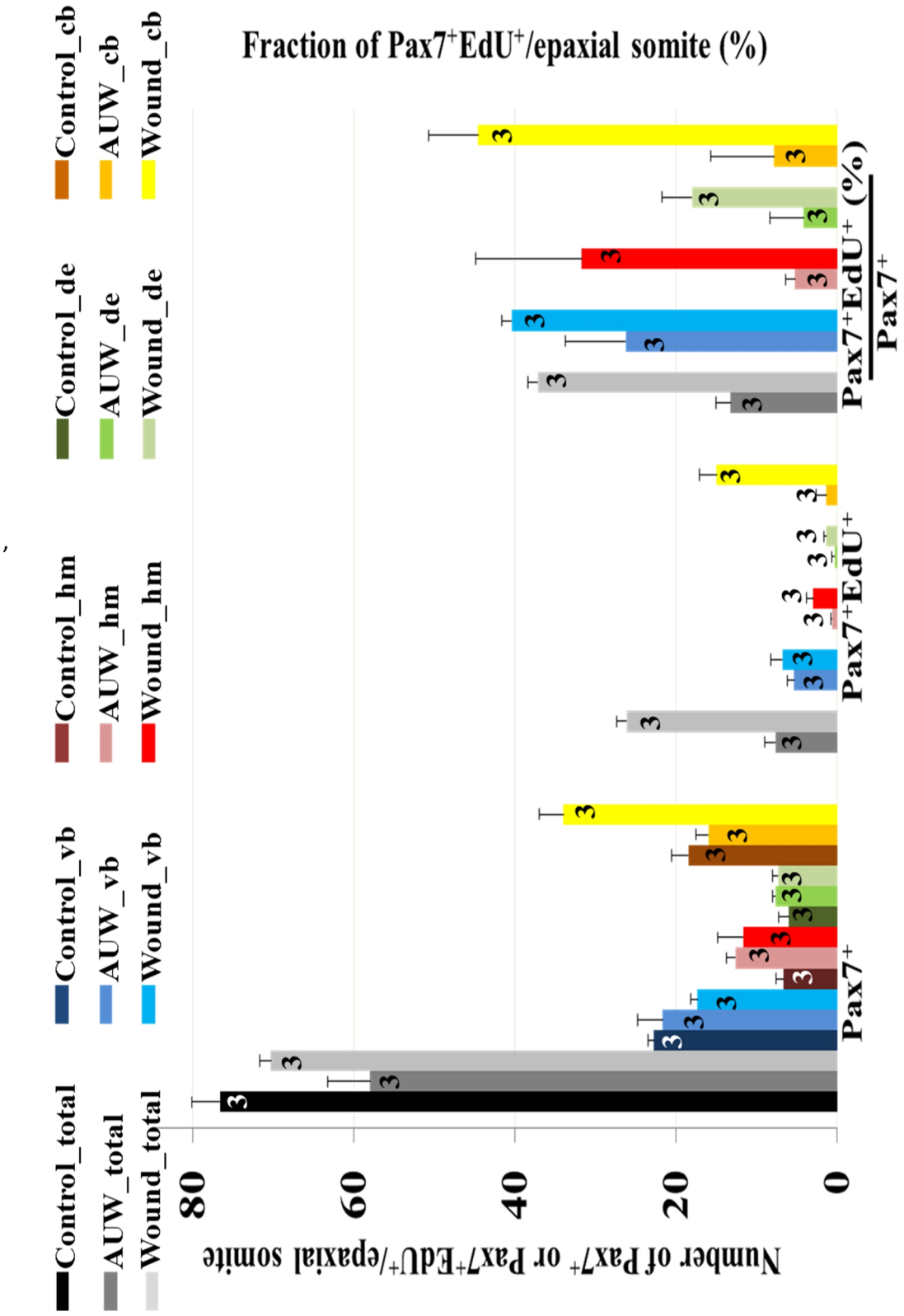


Fig. 4.33 Pax7^{+}EdU^{+} cells increase significantly in a spatiotemporal manner in wounded muscle

Fig. 4.33 At 2 dpw Pax7$^+$ cells in S-phase are primarily located in the wounded central body.
Wholemount wild type larvae at 3 dpf were mechanically wounded and fixed at two days post wounding for immunostaining to detect Pax7$^+$EdU$^+$ cells. Quantification of mononucleate Pax7$^+$ cells was done in age-matched controls, adjacent unwounded and wounded epaxial somites in the number of fish indicated within bars from two separate experiments. The number of Pax7$^+$EdU$^+$ cells and the fraction of Pax7$^+$ in S-phase were examined between wounded and adjacent unwounded in wounded larvae. The number of total Pax7$^+$ cells was similar in wounds compared to controls and adjacent unwounded. Total Pax7$^+$EdU$^+$ cells was significantly increased in wounded epaxial somites compared to adjacent unwounded ($p=0.0009$). The fraction of Pax7$^+$ cells that were in S-phase was significantly increased in wounded epaxial somites compared to adjacent unwounded ($p=0.001$). The number of Pax7$^+$ cells at the vertical borders was similar in wounded compared to controls and adjacent unwounded. The fraction of Pax7$^+$ cells in S-phase was found to be similar at the vertical borders in wounded epaxial somites. The number of Pax7$^+$ cells at the horizontal myoseptum was similar between wounded and adjacent unwounded epaxial somites. The number of Pax7$^+$ cells at the dorsal edge was similar to controls and adjacent unwounded. The number of Pax7$^+$ cells in the wounded central body was significantly increased compared to adjacent unwounded ($p=0.006$). The number of Pax7$^+$EdU$^+$ cells in the central body of wounded epaxial somites was significantly increased compared to adjacent unwounded (0.005). The fraction of Pax7$^+$ cells in S-phase in the central body was also significantly increased in wounded epaxial somites compared to adjacent unwounded ($p=0.02$). Error bars are standard error of the mean. AUW Adjacent unwounded, W Wounded.

To conclude, proliferation changes largely reflect the increase in Pax7$^+$ cell population at specific locations during muscle wound repair, although factors such as migration and differentiation likely play a role in altering the number of Pax7$^+$ cells at a particular location. The data suggests that majority of the proliferating Pax7$^+$ cells are located at the vertical borders at 5 hpw and 1 dpw but in the central body at 2 dpw, strongly suggesting the movement of proliferating Pax7$^+$ cells from the vertical borders to the central body during the course of muscle repair.

4.4 Discussion

The objective of the work described in this chapter was to investigate any regional differences in the response of $Pax7^+$ myogenic precursor cells to muscle wounds in zebrafish larvae. Zebrafish larvae between 2.5 and 4 dpf were anaesthetized and mechanically wounded in the epaxial somitic region. Muscle wounds were found to repair in five to seven days post wounding and regenerated fibres arose by two days post wounding. Slow and fast muscle appeared to regenerate at a similar rate although with minor defects. Cell membranes and nuclei assembly preceded striated actin and myosin expression in regenerating muscle fibres. The number of nuclei in wounds was reduced at 1 dpw but recovered by 2 dpw. Macrophages and neutrophils invade muscle wounds within an hour of injury and leave around 5 hours later. Their numbers are insufficient to account for the number of nuclei in wounds at 1 dpw. In contrast the hypothesis that myogenic cells in wounds account for the number of nuclei at 1 dpw is supported by both time lapse imaging and immunodetection of Pax7 and Myogenin expression in wounds at 1 dpw. The presence of $Pax7^+$ cells in wounds at 1 dpw raises the question how did they get there? Proliferating $Pax7^+$ cells from adjacent unwounded epaxial somites appears to be likely since the fraction of $Pax7^+$ cells in S-phase in wounds and adjacent to wounds increased significantly at 5 hpw and time lapse imaging showed several cells extending into the epaxial wound region from adjacent unwounded epaxial somites at 18 hpw. Proliferation differentiation dynamics were found to vary spatiotemporally during muscle repair. The fraction of $Pax7^+$ cells proliferating increased significantly at the vertical borders whereas the number of proliferative $Pax7^+$ cells and differentiating $Pax7^+Myogenin^+$ cells increased significantly in the central body at 1 dpw. At 2 dpw proliferation increased specifically in the central body and at 3 dpw a surplus of $Pax7{:}gfp^+$ and $Pax7^+$ cells was found in wounded muscle compared to adjacent unwounded. Moreover at 3 dpw, differentiation markers in wounds show a similar expression to adjacent unwounded suggesting that a bulk of muscle repair is completed by this time point. In contrast to the variation in proliferation dynamics at the vertical borders and central body of wounded epaxial somites, that at the horizontal myoseptum and dorsal edge was found to be similar to adjacent unwounded tissue at the various time points. Moreover, many $Pax7^+$ cells were found to enter the wounds from the dorsal edge but not

the horizontal myoseptum. Taken together, these observations indicate a difference in the niches with respect to supporting proliferation and migration of $Pax7^+$ precursor cells. In conclusion, I found region-wise variation in the response of $Pax7^+$ muscle precursor cells to muscle wounds in zebrafish larvae.

4.4.1 Rapid but error prone repair

The present study demonstrates that regenerating muscle fibres appear as early as 48 hours post wounding in zebrafish larvae, as has been suggested by others (Seger et al., 2011). Time-lapse images of muscle wounds in *Pax7:gfp* embryos shows that gfp^+ cells are present in the wounds as early as 18 hpw, although it is not until 2 dpw that they likely fuse and begin to express myosin. Taking into account that the fish are in a growth phase and the primary myotome (consisting of fast and slow fibres) in zebrafish takes only 1 day post fertilization to be established, it appears reasonable that new fibres at the wound can be seen within 2 days post wounding, in a developing embryo. In contrast, regenerating muscle fibres in adult zebrafish were reported 7-11 days post injury, suggesting that time for muscle repair likely varies with age as seen in other models. For example, in some fetal models of wound repair (Nakasone et al., 2007; Rowsell, 1984), regenerating fibres were reported two days post injury whereas many studies in adult mammalian models of muscle regeneration found that the earliest myotubes were first observed between three to seven days post injury (Church and Robertson, 1966; Clark, 1946; d'Albis, 1989; Mastaglia, 1975; Muir et al., 1965; Schmalbruch, 1976; Snow, 1978) and one study investigating the repair timeline in humans and vervet monkeys reported myotubes around 13 dpw and 7 dpw respectively (Allbrook, 1966).

Muscle regeneration was generally rapid with minor defects in fibre orientation and alignment. This finding raises the question how repair can recapitulate embryonic patterning such that a fairly similar number of regenerating slow muscle fibres come to lie superficially underneath the skin overlying the fast muscle. In the developing zebrafish embryo, several developmental cues play a role in accurate patterning. For example, 16-18 adaxial cells differentiate and migrate outward to form the 16—18 superficial slow muscle fibres (Devoto et al., 1996) and this is dependent on the timing on sonic hedgehog (shh) signal as well as the distance of the adaxial cells from the shh signal (Blagden et al.,

1997). Regenerating slow and fast muscle fibres were both found at two days post wound. This is in contrast to the sequence of events during muscle development. Fast muscle formation from precursors in the developing embryo generally varies with their location in the epaxial somite. Fast muscle differentiation of precursors located posteriorly in the epaxial somite follow the wave of slow muscle migration (Devoto et al., 1996; Stellabotte et al., 2007). Moreover, those located laterally are dependent on Fgf8 signaling and differentiate later (Groves et al., 2005).

The finding that myofibre alignment and orientation are perturbed to a certain degree in regenerated muscle in zebrafish larvae is similar to that reported for Gracilis muscle regeneration in rat (Clark, 1946). The finding implicates a regulatory mechanism responsible for myofibre alignment and orientation. Interestingly, wounding perturbs this mechanism, thus providing a model to investigate this phenomenon. Time lapse images in wounded *smyhc1* and *mylz2* often show fibres extending into the neighbouring somite in the absence of a clear border demarcating the two wounded somites. Hence, it is plausible that an emerging fibre in the wounded somite extends further into the neighbouring somite in search for connections to the extracellular matrix specifically found at the vertical septae. The zebrafish wound repair paradigm provides a platform to investigate the cellular basis of patterning.

4.4.2 Proliferation and differentiation dynamics of muscle precursor cells during muscle repair and the role of Pax7$^+$ cells at the various locations

Pax7$^+$ nuclei account for approximately 40% of the epaxial somitic nuclei in four and five dpf larvae (Fig. 4.13 C). At five hours post wound, Pax7$^+$ nuclei in wounds was reduced to approximately half of the Pax7$^+$ nuclei in healthy tissue (Fig. 4.27A and Fig. 4.31). This reduction is similar to that reported in a study of minced muscle in adult rats, where the number of nuclei representing the satellite cell population decreased from 11% in control muscle to 6.3% 8 hours post mincing (Snow, 1978).

The proliferation dynamics of Pax7$^+$ muscle precursor cells was assessed by quantifying the number and fraction of Pax7$^+$ cells in S-phase during the course of muscle repair. Shortly after wounding the fraction of Pax7$^+$ cells in S-phase in wounded larvae was found to be significantly greater than in controls. Both wounded and adjacent unwounded

epaxial somites in wounded animals showed a greater propensity to be in S-phase compared to uninjured animals, suggesting that $Pax7^+$ cells from adjacent somites might provide precursor cells for regeneration. Increase in the fraction of $Pax7^+$ cells in S-phase would suggest an increase in the number of $Pax7^+$ cells in wounded and adjacent unwounded at a later time point. However, at 1 dpw, the number of $Pax7^+$ cells increased significantly in wounds but not in the adjacent unwounded, suggesting a loss of the extra $Pax7^+$ cells in the adjacent unwounded by migration or differentiation. Whereas immunolabeling with Myogenin showed an increase in Myogenin positive nuclei in adjacent unwounded muscle shortly after wounding; at 1 dpw the number of $Myogenin^+$ nuclei in adjacent unwounded was no longer elevated and similar to controls (8-12 $Myogenin^+$ cells, Fig. 3.13C 4 dpf central body and Fig. 4.27D 1 dpw central body). Moreover, the majority of $Myogenin^+$ nuclei at 5 hpw appear to be fibre nuclei, suggesting that an increased number of $Myogenin^+$ cells in this case might not be reflective of increased differentiation, suggesting that the extra $Pax7^+$ cells in adjacent unwounded muscle are unlikely to be lost by differentiation. Time lapse images between 18 and 26 hpw show the entry of an increasing population of $Pax7^+$ cells into wounds from the vertical borders shared with adjacent unwounded epaxial somites and from the dorsal edge of the wounded somites suggesting that extra $Pax7^+$ cells in adjacent unwounded muscle migrate into wounds from these locations. Moreover, at 5 hpw and 1 dpw, immunolabeling indicated that the fraction of $Pax7^+$ cells in S-phase was significantly increased at the vertical borders but not in the central body. Taken together the data suggest that proliferative cells are primarily located at the vertical borders and thereby are a likely source of myogenic cells for muscle repairs. The entry of proliferative $Pax7^+$ cells from vertical borders would suggest an increase in the number of such cells in the central body. As expected, the number of $Pax7^+$ and $Pax7^+EdU^+$ cells was found to be increased in the central body at 1 dpw. Moreover, unlike the vertical borders, the fraction of $Pax7^+$ cells in S-phase did not significantly increase at 1 dpw. Additionally, differentiating $Pax7^+$ cells and $Myogenin^+$ cells were significantly greater in the central body. Taken together, the data suggest that $Pax7^+$ cells at the vertical borders act as a source of extra $Pax7^+$ cells whereas those in the central body are undergoing differentiation.

Differentiating cells at 1 dpw would suggest fibre regeneration and regenerating fibres were detected in live and fixed fish at 2 dpw. By 3 dpw majority of the wounded muscle appeared repaired and the number of differentiating cells was no longer elevated significantly. Unexpectedly, the number of $Pax7^{+}$ cells was found to be significantly increased at 3 dpw in wounded muscle. Immunolabeling 2 dpw fish revealed that the number of $Pax7^{+}$ cells in S-phase was significantly elevated in the central body indicating that ongoing proliferation accompanied by a decrease in differentiation could account for the increased number of $Pax7^{+}$ cells in the central body at 3 dpw. However, the presence of an increased number of $Pax7^{+}$ cells at the borders of wounded epaxial somites at 3 dpw could not be explained by proliferation dynamics alone. Since the number of proliferative $Pax7^{+}$ cells was not elevated significantly at the borders at 2 dpw, it suggests that more $Pax7^{+}$ cells in S-phase at the borders divided or that extra $Pax7^{+}$ cells translocated from the adjacent healthy muscle at 2 dpw. Frequent imaging between 24 and 48 hpw as well as pulsed labeling of $Pax7^{+}$ cells in S-phase could be used to examine the extent of contribution of the rate of cell division versus migration of precursor cells in muscle wounds.

A previous study on zebrafish muscle wounds using a different Pax7 transgenic line (Seger) reported $BrdU^{+}Pax7{:}gfp^{+}$ cells by 24 hpw. Moreover, the number of $Pax7^{+}BrdU^{+}$ cells almost doubled at 24-48 hpw. Our data is in agreement with such observations as we $Pax7^{+}EdU^{+}$ cells are almost doubled at 1 dpw and almost three times increased at 2 dpw. Additionally, region wise comparisons and comparison of wounded, adjacent unwounded and control muscle has revealed changes in the proliferation dynamics of precursor cells, suggesting that muscle regeneration is driven by the migration of $Pax7^{+}$ cells resident at the vertical borders followed by their differentiation via Myogenin expression into regenerated muscle.

The vertical borders have been hypothesized as highways for migration of myogenic cells into the intact (rainbow trout, (Stoiber and Sanger, 1996)) or wounded muscle (adult zebrafish, (Rowlerson et al., 1997)). Time-lapse images in $Pax7{:}gfp^{+}$ fish support the hypothesis that vertical septae could act as highways and additionally raises the idea that the dorsal edge also acts as a highway for myogenic cells. Moreover, quantification of

Pax7$^+$ cells in S-phase with respect to regions indicates that the vertical borders also harbour more proliferative cells pre and post wounding, suggesting that the vertical borders act as a niche supporting an increased fraction of proliferative cells in addition to being accessible for migration. Additionally, the quantitative data distinguishes the dorsal edge to be primarily used for migration, since an actively dividing population of Pax7$^+$ cells was never found at this location pre and post wounding. Unexpectedly, the less proliferative population of Pax7$^+$ cells at the horizontal myoseptum was not found to contribute a significant number of Pax7$^+$ cells to the wound site within the first two days of muscle repair, providing evidence against our hypothesis of a stem-like population at this location.

4.4.3 Immune cell dynamics in muscle wounds

Neutrophils (*MPO:gfp*) and macrophages (*LysC:gfp*) in zebrafish fin amputations arrived at wound site within an hour of wounding, peaked at 6 hpw (Hall et al., 2007) and had exited the wound site by 24 hpw (Renshaw et al., 2006). The number of neutrophils at 6 hpw varied from 10 to 25 in separate experiments (Renshaw et al., 2006). The number of neutrophils and the duration of immune cells in wounds appear to be in the range that was found in our studies. This is interesting because tail fin amputations repair by epimorphic regeneration. Our findings suggest that despite the difference in the mode of regeneration (epimorphic versus tissue mode), the pattern of immune response is similar. Moreover, our study provides a quantitative characterization of the response to neutrophils and macrophages in larval zebrafish muscle wounds. Furthermore, we find that the fraction of myogenic cells in S-phase is increased at the vertical borders in healthy muscle coincident with the dispersal of immune cells from the wound region. Moreover, as described previously (Lescaudron et al., 1999), myogenic cells do not increase in the wound region until after immune cell exit.

Immune cells appear to play a role in many stages of myogenesis during repair by influencing the microenvironment of the muscle precursors or by direct interaction with precursors (Abou-Khalil et al., 2009; Arnold et al., 2007; Bondesen et al., 2004; Chazaud et al., 2003; St Pierre and Tidball, 1994; Tidball and Wehling-Henricks, 2007). Hence, the ability to image muscle cells and immune cells in live wounded zebrafish larvae

provides an immense opportunity for unraveling the dynamics of interactions between these two cell types. The current study demonstrates that majority of the immune cells have exited prior to the entry of muscle precursors. However, a small population of immune cells was found at the wound at 2 dpw and it would be interesting to examine dynamics of this second population with myogenic cells at 2 dpw.

4.4.4 Wound size vs. rate of repair

DIC and confocal imaging on wounded embryos suggest that both small and large muscle wounds are repaired at a similar rate. It is plausible that an intrinsic signal within the tissue controls the rate of repair. Such a rate could be dependent on the number of myogenic cells that are generated at the wound site or attracted to the wound site by chemokines or another as yet unknown factor. The possibility that larger wounds attract more $Pax7^{+}$ cells remains to be tested. A follow-up question relevant in our wounding model is whether muscle growth is altered due to wounding by (a) altering the number of future muscle progenitor cells in regenerated muscle fibres or (b) altering the molecular environment e.g. immediate growth factor availability for further growth of repaired muscle. Compared to unwounded muscle, the number of $Pax7^{+}$ and $Myogenin^{+}$ cells in repaired muscle is higher at 3 dpw and time-lapse images show increased numbers of $Pax7{:}gfp^{+}$ cells in repaired muscle compared to adjacent unwounded muscle at 3 and 6 dpw. Whether the apparent increase in the number of muscle progenitor cells in wounds alters future growth of the wounded muscle is unknown. Following wounded somite growth for a longer duration could begin to address such questions.

4.4.5 Slow and fast muscle repair

In my experiments with embryonic and larval zebrafish, I found that slow and fast muscle repair kinetics were similar. Although, slow muscle appeared to repair quicker initially repair eventually stalled with defects in orientation and alignment. Several studies on adult muscle repair have indicated that slow muscle repair is poor compared to fast muscle repair (Bassaglia and Gautron, 1995; d'Albis, 1989; Hikida and Lombardo, 1974; Moraczewski, 1996; Schmidt, 1985; van Raamsdonk et al., 1982). The cause behind this apparent disparity in the extent of slow muscle repair has been linked to compromised innervation of slow muscle fibres (d'Albis, 1989; Hikida, 1974; Schmidt and Emser, 1985; van Raamsdonk et al., 1982) and differences in the extracellular matrix remodelling

of slow muscle tissue (Bassaglia and Gautron, 1995; Moraczewski, 1996; Zimowska, 2008). The difference in repair kinetics between zebrafish embryos and other adult studies might be linked to innervation and type of myosin produced in the repaired tissue. In the adult studies reposting compromised slow muscle recovery, the early embryonic and neonatal forms of myosin are often expressed normally but the switch to adult slow myosin is delayed or replaced by intermediate forms (Bassaglia and Gautron, 1995; d'Albis, 1989; Hikida, 1974; van Raamsdonk et al., 1982). Similarly, denervation in adult zebrafish abolished adult red (slow) muscle although embryonic red was produced (van Raamsdonk et al., 1982). Since my studies were limited to 13 dpf larvae it is possible that embryonic red and white muscle repair are not compromised by denervation at this stage as shown previously (van Raamsdonk et al., 1982), although the effect of wounding on neuronal connections in muscle wounds was not investigated in the current study.

4.4.6 Slow muscle fibres in fast muscle region

Similar to my observations of the emergence of slow fibres within the deep fast fibre region during muscle repair in zebrafish, at least two other studies have reported similar findings (Rowlerson et al., 1997; van Raamsdonk et al., 1982). Both authors have suggested the presence of 'slow' specific myoblasts amongst the population of myogenic precursors that accidentally get transported into the deeper region during the wounding process.

An alternative hypothesis is that the slow motoneuron makes contact with some cells deep in the fast layer giving them a 'slow character'. To date, however, the role of motoneuron in influencing slow/fast character of muscle fibres of zebrafish between 5-13 dpf has not been demonstrated. Denervation between 1 and 5dpf did not hinder slow/fast muscle identity in the correct locations (van Raamsdonk et al., 1982). Further, in adult zebrafish, upon denervation slow red muscle did not regenerate although superficial and ectopic embryonic red (EER, referring to the slow muscle fibres in deep fast fibre region) were detected suggesting that the emergence of these two types of slow myosin is not nerve dependent.

It could be speculated that the EER arise as an adaptation to the loss of fast fibres. It might be advantageous to develop some slow fibres while the rest of fast fibres are regenerated

since the slow fibres are important for sustained swimming. However, the disarray of the emerging EER is likely to make them dysfunctional with respect to contractility and force. Another possibility is that at the earliest time points post wounding, the skin lies close to the neural tube due to decimation of most slow and fast fibres. It is likely, in my wounding scenario at least, that some of the slow fibres beginning to arise between the skin and neural tube get pushed behind while regenerating fast muscle tissue pushes the skin and other slow fibres back to its normal position.

It has been proposed that the EER were expressing slow myosin before switching to a fast fibre phenotype (van Raamsdonk et al., 1982). Observations made by the other adult zebrafish muscle wounding study (Rowlerson et al., 1997) supports this theory. These authors reported that 3 to 6 weeks post injury, deep smyhc1^{+} fibres were not detected in adult zebrafish muscle wounds, suggesting that the EER had converted to a different phenotype. In my scans, I have noticed the putative slow fibres in the deep region to be sometimes associated with more than one nuclei (generally the character of fast fibres in zebrafish), also supporting the possibility of a switch of myosin phenotype.

Hedgehog (Hh) signaling from the axial midline structures is required for the embryonic red muscle to be established during development (Blagden et al., 1997). It is possible that some surviving myoblasts in wounds come in close contact with a higher Hh gradient close to the axial midline structures, leading them to differentiate into putative slow fibres. However, why only some myoblasts in that location and not others (especially the deep fast fibres) begin to express slow myosin is unclear.

4.4.7 Model of myogenic cell dynamics

Based on our data we propose a **model of myogenic cell dynamics** in zebrafish larval muscle wounds:

a. Shortly after wounding, the number of nuclei is drastically reduced in wounds. Some of these nuclei are likely to be those of mononucleate cells. Also, it is unlikely that majority of the mononucleate precursor cells are killed by direct impact of the needle on individual precursor cells. Whereas quiescent satellite cells under the basal lamina are proposed to be refractory to muscle damage and

largely not killed upon mechanical wounding, actively proliferating myoblasts as in a growing larva might be more sensitive to apoptotic and necrotizing changes in their environment. Receptor expression for anti-apoptotic growth factors or other signaling molecules expressed by satellite cells shortly after their activation are implicated in protecting them from oxidative stress and apoptosis (Goulding et al., 2006; Rathbone et al., 2011; Kami and Senba, 2002). $Pax7^+$ cells at the vertical borders of wounded somites and a short distance away are increasingly found in S-phase. Myogenin expression does not increase in the early wounded tissue, but increases in healthy muscle adjoining the wound possibly as a response to the loss of a large area of muscle tissue.

b. At 1 dpw, the number of $Pax7^+$ cells in wounds has recovered primarily due to proliferative $Pax7^+$ cells at the vertical borders in wounds and adjacent healthy muscle. Proliferative $Pax7^+$ cells migrate from the vertical borders into the central body, thereby increasing the number of proliferative $Pax7^+$ cells in the central body. However, once at this location, $Pax7^+$ cells have an increased propensity to differentiate (based on the significant increase in number of $Pax7^+Myogenin^+$ and $Myogenin^+$ cells) whereas the $Pax7^+$ cells at the vertical borders maintain the increased propensity to proliferate at 1 dpw. Proliferative $Pax7^+$ cells at the vertical borders and central body at 1 dpw likely give rise to progeny that would lead to further increases in $Pax7^+$ cell numbers in the wounds. However, the number of $Pax7^+$ cells remains similar due to continued migration from adjacent healthy muscle and differentiation in the central body of the extra $Pax7^+$ cells.

c. At 2 dpw, $Pax7^+$ cell derived regenerating muscle fibres arise at wound site. Many proliferative mononucleate $Pax7^+$ cells occupy the central body at this time and give rise to the extra $Pax7^+$ cells seen in wounded muscle at 3 dpw.

d. By 3 dpw, $Pax7^+$ cell derived regenerating muscle fibres occupy bulk of the wounded region. The number of $Pax7^+$ cells is significantly increased in regenerated tissue at this time point and appears to remain elevated later, due to a combination of migration of proliferative Pax7+ cells into wounds from adjoining healthy muscle previously and the reduction in differentiation in wounded muscle likely leading to self-renewal.

4.6 Conclusion

I have found that muscle regeneration in zebrafish larvae recapitulates the embryonic patterning in the absence of many of the developmental cues. Regeneration is rapid but imperfect. Immune cells invade and exit the wounded muscle within hours post injury. Proliferation starts to ramp up in adjacent healthy muscle and within the wound around the time of immune cell dispersal from wounds and within the next 12 hours, myogenic cells are found at the wound site. Their proliferation and differentiation dynamics varies spatiotemporally over the next three days during which regenerated muscle is formed at the wound site precursors not expressing differentiation markers implying self-renewal persist in the regenerated tissue. The spatiotemporal dynamics implicate vertical borders as the source of myogenic cells in wounds and Myogenin as the differentiation factor preceding fibre emergence.

Chapter 5: General discussion

Work in this thesis has provided evidence in favor of myogenic cells marked by Pax7 expression and Myogenin expression as drivers of muscle growth and repair in the post hatched zebrafish larvae. In chapter 3, the spatiotemporal dynamics of $Pax7^+$ cells and $Myogenin^+$ cells was followed in post hatched larvae. $Pax7^+$ cells were found to vary with location in terms of number of cells at each location, the incidence in S-phase and whether they expressed differentiation marker Myogenin. Variation in the regional distribution of proliferating and differentiating $Pax7^+$ precursor cells suggested that (i) $Pax7^+$ and $Myogenin^+$ cells in the deep central body contribute to muscle growth in zebrafish larvae and (ii) regional differences in the functional role of muscle precursors. To test the hypothesis that myogenic precursors expressing Pax7 and Myogenin contribute to post-hatched muscle growth in zebrafish, the spatiotemporal distribution of $Pax7^+$ and $Myogenin^+$ precursors was determined in *myod*^{fh261} mutants which show a transient growth defect. The number of $Pax7^+$ and $Myogenin^+$ precursors was elevated in the mutants and distribution of these cells was altered such that they congregated in the deep central body adjacent to fast fibres earlier than siblings. The congregation of an elevated number of $Pax7^+$ and $Myogenin^+$ cells preceded a reduction in the excess number of precursors. This reduction was coincident with myotomal recovery, strongly suggesting that $Pax7^+$ and $Myogenin^+$ cells in zebrafish are involved in muscle growth. To test the second hypothesis that myogenic precursors expressing Pax7 vary functionally based on location, the response of these cells was followed after muscle injury. Zebrafish larvae were wounded mechanically with a fine needle and muscle regeneration was followed from one hour to 6 dpw. Muscle repair was rapid and involved distinct responses of $Pax7^+$ cells at separate somitic locations. Based on the regional variation in the behavior of $Pax7^+$ cells, a role for each region is proposed.

5.1 Dermomyotomal Pax7$^+$ cells are precursors of muscle growth and repair in larval zebrafish

In mouse and chick, Pax7$^+$ cells delaminate from the central portion of the dermomyotome, invade the myotome and are involved in post embryonic growth (Gros et al., 2005; Relaix et al., 2005). Both dermal and myogenic progenitors arise from the delaminating central dermomyotome (Ben-Yair and Kalcheim, 2005). In zebrafish, cells at the anterior portion of the somite were shown to have myogenic or possibly dermal fates (Hollway et al., 2007), suggesting that anterior border cells are equivalent to amniote dermomyotome cells. Following an anterior to lateral movement, cells in the anterior somitic compartment come to lie in the external cell layer or dermomyotome of the 1 day embryo (Hollway et al., 2007; Stellabotte et al., 2007). Moreover, some labeled cells in the external cell layer give rise to medial fast fibres (Hollway et al., 2007; Stellabotte et al., 2007). Dermomyotomal cells in zebrafish are known to express *pax3*, *pax7* as well as dermal progenitor marker *col1a2* (Devoto et al., 2006). Since dermomyotomal Pax7$^+$ cells in amniotes give rise to muscle fibres, it is possible that they have a similar fate in zebrafish. To test the hypothesis that Pax7$^+$ cells in the fish dermomyotome contribute to muscle fibres during growth and repair, the spatiotemporal dynamics of Pax7$^+$ cells was quantitated in growing larvae and after muscle injury. I find several lines of evidence supporting the hypothesis that Pax7$^+$ cells are involved in growth and repair.

In chapter 3, quantitating changes in the number of Pax7$^+$ cells revealed that Pax7$^+$ cells were primarily located superficial to the myotome prior to 4 dpf and gradually increased within the myotome from 4 dpf onwards. Live imaging using a *Pax7:gfp* reporter line between 3 and 4 dpf showed that Pax7$^+$ cells appear in the deep myotome from 4 dpf onwards. The data indicate that entry of Pax7$^+$ cells into the myotome is timed and suggest that as in amniotes, zebrafish Pax7$^+$ cells migrate into the myotome from the dermomyotome. Time lapse images showing Pax7:gfp$^+$ cells extending from superficial positions to deeper location within the myotome support the hypothesis that they can migrate inwards. I find that Pax7$^+$ cells specifically increase in the deep central body region from the time of their proposed migration into the myotome. Moreover, the number of differentiating Pax7$^+$ cells (Myogenin$^+$Pax7$^+$) increases significantly in the

deep central body. By utilizing the *Pax7:gfp* transgenic line, I found that Pax7:gfp$^+$ cells elongated into fibre-like structures in the central body. Moreover, gfp expression in these elongated structures coincided with myosin expression indicating that Pax7:gfp$^+$ cells are myogenic. Taken together the data provide strong evidence in favor of a myogenic role of Pax7$^+$ precursors translocating into the deep central body from the dermomyotome in zebrafish. Moreover the data support the observation that labeled cells in dermomyotome give rise to medial fast fibres located in the central body of somites (Hollway et al., 2007; Stellabotte et al., 2007).

The role of Pax7$^+$ cells in growth of the larval myotome was examined by utilizing *myod*^{fh261} mutants with a transient growth defect. The number of Pax7$^+$ cells was elevated in the dermomyotome (Hammond et al., 2007) and the myotomal volume was significantly reduced compared to siblings (Hinits et al., 2011) at 1 dpf. The myotomal volume increased between 1 and 5 dpf (Hinits et al., 2011) and the increase between 1 and 3 dpf as well as between 3 and 5 dpf was found to correlate with the fold change decrease in the excess number of Pax7$^+$ precursors. Since, majority of the Pax7$^+$ precursors are in the dermomyotome with few Pax7$^+$ cells found in the myotome between 1 and 3 dpf, how could Pax7$^+$ cells contribute to myotome growth between 1 and 3 dpf in mutants? I found that Pax7$^+$ cells were already within the myotome of the *myod*^{fh261} mutants in significant numbers at 3 dpf. Taken together, the number, location and timing of the dynamics of Pax7$^+$ cells in *myod*^{fh261} mutants strongly suggest that Pax7$^+$ cells are the source of myotome recovery, implying that myogenic cells from the dermomyotome marked by Pax7 expression are drivers of muscle growth in larval zebrafish.

The role of Pax7$^+$ cells in muscle regeneration was examined following mechanical injury. The injury resulted in a loss of muscle tissue and a significant reduction in the number of Pax7$^+$ cells throughout the wounded muscle. However in less than 24 hpw the number of Pax7$^+$ cells increased significantly in wounds and were similar to unwounded muscle. Live imaging suggests these Pax7$^+$ cells migrate into the wounds from adjacent healthy muscle and is supported by immunolabeling studies which indicated that the fraction of Pax7$^+$ cells in S-phase significantly increased in adjacent unwounded muscle within 5 hpw and remained elevated significantly at 1 dpw. Pax7:gfp$^+$ cells were seen

elongating into fibre-like structures at 2 dpw correlating with the time at which new fibres are seen in wounded *smyhc1:gfp* (slow muscle) and *mylz2:gfp* (fast muscle) fish. Immunolabeling showed that gfp-labeled elongated structures coincided with myosin heavy chain stain, indicating that Pax7:gfp^{+} cells elongating at the wounds site were contributing to muscle fibre regeneration. To summarize, the data provide strong evidence in favor of the role of Pax7-marked cells in the dermomyotome and myotome of zebrafish as drivers of muscle growth and repair and provide a framework to study the behavior of these cells in the growing zebrafish to investigate the *in vivo* dynamics of muscle precursors during growth and repair.

5.2 Variation in Myogenin expressing myogenic cells as a marker of muscle growth

Hyperplasia in amniotes involves proliferating nuclei positive for Pax7 followed by MRF expression and differentiation into fibres (Gros et al., 2005; Relaix et al., 2005). A similar mechanism has been proposed in fish. Myogenin^{+} and Myogenin^{+}Pax7^{+} cells were reported adjacent to small caliber fast fibres in the deep central body of juvenile zebrafish and larval brown trout and proposed to be involved in muscle growth (Patterson et al., 2008; Steinbacher et al., 2007). However, to date the distribution of Myogenin^{+} cells in growing zebrafish larvae has not been described.

To determine if Myogenin^{+} cells are present in the deep central body of zebrafish larvae in fibre adjacent positions and thereby aid in muscle growth, the spatiotemporal distribution of Myogenin^{+} cells was quantitated in 3 to 6 dpf fish. In 3 dpf larvae, Myogenin transcripts are primarily located at the dorsal and ventral extremes of somites or at the dorsal edge of epaxial somites. I have examined the spatiotemporal distribution of Myogenin expressing nuclei in 3 to 6 dpf fish. At 3 dpf cells with nuclear Myogenin expression were located at the dorsal edge and in the central body. Moreover, the number of Myogenin^{+} cells appeared to be more in dorsal edge at 3 dpf followed by more in the central body by 6 dpf. The location of Myogenin^{+} and Myogenin^{+}Pax7^{+} cells at the dorsal edge and central body are consistent with that reported for pre and post-hatched brown trout, a teleost fish (Steinbacher et al., 2007). The data indicate that Myogenin^{+} cells are located at positions in the myotome (central body and dorsal edge) associated with

hyperplastic growth. Moreover, the small number of Myogenin$^+$ cells suggests a slow rate of fibre addition between 3 and 6 dpf.

To examine a more direct readout of Myogenin expression as a driver of muscle growth, the spatiotemporal distribution of Myogenin$^+$ cells in wounded muscle was assessed. Wounding created a system wherein a large chunk of muscle fibres were lost at once and challenging cells involved in muscle formation to rapidly make new muscle. The number of Myogenin$^+$ cells was found to increase significantly in the central body within 1 day post injury and precede the appearance of new fibres. Moreover, the number of Myogenin$^+$ cells reduced to normal levels by 3 dpw coincident with bulk of muscle repair completed by this time point. The data provide strong evidence in favour of Myogenin$^+$ cells in the myotome of teleost fish as a readout of myotomal growth.

5.3 Regional heterogeneity in muscle precursor dynamics

That muscle precursors are a heterogeneous population in amniotes is known from both in vitro and in vivo work (Biressi and Rando, 2010; Collins et al., 2005; Kuang et al., 2007; Montarras et al., 2005; Ono et al., 2010; Ono et al., 2012; Schultz, 1996). Recent work in the early embryonic zebrafish has shown the existence of heterogeneity in the regulation of Pax7$^+$ cells based on their location in the dermomyotome (Nord et al., 2013; Windner et al., 2012). Work in this thesis supports the aspect of heterogeneity of Pax7$^+$ cells based on location and shows that heterogeneity in the post-hatched larva persists in the form of regional differences in proliferation and differentiation kinetics. Based on the spatiotemporal variation of proliferating and differentiating myogenic precursors, roles of precursors at each location are proposed.

5.3.1 Central body

The number of Pax7$^+$ cells increased in the epaxial somite during normal growth likely due to the translocation of Pax7$^+$ cells from dermomyotome to the myotome for future myotome growth. The number of Pax7$^+$ cells increased in the central body during normal growth. In contrast the number of differentiating Pax7$^+$ cells and Myogenin$^+$ cells remained similar in the central body. Moreover, Pax:gfp$^+$myosin$^+$ cells were also located in the central body, confirming previous studies that cells from the dermomyotome give rise to medial fast fibres (Hollway et al., 2007; Stellabotte et al., 2007). During repair,

Pax7$^+$ cells specifically increased in the central body at 1 dpw and further increased at 3 dpw. The number of Pax7$^+$ cells in S-phase also increased significantly in the central body at 1 dpw but the fraction in S-phase was not elevated indicating that the increased number of Pax7$^+$ cells in S-phase was due to an increase in the number of Pax7$^+$ cells in the central body. Differentiation also increased at 1 dpw and preceded regenerated muscle fibres at 2 dpw. Moreover differentiation returned to normal levels at 3 dpw whereas the fraction in S-phase was significantly increased at this time point in the central body. If differentiation is winding down, why is the fraction of Pax7$^+$ cells in S-phase significantly elevated? The data suggest that many of the Pax7$^+$ cells in the central body are undergoing self-renewal. The excess number of Pax7$^+$ cells at 3 and 6 dpw further suggest a self-renewing Pax7$^+$ population. Thus, observations in this thesis suggest that Pax7$^+$ cells in the central body increasingly differentiate at 1 dpw when there is a lack of 'normal' level of myotome whereas later switch to self-renewal. Increase in the number of differentiating Pax7$^+$ cells and Myogenin$^+$ cells in the central body during repair, as well as in the mutant prior to myotome recovery strongly support the hypothesis that communication between Pax7$^+$ cells and their environment in the central body influences their decision to proliferate or differentiate.

5.3.2 Vertical Borders

During normal growth, the number of Pax7$^+$ cells increases significantly at the vertical borders correlating with a large fraction of Pax7$^+$ cells in S-phase at this location. However, the fraction of Pax7$^+$ cells in S-phase at this location would suggest a greater number of Pax7$^+$ cells than are detected experimentally. This is in contrast to the situation in the central body where an increasing number of Myogenin$^+$Pax7$^+$ and the presence of Myogenin$^+$Pax7$^-$ cells would require the presence of a larger number of Pax7$^+$ cells than what can be accounted for by the fraction of Pax7$^+$ cells in S-phase at this location. The simplest explanation would be that extra Pax7$^+$ cells from the vertical borders translocate to the central body where they differentiate. Time lapse images in control and wounded larvae support this hypothesis. During wound repair, the fraction of Pax7$^+$ cells in S-phase specifically increased at the vertical borders of wounded and adjacent unwounded muscle as early as 5 hpw and remained elevated at 1 dpw. However, the number of Pax7$^+$ cells did not significantly increase at either wounded or unwounded vertical borders till 2 dpw

even though Pax7^{+} cells at this location were not lost by differentiation. Also, time lapse images show Pax7:gfp^{+} cells extending into wounds from the vertical borders of adjacent unwounded muscle. Taken together, the data support the hypothesis that extra Pax7^{+} cells from the vertical borders enter the central body, suggesting that vertical borders act as highways for Pax7^{+} cell transit into the myotome during growth and repair as has been proposed previously (Rowlerson et al., 1997; Stoiber and Sanger, 1996). Additionally, the data show that the vertical borders harbour an actively proliferating but not differentiating population of Pax7^{+} muscle precursors. Since, the number of Pax7^{+} muscle precursors does not increase concomitant with the fraction of Pax7^{+} cells in S-phase, suggests that the vertical border niche supports proliferation and self-renewal along with a loss of extra precursors that move into the central body and differentiate.

5.3.3 Dorsal edge

The number of Pax7^{+} cells at the dorsal edge was found to vary but remain largely similar between three and six dpf. Fewer Pax7^{+} cells at this location were in S-phase compared to the vertical borders and central body and differentiating Pax7^{+} as well as Myogenin^{+}Pax7^{-} cells were present. The data indicate that myogenic cells at this location are not actively proliferating and some cells could be lost via differentiation, suggesting that the low proliferation rate could support a slow increase in the number of Pax7^{+} cells whereas the loss of a small number of cells via differentiation would maintain a similar number of cells over time. The data shows that the environment at the dorsal edge is permissive to both proliferation and differentiation and suggests that these processes might occur at a reduced rate compared to the vertical borders and central body. Live imaging showed many Pax7:gfp^{+} cells entering the myotome from the dorsal edge similar to the vertical borders. However, unlike the vertical borders, proliferation did not increase significantly at the dorsal edge during wound repair. Similarly, unlike the central body, differentiation did not increase at the dorsal edge of wounded epaxial somites. Instead, the role of the dorsal edge during repair appeared to act as a highway for the migration of Pax7^{+} cells that preferred to extend into the wound dorsally compared to extending into the wound closer to the horizontal myoseptum. Taken together, the data in this thesis suggest the hypothesis that the dorsal edge supports a lower level of proliferation and

differentiation compared to the central body and like the vertical borders can act as a migration pathway for myogenic precursor cells.

In the developing zebrafish embryo up to 1 dpf, proliferation of $Pax7^+$ cells at the dorsal edge was found to be regulated by Six1a/b via pSmad 1/5/8 in contrast to direct regulation of $Pax7^+$ cells in the central body and horizontal myoseptum by Six1a/b alone (Nord et al., 2013). Inhibition of Six1a/b reduced the number of $Pax7^+$ cells suggesting decreased proliferation (Nord et al., 2013). BMP signaling acts via pSMAD1/5/8 and over activation led to an increase in $Pax7^+$ myogenic precursor cells as well as delayed their differentiation in 1-2 dpf zebrafish embryos likely via Smad5 (Patterson et al., 2010). However, inhibition of BMP signaling did not lead to downregulation of pSMAD or $Pax7^+$ cell number (Patterson et al., 2010). It is possible that a redundancy exists whereby Six1a/b signaling via pSMAD is able to compensate for the lack of BMP signaling in the zebrafish dermomyotome. Importantly, the $Pax7^+Smad^+$ cells were located at the dorsal and ventral extremes of the somite suggesting that BMP signaling was active at dorsal and ventral edge of the somite in embryos up to 2 dpf.

5.3.4 Horizontal myoseptum

The number of $Pax7^+$ cells at the horizontal myoseptum remained similar between three and six dpf. Differentiating cells were rarely found at the horizontal myoseptum and a low fraction of $Pax7^+$ cells were in S-phase at this location. Taken together, the data suggest a quiescent population of $Pax7^+$ cells at the horizontal myoseptum supporting the observation that $Pax7^+$ cells at this location are found under the basal lamina (i.e. in a satellite cell position) in three dpf fish versus seven dpf for $Pax7^+$ cells in the central body (Hollway et al., 2007). Moreover, since the $Pax7^+$ cells at the horizontal myoseptum were rarely in S-phase or differentiating, in chapter 3 we proposed that $Pax7^+$ cells at the horizontal myoseptum might be more stem-like and expected to see a large number of $Pax7^+$ cells arise at this location post wounding. In contrast, the fraction of $Pax7^+$ cells in S-phase at the horizontal myoseptum did not change significantly between the first two days of muscle repair. Moreover, $Pax7^+$ cells from the epaxial or hypaxial region were rarely found to enter the wounds from the wounded horizontal myoseptum. It is possible that tissue destruction at the horizontal myoseptum affects migration more adversely than

at other locations. HSPGs are glycoproteins associated with the extracellular matrix and capable of defining zones of growth factor activity (Dolez et al., 2011; Meyers et al., 2013) and wounding likely damages or eliminates via destruction of the extracellular matrix. The horizontal myoseptum region has been shown to be sensitive to the lack of HSPG modifying enzymes which can alter and change their affinity towards growth factors (Windner et al., 2013). Specifically, embryos lacking the HSPG modifying enzyme Sulphs1 showed an absence of $Pax7^+$ cells at the horizontal myoseptum and aberrant migration of the lateral line and pigment cells. Hence, the observation of an absence of $Pax7^+$ cells at the horizontal myoseptum following wounding could be attributed to the destruction of extracellular matrix. Immunostaining for HSPG and in situ hybridization of *sulfs* can be used to determine if the lack of HSPG or Sulfs are involved in the absence of $Pax7^+$ cells at the horizontal myoseptum post-wounding.

Whereas the role of $Pax7^+$ cells at the horizontal myoseptum remains unclear from data presented in this thesis, the observations support the view that $Pax7^+$ cells at the horizontal myoseptum appear functionally distinct from $Pax7^+$ cells at the dorsal edge (Windner et al., 2012). The authors in this study found that in developing zebrafish embryos up to 1 dpf, premature differentiation of $Pax7^+$ cells at the horizontal myoseptum is inhibited by *fss/tbx6* (Windner et al., 2012). Moreover, the authors (Windner et al., 2012) noted the absence of $Pax7^+$ cells co-expressing MRFs at the horizontal myoseptum found at other locations in the somite. This is in line with my finding that $Pax7^+Myogenin^+$ cells were generally not observed at the horizontal myoseptum location. Another study found an increase in the number of $Pax3/7^+$ cells at the horizontal myoseptum in 1 dpf *fgf8* morphants (Hammond et al., 2007), suggesting that blocking *fgf8* signaling leads to an increase in proliferation of the Pax3/7 population of cells. Whether *fgf8* signaling regulates proliferation of $Pax7^+$ cells at the horizontal myoseptum in growing larvae remains to be investigated. Yet another study, found a lack of $Pax7^+$ cells at the horizontal myoseptum upon overexpression of BMP signaling (Pownall et al., 2013) contrary to an increase observed in another study (Patterson et al., 2010). A key difference between the two studies was the timing of overexpression which was earlier in the Pownall study, suggesting temporal differences in signal induction.

5.3.5 Deciphering signaling pathways

Variation in the functional behavior of $Pax7^+$ cells and distribution of $Myogenin^+$ cells could be a reflection of intrinsic or extrinsic differences or a combination. Isolation and transcriptome analysis of $Pax7^+$ cells from the various regions could provide static clues regarding intrinsic differences. Extrinsic factors such as subdomains of signaling molecule expression within the myotome could variably modulate the behavior of $Pax7^+$ cells and lead to their heterogeneity. Hence, it is possible that the functional heterogeneity of the myogenic precursors based on location is a reflection of the signaling pathways in play to maintain tissue homeostasis similar to that seen during development. During myogenesis different signaling pathways work spatiotemporally and the balance between signals that promote proliferation, differentiation and self-renewal, regulates skeletal muscle formation (Marcelle et al., 1997; Munsterberg et al., 1995). Hedgehog signals from the notochord and ventral neural tube and Wnts from dorsal neural tube and surface ectoderm generally promote differentiation of muscle precursors whereas Bone morphogenetic protein (BMP) from dorsal neural tube, ectoderm and lateral plate mesoderm inhibits differentiation of dermomyotomal precursors into muscle (Reshef et al., 1998).

As apparent in the previous sections (5.3.1-4), several signaling pathways could operate to influence the heterogeneity of $Pax7^+$ cells in the somite. **Hedgehog signaling** from the notochord and floor plate have been shown to oppose BMP signaling in both chick and zebrafish (Du et al., 1997; Marcelle et al., 1997). Sonic Hedgehog (Shh), a member of the Hh family, is an intracellular signaling protein that acts through the membrane protein Patched (Ptc). Hedgehog (Hh) binding to Patched relieves Patched-mediated inhibition of Smoothened (smo) leading to the activation of GLI transcription factors of which there are three: gli1, 2 and 3 (Jackson and Ingham, 2013). These factors activate or repress Hh target genes. Zebrafish has three Hh genes: Shh expressed in axial midline structures, Echidna Hh (Ehh) expressed in notochord and Twiggywinkle Hh (Twhh) expressed in the floor plate of the neural tube. Hh activity during embryonic myogenesis is essential for slow muscle formation as well as the formation of two engrailed expressing muscle types: engrailed expressing slow (muscle pioneers) and fast muscle (Barresi et al., 2001;

Blagden et al. 1997; Currie et al., 1996; Du et al 1997; Lewis et al, 1999; Roy et al., 2001; Wolff et al., 2003).

In zebrafish, Hh is suggested to promote the differentiation of Pax3/7 expressing cells to fast muscle until the end of segmentation period (1 dpf) (Feng et al., 2006; Hammond et al., 2007). Inhibition of Hh signaling during early muscle development increased Pax3/7 mRNA and protein and decreased fast myogenesis whereas later inhibition after slow and fast muscle formation had no effect on Pax3/7 expressing cells (around 1 dpf), showing that somitic Pax3/7 expression becomes Hh insensitive in zebrafish in a temporal manner (Feng et al., 2006; Hammond et al., 2007). Thus, it is unlikely that Hh signaling influences the fate of Pax7 expressing cells in the growing 3-6 dpf zebrafish studied in this thesis. Similarly in the chick, Pax7 expressing cells were found to become insensitive to Hh signaling towards the end of dermomyotome disintegration and beginning of growth phase (Kahane et al., 2013).

On the other hand, it is possible that Hh signaling influences the proliferation and behavior of Pax7 expressing cells during muscle repair since Hh activity is implicated in muscle regeneration (Straface et al., 2009). Shh increased satellite cell proliferation and survival (Koleva et al., 2005) acting via PI3K/AKT signaling pathway in vitro (Elia et al., 2007). Moreover, Hh inhibition during muscle regeneration impaired muscle repair and inhibited the upregulation of Myf5 and MyoD as well the upregulation of growth factors such as IGF-1 and VEGF. Thus, Hh signaling appears to promote myogenic progression of Pax3/7 expressing muscle precursors during muscle development and repair. A simple method to study the effect of Hh signaling in zebrafish is to expose the fish to cyclopamine in fish water (Chen et al., 2002). Cyclopamine inhibits Hh signaling by binding to smoothened. Additionally, several mutants of the Hh pathway are available to investigate the mechanism by which altered Hh signaling might influence precursor dynamics and are mentioned towards the end of this section.

As previously mentioned, **BMP signaling** has been shown to influence the fate of Pax7 expressing cells in zebrafish at the dorsal edge (Patterson et al., 2010) and horizontal myoseptum (Meyers et al., 2013). BMPs are members of the TGFβ family of growth factors and have been shown to influence Pax7 expressing precursors in other species

(Amthor et al., 1999; Massague et al., 2000; Patterson et al., 2010; Wang et al., 2010). BMP receptors signal by phosphorylation of regulatory Smads 1/5/8 leading to their translocation to the nucleus where in conjunction with Smad4, BMP target genes are transcriptionally regulated (Massague et al., 2005). In amniotes, BMP signaling via Smad 1/5/8 was shown to suppress myogenic precursor differentiation (Amthor et al., 1998) whereas inhibition of BMP signaling led to a reduction in the $Pax7^+$ precursor cell pool during fetal development in chick (Wang et al., 2010). Concomitantly, overexpression of BMP led to an increase in the $Pax7^+$ precursor pool and delayed their differentiation in zebrafish embryos (Patterson et al., 2010) likely via Smad5. Six1a/b can also signal via pSMADs or directly to maintain proliferative $Pax7^+$ precursor cells throughout the zebrafish somitic myotome.

In this thesis, $Pax7^+$ cells at the dorsal edge were characterized in growing larvae from 3 dpf onwards and found to differ in their proliferation and differentiation behavior compared to $Pax7^+$ cells at the central body and horizontal myoseptum, indicating that functional heterogeneity persists and suggesting that differential signaling in different parts of the somite is maintained in the growing larva. Whether BMP or Six1a/b signaling is active in growing larvae and contributes to regulation of $Pax7^+$ cells in the somite remains to be investigated. The availability of heat shock conditional mutants of the bmp pathway make it feasible to inactivate or overexpress the pathway in older larvae during muscle growth or repair and investigate the effects on the proliferation and differentiation of myogenic $Pax7^+$ cells.

Similar to BMP signaling, Notch signaling in general suppresses differentiation of Pax7 expressing precursors. **Notch signaling** (partly reviewed in Section 1.5) is important for maintenance of myogenic precursors via proliferation, self-renewal and controlled differentiation (Mourikis et al., 2012; Schuster-Gossler et al., 2007; Vasyutina et al., 2007). In a study of pectoral fin development in zebrafish embryos, components of the Notch pathway were expressed in the fin mesenchyme and blocking Notch signaling led to a reduction in the number of myogenic $Pax7^+$ cells in the fin (Pascoal et al., 2013). Studies in mice show that Notch ligand Delta-1 and receptor Notch3 are expressed at higher levels in differentiating versus quiescent satellite cells (Fukada et al., 2007; Kuang

et al., 2007). Whether there is a differential level of Notch ligand and receptor expression in the $Pax7^+$ cells in the somite especially at the vertical borders or in the $Pax7^+$ or $Pax7^+Myogenin^+$ cells entering the central body from vertical borders remains to be investigated. Utilizing immunohistochemistry and in situ hybridization, Delta-1, Notch1a and Notch3 and the expression pattern of other notch pathway members in zebrafish somite can be determined. Co-localization with Pax7 expressing cells would indicate Notch pathway components are expressed in the cells of interest within the time periods of our interest (during growth and post-wounding). An alternative mode of asymmetric division is via Notch inhibitor Numb expression (Conboy and Rando, 2002). Immunohistochemistry to stain for Numb protein could clarify whether $Pax7^+$ cells at the vertical borders are subject to Notch signaling. Moreover, treatment with the Notch inhibitor DAPT significantly increased the number of satellite cells committed to differentiation and reduced the number of quiescent $Pax7^+MyoD^-$ cells (Kuang et al., 2007). Similarly, DAPT has been used successfully in fish to study notch signaling (Grotek et al., 2013). Zebrafish can be exposed to DAPT in fish water for a specified duration and investigated for any changes to the proliferation or differentiation dynamics of Pax7 expressing cells. Also, several transgenic fish in which components of the notch pathway can be conditionally activated or inactivated are available in zebrafish making it possible to conditionally activate or inactivate notch signaling pre/post-muscle wounding and exclude developmental defects attributed to Notch pathway. Also, the ability to turn on genes conditionally and constitutively pre/post muscle wounding is useful and will be interesting since in myofibre explant system constitutively active receptor Notch1 increased the rate of myoblast proliferation and reduced myosin expression whereas constitutively active Numb decreased proliferation rates and led to myotube formation (Conboy and Rando, 2002). Moreover, in another study satellite cells with constitutively activated Notch impaired muscle repair due to decreased proliferation and differentiation (Wen et al., 2012).

Contrary to the proposed effects of Notch signaling in suppressing differentiation and promoting quiescence, **Fibroblast growth factor** (FGF) signaling in vivo appears to drive satellite cells out of quiescence (Chakkalakal et al., 2012; Lagha et al., 2008). Fgf8 signaling in zebrafish embryos promotes differentiation of Pax7 expressing

dermomyotomal cells (Groves et al., 2005; Hammond et al., 2007). Retinoic acid (RA) regulated *fgf8* expression in somites and exogenous RA similar to *fgf8* increases *myod* expression and reduces *pax3* expression (Hamade et al., 2006; Hammond et al., 2007). On the other hand, Myostatin (Mstn) TGF-β family member negatively regulates differentiation in chick and zebrafish (Amthor et al., 2006; Xu et al., 2003).

Members of the **Wnt** family have been shown to promote proliferation or differentiation. Wnts are secreted glycoproteins important in various aspects of amniote myogenesis. Briefly, the canonical Wnt pathway works through the stabilization of β-catenin, which then translocates to the nucleus to activate TCF/LEF family of genes (von Maltzahn et al., 2012). In the absence of ligand stabilization of β-catenin, a destruction complex comprising of axin, adenomatous polyposis coli (APC) and glycogen synthase kinase-3 (GSK-3-β) degrade β-catenin and silence the canonical Wnt pathway. When canonical Wnts bind to their respective Frizzled receptors (Fzd) then G proteins and Dishevelled (Dsh) get activated and axin becomes associated with the Fzd co-receptor low-density lipoprotein receptor-related protein (LRP), thereby removing axin from destruction complex which then gets degraded and the inhibition on β-catenin is released. β-catenin is not involved in non-canonical Wnt signaling which may occur through Fzd receptors via or independent of LRP (von Maltzahn et al., 2012).

During myogenesis Wnt signaling appears to promote MRF expression. Myf5 expression in the paraxial mesoderm is activated by the synergistic action of β-catenin dependent Wnt canonical pathway via Wnt1 and Wnt3a expressed in the dorsal neural tube and Gli1 member of Shh signaling pathway (Borello et al., 2006; Tajbakhsh et al., 1998). Similarly, MyoD is activated via non-canonical Wnt pathway by Wnt7a and Wnt6 expressed by the dorsal ectoderm (Tajbakhsh et al., 1998). MyoD activation by the non-canonical Wnt pathway is independent of β-catenin but dependent on protein kinase C (PKC) mediated activation of Pax3 transcription factor (Brunelli et al., 2007). Wnt signaling is also involved in providing directional cues. Orientation of elongating muscle cells in the primary myotome is mediated by Wnt11 (expressed from the dorsal neural tube) via the planar cell polarity (PCP) pathway (Gros et al., 2009). Wnt11 itself is induced by the β-catenin dependent Wnt canonical pathway via Wnt1 and Wnt3a also expressed by the

dorsal neural tube. Wnt1, 3a, and 4 from the dorsal neural tube and Wnt6 from the overlying surface ectoderm are able to maintain Pax3 and Pax7 expression within muscle precursor cells of dermomyotome (Otto et al., 2006).

Several Wnts are upregulated and downregulated during the course of muscle regeneration (Brack et al., 2008). Wnt7a has been shown to induce the expansion of satellite cell pool via symmetric divisions utilizing the non-canonical PCP pathway (Le Grand et al., 2009). Overexpression of Wnt7a enhanced regeneration and increased satellite cell numbers whereas Wnt7a deficient mice have reduced number of satellite cells post repair, suggesting that Wnt7a is involved in maintenance of stem cell population and niche repopulation or self-renewal. Canonical Wnt signaling has been linked to increased muscle mass via increased proliferation and/or differentiation. In zebrafish, gain of function Wnt/β-catenin signaling led to increase in muscle size due to increase in proliferation (Tee et al., 2009). β-catenin signaling was also shown to promote muscle hypertrophy following muscle overload (Armstrong et al., 2005; Armstrong et al., 2006). To summarize depending on the mode of signaling, Wnt proteins could promote proliferation, differentiation and/or self-renewal.

To determine the role of Wnt signaling in regulating Pax7 expressing precursors during growth and repair, wildtype fish can be exposed to chemicals that inhibit or activate Wnt signaling. Moreover, Pax7:gfp fish can be crossed with fish carrying a heat shock inducible promoter to inactivate Wnt signaling during growth or post-wounding or pre-wounding to observe the effect of the inactivation on Pax7 expressing cells in the myotome. This would be possible by utilizing the hs:Dkk1GFP transgenic fish which inactivates Wnt8 by activating Dkk1 (Stoick-Cooper, et al., 2007). Moreover, in situ hybridization can be used to determine the expression pattern of Wnt pathway components to determine which components might be active during growth and post wounding in zebrafish larvae muscle.

In addition to the signaling pathway mutant and transgenic lines available in zebrafish, mutants of somite segmentation lacking the horizontal myoseptum (six of these have notochord: *you, you-too, sonic-you, chameleon, u-boot* and *choker*; five of these have defect in notochord formation: *no tail, floating head, doc, momo* and *dino*) or with

aberration in vertical border development (*beamter*, *deadly seven*, *after eight*, *mindbomb*, and *fused somites*; van Eeden et al., 1996), can be used to determine whether the dynamics of Pax7 and Myogenin expressing cells is altered by the absence of these somitic structures and probably the lack of niche therein. The four mutants *beamter*, *deadly seven*, *after eight*, *mindbomb* are members of the Notch pathway whereas fused somites is a member of the *tbx* gene family. Of the six mutants with notochord but with disrupted horizontal myoseptum, five are members of Hh signaling pathway such that *you* has a mutation in scube2 proposed to be upstream of *smo* (Hollway et al., 2006); *you-too* has mutation in *gli2a* (Wang et al., 2013); *sonic-you* has mutation in *shha* (Du and Dienhart, 2001); *chameleon* is mutated in *dispatched* (Nakano et al., 2004) and *u-boot* has mutation in blimp1/prdm1 which is a target of Hh signaling for slow muscle formation (Elworthy et al., 2008).

An alternate technique to study the effect of niche on precursor cell dynamics would be to transplant Pax:gfp^{+} cells from one location into another. Moreover transplantation could be done from a healthy to wounded/mutant muscle and vice-versa to reveal precursor dynamics in an altered niche.

5.4 Evidence of homeostatic control of myogenic precursors and future perspectives

Findings discussed in this thesis demonstrate that a dynamic balance exists between the number of Pax7^{+} cells and is regulated during growth and repair. During normal growth, Pax7^{+} cells were found to increase in the deep myotome, suggesting that they were translocating from the superficial or adjacent unwounded somites. FGF signaling in amniotes controls timing of epithelial to mesenchymal transformation (EMT) of cells in the dermomyotome and their entry into the myotome (Delfini et al., 2009). Overexpression of FGF led to earlier entry of dermomyotomal cells into the myotome whereas inhibition via dominant negative FGFR4 delayed the epithelial to mesenchymal transition (EMT) of dermomyotomal cells and their entry into the myotome. Moreover, in this study FGF signaling was shown to act via MAPK/ERK/SNAIL1. Similarly EMT of progenitors in lateral dermomyotome to migrate to limb buds is also regulated by FGF via HGF/SF (scatter factor) signaling through c-Met (Bladt et al., 1995; Heymann et al.,

1996). In zebrafish it is not known whether FGF signaling is involved in regulating the timing of Pax7+ cell entry into the myotome. In zebrafish FGF8 mutant embryos, an expansion of Pax3/7 expressing progenitors in the dermomyotome was apparent concomitant with a delay in their differentiation as well as appearance of an *fgf8*-dependent fast fibre population in the myotome (Groves et al., 2005). It is possible that the delay in differentiation occurs due to a delay in dermomyotome to myotome transition in the mutant embryos.

If the $Pax7^+$ cells are translocating from the dermomyotome to the myotome from 4 dpf onwards, a decrease in one location with concomitant increase in the other location would be expected. Instead I found that the number of $Pax7^+$ cells in the superficial myotome did not increase significantly. Since the myotome is growing, implying that differentiation is occurring, one would predict that $Pax7^+$ cells are thereby lost by both migration and differentiation. However, any loss of $Pax7^+$ cells via migration and differentiation appeared to be replenished by proliferation, indicating a dynamic balance between proliferation, migration and differentiation. Study of the dynamics of Pax7 and Myogenin expressing cells by immunohistochemistry of larvae of zebrafish mutants of the previously mentioned signaling pathways (Hh, Notch, BMP, FGF) or molecules (RA, HSPG) could begin to reveal the pathways/molecules involved in influencing muscle homeostasis during growth and repair.

When homeostasis is perturbed as in *myod*^{fh261} mutants, the number of $Pax7^+$ precursors, $Myogenin^+Pax7^+$ and $Myogenin^+$ precursors increase and decrease spatiotemporally correlating with growth recovery. Moreover, the timing of migration is also altered, providing support for an adaptive homeostatic regulation of myogenic precursors. Mechanically wounding the muscle provided an alternative means of examining a system with perturbed homeostasis. In contrast to *myod*^{fh261} mutants with an excess of precursor cells within an intact tissue, the wounding paradigm damaged the tissue and significantly decreased the number of myogenic cells. Despite a damaged niche, the number of $Pax7^+$, $Myogenin^+Pax7^+$ and $Myogenin^+$ precursors increased significantly within a day after injury and were involved in generating muscle fibres a day later. In contrast to the *myod*^{fh261} mutants, the number of $Pax7^+$ cells does not appear to return to control levels

in apparently repaired muscle, at least at the time points examined. Moreover, despite a likely loss of $Pax7^+$ cells by differentiation into fibres, an elevated number of $Pax7^+$ cells persisted which could suggest that repair was still ongoing. However, the decline in both differentiating $Pax7^+$ cells and $Myogenin^+$ cells to levels comparable to unwounded and control muscle indicated that differentiation was winding down. The persistence of numerous mononucleate $Pax7{:}gfp^+$ cells lined up adjacent to fibres in contrast to adjacent unwounded muscle suggests an adaptation to insult.

To summarize, the data indicate regional variation in self-renewal, migration and differentiation of muscle precursors, raising the question as to what signaling mechanism/s control the balance between precursor proliferation, differentiation and quiescence during active muscle growth and repair? This and other questions central to stem cell biology can begin to be answered in a whole animal context by examining the role of different signaling pathways in regulating the *in vivo* dynamics of proliferation and differentiation of muscle precursors in a regional manner. Understanding how the various signaling systems regulate the precursors of satellite cells in zebrafish will begin to unravel details about niche components and mechanisms employed by them to maintain homeostasis in the muscle.

5.5 Clinical relevance of the zebrafish model

Zebrafish are genetically tractable, making them an excellent research tool to understand how cells behave in vivo. The zebrafish genome has been sequenced and revealed a striking 70% similarity to human protein coding sequences and contained greater that 80% of the genes known to be associated with human disease (Howe et al., 2013). Many genetic and molecular tools are available in zebrafish to study genes, signaling pathways, cell behavior and niche dynamics. Genes can be transiently silenced in the embryo by injecting siRNA into one-cell embryos. Moreover, RNA or DNA can be injected into one-cell stage embryos to drive mosaic expression of a gene of interest. Thus a mosaic of cells overexpressing a gene of interest can be obtained in the midst of non-expressing cells, creating an opportunity to observe and compare the behavior of altered and unaltered cells within the same animal. Importantly the ability to create transgenic lines that allow conditional activation or repression, makes it feasible to study gene effects in

a temporal manner (Ni et al., 2012). Also, Maze (mosaic analysis in zebrafish) technology in zebrafish allows the creation of genetically marked clones in a random group of cells which then are indelibly marked by fluorescent protein expression and can also be made to express any molecule of interest. The behavior and ontogeny of these cells can then be followed by in vivo imaging in live fish. Recently, the technical ability to create mutations by introducing specific changes to a gene of interest at the site of interest has revolutionized the use of zebrafish in making quicker strides towards understanding gene functions and deciphering molecular pathways (Sander et al., 2011; Hwang et al., 2013). In summary, a large repertoire of techniques to make changes in genotype/phenotype on zebrafish exists.

In addition to the availability of genetic and molecular tools, zebrafish are relatively cheap and easy to maintain. They produce a large number of progeny, thereby decreasing generation times required to obtain mutants. Importantly, zebrafish are amenable to non-invasive imaging techniques, making it an attractive model for studying cell behavior in vivo. Several lines modeling the pathogenic changes in muscular dystrophies are available in zebrafish and have revealed insights about the underlying the causes of pathogenesis in several muscle diseases (Bassett and Currie, 2003; Berger and Currie, 2013). Recent work in our lab has found a molecular pathway underlying muscle wasting, using the zebrafish model (Yogev et al., 2013). Zebrafish also provide a rapid and low cost method to screen small molecules with therapeutic potential (Johnson et al., 2013). In conclusion, similarity in the genes and proteins of interest between humans and zebrafish, ability to target and manipulate gene expression, availability of a number of mutants in the disease of interest combined with the ability to quickly generate an alternative mutant not yet available and also image in the live animal make zebrafish an attractive model with implications for clinical relevance.

5.6 Conclusion

The behaviour of muscle precursor cells marked by Pax7 and Myogenin expression was characterized in this thesis during normal growth, regeneration and in *myod*^{fh261} mutants. The data provide evidence in favor of muscle precursors marked by Pax7 and Myogenin expression as the precursors of growth and regeneration in zebrafish larvae and show

heterogeneity in regional behavior of muscle precursor cells. The zebrafish model is likely to be useful in understanding the complexity of signaling pathways underlying muscle growth and repair and thereby provide valuable insights for stem cell based therapeutics.

Acknowledgements

I am thankful to my mentors, family and peers for their advice and support which have made this thesis possible. I thank my supervisor Prof. Simon Hughes for his encouragement, patience and support. The Hughes lab, both past and present members have been a great source of inspiration in addition to being supportive and helpful. I would like to thank Jana for introducing me to her project, providing help with the wounding assays and her genuineness. I would like to thank Vikki for being dependable and for her kindness although she had several ongoing projects at any given time. I am grateful to Fernanda, Orli and Yaniv for helping me greatly with their knowledge and invaluable insights. I am also thankful to Jon and Kuoyo for their help and support. Last but not the least, I am thankful to lab newbies Tapan, Duvaraka and Ram for being supportive, helpful and a lot of fun to be around.

Outside of the lab, the Zammits and Mankoos have provided me support, encouragement and interesting conversations. I would especially like to thank Prof. Baljinder Mankoo for his help and guidance throughout the way. I am thankful to my second supervisor Prof. Jon Clarke for his help in shaping my project. I am grateful to Dr. Robert Knight for his advice and help with work using the *Pax7:gfp* fish.

I would like to thank my 'Indian' contingent in the Randall division including Naren, Nikita, Seema, Pahini, Vineetha and Shah. You made my time at King's and in Randall very memorable. I am eternally thankful to my husband Pramod, my parents Shikhi and Subhas, my sister Shulogna and her husband Saheel for always being there for me. This work would not have been possible without your love, faith and encouragement. Thankyou!

Bibliography

Abou-Khalil, R., Le Grand, F., Pallafacchina, G., Valable, S., Authier, F. J., Rudnicki, M. A., Gherardi, R. K., Germain, S., Chretien, F., Sotiropoulos, A., et al. (2009). Autocrine and paracrine angiopoietin 1/Tie-2 signaling promotes muscle satellite cell self-renewal. *Cell stem cell* **5**, 298-309.

Adzick, N. S. and Longaker, M. T. (1991). Animal models for the study of fetal tissue repair. *J Surg Res* **51**, 216-222.

Allbrook, D., Baker, WdeC., Kirkaldy-Willis, W. H. (1966). Muscle regeneration in experimental animals and in man. The cycle of tissue change that follows trauma in the injured limb syndrome. *The Journal of bone and joint surgery. British volume.* **48**, 153-169.

Allen, R. E., Sheehan, S. M., Taylor, R. G., Kendall, T. L. and Rice, G. M. (1995). Hepatocyte growth factor activates quiescent skeletal muscle satellite cells in vitro. *Journal of cellular physiology* **165**, 307-312.

Amthor, H., Christ, B. and Patel, K. (1999). A molecular mechanism enabling continuous embryonic muscle growth - a balance between proliferation and differentiation. *Development (Cambridge, England)* **126**, 1041-1053.

Amthor, H., Christ, B., Weil, M. and Patel, K. (1998). The importance of timing differentiation during limb muscle development. *Current biology : CB* **8**, 642-652.

Amthor, H., Otto, A., Macharia, R., McKinnell, I. and Patel, K. (2006). Myostatin imposes reversible quiescence on embryonic muscle precursors. *Developmental dynamics : an official publication of the American Association of Anatomists* **235**, 672-680.

Andres, V. and Walsh, K. (1996). Myogenin expression, cell cycle withdrawal, and phenotypic differentiation are temporally separable events that precede cell fusion upon myogenesis. *The Journal of cell biology* **132**, 657-666.

Armstrong, D. D. and Esser, K. A. (2005). Wnt/beta-catenin signaling activates growth-control genes during overload-induced skeletal muscle hypertrophy. *American journal of physiology. Cell physiology* **289**, C853-859.

Armstrong, D. D., Wong, V. L. and Esser, K. A. (2006). Expression of beta-catenin is necessary for physiological growth of adult skeletal muscle. *American journal of physiology. Cell physiology* **291**, C185-188.

Armstrong, J. R., Ferguson, M. W. (1995). Ontogeny of the skin and the transition from scar-free to scarring phenotype during wound healing in the pouch young of a marsupial, Monodelphis domestica. *Developmental biology* **169**, 242-260.

Arnold, L., Henry, A., Poron, F., Baba-Amer, Y., van Rooijen, N., Plonquet, A., Gherardi, R. K. and Chazaud, B. (2007). Inflammatory monocytes recruited after skeletal muscle injury switch into antiinflammatory macrophages to support myogenesis. *The Journal of experimental medicine* **204**, 1057-1069.

Bajard, L., Relaix, F., Lagha, M., Rocancourt, D., Daubas, P. and Buckingham, M. E. (2006). A novel genetic hierarchy functions during hypaxial myogenesis: Pax3 directly activates Myf5 in muscle progenitor cells in the limb. *Genes & development* **20**, 2450-2464.

Barresi, M. J., D'Angelo, J. A., Hernandez, L. P. and Devoto, S. H. (2001). Distinct mechanisms regulate slow-muscle development. *Current biology : CB* **11**, 1432-1438.

Barresi, M. J., Stickney, H. L. and Devoto, S. H. (2000). The zebrafish slow-muscle-omitted gene product is required for Hedgehog signal transduction and the development of slow muscle identity. *Development (Cambridge, England)* **127**, 2189-2199.

Bassaglia, Y. and Gautron, J. (1995). Fast and slow rat muscles degenerate and regenerate differently after whole crush injury. *Journal of muscle research and cell motility* **16**, 420-429.

Bassett, D. I. and Currie, P. D. (2003). The zebrafish as a model for muscular dystrophy and congenital myopathy. *Human molecular genetics* **12 Spec No 2**, R265-270.

Bassett, D., Currie, P. D. (2004). Identification of a zebrafish model of muscular dystrophy. *Clinical and experimental pharmacology & physiology*. **31**, 537-540.

Beauchamp, J. R., Heslop, L., Yu, D. S., Tajbakhsh, S., Kelly, R. G., Wernig, A., Buckingham, M. E., Partridge, T. A. and Zammit, P. S. (2000). Expression of CD34 and Myf5 defines the majority of quiescent adult skeletal muscle satellite cells. *The Journal of cell biology* **151**, 1221-1234.

Ben-Yair, R. and Kalcheim, C. (2005). Lineage analysis of the avian dermomyotome sheet reveals the existence of single cells with both dermal and muscle progenitor fates. *Development* **132**, 689-701.

Berger, J. and Currie, P. D. (2012). Zebrafish models flex their muscles to shed light on muscular dystrophies. *Disease models & mechanisms* **5**, 726-732.

Bintliff, S. and Walker, B. (1960). Radioautographic Study of Skeletal Muscle Regeneration. *American Journal of Anatomy* **106**, 233-245.

Bischoff, R. (1997). Chemotaxis of skeletal muscle satellite cells. *Developmental dynamics : an official publication of the American Association of Anatomists* **208**, 505-515.

Biressi, S. and Rando, T. A. (2010). Heterogeneity in the muscle satellite cell population. *Seminars in cell & developmental biology* **21**, 845-854.

Bischoff, R. and Heintz, C. (1994). Enhancement of skeletal muscle regeneration. *Developmental dynamics : an official publication of the American Association of Anatomists* **201**, 41-54.

Blackshaw, S. E. and Warner, A. E. (1976). Low resistance junctions between mesoderm cells during development of trunk muscles. *The Journal of physiology* **255**, 209-230.

Blagden, C. S., Currie, P. D., Ingham, P. W. and Hughes, S. M. (1997). Notochord induction of zebrafish slow muscle mediated by Sonic hedgehog. *Genes & development* **11**, 2163-2175.

Bladt, F., Riethmacher, D., Isenmann, S., Aguzzi, A. and Birchmeier, C. (1995). Essential role for the c-met receptor in the migration of myogenic precursor cells into the limb bud. *Nature* **376**, 768-771.

Bober, E., Franz, T., Arnold, H. H., Gruss, P. and Tremblay, P. (1994). Pax-3 is required for the development of limb muscles: a possible role for the migration of dermomyotomal muscle progenitor cells. *Development (Cambridge, England)* **120**, 603-612.

Bondesen, B. A., Mills, S. T., Kegley, K. M. and Pavlath, G. K. (2004). The COX-2 pathway is essential during early stages of skeletal muscle regeneration. *American journal of physiology. Cell physiology* **287**, C475-483.

Borello, U., Berarducci, B., Murphy, P., Bajard, L., Buffa, V., Piccolo, S., Buckingham, M. and Cossu, G. (2006). The Wnt/beta-catenin pathway regulates Gli-mediated Myf5 expression during somitogenesis. *Development (Cambridge, England)* **133**, 3723-3732.

Borycki, A. G., Li, J., Jin, F., Emerson, C. P. and Epstein, J. A. (1999). Pax3 functions in cell survival and in pax7 regulation. *Development (Cambridge, England)* **126**, 1665-1674.

Brack, A. S., Conboy, I. M., Conboy, M. J., Shen, J. and Rando, T. A. (2008). A temporal switch from notch to Wnt signaling in muscle stem cells is necessary for normal adult myogenesis. *Cell stem cell* **2**, 50-59.

Braun, T., Rudnicki, M. A., Arnold, H. H. and Jaenisch, R. (1992). Targeted inactivation of the muscle regulatory gene Myf-5 results in abnormal rib development and perinatal death. *Cell* **71**, 369-382.

Brent, A. E., Schweitzer, R. and Tabin, C. J. (2003). A somitic compartment of tendon progenitors. *Cell* **113**, 235-248.

Brunelli, S., Relaix, F., Baesso, S., Buckingham, M. and Cossu, G. (2007). Beta catenin-independent activation of MyoD in presomitic mesoderm requires PKC and depends on Pax3 transcriptional activity. *Developmental biology* **304**, 604-614.

Buckingham, M. E. (1994). Muscle: the regulation of myogenesis. *Current opinion in genetics & development* **4**, 745-751.

Buckingham, M. (2001). Skeletal muscle formation in vertebrates. *Current opinion in genetics & development* **11**, 440-448.

Buckingham, M., Bajard, L., Chang, T., Daubas, P., Hadchouel, J., Meilhac, S., Montarras, D., Rocancourt, D. and Relaix, F. (2003). The formation of skeletal muscle: from somite to limb. *Journal of anatomy* **202**, 59-68.

Buckingham, M., Bajard, L., Daubas, P., Esner, M., Lagha, M., Relaix, F. and Rocancourt, D. (2006). Myogenic progenitor cells in the mouse embryo are marked by the expression of Pax3/7 genes that regulate their survival and myogenic potential. *Anatomy and embryology* **211 Suppl 1**, 51-56.

Buckingham, M. and Relaix, F. (2007). The role of Pax genes in the development of tissues and organs: Pax3 and Pax7 regulate muscle progenitor cell functions. *Annual review of cell and developmental biology* **23**, 645-673.

Camargo, A. A., Carvalho, R. F., Dal-Pai, V., Pellizzon, C. H., Dal-Pai-Silva, M. (2004). Morphological aspects of muscle regeneration in the Nile tilapia (Oreochromis niloticus). *Journal of submicroscopic cytology and pathology* **36**, 319-326.

Capers, C. R. (1960). Multinucleation of skeletal muscle in vitro. *J Biophys Biochem Cytol* **7**, 559-566.

Cass, D. L., Meuli, M. and Adzick, N. S. (1997). Scar wars: implications of fetal wound healing for the pediatric burn patient. *Pediatric surgery international* **12**, 484-489.

Chakkalakal, J. V., Jones, K. M., Basson, M. A. and Brack, A. S. (2012). The aged niche disrupts muscle stem cell quiescence. *Nature* **490**, 355-360.

Chakravarthy, M. V., Davis, B. S. and Booth, F. W. (2000). IGF-I restores satellite cell proliferative potential in immobilized old skeletal muscle. *Journal of applied physiology (Bethesda, Md. : 1985)* **89**, 1365-1379.

Chazaud, B., Brigitte, M., Yacoub-Youssef, H., Arnold, L., Gherardi, R., Sonnet, C., Lafuste, P. and Chretien, F. (2009). Dual and beneficial roles of macrophages during skeletal muscle regeneration. *Exercise and sport sciences reviews* **37**, 18-22.

Chazaud, B., Sonnet, C., Lafuste, P., Bassez, G., Rimaniol, A. C., Poron, F., Authier, F. J., Dreyfus, P. A. and Gherardi, R. K. (2003). Satellite cells attract monocytes and use macrophages as a support to escape apoptosis and enhance muscle growth. *The Journal of cell biology* **163**, 1133-1143.

Chen, J. K., Taipale, J., Cooper, M. K. and Beachy, P. A. (2002). Inhibition of Hedgehog signaling by direct binding of cyclopamine to Smoothened. *Genes & development* **16**, 2743-2748.

Chen, X. and Li, Y. (2009). Role of matrix metalloproteinases in skeletal muscle: migration, differentiation, regeneration and fibrosis. *Cell adhesion & migration* **3**, 337-341.

Chen, Y., Lin, G. and Slack, J. M. (2006). Control of muscle regeneration in the Xenopus tadpole tail by Pax7. *Development (Cambridge, England)* **133**, 2303-2313.

Christ, B., Huang, R. and Scaal, M. (2004). Formation and differentiation of the avian sclerotome. *Anatomy and embryology* **208**, 333-350.

Christ, B., Huang, R. and Wilting, J. (2000). The development of the avian vertebral column. *Anatomy and embryology* **202**, 179-194.

Christ, B., Jacob, H. J. and Jacob, M. (1977). [Experimental findings on muscle development in the limbs of the chick embryo]. *Verhandlungen der Anatomischen Gesellschaft*, 1231-1237.

Christ, B. and Ordahl, C. P. (1995). Early stages of chick somite development. *Anatomy and embryology* **191**, 381-396.

Church, J. C.T. (1969). Satellite cells and myogenesis; a study in the fruit-bat web. *Journal of anatomy* **105**, 419-438.

Church, J.C.T., Noronha R.F.X, Allrook D.B. (1966). Satellite Cells and skeletal muscle regeneration. *Br. J. Surg.,* **53**, 638-642.

Church, R. B. and Robertson, F. W. (1966). Biochemical analysis of genetic differences in the growth of Drosophila. *Genetical research* **7**, 383-407.

Cinnamon, Y., Kahane, N. and Kalcheim, C. (1999). Characterization of the early development of specific hypaxial muscles from the ventrolateral myotome. *Development (Cambridge, England)* **126**, 4305-4315.

Clark, W. E. (1946). An experimental study of the regeneration of mammalian striped muscle. *Journal of anatomy* **80**, 24-36.

Coleman, M. E., DeMayo, F., Yin, K. C., Lee, H. M., Geske, R., Montgomery, C. and Schwartz, R. J. (1995). Myogenic vector expression of insulin-like growth factor I stimulates muscle cell differentiation and myofiber hypertrophy in transgenic mice. *The Journal of biological chemistry* **270**, 12109-12116.

Collins, C. A., Olsen, I., Zammit, P. S., Heslop, L., Petrie, A., Partridge, T. A. and Morgan, J. E. (2005). Stem cell function, self-renewal, and behavioral heterogeneity of cells from the adult muscle satellite cell niche. *Cell* **122**, 289-301.

Collins, R. T., Linker, C. and Lewis, J. (2010). MAZe: a tool for mosaic analysis of gene function in zebrafish. *Nature methods* **7**, 219-223.

Colmenares, C., Teumer, J. K. and Stavnezer, E. (1991). Transformation-defective v-ski induces MyoD and myogenin expression but not myotube formation. *Molecular and cellular biology* **11**, 1167-1170.

Conboy, I. M., Conboy, M. J., Smythe, G. M. and Rando, T. A. (2003). Notch-mediated restoration of regenerative potential to aged muscle. *Science (New York, N.Y.)* **302**, 1575-1577.

Conboy, I. M. and Rando, T. A. (2002). The regulation of Notch signaling controls satellite cell activation and cell fate determination in postnatal myogenesis. *Developmental cell* **3**, 397-409.

Coolican, S. A., Samuel, D. S., Ewton, D. Z., McWade, F. J. and Florini, J. R. (1997). The mitogenic and myogenic actions of insulin-like growth factors utilize distinct signaling pathways. *The Journal of biological chemistry* **272**, 6653-6662.

Cooper, W. G., Konigsberg, I. R. (1961). Dynamics of myogenesis in vitro. *The Anatomical record* **140**, 195-205.

Cooper, R. N., Tajbakhsh, S., Mouly, V., Cossu, G., Buckingham, M. and Butler-Browne, G. S. (1999). In vivo satellite cell activation via Myf5 and MyoD in regenerating mouse skeletal muscle. *Journal of cell science* **112 (Pt 17)**, 2895-2901.

Cornelison, D. D., Filla, M. S., Stanley, H. M., Rapraeger, A. C. and Olwin, B. B. (2001). Syndecan-3 and syndecan-4 specifically mark skeletal muscle satellite cells and are implicated in satellite cell maintenance and muscle regeneration. *Developmental biology* **239**, 79-94.

Cornelison, D. D., Olwin, B. B., Rudnicki, M. A. and Wold, B. J. (2000). MyoD(-/-) satellite cells in single-fiber culture are differentiation defective and MRF4 deficient. *Developmental biology* **224**, 122-137.

Cornelison, D. D. and Wold, B. J. (1997). Single-cell analysis of regulatory gene expression in quiescent and activated mouse skeletal muscle satellite cells. *Developmental biology* **191**, 270-283.

Coutelle, O., Blagden, C. S., Hampson, R., Halai, C., Rigby, P. W. and Hughes, S. M. (2001). Hedgehog signalling is required for maintenance of myf5 and myoD expression and timely terminal differentiation in zebrafish adaxial myogenesis. *Developmental biology* **236**, 136-150.

Crow, M. T. and Stockdale, F. E. (1986). The developmental program of fast myosin heavy chain expression in avian skeletal muscles. *Developmental biology* **118**, 333-342.

Currie, P. D. and Ingham, P. W. (1996). Induction of a specific muscle cell type by a hedgehog-like protein in zebrafish. *Nature* **382**, 452-455.

d'Albis, A., Couteaux, R., Janmot, C., Mira, J. C. (1989). Myosin isoform transitions in regeneration of fast and slow muscles during postnatal development of the rat. *Developmental biology* **135**, 320-325.

Dan-Goor, M., Silberstein, L., Kessel, M. and Muhlrad, A. (1990). Localization of epitopes and functional effects of two novel monoclonal antibodies against skeletal muscle myosin. *Journal of muscle research and cell motility* **11**, 216-226.

Darr, K. C. and Schultz, E. (1987). Exercise-induced satellite cell activation in growing and mature skeletal muscle. *Journal of applied physiology (Bethesda, Md. : 1985)* **63**, 1816-1821.

Daughters, R. S., Chen, Y. and Slack, J. M. (2011). Origin of muscle satellite cells in the Xenopus embryo. *Development (Cambridge, England)* **138**, 821-830.

Davis, G. K., D'Alessio, J. A. and Patel, N. H. (2005). Pax3/7 genes reveal conservation and divergence in the arthropod segmentation hierarchy. *Developmental biology* **285**, 169-184.

De Strooper, B., Annaert, W., Cupers, P., Saftig, P., Craessaerts, K., Mumm, J. S., Schroeter, E. H., Schrijvers, V., Wolfe, M. S., Ray, W. J., et al. (1999). A presenilin-1-dependent gamma-secretase-like protease mediates release of Notch intracellular domain. *Nature* **398**, 518-522.

Delfini, M. C., De La Celle, M., Gros, J., Serralbo, O., Marics, I., Seux, M., Scaal, M. and Marcelle, C. (2009). The timing of emergence of muscle progenitors is controlled by an FGF/ERK/SNAIL1 pathway. *Developmental biology* **333**, 229-237.

Della Gaspera, B., Armand, A. S., Lecolle, S., Charbonnier, F. and Chanoine, C. (2012). Mef2d acts upstream of muscle identity genes and couples lateral myogenesis to dermomyotome formation in Xenopus laevis. *PloS one* **7**, e52359.

Denetclaw, W. F., Jr., Berdougo, E., Venters, S. J. and Ordahl, C. P. (2001). Morphogenetic cell movements in the middle region of the dermomyotome dorsomedial lip associated with patterning and growth of the primary epaxial myotome. *Development (Cambridge, England)* **128**, 1745-1755.

Denetclaw, W. F., Jr., Christ, B. and Ordahl, C. P. (1997). Location and growth of epaxial myotome precursor cells. *Development (Cambridge, England)* **124**, 1601-1610.

Denetclaw, W. F. and Ordahl, C. P. (2000). The growth of the dermomyotome and formation of early myotome lineages in thoracolumbar somites of chicken embryos. *Development (Cambridge, England)* **127**, 893-905.

Devoto, S. H., Melancon, E., Eisen, J. S. and Westerfield, M. (1996). Identification of separate slow and fast muscle precursor cells in vivo, prior to somite formation. *Development (Cambridge, England)* **122**, 3371-3380.

Devoto, S. H., Stoiber, W., Hammond, C. L., Steinbacher, P., Haslett, J. R., Barresi, M. J., Patterson, S. E., Adiarte, E. G. and Hughes, S. M. (2006). Generality of vertebrate developmental patterns: evidence for a dermomyotome in fish. *Evolution & development* **8**, 101-110.

Dolez, M., Nicolas, J. F. and Hirsinger, E. (2011). Laminins, via heparan sulfate proteoglycans, participate in zebrafish myotome morphogenesis by modulating the pattern of Bmp responsiveness. *Development (Cambridge, England)* **138**, 97-106.

Droguett, R., Cabello-Verrugio, C., Santander, C. and Brandan, E. (2010). TGF-beta receptors, in a Smad-independent manner, are required for terminal skeletal muscle differentiation. *Experimental cell research* **316**, 2487-2503.

Du, S. J. and Dienhart, M. (2001). Gli2 mediation of hedgehog signals in slow muscle induction in zebrafish. *Differentiation; research in biological diversity* **67**, 84-91.

Du, S. J., Devoto, S. H., Westerfield, M. and Moon, R. T. (1997). Positive and negative regulation of muscle cell identity by members of the hedgehog and TGF-beta gene families. *The Journal of cell biology* **139**, 145-156.

Elia, D., Madhala, D., Ardon, E., Reshef, R. and Halevy, O. (2007). Sonic hedgehog promotes proliferation and differentiation of adult muscle cells: Involvement of MAPK/ERK and PI3K/Akt pathways. *Biochimica et biophysica acta* **1773**, 1438-1446.

Elworthy, S., Hargrave, M., Knight, R., Mebus, K. and Ingham, P. W. (2008). Expression of multiple slow myosin heavy chain genes reveals a diversity of zebrafish slow twitch muscle fibres with differing requirements for Hedgehog and Prdm1 activity. *Development (Cambridge, England)* **135**, 2115-2126.

Epstein, J. A., Shapiro, D. N., Cheng, J., Lam, P. Y. and Maas, R. L. (1996). Pax3 modulates expression of the c-Met receptor during limb muscle development. *Proceedings of the National Academy of Sciences of the United States of America* **93**, 4213-4218.

Epstein, D. J., Vekemans, M. and Gros, P. (1991). Splotch (Sp2H), a mutation affecting development of the mouse neural tube, shows a deletion within the paired homeodomain of Pax-3. *Cell* **67**, 767-774.

Erazo-Pagador, G. D., Mohd Shariff (2001). Rapid Wound Healing In African Catfish, Clarias Gariepinus, Fed Diets Supplemented With Ascorbic Acid *The Israeli Journal of Aquaculture - Bamidgeh* **53**, 69-79.

Fan, Y., Maley, M., Beilharz, M. and Grounds, M. (1996). Rapid death of injected myoblasts in myoblast transfer therapy. *Muscle & nerve* **19**, 853-860.

Fedorov, Y. V., Rosenthal, R. S. and Olwin, B. B. (2001). Oncogenic Ras-induced proliferation requires autocrine fibroblast growth factor 2 signaling in skeletal muscle cells. *The Journal of cell biology* **152**, 1301-1305.

Felsenfeld, A. L., Curry, M. and Kimmel, C. B. (1991). The fub-1 mutation blocks initial myofibril formation in zebrafish muscle pioneer cells. *Developmental biology* **148**, 23-30.

Feng, X., Adiarte, E. G. and Devoto, S. H. (2006). Hedgehog acts directly on the zebrafish dermomyotome to promote myogenic differentiation. *Developmental biology* **300**, 736-746.

Floss, T., Arnold, H. H. and Braun, T. (1997). A role for FGF-6 in skeletal muscle regeneration. *Genes & development* **11**, 2040-2051.

Fukada, S., Uezumi, A., Ikemoto, M., Masuda, S., Segawa, M., Tanimura, N., Yamamoto, H., Miyagoe-Suzuki, Y. and Takeda, S. (2007). Molecular signature of quiescent satellite cells in adult skeletal muscle. *Stem cells (Dayton, Ohio)* **25**, 2448-2459.

Furutani, Y., Umemoto, T., Murakami, M., Matsui, T. and Funaba, M. (2011). Role of endogenous TGF-beta family in myogenic differentiation of C2C12 cells. *Journal of cellular biochemistry* **112**, 614-624.

Gargioli, C. and Slack, J. M. (2004). Cell lineage tracing during Xenopus tail regeneration. *Development (Cambridge, England)* **131**, 2669-2679.

Garry, D. J. and Olson, E. N. (2006). A common progenitor at the heart of development. *Cell* **127**, 1101-1104.

Garry, D. J., Yang, Q., Bassel-Duby, R. and Williams, R. S. (1997). Persistent expression of MNF identifies myogenic stem cells in postnatal muscles. *Developmental biology* **188**, 280-294.

Gillespie, M. A., Le Grand, F., Scime, A., Kuang, S., von Maltzahn, J., Seale, V., Cuenda, A., Ranish, J. A. and Rudnicki, M. A. (2009). p38-{gamma}-dependent gene silencing restricts entry into the myogenic differentiation program. *The Journal of cell biology* **187**, 991-1005.

Gnocchi, V. F., White, R. B., Ono, Y., Ellis, J. A. and Zammit, P. S. (2009). Further characterisation of the molecular signature of quiescent and activated mouse muscle satellite cells. *PloS one* **4**, e5205.

Golding, J. P., Calderbank, E., Partridge, T. A. and Beauchamp, J. R. (2007). Skeletal muscle stem cells express anti-apoptotic ErbB receptors during activation from quiescence. *Experimental cell research* **313**, 341-356.

Gong, Z., Wan, H., Tay, T. L., Wang, H., Chen, M. and Yan, T. (2003). Development of transgenic fish for ornamental and bioreactor by strong expression of fluorescent proteins in the skeletal muscle. *Biochemical and biophysical research communications* **308**, 58-63.

Goulding, M. D., Chalepakis, G., Deutsch, U., Erselius, J. R. and Gruss, P. (1991). Pax-3, a novel murine DNA binding protein expressed during early neurogenesis. *The EMBO journal* **10**, 1135-1147.

Goulding, M.D., Lumsden, A. and Paquette, A. J. (1994). Regulation of Pax-3 expression in the dermomyotome and its role in muscle development. *Development (Cambridge, England)* **120**, 957-971.

Gregorio, C. C., Granzier, H., Sorimachi, H. and Labeit, S. (1999). Muscle assembly: a titanic achievement? *Current opinion in cell biology* **11**, 18-25.

Grimaldi, A., Tettamanti, G., Martin, B. L., Gaffield, W., Pownall, M. E. and Hughes, S. M. (2004). Hedgehog regulation of superficial slow muscle fibres in Xenopus and the evolution of tetrapod trunk myogenesis. *Development (Cambridge, England)* **131**, 3249-3262.

Gros, J., Manceau, M., Thome, V. and Marcelle, C. (2005). A common somitic origin for embryonic muscle progenitors and satellite cells. *Nature* **435**, 954-958.

Gros, J., Scaal, M. and Marcelle, C. (2004). A two-step mechanism for myotome formation in chick. *Developmental cell* **6**, 875-882.

Gros, J., Serralbo, O. and Marcelle, C. (2009). WNT11 acts as a directional cue to organize the elongation of early muscle fibres. *Nature* **457**, 589-593.

Grotek, B., Wehner, D. and Weidinger, G. (2013). Notch signaling coordinates cellular proliferation with differentiation during zebrafish fin regeneration. *Development (Cambridge, England)* **140**, 1412-1423.

Grounds, M. D., Garrett, K. L., Lai, M. C., Wright, W. E., Beilharz, M. W. (1992). Identification of skeletal muscle precursor cells in vivo by use of MyoD1 and myogenin probes. *Cell and tissue research* **267**, 99-104.

Grounds, M. D. and McGeachie, J. K. (1987). Reutilisation of tritiated thymidine in studies of regenerating skeletal muscle. *Cell and tissue research* **250**, 141-148.

Grounds, M., Partridge, T. A., Sloper, J. C. (1980). The contribution of exogenous cells to regenerating skeletal muscle: an isoenzyme study of muscle allografts in mice. *The Journal of Pathology* **132**, 325-341.

Groves, J. A., Hammond, C. L. and Hughes, S. M. (2005). Fgf8 drives myogenic progression of a novel lateral fast muscle fibre population in zebrafish. *Development (Cambridge, England)* **132**, 4211-4222.

Hall, J. M. and McDonnell, D. P. (2007). The molecular mechanisms underlying the proinflammatory actions of thiazolidinediones in human macrophages. *Molecular endocrinology (Baltimore, Md.)* **21**, 1756-1768.

Hamade, A., Deries, M., Begemann, G., Bally-Cuif, L., Genet, C., Sabatier, F., Bonnieu, A. and Cousin, X. (2006). Retinoic acid activates myogenesis in vivo through Fgf8 signalling. *Developmental biology* **289**, 127-140.

Hamilton, L. (1969). The formation of somites in Xenopus. *Journal of embryology and experimental morphology* **22**, 253-264.

Hammond, C. L., Hinits, Y., Osborn, D. P., Minchin, J. E., Tettamanti, G. and Hughes, S. M. (2007). Signals and myogenic regulatory factors restrict pax3 and pax7 expression to dermomyotome-like tissue in zebrafish. *Developmental biology* **302**, 504-521.

Hannon, K., Kudla, A. J., McAvoy, M. J., Clase, K. L. and Olwin, B. B. (1996). Differentially expressed fibroblast growth factors regulate skeletal muscle development through autocrine and paracrine mechanisms. *The Journal of cell biology* **132**, 1151-1159.

Hasty, P., Bradley, A., Morris, J. H., Edmondson, D. G., Venuti, J. M., Olson, E. N. and Klein, W. H. (1993). Muscle deficiency and neonatal death in mice with a targeted mutation in the myogenin gene. *Nature* **364**, 501-506.

Hasty, P., Rivera-Perez, J. and Bradley, A. (1992). The role and fate of DNA ends for homologous recombination in embryonic stem cells. *Molecular and cellular biology* **12**, 2464-2474.

Hatta, K., Bremiller, R., Westerfield, M. and Kimmel, C. B. (1991). Diversity of expression of engrailed-like antigens in zebrafish. *Development (Cambridge, England)* **112**, 821-832.

He, L., Papoutsi, M., Huang, R., Tomarev, S. I., Christ, B., Kurz, H. and Wilting, J. (2003). Three different fates of cells migrating from somites into the limb bud. *Anatomy and embryology* **207**, 29-34.

Herbomel, P., Thisse, B. and Thisse, C. (1999). Ontogeny and behaviour of early macrophages in the zebrafish embryo. *Development (Cambridge, England)* **126**, 3735-3745.

Herbomel, P., Thisse, B. and Thisse, C. (2001). Zebrafish early macrophages colonize cephalic mesenchyme and developing brain, retina, and epidermis through a M-CSF receptor-dependent invasive process. *Developmental biology* **238**, 274-288.

Heymann, S., Koudrova, M., Arnold, H., Koster, M. and Braun, T. (1996). Regulation and function of SF/HGF during migration of limb muscle precursor cells in chicken. *Developmental biology* **180**, 566-578.

Hikida, R. S. and Lombardo, J. A. (1974). Regeneration of pigeon fast and slow muscle fiber types after partial excision and mincing. *The Journal of cell biology* **61**, 414-426.

Hill, E., Boontheekul, T. and Mooney, D. J. (2006). Designing scaffolds to enhance transplanted myoblast survival and migration. *Tissue engineering* **12**, 1295-1304.

Hinits, Y., Osborn, D. P. and Hughes, S. M. (2009). Differential requirements for myogenic regulatory factors distinguish medial and lateral somitic, cranial and fin muscle fibre populations. *Development (Cambridge, England)* **136**, 403-414.

Hinits, Y., Williams, V. C., Sweetman, D., Donn, T. M., Ma, T. P., Moens, C. B. and Hughes, S. M. (2011). Defective cranial skeletal development, larval lethality and haploinsufficiency in Myod mutant zebrafish. *Developmental biology* **358**, 102-112.

Hollway, G. E., Bryson-Richardson, R. J., Berger, S., Cole, N. J., Hall, T. E. and Currie, P. D. (2007). Whole-somite rotation generates muscle progenitor cell compartments in the developing zebrafish embryo. *Developmental cell* **12**, 207-219.

Hollway, G. E., Maule, J., Gautier, P., Evans, T. M., Keenan, D. G., Lohs, C., Fischer, D., Wicking, C. and Currie, P. D. (2006). Scube2 mediates Hedgehog signalling in the zebrafish embryo. *Developmental biology* **294**, 104-118.

Hooper, J. E. (1994). Distinct pathways for autocrine and paracrine Wingless signalling in Drosophila embryos. *Nature* **372**, 461-464.

Howe, K., Clark, M. D., Torroja, C. F., Torrance, J., Berthelot, C., Muffato, M., Collins, J. E., Humphray, S., McLaren, K., Matthews, L., et al. (2013). The zebrafish reference genome sequence and its relationship to the human genome. *Nature* **496**, 498-503.

Huang, R. and Christ, B. (2000). Origin of the epaxial and hypaxial myotome in avian embryos. *Anatomy and embryology* **202**, 369-374.

Hurley, J. V. (1994). Inflammation and repair in the mammalian fetus: a reappraisal. *Microsurgery* **15**, 811-816.

Hutcheson, D. A., Zhao, J., Merrell, A., Haldar, M. and Kardon, G. (2009). Embryonic and fetal limb myogenic cells are derived from developmentally distinct progenitors and have different requirements for beta-catenin. *Genes & development* **23**, 997-1013.

Hwang, W. Y., Fu, Y., Reyon, D., Maeder, M. L., Tsai, S. Q., Sander, J. D., Peterson, R. T., Yeh, J. R. and Joung, J. K. (2013). Efficient genome editing in zebrafish using a CRISPR-Cas system. *Nature biotechnology* **31**, 227-229.

Ingham, P. W., Taylor, A. M. and Nakano, Y. (1991). Role of the Drosophila patched gene in positional signalling. *Nature* **353**, 184-187.

Irintchev, A., Zeschnigk, M., Starzinski-Powitz, A. and Wernig, A. (1994). Expression pattern of M-cadherin in normal, denervated, and regenerating mouse muscles. *Developmental dynamics : an official publication of the American Association of Anatomists* **199**, 326-337.

Ishikawa, H. (1966). Electron microscopic observations of satellite cells with special reference to the development of mammalian skeletal muscles. *Zeitschrift fur Anatomie und Entwicklungsgeschichte* **125**, 43-63.

Jackson, H. E. and Ingham, P. W. (2013). Control of muscle fibre-type diversity during embryonic development: the zebrafish paradigm. *Mechanisms of development* **130**, 447-457.

Jacob, M., Christ, B. and Jacob, H. J. (1978). On the migration of myogenic stem cells into the prospective wing region of chick embryos. A scanning and transmission electron microscope study. *Anatomy and embryology* **153**, 179-193.

Jacob, M., Christ, B. and Jacob, H. J. (1979). The migration of myogenic cells from the somites into the leg region of avian embryos. An ultrastructural study. *Anatomy and embryology* **157**, 291-309.

Johnson, M. N., Farr., Gist, H. F., Maves, L. (2013). The HDAC Inhibitor TSA Ameliorates a Zebrafish Model of Duchenne Muscular Dystrophy. *PLOS Currents Muscular Dystrophy* **1**, doi:10.1371/currents.md.8273cf41db10e2d15dd3ab827cb4b027

Jones, N. C., Fedorov, Y. V., Rosenthal, R. S. and Olwin, B. B. (2001). ERK1/2 is required for myoblast proliferation but is dispensable for muscle gene expression and cell fusion. *Journal of cellular physiology* **186**, 104-115.

Jostes, B., Walther, C. and Gruss, P. (1990). The murine paired box gene, Pax7, is expressed specifically during the development of the nervous and muscular system. *Mechanisms of development* **33**, 27-37.

Kablar, B., Krastel, K., Ying, C., Asakura, A., Tapscott, S. J. and Rudnicki, M. A. (1997). MyoD and Myf-5 differentially regulate the development of limb versus trunk skeletal muscle. *Development* **124**, 4729-4738.

Kahane, N., Cinnamon, Y. and Kalcheim, C. (1998a). The cellular mechanism by which the dermomyotome contributes to the second wave of myotome development. *Development* **125**, 4259-4271.

Kahane, N., Cinnamon, Y. and Kalcheim, C. (1998b). The origin and fate of pioneer myotomal cells in the avian embryo. *Mechanisms of development* **74**, 59-73.

Kahane, N., Cinnamon, Y. and Kalcheim, C. (2002). The roles of cell migration and myofiber intercalation in patterning formation of the postmitotic myotome. *Development* **129**, 2675-2687.

Kahane, N., Ribes, V., Kicheva, A., Briscoe, J. and Kalcheim, C. (2013). The transition from differentiation to growth during dermomyotome-derived myogenesis depends on temporally restricted hedgehog signaling. *Development (Cambridge, England)* **140**, 1740-1750.

Kami, K. and Senba, E. (2002). In vivo activation of STAT3 signaling in satellite cells and myofibers in regenerating rat skeletal muscles. *The journal of histochemistry and cytochemistry : official journal of the Histochemistry Society* **50**, 1579-1589.

Kardon, G., Heanue, T. A. and Tabin, C. J. (2002). Pax3 and Dach2 positive regulation in the developing somite. *Developmental dynamics : an official publication of the American Association of Anatomists* **224**, 350-355.

Kassar-Duchossoy, L., Gayraud-Morel, B., Gomes, D., Rocancourt, D., Buckingham, M., Shinin, V. and Tajbakhsh, S. (2004). Mrf4 determines skeletal muscle identity in Myf5:Myod double-mutant mice. *Nature* **431**, 466-471.

Kassar-Duchossoy, L., Giacone, E., Gayraud-Morel, B., Jory, A., Gomes, D. and Tajbakhsh, S. (2005). Pax3/Pax7 mark a novel population of primitive myogenic cells during development. *Genes & development* **19**, 1426-1431.

Kawakami, A., Kimura-Kawakami, M., Nomura, T. and Fujisawa, H. (1997). Distributions of PAX6 and PAX7 proteins suggest their involvement in both early and late phases of chick brain development. *Mechanisms of development* **66**, 119-130.

Kherif, S., Lafuma, C., Dehaupas, M., Lachkar, S., Fournier, J. G., Verdiere-Sahuque, M., Fardeau, M. and Alameddine, H. S. (1999). Expression of matrix metalloproteinases 2 and 9 in regenerating skeletal muscle: a study in experimentally injured and mdx muscles. *Developmental biology* **205**, 158-170.

Kimmel, C. B., Ballard, W. W., Kimmel, S. R., Ullmann, B. and Schilling, T. F. (1995). Stages of embryonic development of the zebrafish. *Developmental dynamics : an official publication of the American Association of Anatomists* **203**, 253-310.

Koleva, M., Kappler, R., Vogler, M., Herwig, A., Fulda, S. and Hahn, H. (2005). Pleiotropic effects of sonic hedgehog on muscle satellite cells. *Cellular and molecular life sciences : CMLS* **62**, 1863-1870.

Konigsberg, I. R., McElvain, N., Tootle, M., Herrmann, H. (1960). The dissociability of deoxyribonucleic acid synthesis from the development of multinuclearity of muscle cells in culture. *The Journal of Biophysical and Biochemical Cytology* **8**, 333-343.

Kuang, S., Charge, S. B., Seale, P., Huh, M. and Rudnicki, M. A. (2006). Distinct roles for Pax7 and Pax3 in adult regenerative myogenesis. *The Journal of cell biology* **172**, 103-113.

Kuang, S., Kuroda, K., Le Grand, F. and Rudnicki, M. A. (2007). Asymmetric self-renewal and commitment of satellite stem cells in muscle. *Cell* **129**, 999-1010.

Kurth, T., Schwarz, H., Schneider, S. and Hausen, P. (1996). Fine structural immunocytochemistry of catenins in amphibian and mammalian muscle. *Cell and tissue research* **286**, 1-12.

Lagha, M., Kormish, J. D., Rocancourt, D., Manceau, M., Epstein, J. A., Zaret, K. S., Relaix, F. and Buckingham, M. E. (2008). Pax3 regulation of FGF signaling affects the progression of embryonic progenitor cells into the myogenic program. *Genes & development* **22**, 1828-1837.

Le Guyader, D., Redd, M. J., Colucci-Guyon, E., Murayama, E., Kissa, K., Briolat, V., Mordelet, E., Zapata, A., Shinomiya, H. and Herbomel, P. (2008). Origins and unconventional behavior of neutrophils in developing zebrafish. *Blood* **111**, 132-141.

Lefaucheur, J. P. and Sebille, A. (1995). Basic fibroblast growth factor promotes in vivo muscle regeneration in murine muscular dystrophy. *Neuroscience letters* **202**, 121-124.

Le Grand, F., Jones, A. E., Seale, V., Scime, A. and Rudnicki, M. A. (2009). Wnt7a activates the planar cell polarity pathway to drive the symmetric expansion of satellite stem cells. *Cell stem cell* **4**, 535-547.

Lepper, C., Conway, S. J. and Fan, C. M. (2009). Adult satellite cells and embryonic muscle progenitors have distinct genetic requirements. *Nature* **460**, 627-631.

Lescaudron, L., Peltekian, E., Fontaine-Perus, J., Paulin, D., Zampieri, M., Garcia, L. and Parrish, E. (1999). Blood borne macrophages are essential for the triggering of muscle regeneration following muscle transplant. *Neuromuscular disorders : NMD* **9**, 72-80.

Leshem, Y., Gitelman, I., Ponzetto, C. and Halevy, O. (2002). Preferential binding of Grb2 or phosphatidylinositol 3-kinase to the met receptor has opposite effects on HGF-induced myoblast proliferation. *Experimental cell research* **274**, 288-298.

Leshem, Y., Spicer, D. B., Gal-Levi, R. and Halevy, O. (2000). Hepatocyte growth factor (HGF) inhibits skeletal muscle cell differentiation: a role for the bHLH protein twist and the cdk inhibitor p27. *Journal of cellular physiology* **184**, 101-109.

Lewis, K. E., Currie, P. D., Roy, S., Schauerte, H., Haffter, P. and Ingham, P. W. (1999). Control of muscle cell-type specification in the zebrafish embryo by Hedgehog signalling. *Developmental biology* **216**, 469-480.

Lieschke, G. J., Oates, A. C., Crowhurst, M. O., Ward, A. C. and Layton, J. E. (2001). Morphologic and functional characterization of granulocytes and macrophages in embryonic and adult zebrafish. *Blood* **98**, 3087-3096.

Lipton, B. H., Schultz, E. (1979). Developmental Fate of Skeletal Muscle Satellite Cells. *Science (New York, N.Y.)* **205**, 1292-1294.

Liu, F. and Wen, Z. (2002). Cloning and expression pattern of the lysozyme C gene in zebrafish. *Mechanisms of development* **113**, 69-72.

Liu, J. P., Baker, J., Perkins, A. S., Robertson, E. J. and Efstratiadis, A. (1993). Mice carrying null mutations of the genes encoding insulin-like growth factor I (Igf-1) and type 1 IGF receptor (Igf1r). *Cell* **75**, 59-72.

Longaker, M. T., Whitby, D. J., Jennings, R. W., Duncan, B. W., Ferguson, M W., Harrison, M. R., Adzick, N. S. (1991). Fetal diaphragmatic wounds heal with scar formation. *The Journal of surgical research* **50**, 375-385.

Marcelle, C., Stark, M. R. and Bronner-Fraser, M. (1997). Coordinate actions of BMPs, Wnts, Shh and noggin mediate patterning of the dorsal somite. *Development (Cambridge, England)* **124**, 3955-3963.

Marcelle, C., Wolf, J. and Bronner-Fraser, M. (1995). The in vivo expression of the FGF receptor FREK mRNA in avian myoblasts suggests a role in muscle growth and differentiation. *Developmental biology* **172**, 100-114.

Marigo, V., Johnson, R. L., Vortkamp, A. and Tabin, C. J. (1996). Sonic hedgehog differentially regulates expression of GLI and GLI3 during limb development. *Developmental biology* **180**, 273-283.

Martin, B. L. and Harland, R. M. (2001). Hypaxial muscle migration during primary myogenesis in Xenopus laevis. *Developmental biology* **239**, 270-280.

Martin, J. F., Li, L. and Olson, E. N. (1992). Repression of myogenin function by TGF-beta 1 is targeted at the basic helix-loop-helix motif and is independent of E2A products. *The Journal of biological chemistry* **267**, 10956-10960.

Massague, J., Seoane, J. and Wotton, D. (2005). Smad transcription factors. *Genes & development* **19**, 2783-2810.

Mastaglia, F. L., Dawkins, R. L., Papadimitriou, J. M. (1975). Morphological changes in skeletal muscle after transplantation. A light and electron-microscopic study of the initial phases of degeneration and regeneration. *Journal of the neurological sciences.* **25**, 227-247.

Mauro, A. (1961). Satellite cell of skeletal muscle fibers. *J Biophys Biochem Cytol* **9**, 493-495.

Megeney, L. A., Kablar, B., Garrett, K., Anderson, J. E. and Rudnicki, M. A. (1996). MyoD is required for myogenic stem cell function in adult skeletal muscle. *Genes & development* **10**, 1173-1183.

Meyers, J. R., Planamento, J., Ebrom, P., Krulewitz, N., Wade, E. and Pownall, M. E. (2013). Sulf1 modulates BMP signaling and is required for somite morphogenesis and development of the horizontal myoseptum. *Developmental biology* **378**, 107-121.

Miller, K. J., Thaloor, D., Matteson, S. and Pavlath, G. K. (2000). Hepatocyte growth factor affects satellite cell activation and differentiation in regenerating skeletal muscle. *American journal of physiology. Cell physiology* **278**, C174-181.

Mills, P., Lafreniere, J. F., Benabdallah, B. F., El Fahime el, M. and Tremblay, J. P. (2007). A new pro-migratory activity on human myogenic precursor cells for a synthetic peptide within the E domain of the mechano growth factor. *Experimental cell research* **313**, 527-537.

Minchin, J. E. and Hughes, S. M. (2008). Sequential actions of Pax3 and Pax7 drive xanthophore development in zebrafish neural crest. *Developmental biology* **317**, 508-522.

Minchin, J. E., Williams, V. C., Hinits, Y., Low, S., Tandon, P., Fan, C. M., Rawls, J. F. and Hughes, S. M. (2013). Oesophageal and sternohyal muscle fibres are novel Pax3-dependent migratory somite derivatives essential for ingestion. *Development (Cambridge, England)* **140**, 2972-2984.

Mintz, B., Baker, W. W. (1967). Normal mammalian muscle differentiation and gene control of isocitrate dehydrogenase synthesis. *Proceedings of the National Academy of Sciences* **58**, 592-598.

Montarras, D., Lindon, C., Pinset, C. and Domeyne, P. (2000). Cultured myf5 null and myoD null muscle precursor cells display distinct growth defects. *Biology of the cell / under the auspices of the European Cell Biology Organization* **92**, 565-572.

Montarras, D., Morgan, J., Collins, C., Relaix, F., Zaffran, S., Cumano, A., Partridge, T. and Buckingham, M. (2005). Direct isolation of satellite cells for skeletal muscle regeneration. *Science (New York, N.Y.)* **309**, 2064-2067.

Moraczewski, J., Piekarska, E., Zimowska, M., Sobolewska, M. (1996). Activity of mu- and m-calpain in regenerating fast and slow twitch skeletal muscles. *Acta biochimica Polonica* **43**, 693-700.

Moss, F. P. and Leblond, C. P. (1971). Satellite cells as the source of nuclei in muscles of growing rats. *Anat Rec* **170**, 421-435.

Mourikis, P., Gopalakrishnan, S., Sambasivan, R. and Tajbakhsh, S. (2012). Cell-autonomous Notch activity maintains the temporal specification potential of skeletal muscle stem cells. *Development (Cambridge, England)* **139**, 4536-4548.

Muir, A. R., Kanji, A. H. and Allbrook, D. (1965). The structure of the satellite cells in skeletal muscle. *Journal of anatomy* **99**, 435-444.

Munsterberg, A. E., Kitajewski, J., Bumcrot, D. A., McMahon, A. P. and Lassar, A. B. (1995). Combinatorial signaling by Sonic hedgehog and Wnt family members induces myogenic bHLH gene expression in the somite. *Genes & development* **9**, 2911-2922.

Musaro, A., Giacinti, C., Borsellino, G., Dobrowolny, G., Pelosi, L., Cairns, L., Ottolenghi, S., Cossu, G., Bernardi, G., Battistini, L., et al. (2004). Stem cell-mediated muscle

regeneration is enhanced by local isoform of insulin-like growth factor 1. *Proceedings of the National Academy of Sciences of the United States of America* **101**, 1206-1210.

Musaro, A., McCullagh, K., Paul, A., Houghton, L., Dobrowolny, G., Molinaro, M., Barton, E. R., Sweeney, H. L. and Rosenthal, N. (2001). Localized Igf-1 transgene expression sustains hypertrophy and regeneration in senescent skeletal muscle. *Nature genetics* **27**, 195-200.

Myer, A., Wagner, D. S., Vivian, J. L., Olson, E. N. and Klein, W. H. (1997). Wild-type myoblasts rescue the ability of myogenin-null myoblasts to fuse in vivo. *Developmental biology* **185**, 127-138.

Nabeshima, Y., Hanaoka, K., Hayasaka, M., Esumi, E., Li, S., Nonaka, I. and Nabeshima, Y. (1993). Myogenin gene disruption results in perinatal lethality because of severe muscle defect. *Nature* **364**, 532-535.

Nabeshima, Y., Uetsuki, T., Komiya, T., Nabeshima, Y., Asakura, A., Kamijo, K., Yagami, T. and Fujisawa-Sehara, A. (1992). Positive and negative gene regulation in muscle. *Symposia of the Society for Experimental Biology* **46**, 343-353.

Nakano, Y., Kim, H. R., Kawakami, A., Roy, S., Schier, A. F. and Ingham, P. W. (2004). Inactivation of dispatched 1 by the chameleon mutation disrupts Hedgehog signalling in the zebrafish embryo. *Developmental biology* **269**, 381-392.

Nakasone, A., Shibata, S., Suzuki, S., Yamashita, Y. and Ohyama, K. (2007). Laser burn wound healing in naso-labial region of fetal and neonatal mice. *Oral diseases* **13**, 45-50.

Neyt, C., Jagla, K., Thisse, C., Thisse, B., Haines, L. and Currie, P. D. (2000). Evolutionary origins of vertebrate appendicular muscle. *Nature* **408**, 82-86.

Ni, T. T., Lu, J., Zhu, M., Maddison, L. A., Boyd, K. L., Huskey, L., Ju, B., Hesselson, D., Zhong, T. P., Page-McCaw, P. S., et al. (2012). Conditional control of gene function by an invertible gene trap in zebrafish. *Proceedings of the National Academy of Sciences of the United States of America* **109**, 15389-15394.

Nishimura, T., Nakamura, K., Kishioka, Y., Kato-Mori, Y., Wakamatsu, J. and Hattori, A. (2008). Inhibition of matrix metalloproteinases suppresses the migration of skeletal muscle cells. *Journal of muscle research and cell motility* **29**, 37-44.

Nord, H., Nygard Skalman, L. and von Hofsten, J. (2013). Six1 regulates proliferation of Pax7-positive muscle progenitors in zebrafish. *Journal of cell science* **126**, 1868-1880.

Ochi, H. and Westerfield, M. (2007). Signaling networks that regulate muscle development: lessons from zebrafish. *Development, growth & differentiation* **49**, 1-11.

Olguin, H. C. and Olwin, B. B. (2004). Pax-7 up-regulation inhibits myogenesis and cell cycle progression in satellite cells: a potential mechanism for self-renewal. *Developmental biology* **275**, 375-388.

Olwin, B. B. and Rapraeger, A. (1992). Repression of myogenic differentiation by aFGF, bFGF, and K-FGF is dependent on cellular heparan sulfate. *The Journal of cell biology* **118**, 631-639.

Ono, Y., Boldrin, L., Knopp, P., Morgan, J. E. and Zammit, P. S. (2010). Muscle satellite cells are a functionally heterogeneous population in both somite-derived and branchiomeric muscles. *Developmental biology* **337**, 29-41.

Ono, Y., Masuda, S., Nam, H. S., Benezra, R., Miyagoe-Suzuki, Y. and Takeda, S. (2012). Slow-dividing satellite cells retain long-term self-renewal ability in adult muscle. *Journal of cell science* **125**, 1309-1317.

Oustanina, S., Hause, G. and Braun, T. (2004). Pax7 directs postnatal renewal and propagation of myogenic satellite cells but not their specification. *The EMBO journal* **23**, 3430-3439.

Pannese, M., Polo, C., Andreazzoli, M., Vignali, R., Kablar, B., Barsacchi, G. and Boncinelli, E. (1995). The Xenopus homologue of Otx2 is a maternal homeobox gene that demarcates and specifies anterior body regions. *Development (Cambridge, England)* **121**, 707-720.

Parameswaran, M. and Tam, P. P. (1995). Regionalisation of cell fate and morphogenetic movement of the mesoderm during mouse gastrulation. *Developmental genetics* **17**, 16-28.

Partridge, T. A. (2003). Stem cell route to neuromuscular therapies. *Muscle & nerve* **27**, 133-141.

Partridge, T. A., Grounds, M., Sloper, J. C. (1978). Evidence of fusion between host and donor myoblasts in skeletal muscle grafts. *Nature* **273**, 306-308.

Partridge, T. A., Morgan, J. E., Coulton, G. R., Hoffman, E. P. and Kunkel, L. M. (1989). Conversion of mdx myofibres from dystrophin-negative to -positive by injection of normal myoblasts. *Nature* **337**, 176-179.

Pascoal, S., Esteves de Lima, J., Leslie, J. D., Hughes, S. M. and Saude, L. (2013). Notch signalling is required for the formation of structurally stable muscle fibres in zebrafish. *PloS one* **8**, e68021.

Patterson, S. E., Bird, N. C. and Devoto, S. H. (2010). BMP regulation of myogenesis in zebrafish. *Developmental dynamics : an official publication of the American Association of Anatomists* **239**, 806-817.

Patterson, S. E., Mook, L. B. and Devoto, S. H. (2008). Growth in the larval zebrafish pectoral fin and trunk musculature. *Developmental dynamics : an official publication of the American Association of Anatomists* **237**, 307-315.

Pownall, M. E., Gustafsson, M. K. and Emerson, C. P., Jr. (2002). Myogenic regulatory factors and the specification of muscle progenitors in vertebrate embryos. *Annual review of cell and developmental biology* **18**, 747-783.

Rand, M. D., Grimm, L. M., Artavanis-Tsakonas, S., Patriub, V., Blacklow, S. C., Sklar, J. and Aster, J. C. (2000). Calcium depletion dissociates and activates heterodimeric notch receptors. *Molecular and cellular biology* **20**, 1825-1835.

Rathbone, C. R., Yamanouchi, K., Chen, X. K., Nevoret-Bell, C. J., Rhoads, R. P. and Allen, R. E. (2011). Effects of transforming growth factor-beta (TGF-beta1) on satellite cell activation and survival during oxidative stress. *Journal of muscle research and cell motility* **32**, 99-109.

Relaix, F., Montarras, D., Zaffran, S., Gayraud-Morel, B., Rocancourt, D., Tajbakhsh, S., Mansouri, A., Cumano, A. and Buckingham, M. (2006). Pax3 and Pax7 have distinct and overlapping functions in adult muscle progenitor cells. *The Journal of cell biology* **172**, 91-102.

Relaix, F., Polimeni, M., Rocancourt, D., Ponzetto, C., Schafer, B. W. and Buckingham, M. (2003). The transcriptional activator PAX3-FKHR rescues the defects of Pax3 mutant mice but induces a myogenic gain-of-function phenotype with ligand-independent activation of Met signaling in vivo. *Genes & development* **17**, 2950-2965.

Relaix, F., Rocancourt, D., Mansouri, A. and Buckingham, M. (2004). Divergent functions of murine Pax3 and Pax7 in limb muscle development. *Genes & development* **18**, 1088-1105.

Relaix, F., Rocancourt, D., Mansouri, A. and Buckingham, M. (2005). A Pax3/Pax7-dependent population of skeletal muscle progenitor cells. *Nature* **435**, 948-953.

Ren, H., Yin, P. and Duan, C. (2008). IGFBP-5 regulates muscle cell differentiation by binding to IGF-II and switching on the IGF-II auto-regulation loop. *The Journal of cell biology* **182**, 979-991.

Renshaw, S. A., Loynes, C. A., Trushell, D. M., Elworthy, S., Ingham, P. W. and Whyte, M. K. (2006). A transgenic zebrafish model of neutrophilic inflammation. *Blood* **108**, 3976-3978.

Reshef, R., Maroto, M. and Lassar, A. B. (1998). Regulation of dorsal somitic cell fates: BMPs and Noggin control the timing and pattern of myogenic regulator expression. *Genes & development* **12**, 290-303.

Reznik, M. (1969). Origin of myoblasts during skeletal muscle regeneration. Electron microscopic observations. *Laboratory investigation* **20**, 353-363.

Reznik, M. (1976). Origin of the myogenic cell in the adult striated muscle of mammals. A review and a hypothesis. *Differentiation* **7**, 65-73.

Rissanen, T. T., Vajanto, I., Hiltunen, M. O., Rutanen, J., Kettunen, M. I., Niemi, M., Leppanen, P., Turunen, M. P., Markkanen, J. E., Arve, K., et al. (2002). Expression of vascular endothelial growth factor and vascular endothelial growth factor receptor-2 (KDR/Flk-1) in ischemic skeletal muscle and its regeneration. *The American journal of pathology* **160**, 1393-1403.

Robinson, B. W., Goss, A. N. (1981). Intra-uterine healing of fetal rat cheek wounds. *The Celft palate journal.* **18**, 251-255.

Rowlerson, A., Radaelli, G., Mascarello, F. and Veggetti, A. (1997). Regeneration of skeletal muscle in two teleost fish: Sparus aurata and Brachydanio rerio. *Cell and tissue research* **289**, 311-322.

Rowsell, A. R. (1984). The intra-uterine healing of foetal muscle wounds: experimental study in the rat. *British journal of plastic surgery* **37**, 635-642.

Roy, S., Wolff, C. and Ingham, P. W. (2001). The u-boot mutation identifies a Hedgehog-regulated myogenic switch for fiber-type diversification in the zebrafish embryo. *Genes & development* **15**, 1563-1576.

Rudnicki, M. A., Braun, T., Hinuma, S. and Jaenisch, R. (1992). Inactivation of MyoD in mice leads to up-regulation of the myogenic HLH gene Myf-5 and results in apparently normal muscle development. *Cell* **71**, 383-390.

Rudnicki, M. A. and Jaenisch, R. (1995). The MyoD family of transcription factors and skeletal myogenesis. *BioEssays : news and reviews in molecular, cellular and developmental biology* **17**, 203-209.

Rudnicki, M. A., Schnegelsberg, P. N., Stead, R. H., Braun, T., Arnold, H. H. and Jaenisch, R. (1993). MyoD or Myf-5 is required for the formation of skeletal muscle. *Cell* **75**, 1351-1359.

Sabourin, L. A., Girgis-Gabardo, A., Seale, P., Asakura, A. and Rudnicki, M. A. (1999). Reduced differentiation potential of primary MyoD-/- myogenic cells derived from adult skeletal muscle. *The Journal of cell biology* **144**, 631-643.

Sabourin, L. A. and Rudnicki, M. A. (1999). Induction of apoptosis by SLK, a Ste20-related kinase. *Oncogene* **18**, 7566-7575.

Sambasivan, R. and Tajbakhsh, S. (2007). Skeletal muscle stem cell birth and properties. *Seminars in cell & developmental biology* **18**, 870-882.

Sander, J. D., Cade, L., Khayter, C., Reyon, D., Peterson, R. T., Joung, J. K. and Yeh, J. R. (2011). Targeted gene disruption in somatic zebrafish cells using engineered TALENs. *Nature biotechnology* **29**, 697-698.

Sanes, J. R. (2003). The basement membrane/basal lamina of skeletal muscle. *The Journal of biological chemistry* **278**, 12601-12604.

Sassoon, D., Lyons, G., Wright, W. E., Lin, V., Lassar, A., Weintraub, H. and Buckingham, M. (1989). Expression of two myogenic regulatory factors myogenin and MyoD1 during mouse embryogenesis. *Nature* **341**, 303-307.

Satoh, A., Sakamaki, K., Ide, H. and Tamura, K. (2005). Characteristics of initiation and early events for muscle development in the Xenopus limb bud. *Developmental dynamics : an official publication of the American Association of Anatomists* **234**, 846-857.

Scata, K. A., Bernard, D. W., Fox, J. and Swain, J. L. (1999). FGF receptor availability regulates skeletal myogenesis. *Experimental cell research* **250**, 10-21.

Schienda, J., Engleka, K. A., Jun, S., Hansen, M. S., Epstein, J. A., Tabin, C. J., Kunkel, L. M. and Kardon, G. (2006). Somitic origin of limb muscle satellite and side population cells. *Proceedings of the National Academy of Sciences of the United States of America* **103**, 945-950.

Schmalbruch, H. (1976). The morphology of regeneration of skeletal muscles in the rat. *Tissue and cell.* **8**, 673-692.

Schmidt, H. and Emser, W. (1985). Regeneration of frog twitch and slow muscle fibers after mincing. *Muscle & nerve* **8**, 633-643.

Schubert, F. R., Tremblay, P., Mansouri, A., Faisst, A. M., Kammandel, B., Lumsden, A., Gruss, P. and Dietrich, S. (2001). Early mesodermal phenotypes in splotch suggest a role for Pax3 in the formation of epithelial somites. *Developmental dynamics : an official publication of the American Association of Anatomists* **222**, 506-521.

Schultz, E. (1974). A quantitative study of the satellite cell population in postnatal mouse lumbrical muscle. *The Anatomical record* **180**, 589-595.

Schultz, E. (1996). Satellite cell proliferative compartments in growing skeletal muscles. *Developmental biology* **175**, 84-94.

Schultz, E., Gibson, M. C. and Champion, T. (1978). Satellite cells are mitotically quiescent in mature mouse muscle: an EM and radioautographic study. *The Journal of experimental zoology* **206**, 451-456.

Schultz, E. and McCormick, K. M. (1994). Skeletal muscle satellite cells. *Reviews of physiology, biochemistry and pharmacology* **123**, 213-257.

Schuster-Gossler, K., Cordes, R. and Gossler, A. (2007). Premature myogenic differentiation and depletion of progenitor cells cause severe muscle hypotrophy in Delta1 mutants. *Proceedings of the National Academy of Sciences of the United States of America* **104**, 537-542.

Seale, P., Sabourin, L. A., Girgis-Gabardo, A., Mansouri, A., Gruss, P. and Rudnicki, M. A. (2000). Pax7 is required for the specification of myogenic satellite cells. *Cell* **102**, 777-786.

Seger, C., Hargrave, M., Wang, X., Chai, R. J., Elworthy, S. and Ingham, P. W. (2011). Analysis of Pax7 expressing myogenic cells in zebrafish muscle development, injury, and models of disease. *Developmental Dynamics* **240**, 2440.

Seo, H. C., Drivenes, Ellingsen, S. and Fjose, A. (1998). Expression of two zebrafish homologues of the murine Six3 gene demarcates the initial eye primordia. *Mechanisms of development* **73**, 45-57.

Skuk, D., Goulet, M., Roy, B., Chapdelaine, P., Bouchard, J. P., Roy, R., Dugre, F. J., Sylvain, M., Lachance, J. G., Deschenes, L., et al. (2006). Dystrophin expression in muscles of duchenne muscular dystrophy patients after high-density injections of normal myogenic cells. *Journal of neuropathology and experimental neurology* **65**, 371-386.

Slavin, S., Nagler, A., Naparstek, E., Kapelushnik, Y., Aker, M., Cividalli, G., Varadi, G., Kirschbaum, M., Ackerstein, A., Samuel, S., et al. (1998). Nonmyeloablative stem cell transplantation and cell therapy as an alternative to conventional bone marrow transplantation with lethal cytoreduction for the treatment of malignant and nonmalignant hematologic diseases. *Blood* **91**, 756-763.

Snow, M. H. (1977). Myogenic cell formation in regenerating rat skeletal muscle injured by mincing. II. An autoradiographic study. *Anat Rec* **188**, 201-217.

Snow, M. H. (1978). An Autoradiographic Study of Satellite Cell Differentiation into Regenerating Myotubes Following Transplantation of Muscles in Young Rats. *Cell and tissue research* **186**, 535-540.

Snow, M. H. (1983). A quantitative ultrastructural analysis of satellite cells in denervated fast and slow muscles of the mouse. *The Anatomical record* **207**, 593-604.

Sonnet, C., Lafuste, P., Arnold, L., Brigitte, M., Poron, F., Authier, F. J., Chretien, F., Gherardi, R. K. and Chazaud, B. (2006). Human macrophages rescue myoblasts and myotubes from apoptosis through a set of adhesion molecular systems. *Journal of cell science* **119**, 2497-2507.

Soria, B., Roche, E., Berna, G., Leon-Quinto, T., Reig, J. A. and Martin, F. (2000). Insulin-secreting cells derived from embryonic stem cells normalize glycemia in streptozotocin-induced diabetic mice. *Diabetes* **49**, 157-162.

Squire, J. M. (1997). Architecture and function in the muscle sarcomere. *Current opinion in structural biology* **7**, 247-257.

St Pierre, B. A. and Tidball, J. G. (1994). Differential response of macrophage subpopulations to soleus muscle reloading after rat hindlimb suspension. *Journal of applied physiology (Bethesda, Md. : 1985)* **77**, 290-297.

Steinbacher, P., Haslett, J. R., Obermayer, A., Marschallinger, J., Bauer, H. C., Sanger, A. M. and Stoiber, W. (2007). MyoD and Myogenin expression during myogenic phases in brown trout: a precocious onset of mosaic hyperplasia is a prerequisite for fast somatic growth. *Developmental dynamics : an official publication of the American Association of Anatomists* **236**, 1106-1114.

Stellabotte, F., Dobbs-McAuliffe, B., Fernandez, D. A., Feng, X. and Devoto, S. H. (2007). Dynamic somite cell rearrangements lead to distinct waves of myotome growth. *Development (Cambridge, England)* **134**, 1253-1257.

Stickney, H. L., Barresi, M. J. and Devoto, S. H. (2000). Somite development in zebrafish. *Developmental dynamics : an official publication of the American Association of Anatomists* **219**, 287-303.

Stoiber, W. and Sanger, A. M. (1996). An electron microscopic investigation into the possible source of new muscle fibres in teleost fish. *Anatomy and embryology* **194**, 569-579.

Stoick-Cooper, C. L., Weidinger, G., Riehle, K. J., Hubbert, C., Major, M. B., Fausto, N. and Moon, R. T. (2007). Distinct Wnt signaling pathways have opposing roles in appendage regeneration. *Development (Cambridge, England)* **134**, 479-489.

Stone, D. M., Hynes, M., Armanini, M., Swanson, T. A., Gu, Q., Johnson, R. L., Scott, M. P., Pennica, D., Goddard, A., Phillips, H., et al. (1996). The tumour-suppressor gene patched encodes a candidate receptor for Sonic hedgehog. *Nature* **384**, 129-134.

Straface, G., Aprahamian, T., Flex, A., Gaetani, E., Biscetti, F., Smith, R. C., Pecorini, G., Pola, E., Angelini, F., Stigliano, E., et al. (2009). Sonic hedgehog regulates

angiogenesis and myogenesis during post-natal skeletal muscle regeneration. *Journal of cellular and molecular medicine* **13**, 2424-2435.

Tajbakhsh, S., Borello, U., Vivarelli, E., Kelly, R., Papkoff, J., Duprez, D., Buckingham, M. and Cossu, G. (1998). Differential activation of Myf5 and MyoD by different Wnts in explants of mouse paraxial mesoderm and the later activation of myogenesis in the absence of Myf5. *Development (Cambridge, England)* **125**, 4155-4162.

Tajbakhsh, S. and Buckingham, M. (2000). The birth of muscle progenitor cells in the mouse: spatiotemporal considerations. *Current topics in developmental biology* **48**, 225-268.

Tajbakhsh, S., Rocancourt, D. and Buckingham, M. (1996). Muscle progenitor cells failing to respond to positional cues adopt non-myogenic fates in myf-5 null mice. *Nature* **384**, 266-270.

Tajbakhsh, S., Rocancourt, D., Cossu, G. and Buckingham, M. (1997). Redefining the genetic hierarchies controlling skeletal myogenesis: Pax-3 and Myf-5 act upstream of MyoD. *Cell* **89**, 127-138.

Tam, P. P. and Beddington, R. S. (1987). The formation of mesodermal tissues in the mouse embryo during gastrulation and early organogenesis. *Development (Cambridge, England)* **99**, 109-126.

Tatsumi, R., Anderson, J. E., Nevoret, C. J., Halevy, O. and Allen, R. E. (1998). HGF/SF is present in normal adult skeletal muscle and is capable of activating satellite cells. *Developmental biology* **194**, 114-128.

Tatsumi, R., Hattori, A., Ikeuchi, Y., Anderson, J. E. and Allen, R. E. (2002). Release of hepatocyte growth factor from mechanically stretched skeletal muscle satellite cells and role of pH and nitric oxide. *Molecular biology of the cell* **13**, 2909-2918.

Tatsumi, R., Liu, X., Pulido, A., Morales, M., Sakata, T., Dial, S., Hattori, A., Ikeuchi, Y. and Allen, R. E. (2006). Satellite cell activation in stretched skeletal muscle and the role of nitric oxide and hepatocyte growth factor. *American journal of physiology. Cell physiology* **290**, C1487-1494.

Tatsumi, R., Sheehan, S. M., Iwasaki, H., Hattori, A. and Allen, R. E. (2001). Mechanical stretch induces activation of skeletal muscle satellite cells in vitro. *Experimental cell research* **267**, 107-114.

Tee, J. M., van Rooijen, C., Boonen, R. and Zivkovic, D. (2009). Regulation of slow and fast muscle myofibrillogenesis by Wnt/beta-catenin and myostatin signaling. *PloS one* **4**, e5880.

Tidball, J. G. and Wehling-Henricks, M. (2007). Macrophages promote muscle membrane repair and muscle fibre growth and regeneration during modified muscle loading in mice in vivo. *The Journal of physiology* **578**, 327-336.

Toma, C., Pittenger, M. F., Cahill, K. S., Byrne, B. J. and Kessler, P. D. (2002). Human mesenchymal stem cells differentiate to a cardiomyocyte phenotype in the adult murine heart. *Circulation* **105**, 93-98.

Trimble, M. S., Xin, J. H., Guy, C. T., Muller, W. J. and Hassell, J. A. (1993). PEA3 is overexpressed in mouse metastatic mammary adenocarcinomas. *Oncogene* **8**, 3037-3042.

Tylzanowski, P., Mebis, L. and Luyten, F. P. (2006). The Noggin null mouse phenotype is strain dependent and haploinsufficiency leads to skeletal defects. *Developmental dynamics : an official publication of the American Association of Anatomists* **235**, 1599-1607.

van Eeden, F. J., Granato, M., Schach, U., Brand, M., Furutani-Seiki, M., Haffter, P., Hammerschmidt, M., Heisenberg, C. P., Jiang, Y. J., Kane, D. A., et al. (1996). Mutations affecting somite formation and patterning in the zebrafish, Danio rerio. *Development (Cambridge, England)* **123**, 153-164.

van Raamsdonk, W., Pool, C. W., Heyting, C., teKronnie, G. and Veeken, K. (1982). Effects of immobilization and partial denervation on the differentiation of muscle fiber types in the Zebrafish, Brachydanio rerio. *Anatomy and embryology* **164**, 63-74.

Vasyutina, E., Lenhard, D. C., Wende, H., Erdmann, B., Epstein, J. A. and Birchmeier, C. (2007). RBP-J (Rbpsuh) is essential to maintain muscle progenitor cells and to generate satellite cells. *Proceedings of the National Academy of Sciences of the United States of America* **104**, 4443-4448.

Venuti, J. M., Morris, J. H., Vivian, J. L., Olson, E. N. and Klein, W. H. (1995). Myogenin is required for late but not early aspects of myogenesis during mouse development. *The Journal of cell biology* **128**, 563-576.

von Maltzahn, J., Chang, N. C., Bentzinger, C. F. and Rudnicki, M. A. (2012). Wnt signaling in myogenesis. *Trends in cell biology* **22**, 602-609.

Wada, M. R., Inagawa-Ogashiwa, M., Shimizu, S., Yasumoto, S. and Hashimoto, N. (2002). Generation of different fates from multipotent muscle stem cells. *Development (Cambridge, England)* **129**, 2987-2995.

Wagner, W., Ansorge, A., Wirkner, U., Eckstein, V., Schwager, C., Blake, J., Miesala, K., Selig, J., Saffrich, R., Ansorge, W., et al. (2004). Molecular evidence for stem cell

function of the slow-dividing fraction among human hematopoietic progenitor cells by genome-wide analysis. *Blood* **104**, 675-686.

Wang, H., Noulet, F., Edom-Vovard, F., Tozer, S., Le Grand, F. and Duprez, D. (2010). Bmp signaling at the tips of skeletal muscles regulates the number of fetal muscle progenitors and satellite cells during development. *Developmental cell* **18**, 643-654.

Wang, X., Zhao, Z., Muller, J., Iyu, A., Khng, A. J., Guccione, E., Ruan, Y. and Ingham, P. W. (2013). Targeted inactivation and identification of targets of the Gli2a transcription factor in the zebrafish. *Biology open* **2**, 1203-1213.

Waterman, R. E. (1969). Development of the lateral musculature in the teleost, Brachydanio rerio: a fine structural study. *The American journal of anatomy* **125**, 457-493.

Watt, D. J., Lambert, K., Morgan, J. E., Partridge, T. A., Sloper, J. C. (1982). Incorporation of donor muscle precursor cells into an area of muscle regeneration in the host mouse. *Journal of the neurological sciences.* **57**, 319-331.

Weinberg, E. S., Allende, M. L., Kelly, C. S., Abdelhamid, A., Murakami, T., Andermann, P., Doerre, O. G., Grunwald, D. J. and Riggleman, B. (1996). Developmental regulation of zebrafish MyoD in wild-type, no tail and spadetail embryos. *Development (Cambridge, England)* **122**, 271-280.

Weintraub, H. (1993). The MyoD family and myogenesis: redundancy, networks, and thresholds. *Cell* **75**, 1241-1244.

Weintraub, H., Davis, R., Tapscott, S., Thayer, M., Krause, M., Benezra, R., Blackwell, T. K., Turner, D., Rupp, R., Hollenberg, S., et al. (1991). The myoD gene family: nodal point during specification of the muscle cell lineage. *Science (New York, N.Y.)* **251**, 761-766.

Wen, Y., Bi, P., Liu, W., Asakura, A., Keller, C. and Kuang, S. (2012). Constitutive Notch activation upregulates Pax7 and promotes the self-renewal of skeletal muscle satellite cells. *Molecular and cellular biology* **32**, 2300-2311.

Westerfield, M. (1995). *The Zebrafish Book. A Guide for the Laboratory Use of Zebrafish (Danio rerio)* (3rd edn).

Westerfield, M. (2000). *The Zebrafish Book. A Guide for the Laboratory Use of Zebrafish (Danio rerio)* (4th edn).

Weyman, C. M. and Wolfman, A. (1998). Mitogen-activated protein kinase kinase (MEK) activity is required for inhibition of skeletal muscle differentiation by insulin-like growth factor 1 or fibroblast growth factor 2. *Endocrinology* **139**, 1794-1800.

Whitby, D. J., Ferguson, M. W. (1991). The extracellular matrix of lip wounds in fetal, neonatal and adult mice. *Development (Cambridge, England)* **112**, 651-668.

White, J. D., Scaffidi, A., Davies, M., McGeachie, J., Rudnicki, M. A. and Grounds, M. D. (2000). Myotube formation is delayed but not prevented in MyoD-deficient skeletal muscle: studies in regenerating whole muscle grafts of adult mice. *The journal of histochemistry and cytochemistry : official journal of the Histochemistry Society* **48**, 1531-1544.

White, R. M., Sessa, A., Burke, C., Bowman, T., LeBlanc, J., Ceol, C., Bourque, C., Dovey, M., Goessling, W., Burns, C. E., et al. (2008). Transparent adult zebrafish as a tool for in vivo transplantation analysis. *Cell stem cell* **2**, 183-189.

Williams, B. A. and Ordahl, C. P. (1994). Pax-3 expression in segmental mesoderm marks early stages in myogenic cell specification. *Development (Cambridge, England)* **120**, 785-796.

Windner, S. E., Bird, N. C., Patterson, S. E., Doris, R. A. and Devoto, S. H. (2012). Fss/Tbx6 is required for central dermomyotome cell fate in zebrafish. *Biology open* **1**, 806-814.

Wolff, C., Roy, S. and Ingham, P. W. (2003). Multiple muscle cell identities induced by distinct levels and timing of hedgehog activity in the zebrafish embryo. *Current biology : CB* **13**, 1169-1181.

Wright, W. E., Sassoon, D. A. and Lin, V. K. (1989). Myogenin, a factor regulating myogenesis, has a domain homologous to MyoD. *Cell* **56**, 607-617.

Wu, J. C., Sung, H. C., Chung, T. H. and DePhilip, R. M. (2002). Role of N-cadherin- and integrin-based costameres in the development of rat cardiomyocytes. *Journal of cellular biochemistry* **84**, 717-724.

Xu, C., Wu, G., Zohar, Y. and Du, S. J. (2003). Analysis of myostatin gene structure, expression and function in zebrafish. *The Journal of experimental biology* **206**, 4067-4079.

Yablonka-Reuveni, Z., Day, K., Vine, A. and Shefer, G. (2008). Defining the transcriptional signature of skeletal muscle stem cells. *Journal of animal science* **86**, E207-216.

Yablonka-Reuveni, Z. and Rivera, A. J. (1994). Temporal expression of regulatory and structural muscle proteins during myogenesis of satellite cells on isolated adult rat fibers. *Developmental biology* **164**, 588-603.

Yablonka-Reuveni, Z., Rudnicki, M. A., Rivera, A. J., Primig, M., Anderson, J. E. and Natanson, P. (1999). The transition from proliferation to differentiation is delayed in satellite cells from mice lacking MyoD. *Developmental biology* **210**, 440-455.

Yamada, M., Sankoda, Y., Tatsumi, R., Mizunoya, W., Ikeuchi, Y., Sunagawa, K. and Allen, R. E. (2008). Matrix metalloproteinase-2 mediates stretch-induced activation of skeletal muscle satellite cells in a nitric oxide-dependent manner. *The international journal of biochemistry & cell biology* **40**, 2183-2191.

Yamada, M., Tatsumi, R., Kikuiri, T., Okamoto, S., Nonoshita, S., Mizunoya, W., Ikeuchi, Y., Shimokawa, H., Sunagawa, K. and Allen, R. E. (2006). Matrix metalloproteinases are involved in mechanical stretch-induced activation of skeletal muscle satellite cells. *Muscle & nerve* **34**, 313-319.

Yang, X. M., Vogan, K., Gros, P. and Park, M. (1996). Expression of the met receptor tyrosine kinase in muscle progenitor cells in somites and limbs is absent in Splotch mice. *Development (Cambridge, England)* **122**, 2163-2171.

Yogev, O., Williams, V. C., Hinits, Y. and Hughes, S. M. (2013). eIF4EBP3L acts as a gatekeeper of TORC1 in activity-dependent muscle growth by specifically regulating Mef2ca translational initiation. *PLoS biology* **11**, e1001679.

Zammit, P. S., Golding, J. P., Nagata, Y., Hudon, V., Partridge, T. A. and Beauchamp, J. R. (2004). Muscle satellite cells adopt divergent fates: a mechanism for self-renewal? *The Journal of cell biology* **166**, 347-357.

Zimowska, M., Brzoska, E., Swierczynska, M., Streminska, W., Moraczewski, J. (2008). Distinct patterns of MMP-9 and MMP-2 activity in slow and fast twitch skeletal muscle regeneration in vivo. *The International journal of developmental biology* **52**, 307-314.